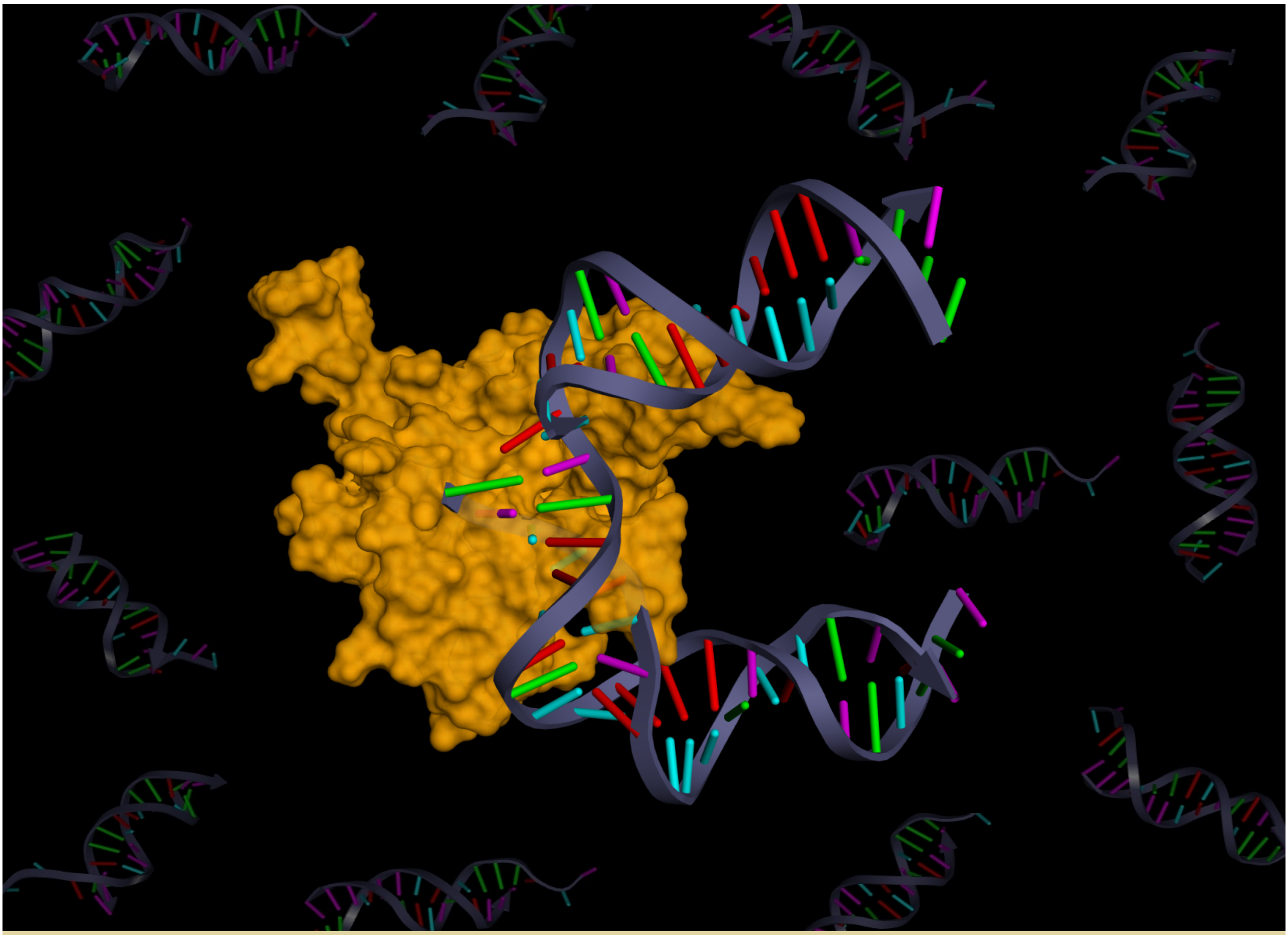

Maria de La Salete de Jesus Baptista

Rational design, synthesis and evaluation of novel anti-cancer chemopotentiators acting on DNA-repair pathways

Doctoral Thesis in Pharmaceutical Sciences in the specialty of Pharmaceutical Chemistry, supervised by Professor Jorge António Ribeiro Salvador and by Professor Maria Manuel Cruz Silva and presented to the Faculty of Pharmacy of the University of Coimbra

December/2017

• U C •

Rational design, synthesis and evaluation of novel anti-cancer chemopotentiators acting on DNA-repair pathways

Thesis submitted to the Faculty of Pharmacy of the University of Coimbra in partial fulfilment of the requirements for the degree of Doctor of Philosophy in Pharmaceutical Sciences in the specialty of Pharmaceutical Chemistry

By

Maria de La Salete de Jesus Baptista

Coimbra, Portugal, 2017

Rational design, synthesis and evaluation of novel anti-cancer chemopotentiators acting on DNA-repair pathways

The present PhD thesis was developed under the supervision of

Professor Jorge António Ribeiro Salvador, PhD

and of

Professor Maria Manuel Cruz Silva, PhD
Laboratory of Pharmaceutical Chemistry, Faculty of Pharmacy, University of
Coimbra, and Centre for Neuroscience and Cell Biology,
University of Coimbra, Portugal

With the collaboration of

Professor Giorgio Colombo, PhD
Istituto di Chimica del Riconoscimento Molecolare - Consiglio Nazionale
delle Ricerche (ICRM-CNR), Milano, Italy

Rational design, synthesis and evaluation of novel anti-cancer chemopotentiators acting on DNA-repair pathways

This work was financially supported by Fundação para a Ciência e a Tecnologia under the Programa Operacional Potencial Humano (POPH) of Quadro de Referência Estratégica Nacional (QREN) Portugal 2007-2013:
SFRH/BD/80975/2011

Front Cover:

Representation of N-terminal DNA-binding domain of PARP-1 bound to a DNA single-strand break.

According to the current legislation, any copying, publication, or use of this thesis or parts thereof shall not be allowed without written permission.

“*You may never know what results come of your actions, but if you do nothing, there will be no results*”

Mahatma Gandhi

À minha família e amigos

AGRADECIMENTOS | *ACKNOWLEDGEMENTS*

Ao Professor Doutor Jorge António Ribeiro Salvador, pela orientação científica desta tese de doutoramento. Pela confiança depositada em mim para desenvolver este projecto. Pela contribuição científica, pelo entusiasmo e disponibilidade demonstrados ao longo de todo este percurso. Pelo seu exemplo de determinação e otimismo. Agradeço ainda as sugestões e a revisão científica do presente documento.

À Professora Doutora Maria Manuel da Cruz Silva, minha co-orientadora científica, pela confiança depositada desde o primeiro momento. Por ser a promotora da minha entrada no mundo da investigação científica, e me ter incentivado e encorajado ao longo de toda esta etapa. Pela disponibilidade e contribuição científica. Agradeço, ainda, as sugestões e a revisão da presente tese.

I am grateful to Doctor Giorgio Colombo for all the support and enthusiasm with this work. I also thank his patience and encouragement, and the warm reception at its research group. I could not have imagined having better support and friendship for my PhD student life abroad.

I thank Sergio Riva, director of *Istituto di Chimica del Riconoscimento Molecolare* (ICRM) for accepting me at this institute and for his great reception and friendship.

À Professora Doutora Teresa Pimenta Dinis e Silva agradeço todo o apoio e orientação facultados. Agradeço ainda a revisão crítica da tese, bem como a simpatia e amabilidade com que sempre me recebeu no Laboratório de Bioquímica da Faculdade de Farmácia da Universidade de Coimbra.

À Fundação para a Ciência e a Tecnologia, pelo apoio financeiro a este projecto (SFRH/BD/80975/2011).

Aos docentes e funcionários do Laboratório de Química Farmacêutica e do Laboratório de Bioquímica da Faculdade de Farmácia pela simpatia e apoio prestados. Um agradecimento especial à D. Graça Santiago pelo encorajamento e

partilha constantes. Pela sua amizade e apoio, que foram de extrema importância ao longo de toda esta etapa. À D. Anabela Pinto, pela boa-disposição e partilha.

A todos os colegas do Laboratório de Química Farmacêutica e do Laboratório de Bioquímica da Faculdade de Farmácia, pela amizade, partilha e boa-disposição demonstradas ao longo de todos estes anos. Ao Bruno Gonçalves e à Vanessa Mendes, pelo apoio e pelas sugestões que contribuíram para a finalização deste trabalho. À Judite Coimbra, pelo encorajamento e partilha, e pelas sugestões pertinentes a esta tese. À Ana Sofia Valdeira, pela amizade ao longo deste percurso. À Daniela Alho e Daniela Marques, pelos bons momentos partilhados. Um agradecimento especial à Sandra, pela sincera e incondicional amizade ao longo deste caminho. Pelas preocupações e sorrisos partilhados. Pelas aventuras vividas. Pela ajuda crucial que em tanto contribuiu para a finalização desta etapa. Por ter sido, provavelmente, a melhor surpresa, que este doutoramento me trouxe. E acima de tudo por me fazer acreditar que haverá sempre mais e melhor.

À Romina Guedes pelo apoio facultado durante a presente tese.

Ao Pedro Silva por todo o apoio prestado ao longo deste trabalho. Pela paciência, amizade e boa disposição.

To Antonella Paladino, Claudio Peri, Elisabetta Moroni, Filippo Marchetti, Gerolamo Vettoretti, Giulia Morra, Giulia Pagani, Massimiliano Meli, Silvia Rinaldi, Riccardo Capelli, the awsome team at Colombo's Lab. Above all, for their friendship, support, and the amazing moments we shared. It was a pleasure to work and learn with them. Each one of them is unique, and their support and friendship meant more than they will ever know. They are the reason why Milan will always be one of my favourite places in Italy.

To Erica Ferrandi for all the friendship and support during my stay in Milan.

À Dra. Ana Melo, por toda a ajuda prestada, que foi crucial para a concretização desta etapa. É sem dúvida um exemplo de que o profissionalismo, a ética e a simpatia podem e devem caminhar lado a lado.

Aos meus pais, aos meus tios, ao meu irmão, à minha cunhada e à minha afilhada. Por todo o apoio e incentivo ao longo desta caminhada. Por terem

acreditado incondicionalmente em mim, mesmo nos momentos mais difíceis. Por serem, sem dúvida, as pessoas mais importantes da minha vida e à quais devo tudo. Um agradecimento especial à minha mãe e à minha tia, por me terem sempre encorajado desde o primeiro dia, e me terem incentivado a ser e a fazer mais e melhor ao longo de toda a vida. À minha afilhada, Lia, que entre as suas brincadeiras e simplicidade de criança, me fez encarar todos os obstáculos com mais leveza, e me ensinou que as coisas mais importantes são por vezes as mais simples e as mais pequenas.

À Cátia Sousa, que foi sem dúvida uma das pessoas mais importantes neste processo. Pelas longas conversas científicas e pelas mais triviais. Pelas gargalhadas sem sentido. Pelo pragmatismo e cuidado com que sempre acompanhou o meu percurso. Pelo apoio constante, pessoal e científico, que em tanto contribuíram para a concretização desta etapa. Por nunca me deixar esquecer que “é nas derrotas que se preparam as vitórias”. E acima de tudo, por ser a amiga insubstituível que é.

À Carolina Macedo, pelo apoio constante ao longo dos últimos anos. Pelo incentivo e encorajamento. E sobretudo, pela sincera e incondicional amizade.

À Mónica Rezende, Filomena Silva, e Susana Monteiro pela boa-disposição e incentivo. Por me acompanharem desde a minha chegada a Coimbra e contribuírem em muito para aquilo que me tornei e alcancei ao longo destes anos.

Aos meus amigos de sempre. À Ana Gonçalves, Edgar Borges, João Pereira, Lígia Abelha e Sara Carvalhais, que ainda que não acompanhassem tão de perto esta caminhada, contribuíram enormemente para a pessoa que hoje sou.

Aos restantes familiares e amigos. Por todo o apoio e motivação. Por sempre me terem encorajado e acreditado em mim.

A todos,

Muito obrigada

Thank you very much

Grazie mille

TABLES OF CONTENTS

ABSTRACT .... **I**

RESUMO .... **III**

LIST OF ABBREVIATIONS .... **VII**

AMINO ACID NOMENCLATURE .... **XIII**

LIST OF FIGURES .... **XV**

LIST OF TABLES .... **XIX**

THESIS ORGANIZATION .... **XXI**

1. CHAPTER I

Introduction **1**

- 1.1. DNA DAMAGE AND CANCER 1
  - 1.1.1. Cancer: general considerations, statistics and success of therapeutics 1
  - 1.1.2. DNA target therapeutics 1
  - 1.1.3. DNA-damaging agents and DNA-repair mechanisms 2
- 1.2. PARP-1 INHIBITORS 22
  - 1.2.1. General considerations 22
  - 1.2.2. PARP-1 inhibitors under clinical evaluation 26
  - 1.2.3. Structural types of PARP-1 inhibitors 31
  - 1.2.4. Mechanisms of the PARP-1 inhibitors 41
  - 1.2.5. Resistance to PARP-1 inhibitors 43
- 1.3. COMPUTER-AIDED DRUG DESIGN IN DRUG DISCOVERY 44
  - 1.3.1. Structure-based drug design methods 47
  - 1.3.2. Ligand-based drug design methods 52

2. CHAPTER II

General objectives **57**

3. CHAPTER III

Design of structure-based pharmacophores for PARP-1 catalytic domain **61**

- 3.1. OVERVIEW 63

3.2. MATERIALS AND METHODS 64
3.2.1. Molecular dynamics simulations 64
3.2.2. MIFs calculation and pharmacophore modelling 65
3.2.3. Database preparation and pharmacophore-based virtual screening 66
3.2.4. Docking studies 67
3.2.5. PARP-1 enzyme assay 68
3.3. RESULTS AND DISCUSSION 69
3.3.1. Characterization of ligand-binding interactions in PARP-1 catalytic domain 69
3.3.2. Molecular interaction fields calculation and receptor-based pharmacophore models generation 70
3.3.3. Pharmacophore-based virtual screening and docking studies 75
3.3.4. PARP-1 inhibitory activity 80
3.4. CONCLUSIONS AND FURTHER DEVELOPMENTS 83

4. CHAPTER IV

Novel PARP-1 inhibitor scaffolds disclosed by a dynamic structure-based pharmacophore approach.. 85

4.1. OVERVIEW 89
4.2. MATERIALS AND METHODS 90
4.2.1. MD simulations 90
4.2.2. Structure-based pharmacophore modelling and validation 91
4.2.3. Database preparation and pharmacophore-based virtual screening 92
4.2.4. Docking Studies 92
4.2.5. PARP-1 enzyme assay 93
4.2.6. Nuclear Magnetic Resonance (NMR) studies 94
4.2.7. NSC131753 MD simulations 94
4.3. RESULTS AND DISCUSSION 94
4.3.1. Structural and dynamic characterization of different complexes with known inhibitors. 94

4.3.2. Pharmacophore model building 101
4.3.3. Pharmacophore-based virtual screening and validation 104
4.3.4. Docking studies 105
4.3.5. PARP-1 inhibition and structure-activity relationship 106
4.4. CONCLUSIONS AND FURTHER DEVELOPMENTS 113

5. CHAPTER V
Bile acid derivatives: from weak PARP-1 inhibitors to novel FXR modulators……115
5.1. OVERVIEW 119
5.2. MATERIALS AND METHODS 123
5.2.1. Database design and preparation 123
5.2.2. Docking studies 126
5.3. RESULTS AND DISCUSSION 128
5.3.1. Structural characterization of the binding interactions of a series of bile acid derivatives into nuclear farnesoid receptor (FXR) 128
5.4. CONCLUSIONS AND FURTHER DEVELOPMENTS 134

6. CHAPTER VI
Concluding remarks……………………………………………………………...................... 137

7. CHAPTER VII
References……………………………………………………….................................... 141

ABSTRACT

Cancer remains a leading cause of death worldwide, with a huge socio-economic impact. Although important improvements in cancer diagnostics and therapeutics have been achieved, their outcomes remain unsatisfactory because of several factors, such as drug resistance, tumour diversity and dose-limiting toxicity, which can be responsible for relapse and/or death.

Targeting DNA repair has emerged as a promising approach to fighting cancer, mostly because the DNA repair inhibition can prevent the survival of cancer cells after DNA damage.

Poly(ADP-ribose)polymerase-1 (PARP-1) is a key effector of DNA repair that plays an important role in the repair of both single-strand and double-strand breaks via different DNA-repair pathways. The PARP-1 inhibitors that have been discovered to date are associated with a lack of target selectivity and the emergence of resistance. Thus, there is a constant demand for new, selective and safer PARP-1 inhibitors that act as anti-cancer agents.

In the present work, the discovery of new and selective PARP-1 inhibitors was pursued. A dynamic receptor-based pharmacophore strategy was first applied, based on the molecular interaction fields calculated on the PARP-1 catalytic domain, which was previously subjected to molecular dynamics (MD) simulations. After a pharmacophore-based virtual screening (VS) against several compound databases, in which the hits that better matched the pharmacophore hypotheses were selected for molecular docking, the top-scoring compounds from the docking calculations were submitted to *in vitro* evaluation, to determine their ability to inhibit PARP-1. As the first approach failed to identify interesting PARP-1 inhibitor candidates, a new strategy was applied.

Taking as starting point the analysis of the interactions established between different inhibitors and the PARP-1 catalytic domain after MD, various dynamic structure-based pharmacophore models were generated and screened against two virtual compound libraries. The drug-like hits retrieved were subjected to molecular docking into the PARP-1 catalytic domain and the top-ranking molecules obtained were submitted to *in vitro* evaluation against PARP-1. Three novel PARP-1 inhibitor scaffolds with interesting activity, i.e., **NSC131753**, **NSC86342** and **NSC121848**, were identified.

Importantly, two cholic acid (CA) derivatives that were designed and evaluated as PARP-1 inhibitors, but without relevant PARP-1 inhibitory activity, were used as the starting point in the design of a bile acid derivative library, which was further subjected to docking calculations. Two chenodeoxycholic derivatives, **5.10** and **5.13**, obtained from that library exhibited a promising binding affinity for the ligand-binding domain of farnesoid X receptor (FXR).

Taken together, these results provided the identification of novel and promising PARP-1 inhibitor scaffolds through an integrated medicinal chemistry strategy that combined a structure-based drug approach, which was based on the dynamics features of active site–ligand interactions, to generate pharmacophore models. This was followed by *in vitro* studies to evaluate the PARP-1 inhibitory activity of the compounds. Furthermore, new potential FXR agonists were identified using a VS strategy by redirecting the target of two CA derivatives that were initially designed and evaluated as PARP-1 inhibitors.

New directions for the investigation of unexplored scaffolds as PARP-1 inhibitors and for the development of novel steroidal FXR agonists were opened through the work developed in this thesis.

Keywords: anti-cancer agents; bile acid derivatives; DNA-repair pathways; FXR; PARP-1; novel scaffolds; structure-based drug design

RESUMO

O cancro é uma das principais causas de morte em todo o mundo, tendo um grande impacto socio-económico. Apesar de todos os avanços no diagnóstico e na terapêutica, os resultados continuam a revelar-se insuficientes, devido, em grande parte, ao desenvolvimento de resistência aos fármacos utilizados, à diversidade tumoral e à toxicidade dos agentes anti-cancerígenos. Todos estes fatores podem contribuir, em última instância, para o aparecimento de recidivas e/ou provocar a morte.

Os mecanismos de reparação do DNA têm vindo a emergir como uma estratégia promissora para combater o cancro, uma vez que a inibição da reparação do DNA pode comprometer a sobrevivência das células tumorais e, consequentemente, travar a sua proliferação. Deste modo, a enzima poly(ADP-ribose)polymerase-1 (PARP-1) representa um potencial alvo terapêutico, dado o seu papel chave na reparação do DNA. Os inibidores da PARP-1 desenvolvidos até agora não apresentaram a seletividade desejada e encontram-se associados a fenómenos de resistência. Assim sendo, a procura de inibidores mais seletivos e mais seguros da PARP-1 que atuem como anti-cancerígenos tem adquirido especial relevo, sendo este o objectivo deste trabalho.

Inicialmente, foi utilizada uma estratégia baseada na criação de modelos dinâmicos de farmacóforos baseados na estrutura do recetor, nomeadamente nos campos de interação molecular no domínio catalítico da PARP-1, que havia sido previamente sujeito a simulações de dinâmica molecular. Após o *screening* virtual de várias bases de dados, utilizando os modelos farmacofóricos criados, os *hits* que apresentaram uma melhor correspondência com os estes modelos foram selecionados para *docking* molecular. Os compostos com melhores resultados nos cálculos de *docking* foram sujeitos a estudos *in vitro*, de modo a avaliar a capacidade destes em inibir a PARP-1. Contudo, devido à incapacidade de identificar candidatos promissores seguindo a metodologia supracitada, uma nova estratégia foi aplicada com vista a obtenção de moléculas mais eficazes na inibição da PARP-1.

Tendo como ponto de partida a análise das interações estabelecidas entre diferentes inibidores e o domínio catalítico da PARP-1 após dinâmica molecular, diferentes modelos farmacofóricos foram gerados e utilizados no *screening* de duas bibliotecas de compostos virtuais. Os *drug-like hits* obtidos foram *dockados* no domínio catalítico da PARP-1 e as moléculas mais promissoras foram testadas *in vitro* para avaliar a sua capacidade em inibir a PARP-1. Como resultado da nova estratégia empregue três novos *scaffolds* de inibidores da PARP-1 com uma importante atividade foram identificados: **NSC131753**, **NSC86342**, e **NSC121848**.

Importa salientar que dois derivados do ácido cólico, desenhados e avaliados como inibidores da PARP-1 mas que não demonstraram uma relevante inibição da mesma, foram usados como ponto de partida para o desenho de uma biblioteca de derivados de ácidos biliares, que foram posteriormente sujeitos a cálculos de *docking* para avaliar a sua interação com o farnesoid X receptor (FXR). Dois derivados do ácido quenodesoxicólico, **5.10** e **5.13** demonstraram uma promissora afinidade com o domínio de ligação do FXR.

Resumindo, estes resultados permitiram a identificação de novos e promissores *scaffolds* de inibidores da PARP-1 através de uma estratégia de química medicinal integrada, que combinou uma abordagem baseada na estrutura do recetor, que teve em conta as características dinâmicas das interações de diferentes ligandos com o local ativo da PARP-1 para gerar modelos farmacofóricos, com estudos *in vitro*, para testar a inibição da atividade da PARP-1. Além disso, novos potenciais agonistas do FXR foram identificados, através de *screening* virtual, partindo de dois derivados do ácido cólico que haviam sido inicialmente desenhados e avaliados como inibidores da PARP-1 e que foram posteriormente usados como base para o desenho de uma biblioteca virtual de derivados dos ácidos biliares usados no *screening*.

Em termos gerais, esta tese contribuiu para a identificação de novos *scaffolds* para o desenvolvimento de inibidores da PARP-1 e para o desenvolvimento de novas moléculas esteróides como agonistas do recetor FXR.

Palavras-chave: anti-cancerígenos; derivados dos ácidos biliares; *design* de fármacos baseado na estrutura; FXR; novos *scaffolds*; PARP-1; Vias de reparação do DNA

LIST OF ABBREVIATIONS

3-AB	3-Aminobenzamide
5′dRP	5′-Deoxyribose-5-phosphate (5′dRP)
5-FU	5-Fluorouracil
6-ECDCA	6α-Ethyl-chenodeoxycholic acid
ADMET	Absorption, distribution, metabolism, excretion and toxicity
ADP	Adenosine diphosphate
Alt-NHEJ	Alternative non-homologous end-joining
APE1	Human apurinic/apyrimidinic endonuclease 1
AP	Apurinic/apyrimidinic
ANK	Ankyrin
APLF	Aprataxin-like factor
ART	ADP-ribosyltransferase
ARTDs	ART dipheteria toxin-like
ATM	Ataxia telangiectasia mutated
ATR	Ataxia telangiectasia and Rad3-related
BA	Bile acid
BAR	Bile acid receptor
BER	Base excision repair
BIR	Break-induced replication
BRCA1	Breast cancer type 1
BRCA2	Breast cancer type 2
BRCT	BRCA1 C-terminus
BRIP1	BRCA1-interacting protein C-terminal helicase 1
BTD	Breakthrough therapy designation
cAbl	Cellular form of the Abelson leukemia virus tyrosine kinase
CA	Cholic acid
CADD	Computer-aided drug design
CAT	Catalytic domain
CDCA	Chenodeoxycholic acid
CETN2	Centrin 2
C-NHEJ	Canonic non-homologous end-joining
cryo-EM	Cryo-electron microscopy

CtIP	CtBP-interacting protein
ddR5P	2,3-didehydro-2,3-dideoxy-ribose
dHj	Double holliday junction
DCA	Deoxycholic acid
DGs	DNA glycosylases
DMSO	Dimethyl sulfoxide
DNA	Deoxyribonucleic acid
DNA-PK	DNA-dependent protein kinase
DNA-PK$_{CS}$	DNA-PK catalytic subunit
DPC	DNA-protein cross-link
DBD	DNA-binding domain
DDR	DNA damage response
DRY	Hydrophobic probe
DSB	Double-strand break
dsDNA	Double-stranded DNA
DSBR	DSB repair
EGFR	Epidermal growth factor receptor
EMA	European Medicines Agency
ERCC1	ERCC excision repair 1
EXO1	Exonuclease 1
FA	Fanconi anaemia
FAAP	FA core complex-associated protein
FANC	FA complemention group
FDA	Food and Drug Administration
FEN1	Flap endonuclease 1
FXR	Farnesoid X receptor
GAFF	Generalized Amber Force Field
GG-NER	Global genomic nucleotide excision repair
HBA	Hydrogen bond acceptor
HBD	Hydrogen bond donor
HD	Helical domain
HR	Homologous recombination
HRR	HR repair
HPS	Histidine-proline-serine rich domain
Hsp90	Heat-shock protein 90

HTS	High-throughput screening
IC_{50}	Concentration of compound required to inhibit 50% of evaluated effect
ICL	Interstrand cross-link
ID	Identification
IR	Ionizing radiation
K_D	Dissociation constant
K_i	Inhibitory constant
Ku70/80	XRCC6/XRCC5
LBD	Ligand-binding domain
LBDD	Ligand-based drug design
LBVS	Ligand-based virtual screening
Lig	DNA ligase
logP	Octanol/water partition coefficient
LCA	Lithocholic acid
MC	Monte Carlo
MD	Molecular dynamics
MDR	Multi-drug resistance
MGMT	O^6-Methylguanine DNA methyltransferase
MLH1	mutL homolog 1
MIF	Molecular interaction field
MMR	Mismatch repair
MRN	MRE11-RAD50-NBS1
MSH	mutS homolog
mTOR	mammalian target of rapamycin
MutS	Mutator S
MVP-ID	Major vault protein interaction domain
NAD^+	Nicotine adenine dinucleotide
NAFLD	Non-alcoholic fatty liver disease
NCI	National Cancer Institute
NER	Nucleotide excision repair
NHEJ	Non-homologous end-joining
NMR	Nuclear magnetic resonance
NR	Nuclear receptor
NSCLC	Non-small cell lung cancer
NVT	Constant temperature, constant volume

O^6-BG	O^6-Benzylguanine
O^6-meG	O^6-Methylguanine
O^6-meT	O^6-Methylthymine
OCA	Obeticholic acid
ORR	Objective response rate
PALB2	Partner and localizer of BRCA2
PAR	Poly(ADP-ribose)
PARG	Poly(ADP-ribose) glycohydrolase
PARP	Poly(ADP-ribose)polymerase
PBC	Primary biliary cholangitis
PCNA	Proliferating cell nuclear antigen
PDB	Protein data bank
P-gp	P-glycoprotein
PI3K	Phosphatidylinositol 3-kinase
PK/PD	Pharmacokinetic/pharmacodynamic
PLD	Pegylated liposomal doxorubicin
PNKP	Polynucleotide kinase phosphatase
Pol	DNA Polymerase
PSA	Polar surface area
QSAR	Quantitative structure-activity relationship
RFA	Replication factor A
RFC	Replication factor C
RMSD	Root mean square deviation
RMSF	Root mean square fluctuation
RNA	Ribonucleic acid
RNAP	RNA polymerase
RPA	Replication protein A
SAM	Sterile alpha motif
SAR	Structure-activity relationship
SBDD	Structure-based drug design
SBVS	Structure-based virtual screening
SDSA	Synthesis-dependent strand annealing
SEM	Standard error of the mean
SNP	Single-nucleotide polymorphism
SP	Standard precision

ssDNA	Single-stranded DNA
SSB	Single-strand break
TANKS	Tankyrase
TC-NER	Transcription-coupled nucleotide excision repair
TFIIH	Transcription factor IIH
TIP3P	Transferable intermolecular potential with 3 points
TMZ	Temozolomide
TLS	Translesion synthesis
TNBC	Triple negative breast cancer
TRITON	Trial of RucaparIb in ProsTate IndicatiONs
UDCA	Ursodeoxycholic acid
UV	Ultraviolet
VEGFR	Vascular endothelial growth factor receptor
VIT	Vault protein inter-alpha-trypsin domain
VS	Virtual screening
VMD	Visual Molecular Dynamics
VWA	Von Willebrand factor type A domain
XLF	XRCC4-like factor
XRCC	X-ray cross-complementing protein
XP	Extra precision
XPA	Xeroderma pigmentosum group A-complementing protein
XPB	Xeroderma pigmentosum group B-complementing protein
XPC	Xeroderma pigmentosum group C-complementing protein
XPD	Xeroderma pigmentosum group D-complementing protein
XPF	Xeroderma pigmentosum group F-complementing protein.
XPG	Xeroderma pigmentosum group G-complementing protein
ZnF	Zinc finger
WGR	Tryptophane- glycine- arginine rich domain

AMINO ACID NOMENCLATURE

Amino acid	One Letter	Three Letter
Alanine	A	Ala
Cysteine	C	Cys
Aspartic acid	D	Asp
Glutamic acid	E	Glu
Phenylalanine	F	Phe
Glycine	G	Gly
Histidine	H	His
Isoleucine	I	Ile
Lysine	K	Lys
Leucine	L	Leu
Methionine	M	Met
Asparagine	N	Asn
Proline	P	Pro
Glutamine	Q	Gln
Arginine	R	Arg
Serine	S	Ser
Threonine	T	Thr
Valine	V	Val
Tryptophan	W	Trp
Tyrosine	Y	Tyr

LIST OF FIGURES

Figure 1.1 Simplified schematic representation of the main types of DNA damage and the major DNA-repair pathways involved in their repair.. 3
Figure 1.2 The main mechanism involved in the direct repair, MGMT repair. 4
Figure 1.3 Simplified schematic representation of DNA damage repair via the BER pathway. 6
Figure 1.4 Simplified schematic representation of the NER pathway.. 10
Figure 1.5 Simplified schematic representation of the MMR pathway. 12
Figure 1.6 Simplified overview of DNA DSB repair by HR.. 16
Figure 1.7 Simplified schematic representation of classical NHEJ.. 18
Figure 1.8 Structural domains of the human PARPs.. 23
Figure 1.9 Representation of the major PARP-1 domains.. 24
Figure 1.10 Simplified schematic representation of PARP-1 activity in DNA repair pathways and the major effects of PARP-1 inhibitors.. 25
Figure 1.11 PARP-1 inhibitors that have entered clinical trials.. 27
Figure 1.12 First A) and second B) generations of PARP-1 inhibitors. 32
Figure 1.13 The binding mode of NAD$^+$ at the donor site of PARP-1 catalytic domain. ... 32
Figure 1.14 PARP-1 inhibitors obtained by modification of the pyrrolo[1,2-a] pyrazine-1(2H)-one (1.24 and 1.25), dimethylpyridazin-3-one (1.26) or phthalazinone (1.27) scaffolds. 34
Figure 1.15 PARP-1 inhibitors derived from dihydroquinolinone core. 36
Figure 1.16 PARP-1 inhibitors containing a benzo[de][1,7]naphthyridin-7(8H)-one core. 36
Figure 1.17 PARP-1 inhibitors obtained by modification of quinazolinone (1.34) and quinazolinedione (1.35) scaffolds. 37
Figure 1.18 PARP-1 inhibitors bearing pseudo-bicyclic lactams. 38
Figure 1.19 PARP-1 inhibitors not bearing an amide group. 39
Figure 1.20 Selective PARP-1 inhibitors. 40
Figure 1.21 CADD in drug discovery and development process.. 45
Figure 1.22 The most widely used methods in CADD.. 47
Figure 3.1 Representation of the main interactions established for each co-crystallised ligand with PARP-1 catalytic domain along MD run.. 70
Figure 3.2 Pharmacophore models generated from MIFs calculation.. 72
Figure 3.3 PARP-1 binding pocket.. 73

Figure 3.4 Superposition of crystal structure and MD reference snapshot of wild-type A) and PARP-1 Val101Ala B) catalytic domain.... 76

Figure 3.5 The top-scoring compounds selected from docking studies for further PARP-1 *in vitro* evaluation.. 77

Figure 3.6 Binding mode of the selected hits into MD reference snapshot of PARP-1 Val101Ala (A and B) and wild-type (C and D) PARP-1 catalytic domain.. 78

Figure 3.7 Binding mode of 3.3 and 3.4 into crystal structure A) and MD reference snapshot B) of wildtype PARP-1 catalytic domain.. 80

Figure 3.8 Betulinic acid derivatives selected from ST database for *in vitro* studies against PARP-1 due to their promising docking results. 81

Figure 4.1 Superposition of the starting crystal structures of 2RCW, 3L3L, 3GN7 and 3GJW 95

Figure 4.2 The plot distances involving the tyrosine residues and ligands along MD trajectories.. 96

Figure 4.3 2D-Ligand interaction diagrams for each ligand complexed with PARP-1 catalytic domain along MD run.. 98

Figure 4.4 Representation of the PARP-1 binding site with excluded volume spheres.. 100

Figure 4.5 RMSFs of complexes along 20 ns MD run. 101

Figure 4.6 Asp105 side chain orientation in the crystal structure and after MD simulations (representative structure).. 102

Figure 4.7 Representation of structure-based pharmacophore models obtained from crystal structures and the dominant conformations after MD simulations.. 103

Figure 4.8 Superposition of the docked pose (magenta) of A620223 with its crystal structure conformation (yellow).. 105

Figure 4.9 Dose-response curves of the three most promising hits: A) NSC131753; B) NSC86342; C) NSC121848.. 106

Figure 4.10 PARP-1 inhibitory activity and docking score data for the most promising hits. 107

Figure 4.11 NOESY spectrum of NSC121848. 108

Figure 4.12 NOESY spectrum of NSC86342. 109

Figure 4.13 The binding mode of the most promising PARP-1 inhibitors at the PARP-1 catalytic domain.... 110

Figure 4.14 The binding mode of A) NSC153161, B) NSC102534, C) NSC65378 and D) NSC11907 at the PARP-1 catalytic domain.. 111

Figure 4.15 Conformational statistics obtained for (*R*)- and (*S*)-NSC131753, along 100 ns MD run.. 112

Figure 5.1 The different FXR isoforms and the 3D structure of FXR-LBD, which is conserved among all isoforms (PDB code: 4QE6). 120

Figure 5.2 Primary (CDCA 5.1 and CA 5.2) and secondary (DCA 5.3, LCA 5.4 and UDCA 5.5) endogenous bile acids. 122

Figure 5.3 The first-in class FXR agonist, OCA. 122

Figure 5.4 Virtual database of BAs derivatives including the endogenous BAs used as starting point to their preparation. A) CA derivatives; B) DCA derivatives; C) CDCA derivatives; D) UDCA derivatives.. 126

Figure 5.5 Representation of the hydrophobic receptor surface (PDB code: 4QE6) around 3.3.. 130

Figure 5.6 The binding mode of the 3.3, 5.10, 5.13, and 5.20 at the FXR-LBD. A) 4QE6; B) 1OSV.. 132

Figure 5.7 2D-Ligand interaction diagrams for 5.13 complexed with the FXR-LBD. A) 4QE6; B) 1OSV.. 133

LIST OF TABLES

Table 1.1 Clinical trials that are currently under way for PARP-1 inhibitors..................... 29

Table 3.1 Docking score data and PARP-1 inhibition activity for the hits studied............ 79

Table 4.1 A) Hydrogen bonds, B) hydrophobic interactions (namely alkyl and π–alkyl interactions) and C) charge-charge interactions with greater occupancy during MD trajectories for 2RCW, 3L3L, 3GN7 and 3GJW complexes.. 97

Table 4.2 Statistical data of structure-based pharmacophore models. 104

Table 5.1 Docking score data for the BAs under investigation.. 131

THESIS ORGANIZATION

This thesis is structured as follows:

Chapter 1 presents a general introduction to DNA damage and cancer, including cancer statistics and DNA target therapeutics. Additionally, different DNA-repair mechanisms are discussed briefly, as are the inhibitors of each DNA-repair pathway that have been disclosed to date. Furthermore, a brief description of the structure and functions of the poly(ADP-ribose)polymerase (PARP) family is provided, especially regarding PARP-1 and its key role in DNA-repair pathways. Moreover, the structural types of PARP-1 inhibitors and their mechanisms of action are discussed, as well as their associated resistance phenomena. In the last part of this chapter, computer-aided drug design (CADD) is highlighted, namely the different approaches applied and the methods that are most widely used in drug discovery pipeline.

Chapter 2 describes the purposes of the work presented in this thesis.

Chapters 3 and **4** aim the discovery of novel PARP-1 inhibitors. Two different structure-based pharmacophore approaches, followed by virtual screening (VS) against different compound databases and subsequent docking studies into PARP-1 catalytic domain are described. In these two chapters, the results on the top-scoring docked compounds, further studied in *in vitro* studies to evaluate their ability to inhibit PARP-1 activity, are presented and discussed.

Chapter 5 focuses on the design of a series of bile acid (BA) derivatives and on their molecular docking into the farnesoid X receptor-ligand binding domain (FXR-LDB), in which two cholic acid (CA) derivatives previously tested as PARP-1 inhibitors are used as the starting point to the library design.

Chapters 3–5 are similarly organized and include an overview, a materials and methods section and the main results and discussion. Each chapter ends with conclusions and future perspectives.

Chapter 6 states the main outcomes drawn from this work and proposals for future work.

Chapter 7 includes the supporting references used in this thesis.

CHAPTER I

INTRODUCTION

1. CHAPTER I

Introduction

1.1. DNA DAMAGE AND CANCER

1.1.1. Cancer: general considerations, statistics and success of therapeutics

Cancer is a complex and multifactorial disease that results from uncontrolled cell division, which can ultimately lead to tumour generation and spreading to different parts of the body via the blood or the lymph system, causing death [1, 2]. Despite the many efforts toward the development of novel therapies targeting cancer, it remains a major cause of morbidity and mortality worldwide [3]. In fact, cancer is the first cause of death among specific age groups (women aged 40–79 years and men aged 45–79 years), and it is estimated that the cancer rate will increase by about 70% within the next 20 years [4, 5]. The main risk factors associated with cancer development include exposure to chemicals or radiation, obesity, tobacco, alcohol and inherited genetic mutations (e.g., *breast cancer type 1/2* (*BRCA1/2* mutations)), which are deeply involved in about 5–10% of all cancers [4]. Despite the different approaches used to treat cancer, such as surgery, chemotherapy, radiotherapy and immunotherapy, the success of cancer treatments remains limited, mostly because of multidrug resistance, tumour diversity and dose-limiting toxicity, which often involve relapse [6]. Furthermore, the costs associated with cancer therapeutics are extremely high. In 2010, the total annual economic impact of cancer was evaluated at US$ 1.16 trillion by the World Cancer Report 2014 [7]. Therefore, novel and safer treatments for cancer are needed to overcome this lethal disease, which has a huge economic impact worldwide.

1.1.2. DNA target therapeutics

Compared with non-tumour cells, cancer cells often display a diminished ability regarding DNA-repair and DNA-damage signalling. They also exhibit upregulation of some mutagenic repair pathways, which contributes to cancer development. Therefore, it is not surprising that DNA damage response (DDR) inhibition can especially compromise cancer cells *versus* non-tumour ones, as the former are usually more dependent on particular repair pathways. In fact, impaired DNA-repair activity and defective cell-cycle checkpoint activation lead to replication stress and a consequent increase in DNA damage in cancer cells. Moreover, the overcoming of the dysfunctional redox homeostasis that is usually associated with cancer cells is also dependent on DDR repair mechanisms. Thus, the development of compounds that potentiate processes that are dependent on the DDR, like replication and oxidative stress, as well as its inhibition itself, have been actively pursued as a promising weapon in cancer treatment [8].

1.1.3. DNA-damaging agents and DNA-repair mechanisms

Each cell can accumulate tens of thousands of DNA lesions per day, which are induced by either exogenous or endogenous agents [9]. Endogenous sources of lesions comprise spontaneous chemical reactions, such as hydrolysis, or genotoxic agents generated by cellular metabolism, like reactive oxygen, nitrogen and carbonyl species, alkylating agents or even lipid peroxidation products. On the other hand, exogenous sources, such as ultraviolet (UV), X-ray and ionizing radiation (IR) and chemical agents, like some drugs used in cancer treatment, are also able to damage DNA [9, 10].

DNA damage can be classified in different types: base modifications, intrastrand and interstrand cross-links (ICLs), DNA–protein cross-links (DPCs), single-strand breaks (SSBs) and double-strand breaks (DSBs) [11, 12]. Depending on the type and location of the DNA damage in the genome, the cell type that suffer the injury and the stage of the cell-cycle, different lesions can appear with different degrees of mutagenicity and cytotoxicity [13]. The evolution of DNA damage into mutations due to unrepaired or incorrectly repaired lesions leads to permanent changes in the original nucleotide sequence of the DNA and may cause different genetic diseases, including cancer or even cell death. Thus, to preserve genome integrity by keeping changes in DNA to a minimum, cells evoke the DDR, which involves DNA damage recognition and signalling, transcriptional regulation and DNA-repair, as well as cell-cycle and apoptosis regulation [10, 14].

Different DNA-repair pathways are engaged according to the specific types of DNA damage and can act independently or coordinated with each other (**Figure 1.1**) [15]. The major DNA-repair pathways, as well as the inhibitors associated with them, are discussed below.

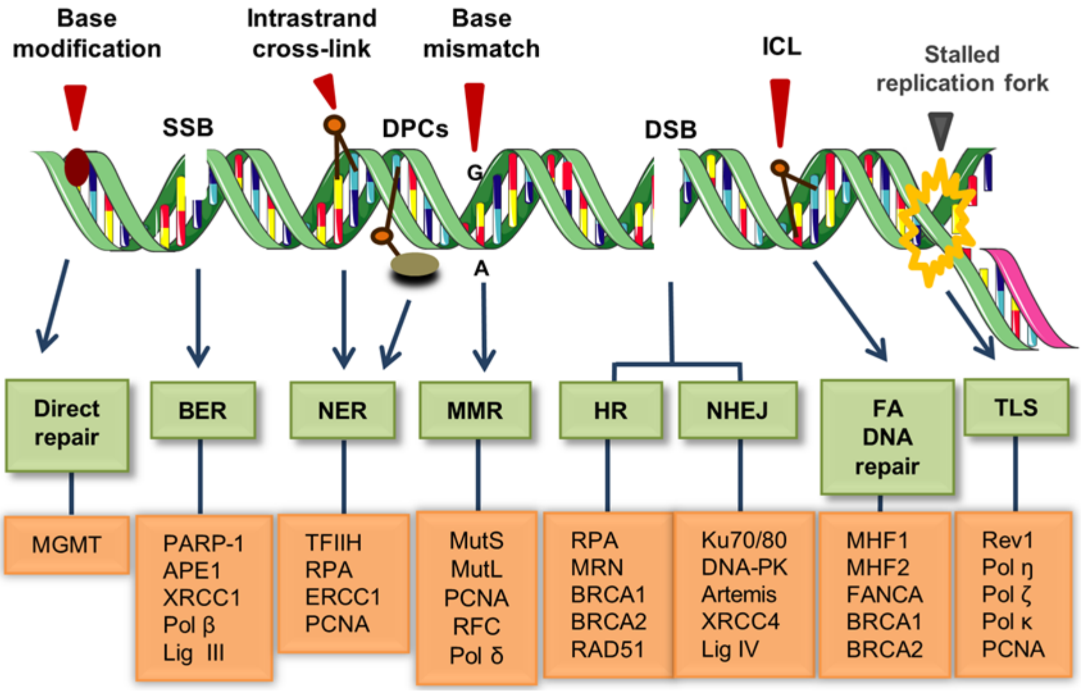
Base modification
Intrastrand cross-link
Base mismatch
ICL
Stalled replication fork
SSB
DPCs
DSB
G
A
Direct repair
BER
NER
MMR
HR
NHEJ
FA DNA repair
TLS
MGMT
PARP-1
APE1
XRCC1
Pol β
Lig III
TFIIH
RPA
ERCC1
PCNA
MutS
MutL
PCNA
RFC
Pol δ
RPA
MRN
BRCA1
BRCA2
RAD51
Ku70/80
DNA-PK
Artemis
XRCC4
Lig IV
MHF1
MHF2
FANCA
BRCA1
BRCA2
Rev1
Pol η
Pol ζ
Pol κ
PCNA

Figure 1.1 Simplified schematic representation of the main types of DNA damage and the major DNA-repair pathways involved in their repair. The main proteins engaged in DNA damage repair are also presented.

1.1.3.1. Direct repair pathway

Direct repair pathway refers to a process that promotes the direct repair of modified bases without disruption or removal of the phosphodiester backbone. The O^6-methylguanine DNA methyltransferase (MGMT) is the main component of this repair pathway. It removes the alkyl group from the O^6-guanine position and transfers it to a cysteine residue in its active site, after which it becomes inactivated and it is subjected to ubiquitin-mediated degradation. This reaction is irreversible and stoichiometric, i.e., one molecule of MGMT can transfer and accept only one alkyl group (**Figure 1.2**). Even though O^6-methylguanine (O^6-

meG) accounts for less than <8% of total alkylation, it is the main factor responsible for the mutagenic, carcinogenic and apoptotic effects induced by methylating agents, such as temozolomide (TMZ), at the oxygen atom of the DNA bases. Nevertheless, MGMT overexpression has been related to chemo-resistance phenomena [16]. On the other hand, in the absence of MGMT, unrepaired base damages can lead to base pair mismatches during replication, namely O^6-meG/T, which can activate the DNA mismatch repair (MMR), induce DSBs and ultimately trigger other repair pathways or even apoptotic cell death [17]. Moreover, the methylation of the *MGMT* promoter with consequent MGMT inactivation has been described in different types of tumours, such as colorectal [18], gastric [19] and head and neck cancers [20], as well as in gliomas [21]. In the latter case, the absence of MGMT activity leads to an increased responsiveness to TMZ. Therefore, efforts have been made to develop MGMT inhibitors. O^6-Benzylguanine (O^6-BG) is the most widely studied MGMT inhibitor identified and several studies are currently under way to identify novel MGMT inhibitors [17, 22].

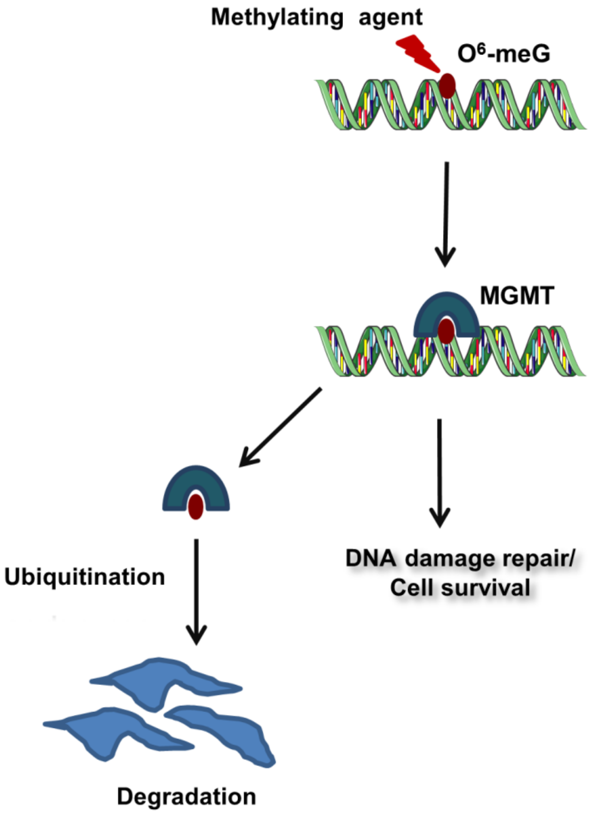

Figure 1.2 The main mechanism involved in the direct repair, MGMT repair (adapted from [17]).

1.1.3.2. Base excision repair

Base excision repair (BER) refers to the repair of small non-helix-distorting base lesions that can be induced by different processes, such as IR, deamination, alkylation and oxidative damage and plays a key role in SSB repair [11, 23]. The BER pathway is activated by one of the 11 damage-specific DNA glycosylases (DGs) that recognize damaged or inappropriate DNA bases and catalyse the cleavage of the *N*-glycosidic bond, thus removing the base and generating apurinic/apyrimidinic (AP) sites [24].

DGs can be classified as monofunctional or bifunctional. In the case of monofunctional DGs, such as uracil-DNA glycosylases, the resulting baseless site is processed by an AP endonuclease (apurinic/apyrimidinic endonuclease 1 (APE1) in humans) that cleaves the phosphodiester bond, creating a single-stranded DNA (ssDNA) in which the gap is flanked by 3′-hydroxyl and 5′-deoxyribose-5-phosphate (5′dRP) ends. On the other hand, bifunctional DGs have an additional lyase activity that is responsible for processing the AP site via β or β,δ-elimination. In this case, a gap flanked by a 5′-phosphate and a 3′-α,β-unsaturated aldehyde (β-elimination) or a 5′-phosphate and a 3′-phosphate (β,δ-elimination) is generated. In order to render the DNA termini accessible to polymerases, the 3′-α,β-unsaturated aldehyde and the 3′-phosphate termini are further processed by APE1 and polynucleotide kinase phosphatase (PNKP), respectively, to afford a 3′-hydroxyl end, which corresponds to the same product that is obtained by the combined action of monofunctional DGs and APE1 [25].

The gap filling and ligation processes proceed via a short-patch or long-patch, depending on the type of DNA damage, the DNA glycosylase involved, the cell-cycle phase and the differentiation status [26]. The short-patch pathway involves a polymerase, Pol β, to incorporate a new nucleotide in the single nucleotide gap and to remove the 5′dRP, which allows the sealing of the DNA ends by the DNA ligase IIIα (Lig IIIα)/X-ray cross-complementing protein 1 (XRCC1) complex, thus finalizing the DNA-repair process. Conversely, in the long-patch repair, two or more nucleotides are added. Even though the first nucleotide is also incorporated by Pol β, the elongation step is likely performed by Pol σ/ϵ, creating a 5′-DNA flap structure that is refractory to ligation. This is further excised by the flap endonuclease 1 (FEN1) in a proliferating cell nuclear antigen (PCNA)-dependent manner, thus allowing nick sealing by DNA ligase I (Lig I), which completes the repair [23, 24]. A simplified schematic representation of the BER pathway is presented in **Figure 1.3**

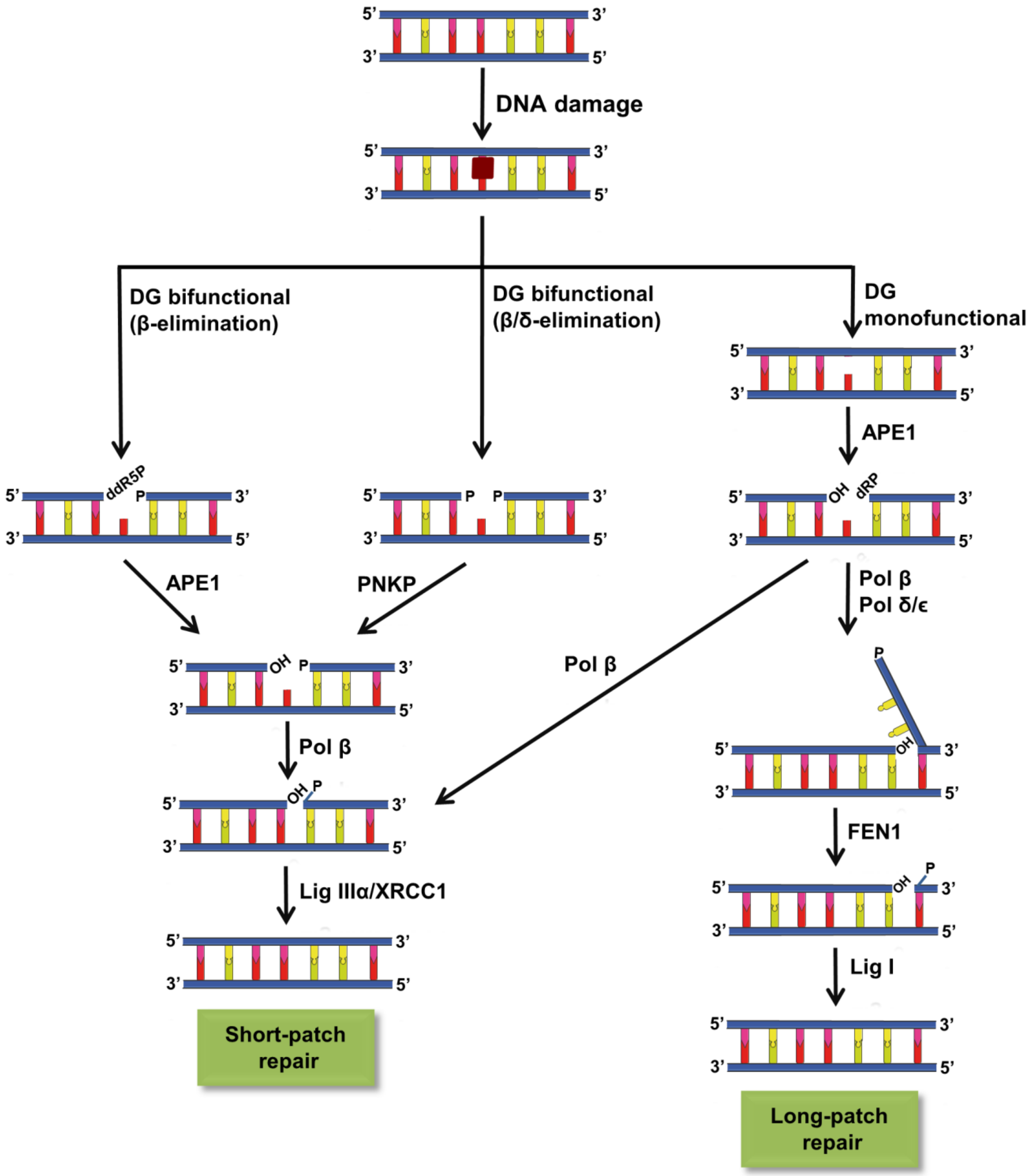
5'
3'
DNA damage
DG bifunctional (β-elimination)
DG bifunctional (β/δ-elimination)
DG monofunctional
APE1
ddR5P
P
OH
dRP
APE1
PNKP
Pol β
Pol δ/ϵ
Pol β
Pol β
FEN1
Lig IIIα/XRCC1
Lig I
Short-patch repair
Long-patch repair

Figure 1.3 Simplified schematic representation of DNA damage repair via the BER pathway.

It is noteworthy that XRCC1 plays a key role in BER, despite its lack of catalytic activity. This scaffold protein interacts with several proteins that are directly involved in BER, such as Lig III and Pol β, holding together the repairing complex and thus allowing them to perform their enzymatic activities. It also interacts with poly(ADP-ribose)polymerase-1 (PARP-1), an enzyme that is responsible for detecting direct and indirect SSBs and for catalysing the formation and addition of poly(ADP-ribose) (PAR) to several acceptor targets, therefore promoting the recruitment of proteins involved in the DNA-repair. Moreover, PARP-1 facilitates the assembly and activation of the BER machinery [27-30].

The BER pathway plays an important role in the repair of DNA damage caused by some anti-cancer drugs, such as taxanes and, alkylating and platinating agents. Consequently, the inhibition of this pathway appears to be a strategy to overcome the resistance to those antitumour drugs. Among the several proteins that are involved in the BER pathway, four (PARP-1, APE1, Pol β and FEN1) have been reported as promising targets because of their specific and/or relevant activity on BER pathway [16]. PARP-1 is the most extensively studied, with three inhibitors recently approved and several clinical trials of different promising inhibitors under way, either in monotherapy or in combination with other anti-cancer agents, like alkylating agents (e.g., TMZ and cyclophosphamide) and topoisomerase inhibitors (e.g., topotecan) [31]. A more detailed description of PARP-1 inhibitors will be presented in section 1.2.

The development of APE1 inhibitors has also been pursued actively, and some molecules have entered clinical trials, namely Lucanthone and TRC102 (methoxyamine hydrochloride) [32]. Despite showing interesting results, TRC102 seems to be a non-specific APE1 inhibitor; rather, it appears to be a BER inhibitor. Nevertheless, other molecules showed promising specific APE1 inhibition, like E3330 (or APX3330), which yielded interesting results in several types of tumours [33].

Moreover, the inhibition of Pol β has been extensively studied, even though no particular Pol β inhibitor has entered clinical trials, usually due to a lack of specificity. Cytarabine, an antimetabolic agent that is used extensively in chemotherapy, also acts as a Pol β inhibitor. It is worth noting that edgeworin, betulinic acid, kohamaic acid A and oleanolic acid are natural compounds that have shown an interesting, but not very potent, Pol β inhibitory activity [32, 34].

On the other hand, FEN1 has also been identified as a promising BER target. Moreover, overexpression of this protein has been associated with different types of cancer, such as pancreatic, prostate, breast and brain cancers [35]. Despite the many efforts toward the discovery of selective and potent FEN1 inhibitors, none has been disclosed to date [16].

1.1.3.3. Nucleotide excision repair

Nucleotide excision repair (NER) promotes the repair of a broad spectrum of DNA damages with very different structures, namely bulky and helix-distorting base lesions (e.g., intrastrand and DNA-protein cross-links) caused by several carcinogenic and mutagenic chemicals, as well as UV irradiation. The efficiency of this pathway depends on different factors, such as the type of tissue damaged and the degree of distortion arising from the lesion (adduct or unusual structure). The NER mechanism comprises 4 essential steps: DNA damage recognition, incision/excision of the oligonucleotide damaged, re-synthesis using the undamaged complementary strand as a template and ligation [36]. The recognition of the lesions is triggered either by the global genome repair mechanism, global genomic NER (GG-NER) or by the transcription-coupled NER (TC-NER). While in the GG-NER sensor proteins, namely the xeroderma pigmentosum group C-complementing protein (XPC), complex with hRAD23B and centrin 2 (CETN2), scan the genomic DNA and recognize distortions and chemical modifications, in TC-NER, the RNA polymerase (RNAP) stalls at DNA damage site, acting as a damage sensor in a transcription-dependent manner. Despite the differences in the initial DNA lesion detection, both NER sub-pathways converge when transcription factor IIH (TFIIH) is recruited at the site of the DNA lesion to verify the presence of damage. Among the ten proteins that constitute this complex are xeroderma pigmentosum group B-complementing protein (XPB) and xeroderma pigmentosum group D-complementing protein (XPD), which are ATPases/helicases, and are responsible for unwinding the DNA double helix and exposing a 20–30 nucleotide bubble [36, 37]. Once the DNA is unwound, xeroderma pigmentosum group A-complementing protein (XPA), replication protein A (RPA) and xeroderma pigmentosum group G-complementing protein (XPG) are recruited. While XPA binds to DNA near the 5′ side of the DNA bubble, RPA binds to the opposite undamaged DNA strand, protecting it from degradation and coordinating excision and repair events. Both XPA and RPA stabilize the damaged DNA and are responsible for the recruitment of other proteins to the bubble site. After association with TFIIH, xeroderma pigmentosum group F-complementing protein/ERCC excision repair 1 (XPF/ERCC1) complex and XPG trigger the dual incision at the 5′ and 3′ sides of the bubble, respectively. Subsequently, the damaged oligonucleotide is released, as are the TFIIH and XPA, allowing gap filling and DNA sealing [38] (**Figure 1.4**). For this event, different polymerases and DNA ligases are recruited, depending on the replicative state of the cells. Pol ϵ and Lig I promote DNA synthesis and ligation, respectively, in replicating cells, while Pol σ and k and Lig IIIα/XRCC1 play corresponding roles in quiescent cells [39-41]. The polymerase activity is coordinated by PCNA, which is loaded onto DNA by the replication factor C (RFC) and RFA [42]. In total, more than 30 proteins are involved in the NER pathway [43].

The NER activity appears to contribute to the chemo-resistance to platinating agents, because of the ability of this pathway to repair the DNA damage caused by those drugs [16]. Thus, the inhibition of NER has been pursued using F11782 [44], UCN-01 [45] and Et743 [46], the first inhibitors reported, even though they are not very potent or specific. Furthermore, UCN-01 was lately classified as a checkpoint inhibitor [43]. Presently, the search for NER inhibitors is mostly focused on ERCC1, namely on the ERCC1–XPA and ERCC1–XPF interactions. NER101 and NER102 are the representative inhibitors of each complex, respectively [43]. The attempt to block the ERCC1–XPA or ERCC1–XPF interactions arises from the crucial and singular role of ERCC1 in the NER pathway, because its overexpression has been related with resistance to platinating agents [11, 16].

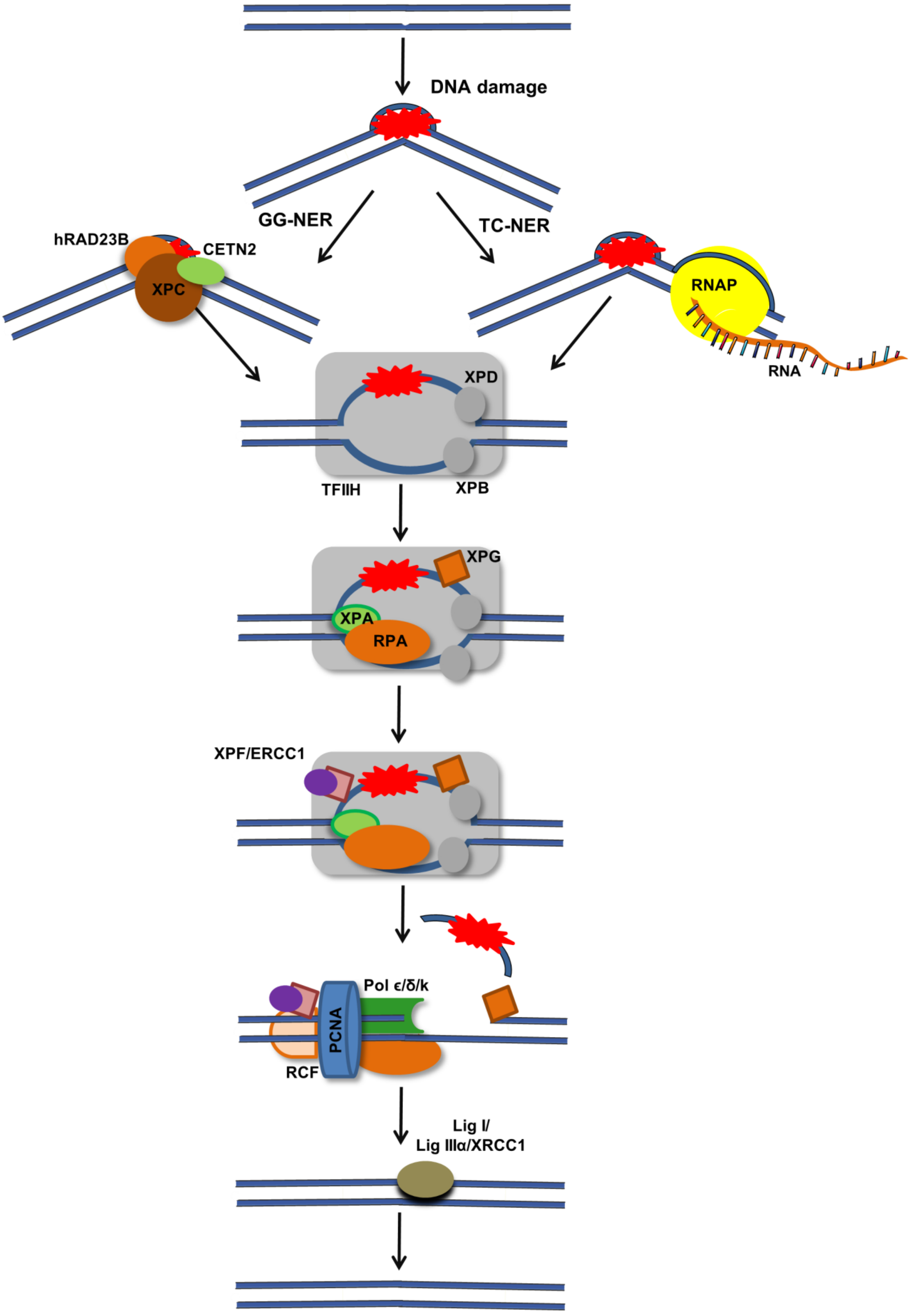
DNA damage
GG-NER
TC-NER
hRAD23B
CETN2
XPC
RNAP
RNA
XPD
TFIIH
XPB
XPG
XPA
RPA
XPF/ERCC1
Pol ϵ/δ/k
PCNA
RCF
Lig I/
Lig IIIα/XRCC1

Figure 1.4 Simplified schematic representation of the NER pathway. The TC-NER and GG-NER sub-pathways are represented. Despite the differences in DNA damage detection, both mechanisms utilize the same machinery to excise and repair the damage (adapted from [36]).

1.1.3.4. DNA mismatch repair

MMR plays a leading role in the repair of post-replicative mismatches, namely base–base mismatches and insertion–deletion loops generated during DNA replication [47]. The correction of mismatch errors occurs during DNA recombination. The mediation of the response to some DNA-damaging drugs, such as methylating and oxidizing agents, is also triggered by MMR [47, 48]. A mutator S (MutS) dimer recognizes and binds to the site of a mismatch and recruits MutL, which mediates downstream events in the MMR pathway. Despite some controversy regarding the signalling downstream MMR events that occur after mismatch recognition, one of the generally described models of MMR, i.e., the *cis* activation model, emphasizes that the MutS/MutL complex will slide along the DNA double helix, releasing the site of mismatch and allowing exonuclease 1 (EXO1) to access and excise the daughter DNA strand. The MutS/MutL complex travels along the DNA until it encounters a gap in the single-strand, coordinated with PCNA and RFC, which works as a signal for the excision step [47, 49, 50]. Subsequently, a DNA polymerase (Pol σ) synthesizes new DNA at the excision site using the parental DNA strand as a template. Lig I finishes the process by sealing the DNA (**Figure 1.5**) [49]. Different MutS heterodimers are recruited depending on the type of mismatch. The MutSα (MSH2–MSH6) heterodimer targets base–base mismatches and small insertion-deletion loops (1–2 nucleotides). Conversely, MutSβ (MSH2–MSH3) only targets insertion–deletion loops, both small and large (~10 nucleotide loops) [47].

Impaired or deficient MMR can lead to an increment in the mutation rates of cells of up to 1000-fold and consequently to an increase in cancer incidence rates. Up to 20% of sporadic cancers have been associated with MMR defects, as have some hereditary cancers, such as hereditary nonpolyposis colon cancer, which is related to mutations in four MMR genes (*MSH2*, *MSH6*, *MLH1* and *PMS2*) [47]. An increase in recombination between DNA sequences homologues (but not fully identical sequences) is also associated with MMR deficiency [51].

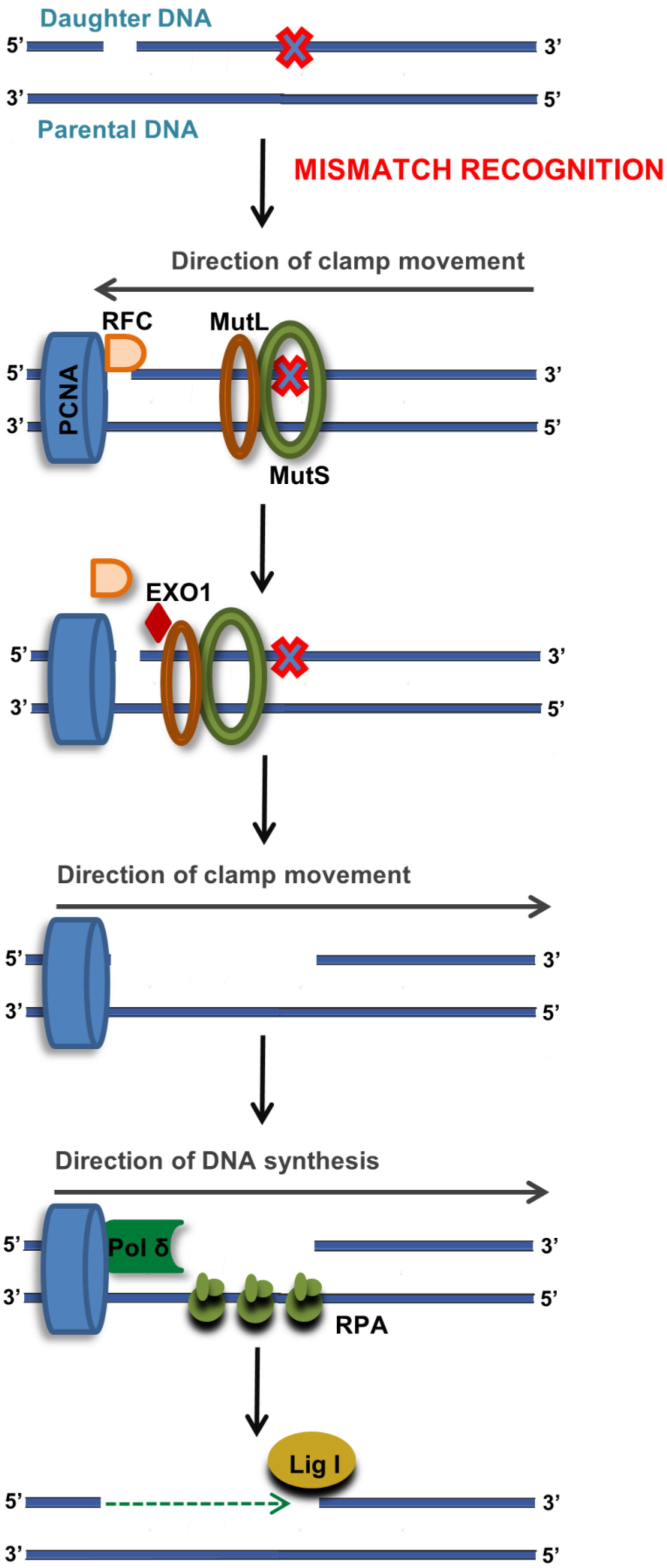
Daughter DNA
5'
3'
3'
5'
Parental DNA
MISMATCH RECOGNITION
Direction of clamp movement
RFC
MutL
PCNA
MutS
EXO1
Direction of clamp movement
Direction of DNA synthesis
Pol δ
RPA
Lig I

Figure 1.5 Simplified schematic representation of the MMR pathway (adapted from [47]).

Because of the contribution of deficient MMR to mutagenicity and chemo-resistance, its inhibition/deficiency has only been explored within the scope of synthetic lethality as anti-cancer activity. Different studies reported an enhancement of oxidative stress in cells carrying MMR deficiency, which can trigger synthetic lethality in the case of other impaired DNA-repair pathways [11, 16].

1.1.3.5. Double-strand break repair

The repair of DSBs, which are the most harmful type of DNA damage, is particularly difficult compared with other types of DNA damage. A deficient DSB repair leads to harmful consequences, such as several mutagenic events (e.g., chromosome deletion, translocation), which can trigger genomic instability and carcinogenesis, or even cell death [52].

DSBs can arise from endogenous sources, such as reactive oxygen species and collapsed replication forks, or exogenous sources, such as IR, UV light and some chemotherapeutic agents (e.g., cisplatin and topoisomerase inhibitors) [15, 52, 53]. Two major mechanisms are involved in DNA DSB repair: homologous recombination (HR) and non-homologous end-joining (NHEJ), which can compete or co-operate with each other to repair DSBs and maintain the genomic stability [53]. HR is the most accurate pathway and it is responsible for the repair of the most severe types of DSB damage [16]. Unlike NHEJ, HR involves the presence of an identical and undamaged DNA sequence, most often derived from the sister chromatid, or exceptionally from the homologous chromosome. As the sister chromatid is present only at S and G2 cell-cycle phases, HR is the predominant DSB repair mechanism at these phases. On the other hand, NHEJ triggers DBS repair throughout the entire cell-cycle, with particular relevance in the G0 and G1 phases. This pathway promotes the re-joining of two broken DNA ends directly [54, 55].

The two primary mechanisms involved in DSB repair, HR and NHEJ, are described further below.

Homologous recombination

HR is responsible for the repair of complex DNA damage events, such as ICLs and DSBs, and also plays a key role in the suppression of genomic instability [56]. This complex pathway involves different steps, such as the unwinding and resection of DNA DSBs to generate single-strand ends, homology search, DNA strand invasion, re-synthesis and resolution [52, 53]. The first stage of HR, DNA-end resection, involves CtBP-interacting protein (CtIP) and BRCA1, as well as the MRN (MRE11–RAD50–NBS1) complex, which binds to DNA ends at each side of the break and triggers the recruitment of other proteins (e.g., nucleases), culminating in 5′ → 3′ DNA resection [57, 58]. The resulting ssDNA is then coated by RPA, which melts the DNA's secondary structure, followed by replacement by RAD51 recombinase, which binds to ssDNA and forms a nucleoprotein filament along the unwound DNA strand [59, 60]. This step involves BRCA2, which plays a key role in HR. It binds and recruits RAD51 to the dsDNA–ssDNA junction, thus fostering the loading and aggregation of the RAD51 filaments onto ssDNA [12, 58].

A search for a homologous dsDNA template will then proceed, which leads to DNA strand invasion, if the location of a complementary ssDNA region in the homologous duplex is successful. Subsequently, a heteroduplex DNA is generated to allow the physical connection between the invading DNA strand and the homologous duplex DNA template. The last two steps, DNA strand invasion and heteroduplex DNA formation are both mediated by RAD51 [56].

Once DNA synthesis is primed, HR can be performed via at least three different sub-pathways: double-strand break repair (DSBR), synthesis-dependent strand annealing (SDSA) and break-induced replication (BIR) (**Figure 1.6**). The DSBR model predicts that the second overhanging 3′ end of DSB is captured and triggers leading strand DNA synthesis, generating a double Holliday junction (dHj) intermediate, the resolution of which can lead to crossover or non-crossover products. In the SDSA model, the heteroduplex DNA is unwound and the invading strand, extended by DNA synthesis, anneals to a complementary sequence at the other side of the break, exposed after resection. Similarly to DSBR, the repair finishes with DNA synthesis and re-sealing. In contrast to DSBR, SDSA only generates non-crossover products and it is the favoured HR pathway during mitosis. The third sub-pathway, BIR, is mainly triggered when only one DNA end is present, as it happens in the repair of broken or shortened telomeres. In this pathway, a replication fork is established and DNA synthesis occurs [56].

Tumours carrying a deficient homologous recombination repair (HRR) showed a higher sensitivity to DNA-damaging agents [56]. For instance, *BRCA1/2*-deficient cells were very sensitive to chemotherapy and IR, and exhibited increased chromosomal instability [61]. Furthermore, the inhibition of an additional DNA-repair pathway by some anti-cancer therapies may trigger synthetic lethality in HR-deficient tumours cells [56]. It was reported that tumours harbouring *BRCA1/2* deficiency (and consequent HR impairment) showed a better response to PARP inhibitors than did HR-proficient cells [62, 63]. Despite the involvement of more than 200 proteins in HR [60], few inhibitors target HR proteins directly, with the exception of RAD51 or RAD54, which seem to be inhibited by B02, A03, A10 and RI-1 (RAD51) or streptonigrin (RAD54), as shown in pre-clinical studies [64-66]. Nevertheless, some molecules can inhibit HR via an indirect way, by affecting HR-related proteins, such as heat-shock protein 90 (Hsp90) and some tyrosine kinases (e.g., Abelson leukemia virus tyrosine kinase (cAbl)). Inhibition of both Hsp90 and cellular form of the cAbl is associated with the decrease of RAD51 activity, which may compromise HR and ultimately lead to apoptosis [12, 16]. 17-Alkylamino-17-demethoxygeldanamycin is an example of an Hsp90 inhibitor that is able to radio-sensitize human tumour cells via the inhibition of RAD51 [67]. Moreover, erlotinib and gefitinib, two tyrosine kinases inhibitors, are also HR inhibitors [11].

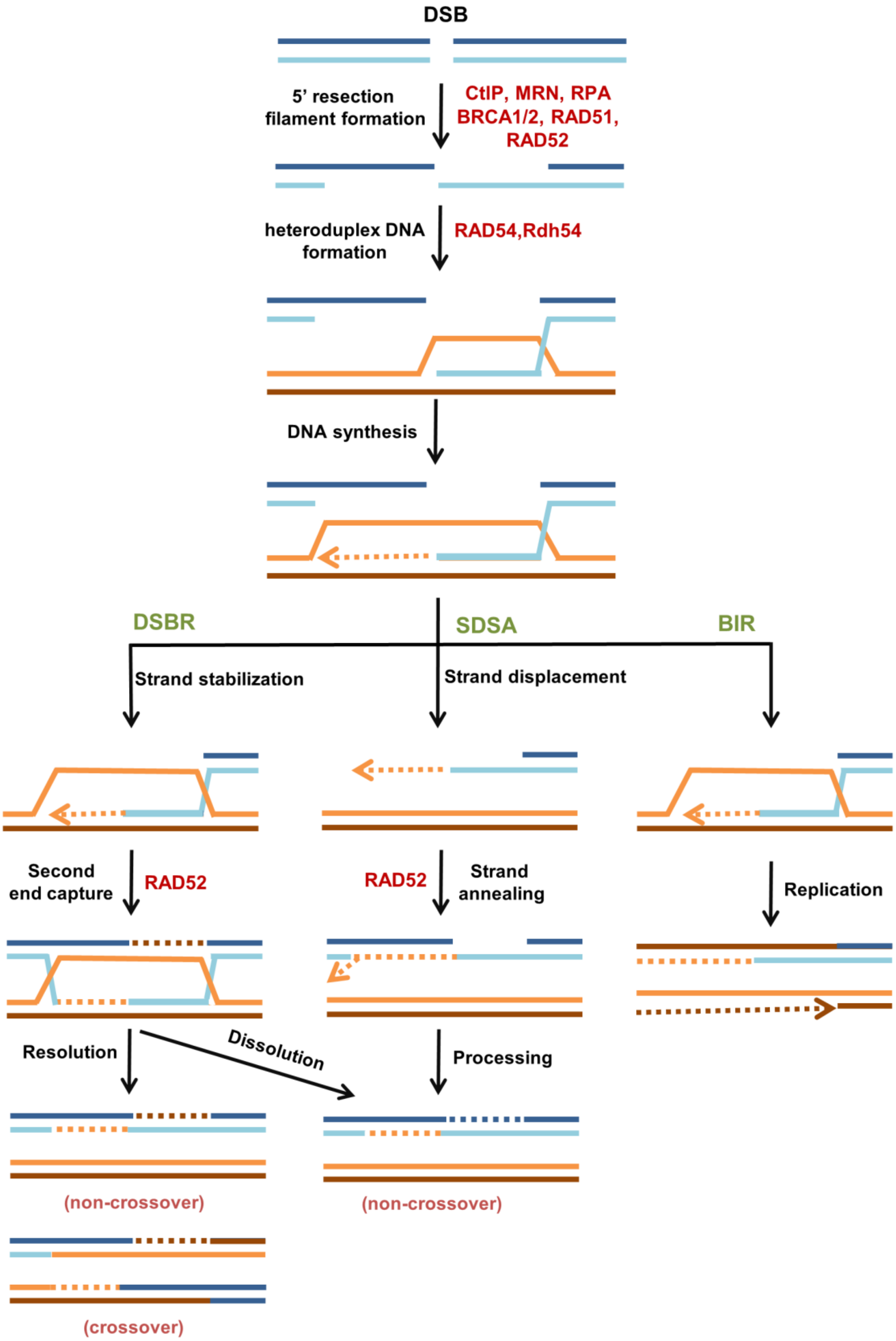
DSB
5' resection
filament formation
CtIP, MRN, RPA
BRCA1/2, RAD51,
RAD52
heteroduplex DNA
formation
RAD54,Rdh54
DNA synthesis
DSBR
SDSA
BIR
Strand stabilization
Strand displacement
Second
end capture
RAD52
RAD52
Strand
annealing
Replication
Resolution
Dissolution
Processing
(non-crossover)
(non-crossover)
(crossover)

Figure 1.6 Simplified overview of DNA DSB repair by HR. After resection of DNA DSBs, RAD51 filaments are formed and initiate strand invasion into the homologous template, to form heteroduplex DNA structures. When DNA synthesis is initiated, three different mechanisms can be further activated: DSBR, SDSA and BIR. In DSBR, the resolution of dHJs can originate crossover and non-crossover products, while dHJ dissolution leads to non-crossover products. Conversely, in SDSA, only non-crossover products are generated. In BIR, the heteroduplex DNA intermediate evolves into a replication forks, followed by DNA strand synthesis. The dashed lines denote the newly synthesized DNA (adapted from [56]).

Non-homologous end-joining

NHEJ can be summarized in three essential steps: detection of DSBs, processing of DNA ends and re-ligation of compatible processed DSBs ends. The DBS repair mediated by NHEJ begins with the recognition and binding of the Ku70/80 heterodimer to both DSB DNA ends, thus creating a scaffold that is able to aggregate other NHEJ-intervenient proteins, such as the DNA-dependent protein kinase catalytic subunit (DNA-PK_{CS}). The DNA-PK_{CS} of each DSB end are then linked together, auto-phosphorylated and assembled with DNA ends and Ku70/80. At this point, the non-compatible DNA termini are processed by several enzymes, such as nucleases and polymerases, to allow the re-ligation of the DNA ends (**Figure 1.7**). This step generally leads to small DNA sequence deletions, which promotes erroneous repairs and leads to a lower repair accuracy compared with HR. To finalize the repair, the X-ray cross-complementing protein 4 (XRCC4) complex with XRCC4-like factor (XLF) and DNA ligase IV (Lig IV) and the ligation of both DSBs termini is promoted [68-70].

In addition to this classical or canonical NHEJ (also termed C-NHEJ), an alternative form of NHEJ (Alt-NHEJ) also involves DSB end-joining. However, this repair mechanism occurs without the key factors that are required by C-NHEJ, such as Ku70/Ku80, DNA-PKcs and Lig IV [71]. It is worth mentioning that Alt-NHEJ is more error prone than C-NHEJ, often leading to sequence alterations and translocations and, ultimately, to genomic instability and cancer development [71, 72]. Like HR, Alt-NHEJ involves DNA end resection, and it has been suggested that this DNA-repair pathway works as a back-up mechanism in the repair of DSBs in case of HR deficiency. The key role that PARP-1 seems to play in Alt-NHEJ may also contribute to the promising responses showed by PARP-1 inhibitors in HR-deficient cells [58].

Similar to mismatch repair, a loss or deficiency of NHEJ is associated with an increment of chemo-resistance and cancer development. Nevertheless, NHEJ inhibition has been pursued in terms of synthetic lethality in HRR-deficient cells, which lose the ability of repairing DSBs using HR [16]. The NHEJ compromise can promote HR, which is lethal in cancer cells carrying a deficiency in the HR pathway.

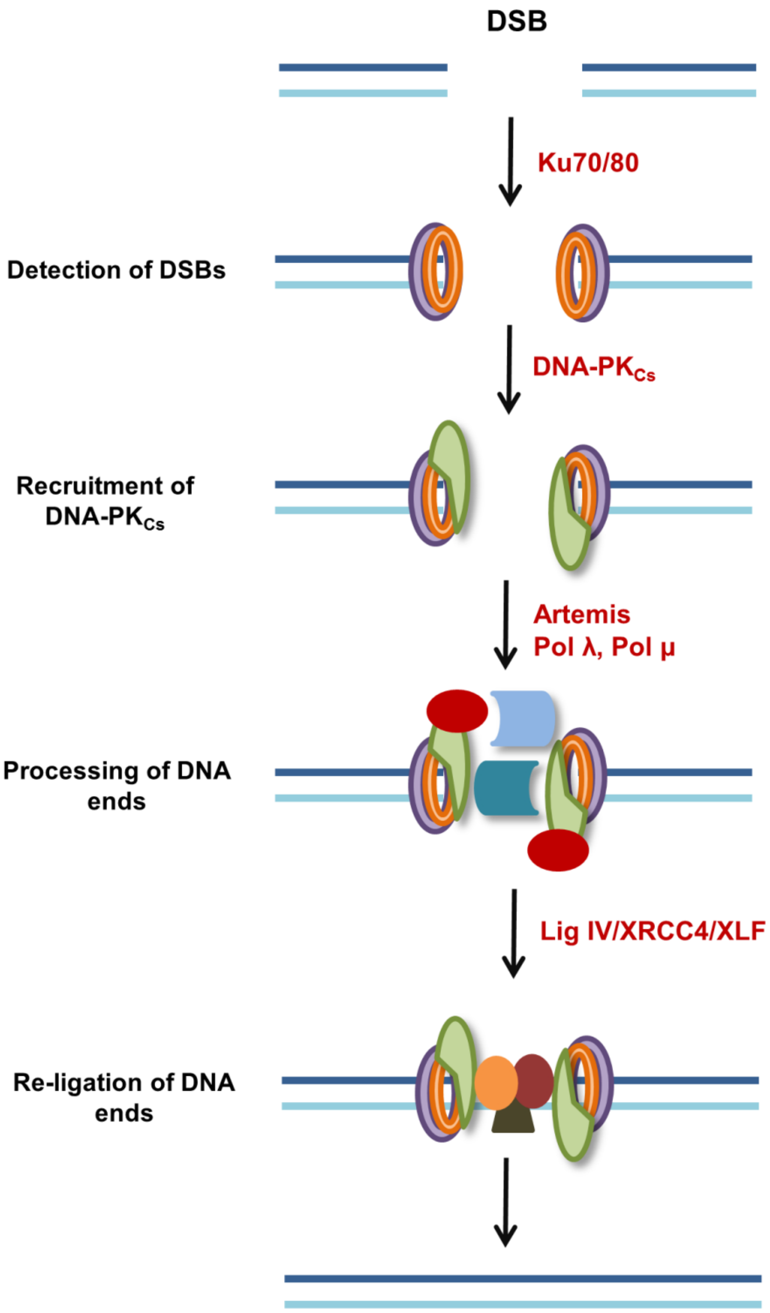
DSB
Ku70/80
Detection of DSBs
DNA-PKCs
Recruitment of DNA-PKCs
Artemis
Pol λ, Pol μ
Processing of DNA ends
Lig IV/XRCC4/XLF
Re-ligation of DNA ends

Figure 1.7 Simplified schematic representation of classical NHEJ. DSBs are detected by the Ku70/80 heterodimer, which is loaded onto DSB ends and recruits DNA-PK$_{CS}$. DNA-PKCS facilitates the processing of DNA ends by Artemis and other substrates, like DNA polymerases, through phosphorylation of those targets and self-phosphorylation. Finally, Lig IV/XRCC4/XLF complex ligates the broken ends.

Direct NHEJ inhibitors have been developed that target DNA-PK, a key NHEJ protein, the overexpression of which is correlated with radio-resistance in lung carcinoma, oesophageal cancer and oral squamous cell carcinoma [73, 74]. Some potent and specific DNA-PK inhibitors have been identified, such as

NU7026 and NU7441; they were able to enhance the sensitivity to DNA-damaging agents and IR in pre-clinical studies [75]. However, specific DNA-PK inhibitors have been associated with a poor pharmacokinetic profile and high levels of toxicity in non-tumour cells [12, 75]. Thus, the only two DNA-PK inhibitors that are currently in clinical trials, CC-115 and CC-122, are dual-action inhibitors that also display mammalian target of rapamycin (mTOR) inhibitory effects and pleiotropic pathway modulation, respectively [16, 31].

It is worth noting that other proteins are being studied as potential targets of NHEJ inhibition, namely Lig IV. DNA ligases are engaged in different DNA-repair pathways, such NHEJ, Alt-NHEJ, BER and NER. Their inhibition was shown to increase the cytotoxicity of DNA-damaging agents [12]. SCR7 has been identified as an inhibitor of Lig IV, the DNA ligase that is involved in the NHEJ pathway. This inhibitor potentiates the cytotoxic effect of anti-cancer drugs that cause DSBs, ultimately leading to cell death due to unrepaired DSBs accumulation [76]. L67 is another DNA ligase inhibitor that was reported recently. This molecule acts as a Lig I and IIIα inhibitor, thus affecting Alt-NHEJ, BER and NER pathways [77].

In fact, some molecules that inhibit more than one DNA-repair pathway were identified as part of a promising strategy to develop new anti-cancer agents. These compounds modulate the activity of specific proteins that are involved in several of those pathways, such as histone deacetylases (HDACs) and PARP-1, or even in other DNA damage response targets, such as ataxia telangiectasia mutated/Ataxia telangiectasia and Rad3-related (ATM/ATR) and the MRN complex.

HDACs, for instance, play an essential role in the maintenance of genome stability, and their inhibition downregulates several components of the DDR and DNA-repair pathways, namely the MRN complex, ATM, HR and NHEJ [78]. The combination of HDAC inhibitors with DNA-damaging agents seems to be an interesting approach in anti-cancer therapy [79].

On the other hand, some MRN complex inhibitors with promising outcomes have also been reported. For example, telomelysin is a MRN complex inhibitor [80] that is currently in clinical trials.

Another interesting target in DNA-repair-mediated anti-cancer therapy is PARP-1. This protein plays an important role in both SBS and DSB repair by binding to sites of DNA damage and recruiting other proteins that are key for DNA-repair, such as XRCC1 (BER) or NBS1 and MRE11 (HR) [81]. Moreover, PARP-1 seems to supress NHEJ via PARylation of Ku70/80, which is responsible for the recognition of, and binding to DSBs, as previously mentioned. Therefore, repair by HR is fostered [81, 82]. PARP-1 inhibition reverts this situation, which leads to NHEJ activation, especially in HR-deficient cancer cells. Because NHEJ is a more error-prone pathway than HR, PARP-1 inhibition can lead to an increase in mutation rates and consequent cell death [81]. An extensive description of the PARP-1 inhibitors that have been approved or are under investigation will be presented in section 1.2.

1.1.3.6. Fanconi anaemia DNA-repair pathway

Fanconi anaemia (FA) DNA-repair pathway plays a key role in the repair of ICLs, which is an extremely hazardous type of DNA damage. Various endogenous (e.g., reactive aldehydes) and exogenous agents are able to generate ICLs. Among the exogenous sources of DNA damage, chemotherapeutic agents like cisplatin or even mitomycin C, which is a natural compound, are widely recognized as cross-linking compounds. Depending on the agents that generate the ICLs, different cellular responses will be obtained. Subsequently, a complex DDR is promoted, including the activation of the FA DNA-repair pathway and cell-cycle checkpoint. Nineteen FA proteins are involved in ICL repair. These are often divided into three groups, in line with their role in this DNA repair pathway: the FA core complex, the FANCD2/FANCI complex and the effector proteins [83]. It is noteworthy that 95% of patients with FA, which is a rare inherited syndrome characterized by congenital abnormalities, bone marrow failure and increased risk of some types of cancer, display FA gene mutations [83, 84].

Once installed into DNA, ICLs are recognized by the FANCM–FAAP24–MHF1–MHF2 anchor complex, followed by the triggering of the core complex formed by FANCA, FANCB, FANCC, FANCE, FANCF, FANCG, FANCL, FANCM, FAAP20, FAAP24 and FAAP100 [83, 84]. Subsequently, the FANCD2/FANCI complex is recruited to the ICLs, after mono-ubiquitination by the core complex. Finally, the effector proteins play a key role in the later stages of ICL repair. These proteins include FANCD1 (BRCA2), FANCJ (BRIP1), FANCN (PALB2), FANCO (RAD51C), FANCP (SLX4), FANCQ (XPF), FANCR (RAD51) and FANCS (BRCA1) [83].

Induction and upregulation of the FA DNA-repair pathway has been reported as a mechanism of resistance to DNA cross-linking agents in a broad range of cancers, such as gliomas [85], leukaemia [86], squamous cell head and neck tumours [87] and multiple myeloma [88]. Thus, the inhibition of the FA pathway has been pursued as a strategy to overcome the resistance to ICL-inducing agents [89].

1.1.3.7. Translesion synthesis

Translesion synthesis (TLS), often described as a DNA-repair pathway, is rather a DNA damage tolerance process that promotes replication, despite the presence of some DNA lesions, such as AP sites. This implies the use of specialized DNA polymerases that promote DNA synthesis (e.g., Rev1, Pol ŋ and ζ). This DNA damage tolerance is an important mechanism of survival after the occurrence of DNA lesions, despite the fact that it is an intrinsically error-prone process and a major source of mutagenesis induced by DNA damage [90, 91]. Moreover, this mechanism is associated with acquired resistance to the genotoxic agents used in anti-cancer therapy, due to an enhancement of cancer cells survival after chemotherapy, which may increase the mutagenesis rate in tumours. Consequently, TLS inhibition has been reported as an interesting approach to overcome that resistance and to improve the efficacy of those drugs. The development of TLS inhibitors has been actively pursued, even though no specific TLS inhibitor has been identified to date. Therefore, further studies are needed to understand fully the potential of these compounds [92].

1.2. PARP-1 INHIBITORS

1.2.1. General considerations

1.2.1.1. The PARP family: structure and function

The poly(ADP-ribose)polymerases (PARP) family comprises a group of enzymes that share the ability to catalyse the attachment of ADP-ribose moieties to specific acceptor proteins and transcription factors, using nicotine adenine dinucleotide (NAD^+) as a substrate [93]. The PARP family includes at least 17 isoforms that share a homologous catalytic domain, which includes a highly conserved sequence of amino acids, the PARP signature motif (residues 859-908 in human PARP-1) [94], which defines the PARP family of proteins [95].

Additional similarities other than the catalytic domain are observed among some PARP members and may underlie the common functions observed between them [96]. For instance, PARP-1, PARP-2 and PARP-3 display a common tryptophan-, glycine-, arginine-rich (WGR) domain that seems to play an important role in their DNA-dependent activity [96, 97] (**Figure 1.8**). Moreover, PARPs have been grouped in different classes, according to their multi-domain structure architecture, cellular location or enzymatic functions [98, 99]. According to the new nomenclature proposed by Hottiger *et al*. [100], the human PARP family (hPARP) can be divided into three groups, taking into account their motifs and activities:

a) PARP-1,-2 and 4, and tankyrases 1 (PARP-5A) and 2 (PARP-5B), which catalyse poly (ADP-ribosyl)ation;

b) PARP-3, 6–8, 10–12 and 14–16, which have an accepted or putative mono (ADP-ribosyl)ation activity;

c) PARP-9 and 13, which are likely enzymatically inactive.

Therefore, only five members display true PARP activity, which leads to their renaming as ADP-ribosyltransferase diphtheriatoxin-like (ARTD) proteins. This designation reflects better the transferase activity described above that is common to all members of the family. However, the term PARP is generally accepted.

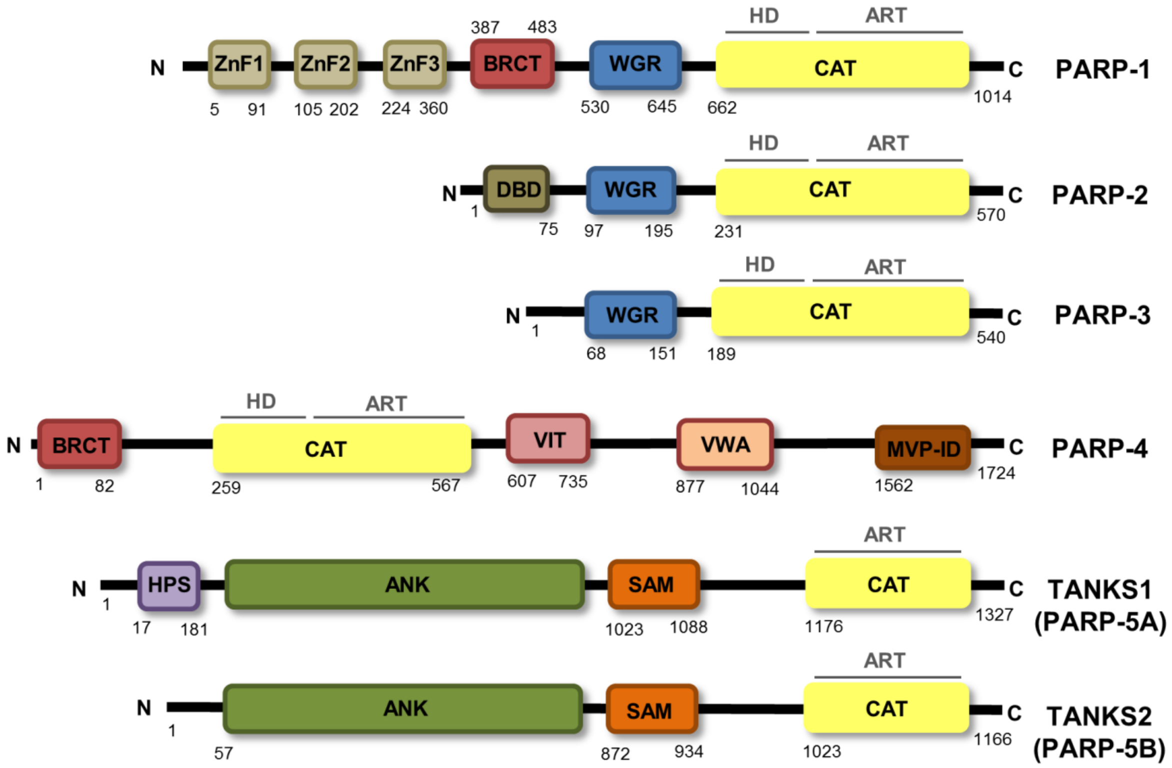
HD
ART
387 483
N
ZnF1
ZnF2
ZnF3
BRCT
WGR
CAT
C
PARP-1
5 91 105 202 224 360
530 645 662
1014
HD
ART
N
DBD
WGR
CAT
C
PARP-2
1
75 97 195 231
570
HD
ART
N
WGR
CAT
C
PARP-3
1
68 151 189
540
HD
ART
N
BRCT
CAT
VIT
VWA
MVP-ID
C
PARP-4
1 82 259 567 607 735 877 1044 1562
1724
ART
N
HPS
ANK
SAM
CAT
C
TANKS1
(PARP-5A)
1
17 181 1023 1088 1176
1327
ART
N
ANK
SAM
CAT
C
TANKS2
(PARP-5B)
1
57 872 934 1023
1166

Figure 1.8 Structural domains of the human PARPs. Only the members that have a true poly(ADP-ribosyl)ation activity (PARP-1, 2, 4 and 5) and/or display a DNA-dependent activity (PARP-1, 2, and 3) are represented. Each member displays a catalytic domain containing an ADP-rybosyltransferase (ART) domain. PARPs 1–4 have an additional helical domain (HD), which is involved in allosteric regulation. PARPs 1–3 contain a WGR domain that plays a key role in DNA-dependent catalytic activation.

PARP-1 is the best characterized isoform among the PARP family members and is responsible for 85%–90% of poly(ADP-ribosyl)ation activity [101]. It plays an active role in several biological processes, including inflammation, hypoxic response, transcriptional regulation, maintenance of chromosome stability, DNA-repair, and cell death [101-105]. This 113 kDa nuclear enzyme is composed of three major domains: an *N*-terminal DNA-binding domain (DBD), an auto-modification domain (which is able to establish protein–protein interactions, namely with BRCA1) and a catalytic domain ((CAT) where enzymatic activity takes place) [81] (**Figure 1.9**).

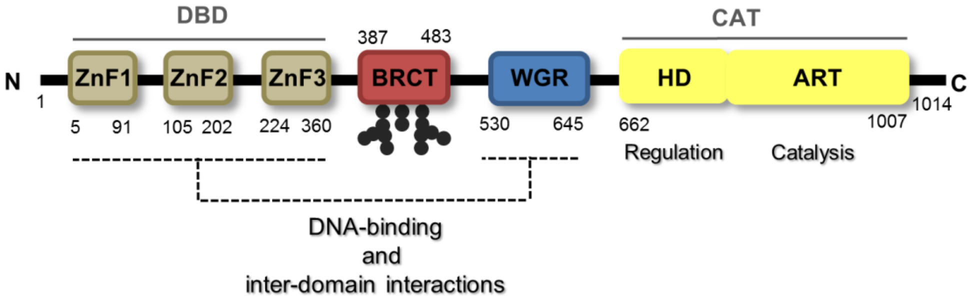

Figure 1.9 Representation of the major PARP-1 domains. The DNA-binding domain (DBD) contains three zinc-finger motifs: ZnF1, ZnF2 and ZnF3. The BRCA1 C-terminus (BRCT) is involved in protein–protein interactions. The catalytic domain (CAT) is divided into two sub-domains, the helical domain (HD) and the ART domain.

Among the different biological processes in which PARP-1 can take place, its key role in DNA-repair has been amply studied [61]. This protein recognizes and binds to DNA strand breaks via its *N*-terminal region, which promotes a conformational change in the *C*-terminal catalytic domain. As a result, this domain becomes activated, exposing the activation site to NAD^+ and leading to the attachment of poly (ADP-ribose) chains to many targets, including key proteins for DNA-repair and replication and PARP-1 itself, in a process that is known as "PARylation" [81, 102, 106, 107]. The PARP-1 catalytic activity is increased by to 500 times upon binding to damaged DNA. The negative charge of PAR decreases the interaction between histones and DNA, thus allowing the access of DNA-repair enzymes, such as XRCC1 and Lig IIIα (in BER pathway), to the site of damage. Simultaneously, PARP-1 is rapidly inactivated by poly(ADP-ribose) glycohydrolase (PARG), which renders the DNA damage site even more accessible to the DNA-repair machinery. Consequently, the enzyme becomes inactivated and dissociates from the DNA. In this way, the DNA-repair can proceed. The total repair cycle can be processed in a few minutes [107]. In addition to its key role in BER, PARP-1 has been described as a promoter of HR over NHEJ, and to have a critical function in Alt-NHEJ activation [58, 81] (**Figure 1.10**).

PARP-2 and PARP-3, together with PARP-1, are also involved in DNA-repair and genomic maintenance. PARP-2, which exhibits 69% similarity with the PARP-1 catalytic domain, is its closest relative and displays overlapping functions. A double knockout of PARP-1 and PARP-2 is embryonically lethal in mice, while knockouts of either PARP-1 or PARP-2 bear only mild phenotypes.

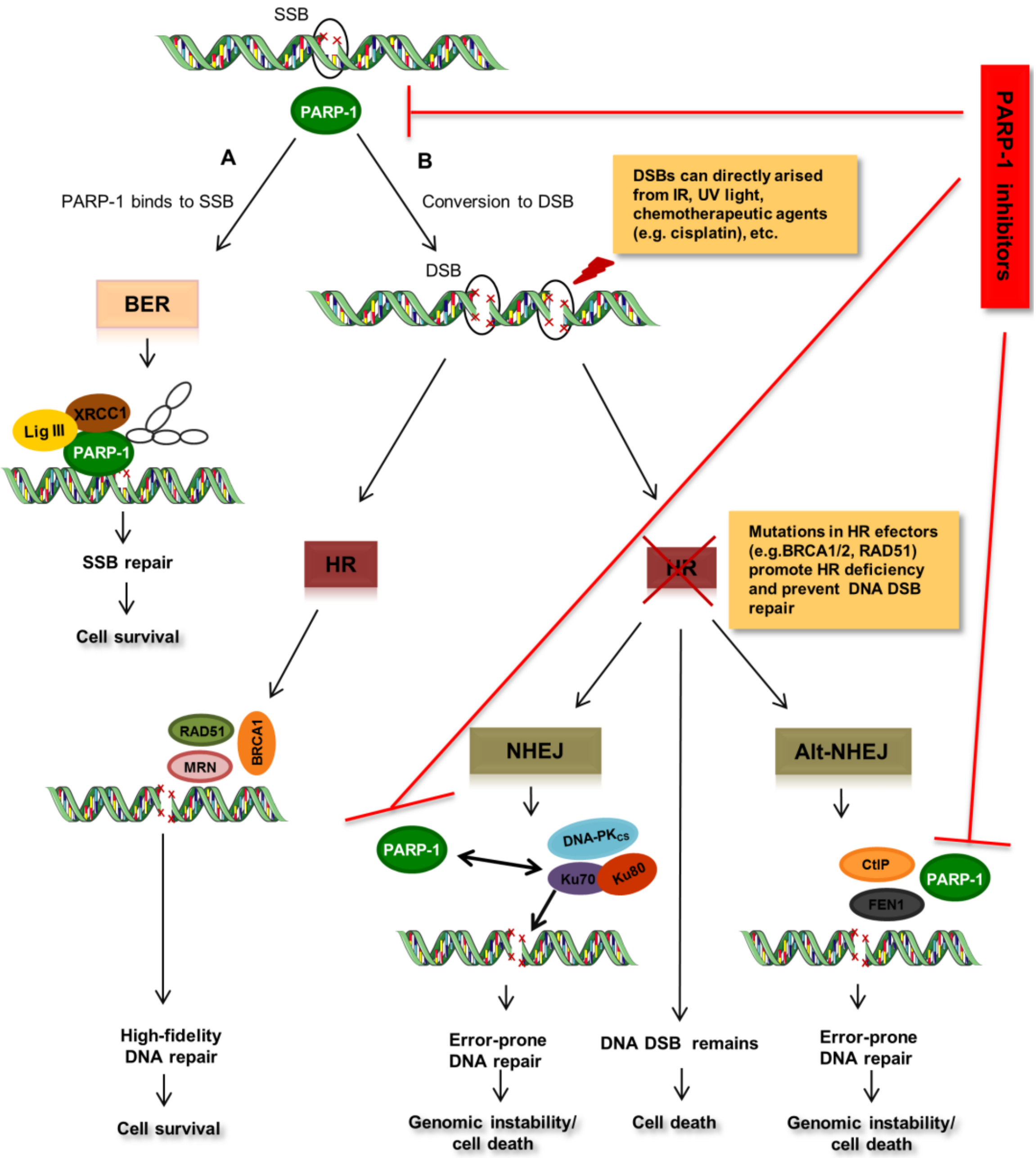
SSB
PARP-1
A
PARP-1 binds to SSB
B
Conversion to DSB
DSBs can directly arised from IR, UV light, chemotherapeutic agents (e.g. cisplatin), etc.
PARP-1 inhibitors
BER
DSB
XRCC1
Lig III
PARP-1
SSB repair
Cell survival
HR
HR
Mutations in HR efectors (e.g.BRCA1/2, RAD51) promote HR deficiency and prevent DNA DSB repair
RAD51
BRCA1
MRN
NHEJ
Alt-NHEJ
PARP-1
DNA-PKcs
Ku70
Ku80
CtIP
PARP-1
FEN1
High-fidelity DNA repair
Cell survival
Error-prone DNA repair
Genomic instability/ cell death
DNA DSB remains
Cell death
Error-prone DNA repair
Genomic instability/ cell death

Figure 1.10 Simplified schematic representation of PARP-1 activity in DNA repair pathways and the major effects of PARP-1 inhibitors. A) SSB repair by the BER pathway. **B)** DNA-repair mechanisms involved in DNA DSBs, in HR-proficient and HR-deficient cells, and the consequences of PARP-1 inhibition in DNA DSB repair. Only the main components of each pathway are displayed.

Nevertheless, different targets have been reported for PARP-1 and PARP-2, which might indicate that the two proteins carry out specific biological functions, namely in the DDR [95]. In contrast with PARP-1, genetic disruption of PARP-2 in mice affects several processes, such as adipogenesis [108], spermatogenesis [109], and thymocyte survival [110]. On the other hand, the involvement of PARP-3 in DNA-repair implies the recruitment of the aprataxin-like factor (APLF) at DSBs, which triggers the recruitment/retention of the XRCC4/Lig IV complex at DNA breaks, thus facilitating DSB repair [97]. Despite this, deletion of PARP-3 has shown that this protein is not essential for cell survival upon DNA damage [95].

Tankyrases 1 and 2 have also emerged as potential drug targets, as they play a key role in many biological processes, such as telomere homeostasis, glucose metabolism, Wnt/β-catenin signalling and cell progression. The two tankyrases display 82% of homology between them and are unique members among the ARTD family, as they contain a sterile alpha motif (SAM) that is responsible for tankyrase multimerization, as well as an ankyrin (ANK) domain, which is formed by several ankyrin repeats and acts as a protein interaction module [111].

1.2.2. PARP-1 inhibitors under clinical evaluation

At least 15 molecules have entered clinical trials as PARP-1 inhibitors (**Figure 1.11**). Among them, four were discontinued (iniparib **1.12**, the prodrug CEP-9722 **1.13** [112, 113], INO-1001 **1.14** [114, 115], and AZD-2461 **1.15**), two completed the earliest phase studies without additional information (E7016 **1.6** and E7449 **1.7** [116]) and nine are currently progressing in different phases of clinical trials (olaparib **1.1** (Lynparza^{TM}), rucaparib **1.2**, niraparib **1.3** [117], veliparib **1.4** [118], talazoparib **1.5** (also known as BMN-673) [119], fuzuopali **1.8**, BGB-290 **1.9**, ABT-767 **1.10** and fluzoparib **1.11**). All of these inhibitors contain a benzamide pharmacophore that mimics the natural PARP-1 substrate NAD$^+$, thus suggesting their activity as competitive inhibitors. Moreover, they display a high, but not selective, PARP-1 inhibitory activity. These molecules are PARP-2 inhibitors as well, and, in some cases, are able to inhibit Tankyrases 1 and 2 [116]. It is important to mention that iniparib **1.12** is not a true PARP inhibitor, and its poor therapeutic effectiveness against PARP-1 explains the discontinuation of its clinical evaluation during phase III clinical trial testing. Compounds **1.13**, **1.14** and

1.15 were also discontinued, due to the poor pharmacokinetic profile or safety/efficacy issues [113].

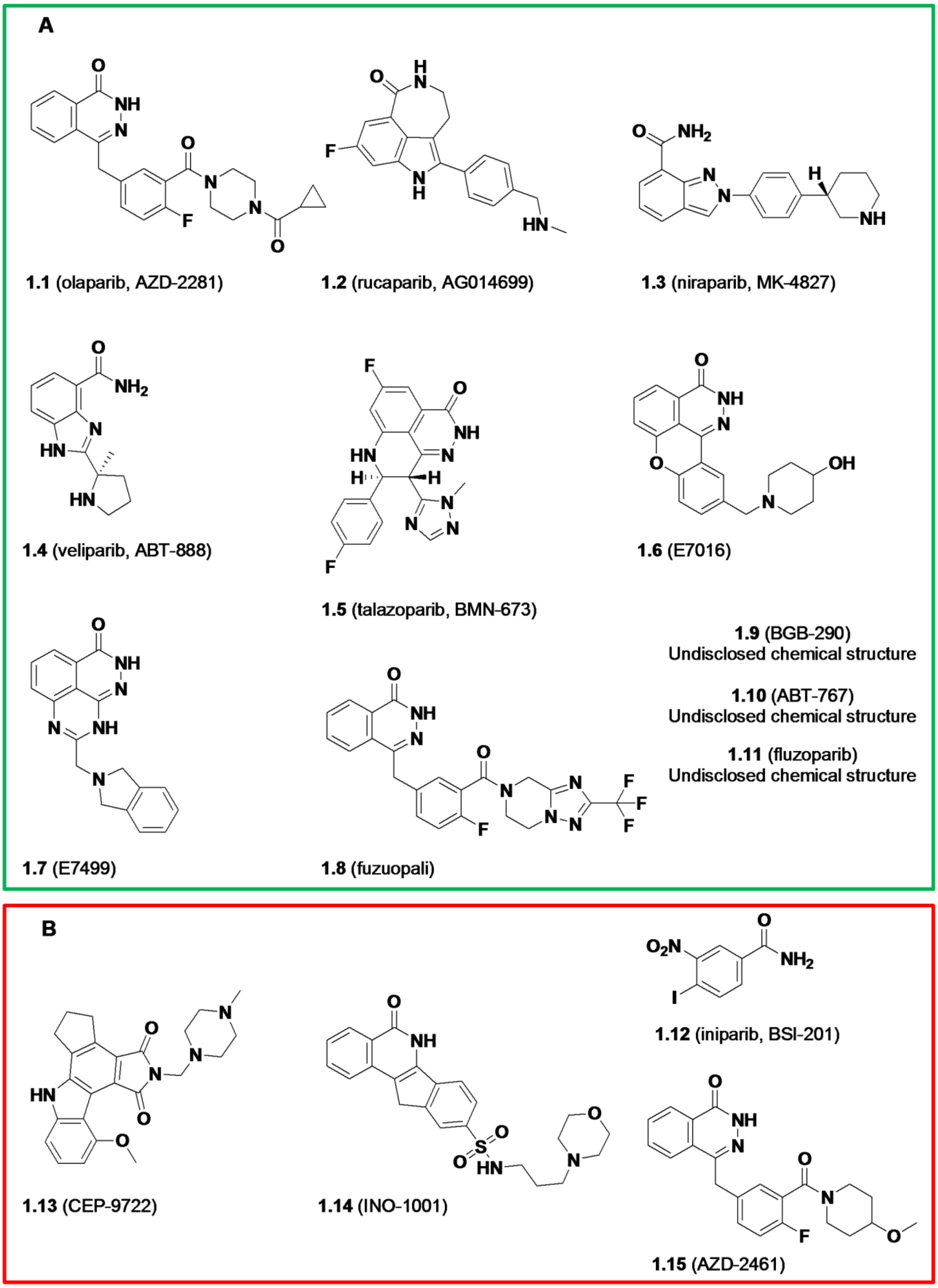

1.1 (olaparib, AZD-2281)

1.2 (rucaparib, AG014699)

1.3 (niraparib, MK-4827)

1.4 (veliparib, ABT-888)

1.5 (talazoparib, BMN-673)

1.6 (E7016)

1.7 (E7499)

1.8 (fuzuopali)

1.9 (BGB-290)
Undisclosed chemical structure

1.10 (ABT-767)
Undisclosed chemical structure

1.11 (fluzoparib)
Undisclosed chemical structure

1.12 (iniparib, BSI-201)

1.13 (CEP-9722)

1.14 (INO-1001)

1.15 (AZD-2461)

Figure 1.11 PARP-1 inhibitors that have entered clinical trials. A) Inhibitors that are currently in clinical evaluation. **B)** Inhibitors that were discontinued.

Among the inhibitors that are presently undergoing active clinical trials, four compounds are in the earliest phase studies (**1.8**–**1.11**; **Table 1.1**). The remaining five molecules (**1.1**–**1.5**) have reached the late-stage of clinical development. In the majority of the current clinical trials, the compounds are being tested as stand-alone therapies against different types of cancer with *BRCA1/2* mutations, such as breast, ovarian or pancreatic cancers. The combination of PARP inhibitor candidates with common anti-cancer agents is also being investigated against solid tumours, such as glioblastoma and non-small cell lung cancer (NSCLC) (**Table 1.1**). Among the molecules in the later clinical evaluation phases, olaparib **1.1**, rucaparib **1.2** and niraparib **1.3** are particularly interesting, as they are the only PARP inhibitors that have been approved to date, for some particular clinical uses.

Olaparib **1.1** is the first-in-class PARP inhibitor and was approved in 2014. The European Medicines Agency (EMA) has granted it market approval as a maintenance monotherapy for patients carrying platinum-sensitive *BRCA*-mutant (germline and somatic) ovarian cancer. Despite the fact that Food and Drug Administration (FDA) did not approved it simultaneously, this agency granted approval to olaparib **1.1** a few months later, for the treatment of advanced ovarian cancer in women with germline *BRCA1/2* mutation who had been treated previously with at least three chemotherapeutic lines [120].

Olaparib **1.1** is the PARP-1 inhibitor that has been evaluated most extensively. Since 2013, more than 60 clinical trials have initiated to evaluate this molecule as a stand-alone agent or as a combination therapy, with some encouraging results. Eight phase II monotherapy studies have been reported for breast, ovarian, pancreatic and prostate cancer or for Ewing sarcoma, with different levels of therapeutic responses. The best responses were observed in the treatment of *BRCA*-mutated ovarian cancer [121-128]. Current phase III studies are under way to evaluate the use of olaparib **1.1** not only as a maintenance therapy after platinum-based chemotherapy for women with newly diagnosed or recurrent ovarian cancer, but also as a single agent for the treatment of recurrent ovarian cancer with *BRCA* mutations [129].

Table 1.1 Clinical trials that are currently under way for PARP-1 inhibitors. Only the clinical trials in the highest clinical phases for each drug are presented. The data were obtained from www.clinicaltrials.gov, accessed 7/11/2017, with exception of compound **1.8**.

Drug	Company	Highest clinical phases	Study identifiers	Cancer type	*BRCA1/2* testing	Combination
1.1*	AstraZeneca	III	NCT01844986	Ovarian	Yes	No
		III	NCT01874353	Ovarian	Yes	No
		III	NCT01924533	Gastric	No	+ paclitaxel
		III	NCT02000622	Breast	Yes	No
		III	NCT02032823	Breast	Yes	No
		III	NCT02184195	Pancreatic	Yes	No
		III	NCT02282020	Ovarian	Yes	No
		III	NCT02446600	Ovarian	Yes	+ cediranib
1.2	Clovis Oncology	III	NCT01968213	Ovarian	Yes	No
		III	NCT02855944	Ovarian	Yes	No
		III	NCT02975934	Prostate	Yes	No
1.3	Tesaro	III	NCT01905592	Breast	Yes	No
		III	NCT02655016	Ovarian	Yes	No
1.4	AbbVie	III	NCT02032277	TNBC	No	+ carboplatin
		III	NCT02106546	NSCLC	No	+ carboplatin + paclitaxel
		III	NCT02152982	Glio-blastoma	No	+ TMZ
		III	NCT02163694	Breast cancer	Yes	+ carboplatin + paclitaxel
		III	NCT02264990	NSCLC	No	+ carboplatin + paclitaxel
		III	NCT02470585	Ovarian Cancer	No	+ carboplatin + paclitaxel
1.5	BioMarin Pharmaceutical	III	NCT01945775	Breast cancer	Yes	No
1.8	Jiangsu Hengrui Medicine Co.	I	CTR20131369	Advanced solid tumours	No	No
1.9	BeiGene	I/II	NCT03150862	Glio-blastoma	No	+ TMZ and/or Radiation therapy
1.10	AbbVie	I	NCT01339650	Solid tumours	Yes	No
1.11	Jiangsu Hengrui Medicine Co.	I	NCT02575651	Advanced solid tumours	No	No

* Seventeen clinical studies are undergoing for olaparib **1.1**. Only the first eight to enter phase III clinical trials are represented.

A phase III clinical trial was also initiated to test olaparib **1.1** against metastatic pancreatic cancer in individuals with germline *BRCA1/2* mutation who had not progressed after the first-line platinum-based chemotherapy (**Table 1.1**). Moreover, promising results obtained in patients with metastatic castration-resistant prostate cancer who carry *BRCA* or *ATM* mutations led to the classification of olaparib **1.1** by the FDA as breakthrough therapy designation (BTD) for prostate cancer.

Furthermore, olaparib **1.1** has been displaying promising results in combination therapy. The combination of olaparib **1.1** with placitaxel has led to a high objective response rate (ORR) in patients with gastric cancer who have low expression of ATM [130]. A phase III study, named NCT01924533, is under way for further investigation (**Table 1.1**). Additional clinical benefits in patients with ovarian cancer were observed by the combination of olaparib **1.1** with the vascular endothelial growth factor receptor (VEGFR) inhibitor cediranib in both phase I and II studies, and by its combination with the pan-phosphatidylinositol 3-kinase (PI3K) inhibitor 5-(2,6-dimorpholinopyrimidin-4-yl)-4-(trifluoromethyl)pyridin-2-amine (BKM120) or even the epidermal growth factor receptor (EGFR) inhibitor gefitinib in advanced NSCLC with positive *EGFR* mutation [131-133].

Despite the absence of inter-ethnic differences in its tolerability, safety and pharmacokinetic/pharmacodynamics (PK/PD) profiles, olaparib **1.1** was associated with myelosuppression and gastrointestinal issues as its primary toxicity, particularly in combination with other chemotherapeutic drugs [134-136]. In fact, complete clinical trials that evaluated olaparib **1.1** in combination with cisplatin, carboplatin and the topoisomerase II inhibitor pegylated liposomal doxorubicin (PLD) demonstrated that olaparib **1.1** potentiates the toxicity associated with those drugs, despite the fact that it increases their therapeutic response [137-139]. Moreover, the combination of olaparib **1.1** with dacarbazine, topotecan or even cisplatin plus gentamicine could not be tolerated because of an increment in the toxicity [140, 141].

The other recently approved PARP inhibitor, rucaparib **1.2** was the first to enter clinical trials in 2003; it was used in combination with TMZ to treat advanced solid tumours [142]. A chemo-potentiation benefit was afforded by the combination of rucaparib **1.2** with TMZ or 5-fluorouracil (5-FU) in patients with metastatic melanoma and acute leukaemia, respectively [143, 144]. With a demonstrated anti-ovarian cancer activity *in vitro* and *in vivo* [145], rucaparib **1.2** was recently approved by the FDA for the treatment of patients with advanced ovarian cancer with *BRCA1/2* mutation who were previously treated with two or more chemotherapeutic protocols [146]. Moreover, a phase III study is under way to test the use of rucaparib **1.2** in patients with metastatic castration-resistant prostate cancer and homologous recombination gene deficiency (TRITON3–NCT02975934; **Table 1.1**)

Niraparib **1.3** was the latest PARP-1/2 inhibitor approved by the FDA as a maintenance treatment for adult patients with recurrent epithelial ovarian, fallopian tube or primary peritoneal cancer who exhibit partial or complete response to platinum-based chemotherapy [147]. Its clinical use in Europe, for the same indication, was recently granted by EMA [148].

It is worth mentioning that all five PARP-1 candidates that are in late-stage clinical trials induced toxicity, even in monotherapy. Even though they are relatively well-tolerated, these molecules yielded different side effects. The most severe side effects include nausea, fatigue and neutropenia, among other hematologic toxicities. Among these five molecules, olaparib **1.1** shows a higher clinical toxicity, although other PARP-1 inhibitors, such as rucaparib **1.2** and niraparib **1.3**, also display severe side effects, including increased liver enzyme levels and thrombocytopenia, respectively [81].

1.2.3. Structural types of PARP-1 inhibitors

Nicotinamide **1.16** (**Figure 1.12**), which is the by-product of NAD^+ cleavage, has been used as the structural basis for the discovery of PARP-1 inhibitors. Most of the PARP-1 inhibitors described in the literature are nicotinamide/benzamide derivatives and bind at the nicotinamide-binding pocket in the donor site of the PARP-1 catalytic domain, thus competing with NAD^+ (**Figure 1.13**).

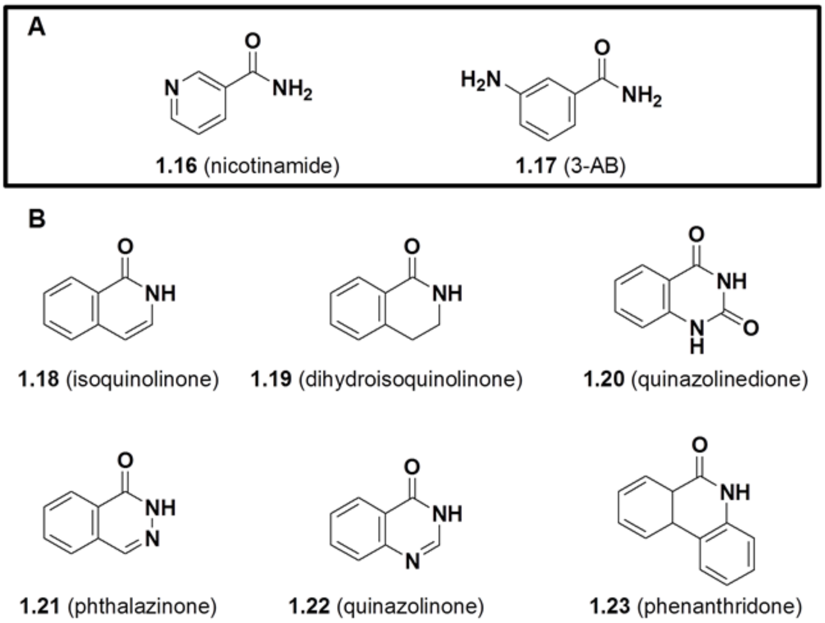
A
N
O
NH₂
H₂N
O
NH₂
B
O
NH
O
NH
O
NH
N
H
O
O
NH
N
O
NH
N
O
NH

1.16 (nicotinamide)
1.17 (3-AB)
1.18 (isoquinolinone)
1.19 (dihydroisoquinolinone)
1.20 (quinazolinedione)
1.21 (phthalazinone)
1.22 (quinazolinone)
1.23 (phenanthridone)

Figure 1.12 First A) and second B) generations of PARP-1 inhibitors.

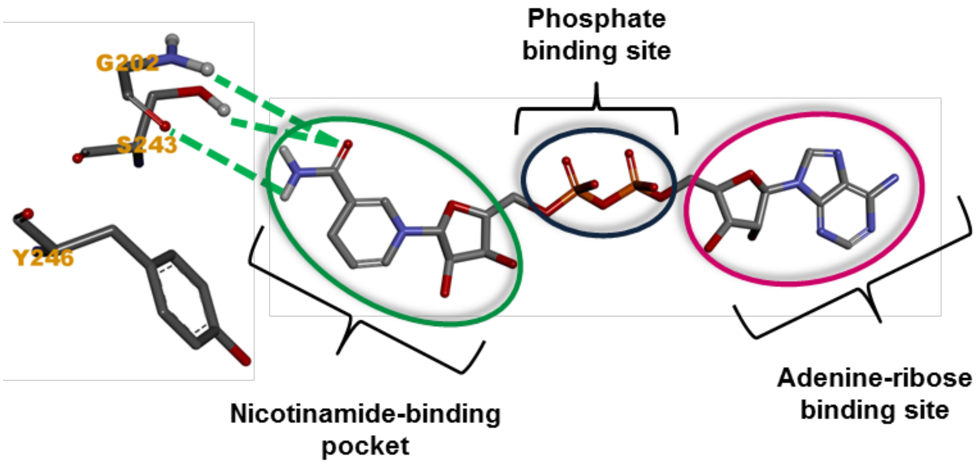
Phosphate binding site
G202
S243
Y246
Nicotinamide-binding pocket
Adenine-ribose binding site

Figure 1.13 The binding mode of NAD^+ at the donor site of PARP-1 catalytic domain.

This mode of binding suggests that these inhibitors establish classical hydrogen bonds with Ser243 and Gly202, as well as π–π interactions with Tyr246, also established by nicotinamide at the binding site. Nicotinamide **1.16** itself and 3-aminobenzamide (3-AB) **1.17** were the earliest PARP-1 inhibitors identified in the 1980s, with an activity falling into the micromolar range (**Figure 1.12**) [107, 149]. However, the low inhibitory potency and the lack of specificity of those compounds prevented their further development [150]. To improve the potency of the first generation of PARP-1 inhibitors, mainly 3-substituted benzamides, different structure-activity relationships (SARs) and drug design studies were pursued.

1.2.3.1. Bicyclic lactam-containing PARP-1 inhibitors

Based on a screening of more than 100 compounds, Banasik and co-workers identified a second generation of PARP-1 inhibitors formed by bicyclic and tricyclic lactams [151]. The restricted rotation of the amide within the heterocyclic system maintains the carbamoyl group in the *anti* (*cis*) favourable configuration, which facilitates hydrogen bonding with Ser243 and Gly202. Moreover, the aryl system also contributes to the interaction between the carboxamide and the nicotinamide-binding residues, via an increment in the electron-donor capacity of the carbamoyl group [152]. Isoquinolinone **1.18** [153], dihydroisoquinolinone **1.19** [154], quinazolinedione **1.20**, phthalazinone **1.21**, quinazolinone **1.22** and phenanthridone **1.23** are examples of bicyclic (**1.18**–**1.22**) and tricyclic (**1.23**) lactams derivatives that showed promising PARP-1 inhibitory activity (**Figure 1.12**) [151]. However, due to the micromolar range of the PARP-1 inhibition activity of these compounds, further studies using these scaffolds were developed to discover new promising molecules, including some that are currently in clinical trials (**Table 1.1**). For instance, the structural modification of early phthalazinone **1.21** derivatives led to the discovery of the recently approved PARP inhibitor olaparib **1.1** (**Figure 1.11**) [107, 150]. Moreover, in an attempt to overcome the failed responses to long-term treatment with this inhibitor, AstraZeneca developed AZD2461, which is structurally similar to olaparib **1.1** but a poor substrate of the P-glycoprotein (P-gp) efflux pump, one of the mechanisms that is associated with resistance to PARP inhibitors [106, 155, 156]. However, despite its entry in phase I clinical trials, the development of AZD2461 was stopped because of safety/efficacy issues [157]. Additional structural modifications of the phthalazinone **1.21** scaffold were performed to enhance the aqueous solubility and low bioavailability associated with these compounds, including olaparib **1.1**.

In 2010, Pescatore and co-workers reported a new PARP inhibitor class, containing a pyrrolo[1,2-a]pyrazine-1(2H)-one core. Among the compounds designed, **1.24** and **1.25** (**Figure 1.14**) showed high potency against PARP-1, as well as a significant cytotoxicity against *BRCA1*-deficient cells. Nevertheless, further studies were disrupted due to high plasma clearance [158]. The substitution of the pyrrole moiety with a dimethylpyridazin-3(2H)-one core led to the discovery of compound **1.26** (**Figure 1.14**), which has interesting PARP-1 inhibitory and cytotoxic activities, but also high clearance and metabolic instability, thus preventing further development [159]. In another attempt to improve the solubility profile of the phthalazinone **1.21** scaffold derivatives, Zhu and co-workers developed tetrahydropyridopyridazinone analogues. The replacement of the phenyl moiety in the phthalazinone **1.21** scaffold with a piperidine ring may promote the establishment of an additional water-mediated hydrogen bond between the amine moiety of piperidine and Glu327 at the nicotinamide-binding pocket of the PARP-1 catalytic domain, which would enhance the water solubility of these new compounds. A novel compound, **1.27**, displaying high PARP-1 inhibitory potency and high cytotoxicity against *BRCA1*-deficient cells was obtained (**Figure 1.14**) [160].

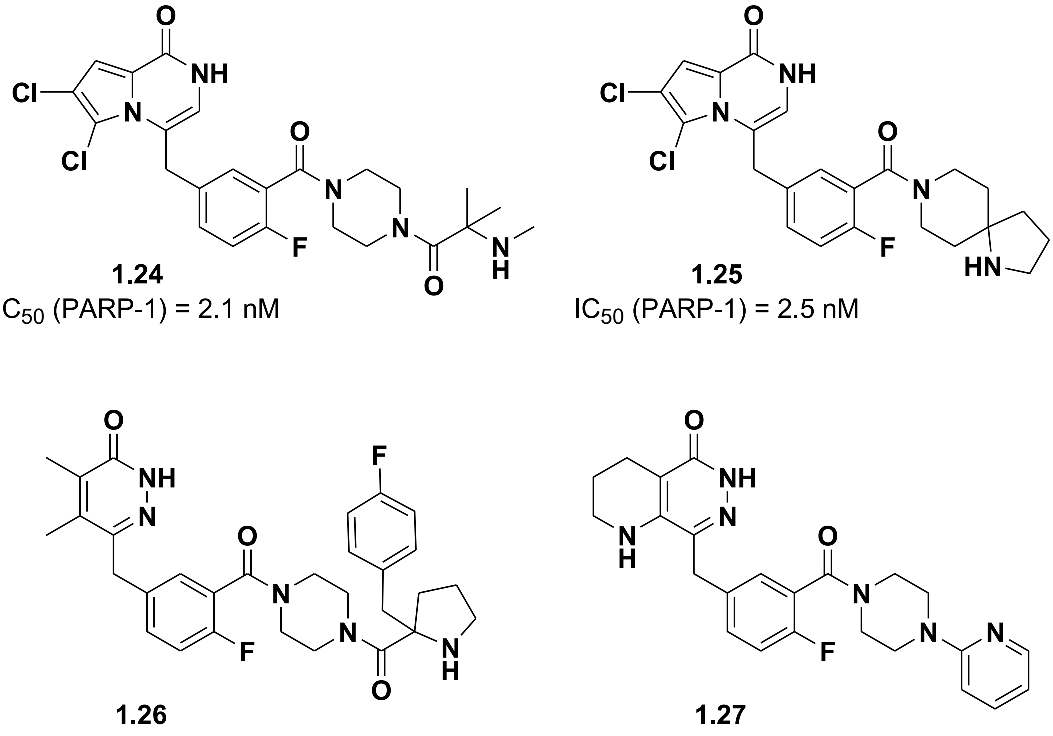

1.24
IC_{50} (PARP-1) = 2.1 nM

1.25
IC_{50} (PARP-1) = 2.5 nM

1.26
IC_{50} (PARP-1) = 3.6 nM

1.27
K_i (PARP-1) = 0.9 nM

Figure 1.14 PARP-1 inhibitors obtained by modification of the pyrrolo[1,2-a] pyrazine-1(2H)-one (1.24 and 1.25), dimethylpyridazin-3-one (1.26) or phthalazinone (1.27) scaffolds.

Polycyclic compounds bearing a lactam moiety were designed as PARP-1 inhibitors. E7016 **1.6** and E7449 **1.7** (**Figure 1.11**), which were both developed by Eisai, are two examples of tetracyclic and tricyclic PARP-1 inhibitors, respectively, which entered clinical trials as drug candidates. Rucaparib **1.2** (**Figure 1.11**), initially developed by Cancer Research Technology/Pfizer (subsequently transferred to Clovis Oncology), is another example of a potent tricyclic lactam-containing PARP-1 inhibitor.

Moreover, BioMarin Pharma developed a new class of tricyclic PARP-1 inhibitors based on the combination of the benzimidazole and phthalazinone **1.21** cores, which led to the discovery of the most potent PARP-1 inhibitor under clinical investigation, talazoparib **1.5** (IC_{50} = 0.57 nM (**Figure 1.11**)). The fused tricyclic core generated is able to establish the same key interactions as the phthalazinone core in olaparib **1.1**. In addition, new hydrogen bonds and π–π stackings with binding site residues, shown by X-ray co-crystallisation of talazoparib **1.5** with the PARP-1 catalytic domain, contribute to its potency. In this case, the stereochemistry also plays a key role, as talazoparib **1.5** is 240- and 340-fold more potent than its enantiomer, BMN-674, in PARP-1 enzymatic and cellular assays [119, 161]. A good oral bioavailability, improved by the presence of the triazole moiety, associated with optimal plasma clearance and a long half-life render talazoparib **1.5** an excellent PARP-1 inhibitor candidate. It is currently in phase III clinical trials as a stand-alone agent or in combination therapy with other anti-cancer agents.

The dihydroquinolinone core, which is a reported PARP-1 inhibitor scaffold, was also used in different drug design approaches for the development of new promising inhibitors. Compounds **1.28**, **1.29**, **1.30** and **1.31** (**Figure 1.15**) are examples of molecules that were obtained from structural modifications of this core. However, despite their promising PARP-1 inhibitory activity, those compounds were not further evaluated due to poor pharmacokinetics (**1.28**), safety issues (**1.29**) or even low cellular potency in *BRCA* mutant cells (**1.30**, **1.31**) [162-164].

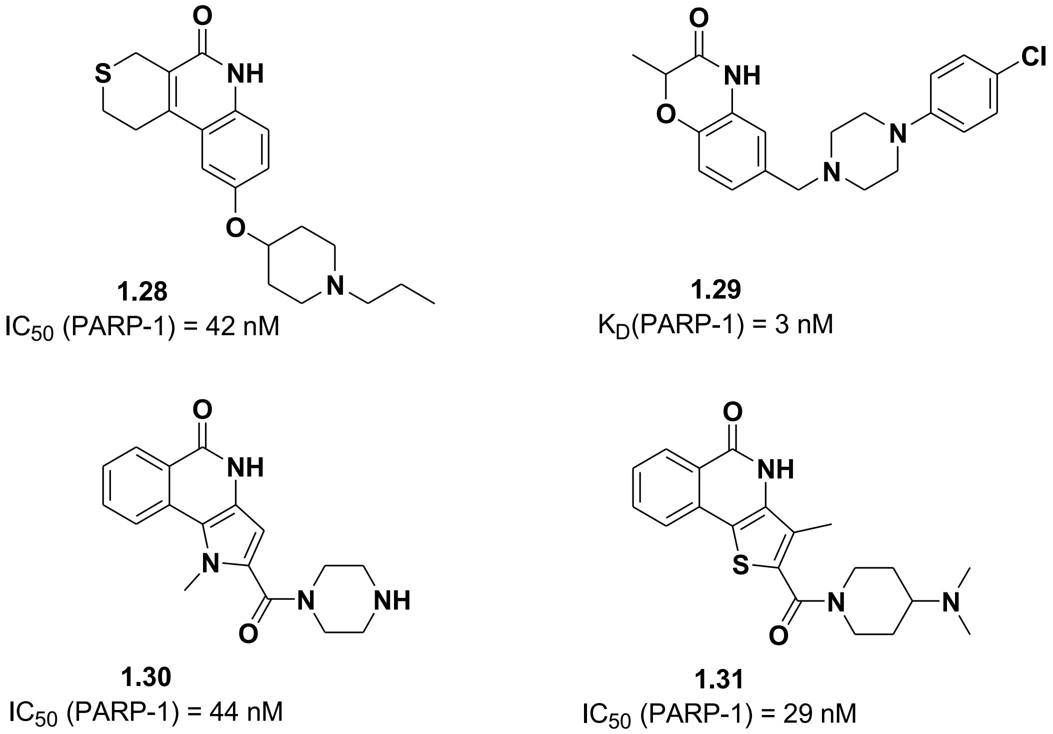

1.28
IC$_{50}$ (PARP-1) = 42 nM

1.29
K$_D$(PARP-1) = 3 nM

1.30
IC$_{50}$ (PARP-1) = 44 nM

1.31
IC$_{50}$ (PARP-1) = 29 nM

Figure 1.15 PARP-1 inhibitors derived from dihydroquinolinone core.

Another approach was used in 2013 by Zhang and co-workers to synthesize new and potent PARP-1 inhibitors. Using apomorphine, which is a dopamine agonist, as the starting point, those authors developed a series of benzo[de][1,7]naphthyridin-7(8H)-ones, among which the two most promising PARP-1 inhibitors are compound **1.32** and its derivative **1.33** (**Figure 1.16**), both bearing the phthalazin-1(2H)-one core structure of olaparib **1.1** [165].

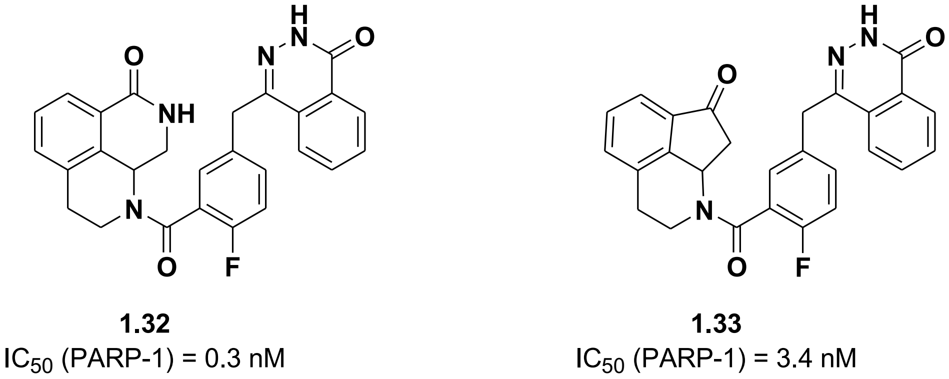

1.32
IC$_{50}$ (PARP-1) = 0.3 nM

1.33
IC$_{50}$ (PARP-1) = 3.4 nM

Figure 1.16 PARP-1 inhibitors containing a benzo[de][1,7]naphthyridin-7(8H)-one core.

It is worth mentioning that structural modification of known PARP-1 scaffolds, such as quinazolinones **1.22** and quinazolinedione **1.20** cores, recently provided the discovery of new promising PARP-1 inhibitors, such as compounds **1.34** and **1.35** (**Figure 1.17**). Both molecules showed a high PARP-1 enzymatic activity [166, 167].

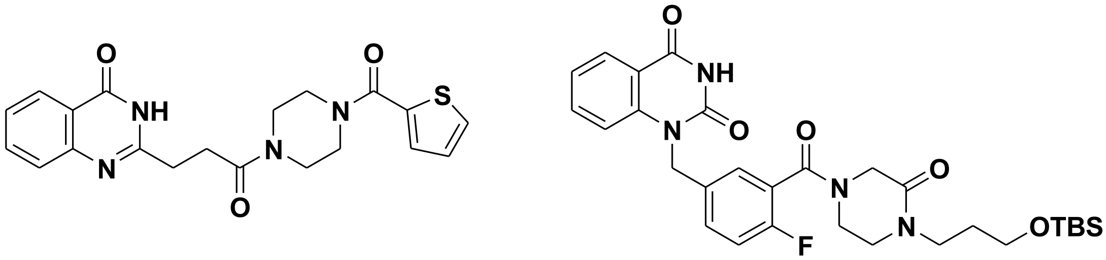

1.34
IC_{50} (PARP-1) = 9.8 nM

1.35
IC_{50} (PARP-1) = 1.3 nM

Figure 1.17 PARP-1 inhibitors obtained by modification of quinazolinone (1.34) and quinazolinedione (1.35) scaffolds.

1.2.3.2. Pseudo-bicyclic lactam-containing PARP-1 inhibitors

In the 1990s, the research group of Roger Griffin and Bernard Golding at University of Newcastle reported two new PARP-1 inhibitor scaffolds, the imidazole and benzoxazole carboxamides [168]. The imidazole/benzoxazole nitrogen is able to establish an intramolecular hydrogen bond with the amide moiety, which acts as a hydrogen bond donor. Thus, a pseudo-ring is formed, maintaining the amide in the most favourable configuration for PARP-1 binding, as happens with bicyclic and tricyclic lactams [107]. Due to the high PARP-1 inhibitory potency exhibited by these cores, especially by benzimidazole carboxamides (Ki = 95 nM), several drug design approaches were developed to identify novel and potent PARP-1 inhibitors, leading to the discovery of two potent candidates, niraparib **1.3** and veliparib **1.4** (**Figure 1.11**), one of which (niraparib **1.3)** recently approved as PARP inhibitor.

Based on these molecules, novel series of derivatives were identified. Zhu and co-workers reported a series of imidazo[4,5-c]pyridine carboxamide derivatives acting as PARP-1 inhibitors, namely the compound **1.36** (**Figure 1.18**). It displayed not only an interesting PARP-1 inhibitory activity (IC_{50} = 528 nM), but also a potentiation of TMZ cytotoxicity against several cancer cell lines. Moreover, an improved anti-cancer efficacy was observed by combining **1.36** with cisplatin, similar to the combination of veliparib **1.4** with cisplatin, in mouse [169].

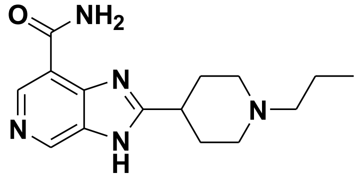

1.36
IC_{50} (PARP-1) = 528 nM

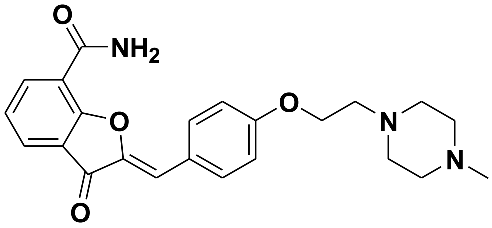

1.37
IC_{50} (PARP-1) = 114 nM

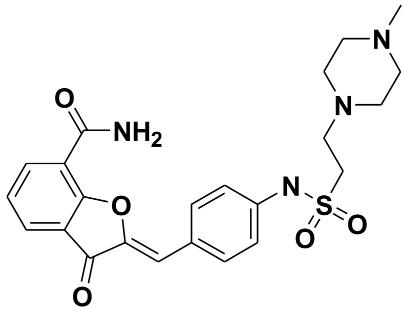

1.38
IC_{50} (PARP-1) = 79 nM

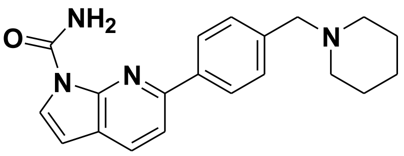

1.39
IC_{50} (PARP-1) = 70 nM

Figure 1.18 PARP-1 inhibitors bearing pseudo-bicyclic lactams.

Patel and co-workers recently reported dihydrobenzofuran carboxamides as PARP-1 inhibitors. Two molecules with promising inhibitory activity were identified: **1.37** and **1.38** (**Figure 1.18**). However, only a moderate activity against *BRCA2*-deficient DT40 cells was shown for compound **1.37** [170]. It is worth noting that, in 2014, Cincinelli and co-workers described a new class of pseudo-bicyclic lactam PARP-1 inhibitors, 7-azaindole-1-carbaxamides. The most potent compound, **1.39** (**Figure 1.18**), showed an IC_{50} value of 70 nM against PARP-1, as well as a lower recognition by P-gp compared with olaparib **1.1** in P-gp overexpressing cells [171].

1.2.3.3. PARP-1 inhibitors not containing an amide moiety

In 2013, Yu-Ru and co-workers reported a series of anthraquinone derivatives among which the most active compound, NSC747854 **1.40** (**Figure 1.19**), a non-amide molecule derivative, displayed an interesting PARP-1 inhibitory activity [172]. Moreover, Song and co-workers used a virtual screening strategy to identify a set of commercially available natural compounds that act as PARP-1 inhibitors. Among those compounds, puerarin **1.41**, chlorogenic acid **1.42**, biochanin A **1.43** and phloretin **1.44**, represented in **Figure 1.19**, appeared to be the most promising molecules, with IC_{50} values of 6, 25, 86 and 470 nM, respectively. Interestingly, none of these compounds contain the amide moiety in their structure [173].

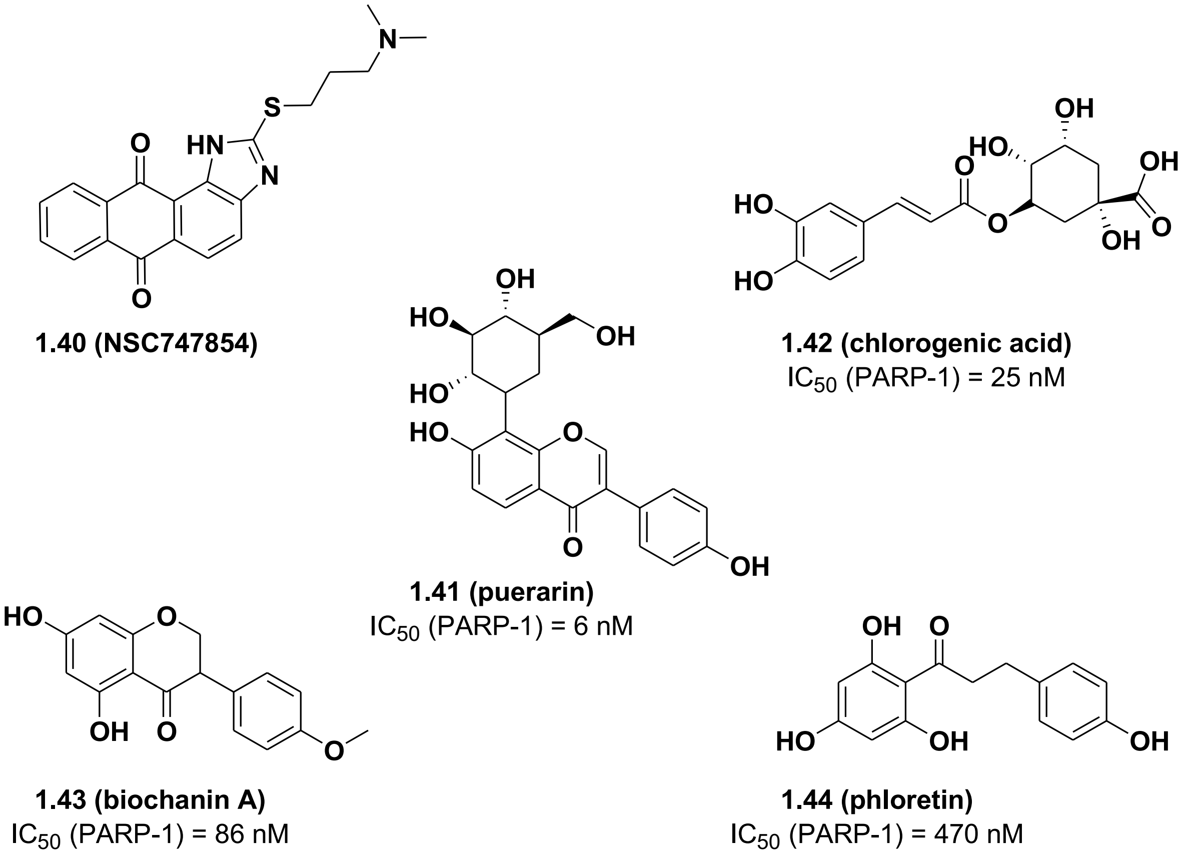

1.40 (NSC747854)

1.42 (chlorogenic acid)
IC_{50} (PARP-1) = 25 nM

1.41 (puerarin)
IC_{50} (PARP-1) = 6 nM

1.43 (biochanin A)
IC_{50} (PARP-1) = 86 nM

1.44 (phloretin)
IC_{50} (PARP-1) = 470 nM

Figure 1.19 PARP-1 inhibitors not bearing an amide group.

1.2.3.4. Selective PARP-1 inhibitors

Despite decades of research on this subject, most of the PARP-1 inhibitors developed to date display poor or no selectivity over PARP-2, including those currently in clinical trials or even recently approved. The most notorious example is olaparib **1.1**, a PARP-1/2 inhibitor with an IC_{50} of 5 nM/1 nM. Moreover, some of those molecules are able to inhibit other members of the PARP family, like Tankyrases 1 and 2.

In an attempt to discover selective PARP-1 inhibitors, Hattori and co-workers reported, in 2006, a series of quinazolinone **1.22** analogues that displayed a modest PARP-1 selectivity over PARP-2. The representative compound, **1.45** (**Figure 1.20**), displayed an IC_{50} value of 13 nM for PARP-1, which represents a more than 38-fold PARP-1/PARP-2 selectivity [174]. Moreover, isoquinolindione derivatives showed a preferential PARP-1 inhibition over PARP-2. The illustrative compound **1.46** (**Figure 1.20**), for instance, exhibited an IC_{50} value of 45 nM and 4000 nM for PARP-1 and PARP-2, respectively [175].

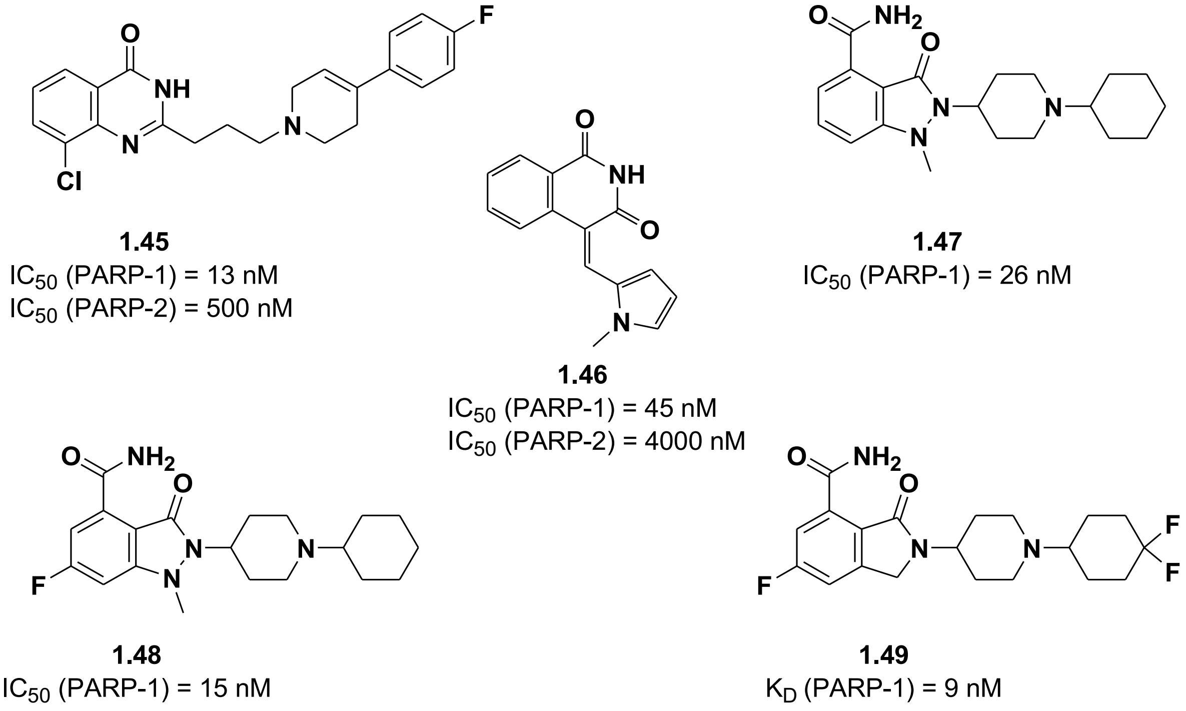

1.45
IC_{50} (PARP-1) = 13 nM
IC_{50} (PARP-2) = 500 nM

1.46
IC_{50} (PARP-1) = 45 nM
IC_{50} (PARP-2) = 4000 nM

1.47
IC_{50} (PARP-1) = 26 nM

1.48
IC_{50} (PARP-1) = 15 nM

1.49
K_D (PARP-1) = 9 nM
K_D (PARP-2) = 1300 nM

Figure 1.20 Selective PARP-1 inhibitors.

On the other hand, Papeo and co-workers reported 3-oxo-2,3-dihydro-1H-indazole-4-carboxamide derivatives as selective PARP-1 inhibitors. Among the promising molecules, compounds **1.47** and **1.48** (**Figure 1.20**) display a high PARP-1 enzymatic inhibition, as well as good selectivity (2/3-fold over their PARP-2 or PARP-3 inhibitory activity) and pharmacokinetic profile [176]. Furthermore, the same research group identified a set of molecules derived from the structural optimization of isoindole-4-carboxamides that display an important selectivity for PARP-1. Among these, compound **1.49** (**Figure 1.20**), with a K_D value of 9 nM/1300 nM for PARP-1/PARP-2, displays a remarkable PARP-1 selectivity over PARP-2. Additionally, it exhibits a good performance either as a stand-alone agent or in combination with TMZ in *BRCA1/2*-deficient cells. The analysis of the active site–ligand interactions of this compound co-crystallised with the PARP-1 and PARP-2 catalytic domains showed that compound **1.49** established similar interactions at the nicotinamide-binding pocket of both proteins. The PARP-1 selectivity observed may be attributed to the better accommodation of the 4,4-difluorocyclohexyl group into the adenine-ribose binding site, because of the formation of a larger pocket in PARP-1 over PARP-2. This may be induced by slight differences in the α-helix orientation of the two proteins [177].

1.2.4. Mechanisms of the PARP-1 inhibitors

1.2.4.1. PARP trapping

The first mechanism proposed for the PARP-1/2 inhibitors activity is the inhibition of the enzymatic activity of PARP-1/2, which compromises the SSB repair, leading to the conversion of these into DSBs after duplication of DNA strands. This may potentiate some anti-cancer agents that act by damaging DNA, or even, in the case of HRR-deficient cancers, triggers cell death based on an inability to repair the DSBs generated [150, 178]. Nevertheless, differences in the cytotoxic activities of several PARP-1/2 inhibitors that display a similar potency in inhibiting the PARP-1/2 catalytic domain have been reported, which suggests the existence of an additional mechanism underlying these discrepancies. Olaparib **1.1** and niraparib **1.3**, for instance, show a higher cytotoxicity than veliparib **1.4**, despite the great PARP-1/2 catalytic activity displayed by all of them [179, 180]. Moreover, PARP-1/2 inhibitor cytotoxicity seems to be greater in cancer cells with a wild-type *PARP* gene, compared with *PARP-1/2* knockout cells, which cannot be explained by PARP-1/2 catalytic inhibition [181]. It has been suggested that the binding of PARP-1/2 inhibitors to the nicotinamide-binding pocket induces an allosteric conformational change in PARP-1/2 that stabilizes its interaction with DNA, thus trapping PARP-1 in the damaged DNA. The persistent DNA–PARP-1 complexes, which generally exist as noncovalent complexes in intact cells, act as a physical barrier to the DNA-repair machinery, which can ultimately lead to cell death. This is particularly true during the S phase, in which DNA trapping promotes the generation of DSBs, which are lethal in HRR-deficient cells. Furthermore, the differences between PARP-1/2 catalytic inhibitory and trapping activities appear to be related with differences in synergism, after combining PARP-1/2 inhibitors with anti-cancer agents, such as TMZ. However, the high correlation between PARP-1 inhibitors cytotoxicity and HRR deficiency may not be completely explained by DNA–PARP-1 trapping [179, 180]. Additionally, PARP-1 inhibitors with different trapping abilities are able to induce comparable efficacy at the maximum tolerated dose (MTD) *in vitro* [182]. On the other hand, the amount of SSBs did not appear to increase in *BRCA2*-deficient cells treated with PARP-1 inhibitors. Taken together, these finds suggest that further investigation of DNA–PARP trapping mechanism is necessary to understand fully its real role in the cytotoxicity induced by PARP-1 inhibitors, in addition to the other PARP-1 mechanisms suggested [150].

1.2.4.2. Synthetic lethality

Synthetic lethality occurs when the combination of mutations in two or more genes becomes lethal to the cell or organism, whereas the mutation of each gene alone is not [183]. It has been reported as the mechanism via which PARP-1 inhibitors act as single agents and is mainly associated with HRR deficiency. Three different models have been proposed to explain how the anti-cancer PARP-1 inhibitory activity depends on synthetic lethality, namely the inhibition of BER, NHEJ activation and Alt-NHEJ inactivation.

BER inhibition

As mentioned above, PARP-1 plays a key role in BER, which is one of the main mechanisms involved in SSB repair. Thus, PARP-1 inhibitors will promote the accumulation of unrepaired SSBs, and consequently of DSBs, after DNA strand duplication. In HRR-deficient cells, the DSBs are left unresolved, thus compromising cell viability and leading to cell death [81, 184]. Nevertheless, it is worth mentioning that the absence of XRCC1 (a key scaffold protein in BER) does not compromise cell viability in HRR-deficient cells, demonstrating the crucial role of PARP-1 over a deficiency in the BER pathway in cells carrying defects in HRR [61].

NHEJ activation

PARP-1 is responsible for the PARylation of many targets, including key proteins involved in the NHEJ pathway, like Ku70/80 and DNA-PKcs [28, 185, 186]. This process leads to the suppression of NHEJ [187-189]. PARP-1 inhibition seems to reverse this process, thus increasing NHEJ activity. Consequently, in HR-deficient cells, the error-prone NHEJ pathway is activated, leading to an increase of, chromosomal rearrangements and mutations, which can ultimately promote cell death [190, 191].

Alt-NHEJ inactivation

PARP-1 has also been described as a player in mutagenic Alt-NHEJ by recruiting Pol ʋ to the DNA damage sites, to foster DSB repair. In HRR-deficient cells that pathway is promoted as an alternative to HR, to allow DSB repair. Thus, PARP-1 inhibition leads to the suppression of Alt-NHEJ, which is lethal in cells harbouring impaired HRR [61, 150].

1.2.5. Resistance to PARP-1 inhibitors

Despite the promising clinical studies involving PARP-1 candidates and the market approval of olaparib **1.1**, rucaparib **1.2** and niraparib **1.3**, resistance to PARP-1 inhibitors seems to be a significant clinical challenge. Several resistance mechanisms have been identified, such as the decreased intracellular availability of PARP-1 inhibitors, the restoration of HR function in cells carrying HRR deficiency and loss or decrease of PARP-1 expression [192].

Multi-drug resistance (MDR) efflux transporters have been reported as a primary mechanism of resistance to several drugs. For instance, the overexpression of P-gp has been correlated with the resistance to PARP-1 inhibitors. It is suggested that PAR is able to inhibit P-gp. The decrease of PAR synthesis due to PARP-1 inhibition may lead to the increase of P-gp and, consequently, of drug efflux [193]. Pre-clinical studies using olaparib **1.1** have suggested that it acts as a P-gp substrate, as shown by the resistance of P-gp-overexpressing cancer cells to that PARP-1 inhibitor [156, 194]. However, further studies are needed to establish a true correlation between PARP-1 inhibitors resistance and P-gp overexpression in cancer cells [150].

Another resistance mechanism that has been identified is the recovery of HR function in HRR-deficient cells. Secondary mutations in mutated *BRCA* that are able to restore its function have been the most identified resistance mechanism. Those mutations can include the restoration of the wild-type *BRCA*, or even the codification of a new form of *BRCA*, both of which are capable of re-establishing the BRCA and HRR functions. Once HRR is restored, PARP-1 inhibitors may lose their activity as stand-alone agents or in combination with anti-cancer drugs. Examples of secondary mutations have been reported for *BRCA*-mutated ovarian and breast cancers, after which they become resistant to PARP-1 inhibitors [150].

A third frequently reported resistance mechanism is the decrease or loss of PARP-1 expression, as the effectiveness of PARP-1 inhibitors in anti-cancer therapy depends on the availability of the PARP-1 protein [150, 193]. It has been demonstrated that the absence of PARP-1 promotes resistance to olaparib **1.1** and talazoparib **1.5**. Moreover, continued treatment with veliparib **1.4** is associated with a decrease in PARP-1 protein levels. However, it is worth mentioning that changes in the levels of PARP-1 expression during different stages of breast cancer, for instance, are correlated with differences in the level of miR-210, which is a suppressor of PARP-1 expression. Thus, the resistance to PARP-1 inhibitors may ultimately be dependent on miR-210 and the cancer stage [193, 195].

1.3. COMPUTER-AIDED DRUG DESIGN IN DRUG DISCOVERY

Despite all the efforts that have been made in the search for novel, safer and more potent drugs, the high cost and time associated with their development have led to the development of different tools to achieve this goal more efficiently, namely computer-aided drug design (CADD), aiming to save time and resources [196]. Using scientifically accurate knowledge, it is estimated that about $2.6 billion dollars are involved in the drug development process of bringing a promising molecule to the market [197], which takes 10–15 years [198, 199]. Moreover, the rate of molecules that fail in the late-stage of clinical trials and do not enter the market is extremely high. In fact, up to 90% of drug candidates that reach clinical trials are not approved further [200].

Although high-throughput screening (HTS) has assumed an important role in the identification of novel and promising hits, because it allows the screening of thousands of molecules using an integrated robotic system, it still involves a considerable financial effort and is limited by the availability of targets and ligands for testing [197]. Thus, CADD has emerged as a key tool in drug discovery (**Figure 1.21**), either used in combination with or as an alternative to HTS, as computational tools are usually quicker, cheaper and easier to establish than is HTS [196].

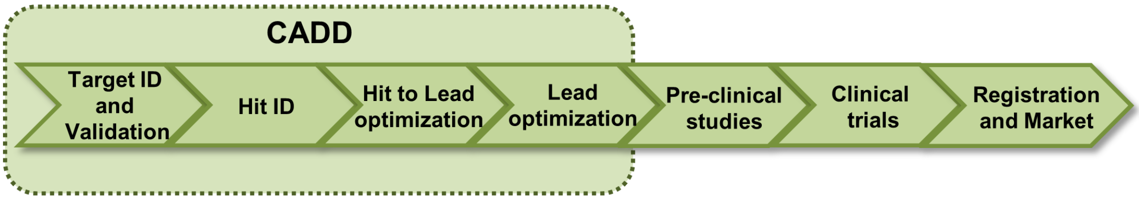

Figure 1.21 CADD in drug discovery and development process. CADD is particularly important at the early stages of drug discovery, namely in lead identification and optimization, aiming the selection of active and safe drug candidates.

CADD refers to the application of all computer-assisted methods aiming at the discovery, design and optimization of biologically active molecules [199]. Furthermore, it allows the screening of thousands or millions of small molecules, most of which do not exist physically, in a process that is termed virtual screening (VS) [201, 202].

VS is likely the most widely used method among the CADD methodologies. It consists in the computational screening of large compound databases to identify a small set of drug-like candidates that display a high probability to bind to a specific target and to be further evaluated experimentally [199, 201, 203]. The electronic libraries used are composed of commercially available compounds or virtual molecules, the chemical synthesis of which is theoretically achievable [196, 204]. This strategy has become popular in both the pharmaceutical industry and academia, as it prevents the synthesis of a huge number of inactive compounds for a specific target, consequently saving money and resources [197].

In addition, CADD promotes the design and optimization of new leads, thus providing insights into the structure and physicochemical properties of the molecules, as well as into their absorption, distribution, metabolism, excretion and pharmacokinetic (ADME/PK) profile, or even their binding affinity to a specific target. Ultimately, CADD directs the synthesis of new promising compounds and/or identifies novel targets for well-known and active molecules. [196, 202, 204]. Some approved drugs, such as captopril (angiotensin-converting enzyme inhibitor) [205], zanamivir (neuraminidase inhibitor) [206], dorzolamide (carbonic anhydrase inhibitor) [207], saquinavir [208] and tiprinavir (HIV-1 protease inhibitors) [209], rilpivirine (HIV transcriptase reverse inhibitor) [210], aliskiren (renin inhibitor) [211] and nilotinib (tyrosine kinase inhibitor) [212] are successful examples of the implementation of CADD in the drug development pipeline.

Conceptually, CADD methodologies are divided into two approaches, structure-based and ligand-based drug design.

Structure-based drug design (SBDD) requires the availability of the three-dimensional (3D) structure of the target, which is generally obtained from experimental data, such as X-ray crystallography, nuclear magnetic resonance (NMR) or cryo-electron microscopy (cryo-EM), to discover active and selective drug candidates based on their predicted interactions with the receptor binding site. The promising molecules obtained are further evaluated *in vitro* [197].

Conversely, **ligand-based drug design (LBDD)** takes advantage of a group of molecules, for which the activity and potency against a specific target is known. LBDD generates theoretical predictive models that allow either the structural optimization of the known ligands to improve their potency, or the identification of new active scaffolds via VS of different compound libraries [198].

Nevertheless, the two strategies yield interesting results in the drug discovery pipeline. The combination of SBDD with LBDD has emerged as a promising way to overcome the shortcomings of each approach individually, thus converging efforts in the discovery of novel and promising drugs [198]. A brief description of SBDD and LBDD, as well as of some of the most widely used methods in CADD, is presented below and summarized in **Figure 1.22**.

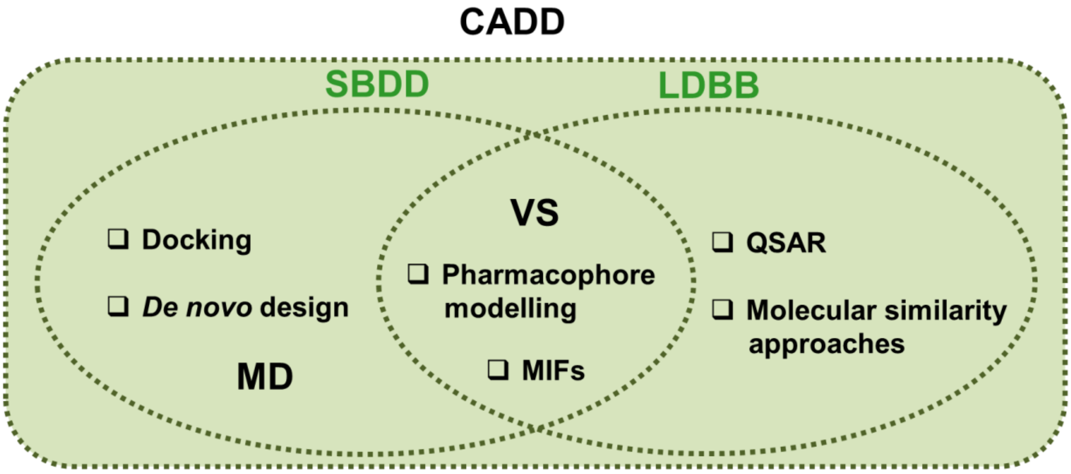

Figure 1.22 The most widely used methods in CADD. A structure-based drug design (SBDD) or a ligand-based drug design (LBDD) can be applied depending on the availability of the 3D structure of the target (SBDD) or of active ligands (LBDD). Some methods can be used in both approaches, such as molecular interaction fields (MIFs) and pharmacophore modelling. Molecular dynamics (MD) is broadly applied as a complement of SBDD, namely to take into consideration target flexibility.

1.3.1. Structure-based drug design methods

SBDD is usually the CADD approach of choice when valid structural information of the target is available. In cases in which an experimentally obtained 3D structure is not accessible, receptor structure can be predicted by implementing distinct computational methods, such as homology modelling [213, 214], threading approaches [215] and *ab initio* folding [216, 217].

Typically, two main techniques are associated with SBDD, i.e., molecular docking and *de novo* design.

1.3.1.1. *De novo* design

Rather than molecular docking, which will be discussed below, the *de novo* approach involves the design and synthesis of novel molecules [197]. In fact, *de novo* design approach considers insights from the 3D receptor to generate new promising drug-like molecules that can be synthesized. Either linking or growing algorithms can be applied. The former algorithms involves the combination of different small fragments or functional groups that bind to the different regions of the target pocket, whereas growing algorithms pursue an incremental construction of the ligand, in which a first fragment is docked into the binding site, followed by the inclusion or removal of others to ultimately design novel potent lead compounds [200, 218-220].

1.3.1.2. Molecular docking

Molecular docking is likely the most widely used method in SBDD. It requires the availability of the target structure (usually a protein) and ligand molecules. The docking process involves a search algorithm, which samples possible ligand conformations and orientations (poses) into the target binding pocket and a scoring function that predicts the binding ligand affinity of the docking poses generated previously by the search algorithm, thus ranking them by a score [197]. Therefore, molecular docking is able to predict the putative binding mode of a ligand into the target-binding pocket, and to estimate the binding affinity between the receptor and the ligand, determining which it the most favourable ligand pose in the receptor-binding site [221, 222]. Despite the steady improvement of computer performance, searching the conformational space is usually a demanding and time-consuming process [223]. Consequently, efficient search methods and trustworthy scoring functions are essential elements of docking algorithms.

In general, docking algorithms can be divided into three categories, depending on the search algorithm applied: rigid-body, flexible-ligand and flexible-ligand and receptor approaches [199, 224].

Rigid-body search algorithms were the earliest applied docking approaches. They take only into account the geometrical complementarity between the receptor and the ligand in the docking process. The ligand is subjected to rotation and translation in order to be docked into the target-binding pocket, in which the flexibility of the receptor or the ligand is not considered in the calculation. This is ultimately associated with a lack of accuracy in the docking process, despite it being the fastest search algorithm approach available [225] [226, 227].

On the other hand, the most commonly applied docking approaches, the **flexible-ligand search algorithms**, treat the receptor, but not the ligand, as a rigid-body and take into account the whole conformational space of the ligand in an attempt to maximise the degrees of freedom of the ligands involved in the docking calculation. Nevertheless, the absence of target flexibility may be associated with unsuccessful docking results, especially among some types of proteins in which receptor conformational changes play a key role in their ligand-binding mode and, consequently, in their biological activity [228-232]. Thus, the **flexible-ligand and receptor search algorithms**, which taking into consideration the flexibility of both the ligand and the receptor, were developed to better predict ligand-receptor binding [228].

Different approaches are applied to take into consideration the receptor flexibility, such as molecular dynamics (MD) [233, 234] and Monte Carlo (MC) [235] simulations, rotamer libraries [236-239], protein ensemble grids [240, 241] and soft-receptor modelling [240, 242]. Despite all the efforts spent in the application of flexible-ligand and receptor search algorithms, the flexible-ligand algorithms remain the most used in docking calculations, especially in VS studies, when a huge number of small molecules are tested. Other than the good docking results afforded by the latter search algorithm, its high costs in terms of time and computational resources can explain the preference of the flexible-ligand algorithms [199].

In addition to the search algorithms, scoring functions play an essential role in the docking process, as they are used to estimate the binding free energy of small molecules complexed with a specific target and to rank them according to that. Accuracy in the scoring and ranking of compounds is an essential step in docking performance. Nevertheless, if thousands of compounds are evaluated, the comparison of the binding free energy among them may be a very slow process. As scoring functions are simplified approximated mathematical methods, they are able to predict the receptor-ligand binding affinity in a very fast way without using computational resources that are too demanding. Although the number of scoring functions has been increasing incredibly in the last years, the choice of a function that combines good accuracy with speed remains a challenge [198, 199].

According to the literature, four main groups of scoring functions are available: force field-based, empirical, knowledge-based and consensus-based scoring functions [197].

Force field-based scoring functions compute the binding affinity derived from physical atomic contacts between the receptor and the ligand by implementing classical molecular mechanics [243, 244]. GOLDScore [245] (employed in the GOLD docking software [246, 247]), DOCK [248] and AutoDOCK [249] are examples of docking programs that use this type of scoring function, and the latter two are based on the molecular dynamics AMBER force field [250].

Empirical scoring functions usually use simpler energy terms compared with force field-based scoring functions. The binding free energy is computed as the sum of several terms (e.g., hydrogen bonds, hydrophobic interactions), the weight of which in the function is often obtained by regression analysis. The parameters used take into account the experimental binding affinity data [251-253]. Among the many empirical scoring functions available currently, ChemScore [245, 251] (implemented in the GOLD docking software [246, 247]) and Glide SP/XP [254] are two popular examples of empirical scoring functions.

Knowledge-based scoring functions use statistical analyses to predict the occurrence of different interactions among a huge set of receptor-ligand complexes obtained from experimental structures. Unlike the force field-based and empirical scoring functions, knowledge-based scoring functions try to describe experimental structures rather than binding affinities [255, 256]. DrugScore [256, 257] is a well-known example of this type of scoring function.

Consensus-based scoring functions are the latest approach in the development of accurate scoring functions. They combine different types of scoring functions in an attempt to overcome the individual drawbacks of each of the classes of scoring functions [258]. X-CSCORE is an example of a consensus-based scoring function that incorporates three empirical scoring functions, namely SCORE, ChemScore and Bohm’s scoring functions [259].

Despite all of the efforts aimed at developing more accurate scoring functions, the approximations applied in molecular docking studies often lead to inadequate approaches into receptor conformational changes [260]. The main targets in the drug discovery pipeline, proteins, are dynamic molecules with a conformation that is often affected by ligand recognition and binding. Moreover, their biological role is regularly dependent on these changes, as happens in some enzymatic reactions, in which the enzyme motions are directly involved in the success of the chemical reaction [261]. Thus, molecular dynamics (MD) has emerged as a leading method to overcome target flexibility issues.

1.3.1.3. Molecular Dynamics

MD is a computational method that is used extensively to study biological systems, namely proteins, as it provides insights into their dynamic features at the atomic level [260]. Through the application of a physics-based energy function (also called force field) like AMBER [262], CHARMM [263] and GROMOS [264], this method allows the identification of different relevant conformations experienced by proteins during different timescales, in agreement with Newton’s equation of motion. Moreover, MD simulations provide insights into dynamic molecular interactions of proteins, which could not be achieved via the use of a single static structure. This can ultimately disclose important information about both protein function and stability [265]. Due to great advances in computational resources observed in the last years, MD simulations have been applied to large systems that include explicit solvent and membrane environments, in an effort to mimic real biological systems [266]. Furthermore, MD simulations have been extensively used in drug discovery with different purposes, such as prediction of target selectivity [267], allosteric regulation [261, 268, 269], flexible docking (using representative structures that take into consideration the conformal changes in the protein) [228], development of dynamic structured-based pharmacophores [270-275], protein homology models refinement [276] and calculation of the free energy of binding [260, 277].

1.3.2. Ligand-based drug design methods

LBDD is the approach of choice when protein structure is not available, either experimentally or computationally. Nevertheless, the application of LDBB implies the availability of a set of small molecules that are able to bind to the target under investigation and provide additional insights about the physicochemical and structural features involved in their target bioactivity [197, 198]. Among the LBDD techniques, quantitative structure-activity relationship (QSAR), molecular similarity approaches, and pharmacophore modelling are well-known and widely used methods [197].

1.3.2.1. Quantitative structure-activity relationship

QSAR studies use statistical models to establish a correlation between the structural features of a series of compounds and their biological activity against a specific target. This method assumes that structurally similar compounds likely have a similar biological function. After the identification of a set of active ligands, which biological activity against a particular target was experimentally determined, different molecular descriptors that represent the structural and physicochemical properties of the molecules are selected. Subsequently, mathematical models that correlate those descriptors with a specific biological activity are built. Furthermore, these models are used to predict the activity of new compound analogues that present some differences in molecular properties [278, 279]. Although classical QSAR methods are based on 2D descriptors, namely the physicochemical properties of ligands, more recent approaches have been developed. Specifically, 3D, 4D, 5D and 6D-QSAR have been developed in an attempt to take into consideration additional features, such as ligand shape (3D-QSAR), ligand conformation and orientation (4D-QSAR), receptor flexibility and induced-fit effects (5D-QSAR) or even solvation effects (6D-QSAR) [280]. It is worth mentioning that the generation of a trustworthy QSAR model implies a minimum set of compounds (usually 20), with biological activity values that can be compared [281, 282].

1.3.2.2. Molecular similarity approaches

Molecular similarity approaches are based on the physicochemical and structural similarity among a set of well-known target binders, aiming at the identification of novel promising compounds. Generally, the molecular fingerprint of a set of active molecules for a specific target is used to screen compound databases, after which novel molecules with similar fingerprint profile are selected [197, 283].

Unlikely QSAR, these approaches do not take into consideration the bioactivity data of the molecules against a specific target [197]. Both 2D and 3D similarity methods can be used in molecular similarity calculations [284].

1.3.2.3. Pharmacophore modelling

Pharmacophore modelling is a widely used method in drug discovery. A pharmacophore represents a set of steric and electronic features of a molecule that are ultimately engaged in its recognition and biological activity against a specific target [285]. In a ligand-based approach, pharmacophore modelling implies the alignment and superimposition of active ligands that are known to interact and bind similarly to a particular target, to disclose common molecular features, which are further used to generate pharmacophore models [197]. Several features are considered in pharmacophore generation, such as hydrogen bond acceptors (HBA)s, hydrogen bond donors (HBD)s, negative and/or positive ionizable groups, aromatic rings and hydrophobic regions. Moreover, the 3D spatial arrangement derived from the superposition of known active molecules is also taken into consideration during pharmacophore modelling [286, 287]. This is particularly relevant when the pharmacophore approach is used to identify new promising molecules, as the pharmacophore models are able to capture not only the essential chemical features, but also the relative orientation of the newly discovered compounds [286].

Although they were originally reported as ligand-based methods, structured-based pharmacophores have also been described. This approach, which is only applied when the target structure is available, usually provides further insights into binding interactions, as well as further information about steric target requirements. Therefore, a further pharmacophoric feature may be obtained in structure based-pharmacophore models, excluded volumes spheres. These represent the steric region at the binding site, in which ligand substituent groups may not be engaged [287].

A further important point in pharmacophore generation is the conformational flexibility of both the ligand and the receptor, if available. Generally, low-energy geometries of active ligands are used to build pharmacophore models in an attempt to reproduce bioactive conformations [288, 289]. On the other hand, the tolerance radii of chemical features, as well as the excluded volume spheres, partially contribute to the introduction of receptor flexibility in pharmacophore generation [290]. Nonetheless, a major account in protein flexibility was introduced by dynamic structured-based pharmacophore models. In these cases, pharmacophore models are built using representative structures obtained from the MD simulations of a specific target, based on the *apo* and/or *holo* forms, in order to disclose conserved interactions regions, or even those that cannot be occupied by any active ligand [287]. Thus, a more trustworthy pharmacophore model may be generated.

Different programs are used in pharmacophore modulation, such as Catalyst [291], Phase [292] and MOE [293]. Generally, several pharmacophoric hypotheses are generated and the choice of the best pharmacophore model is often based on both the sensitivity and specificity of the hypotheses obtained after a screening of these against an external compound database formed by active and inactive ligands [198].

As one of the most powerful CADD techniques, the pharmacophore modelling strategy may be applied in different phases of the drug discovery pipeline, such as hits identification [294], lead optimization [295] and prediction of toxicity [296] and side effects [297], or even to disclose ligand activity *in silico* [298] and predict drug-drug interactions [299].

1.3.2.4. Molecular Interaction Fields

Molecular interaction fields (MIFs) calculation is also a well-known method in CADD that has a broad range of applications in the drug development pipeline. This tool identifies the favourable energy interaction between a target and a chemical probe, ultimately predicting the way in which molecules may interact [300, 301]. The probes used, which can be only an atom or a functional group, reflect the different chemical properties of the binding partner. In an SBDD approach, MIFs calculation outlines regions in the binding site where chemical probes may interact with higher probability, thus directing the design of promising new ligands. On the other hand, in the absence of the 3D structure of the target molecule, MIFs can be calculated considering a set of known active ligands that bind to the receptor in a similar way. In this situation, the energetically favoured sites obtained represent the positions that may preferably interact with the receptor [302]. MIFs can be extensively applied in drug discovery, namely in hit identification and design, lead optimization, ADME/PK and toxicity prediction, as well as to provide insights into protein-ligand and protein-protein interactions [300].

Several *in silico* methods have been used in the search for potent and selective drugs that act on individual targets, and different choices are made depending on the information available about the structure of the target and/or active ligands. Nevertheless, the combination of SBDD with LBDD is been actively pursued to investigate particular target ligands and to propose new selective drugs. Moreover, some CADD methodologies cannot be included in a specific group, SBDD or LBDD, such as VS and MIFs calculation.

Molecular docking and pharmacophore-based searching are two examples of widely used structure-based virtual screening (SBVS) and ligand-based virtual screening (LBVS) strategies, respectively. The former approach takes into consideration the receptor structure to rank molecules within a virtual database according to the prediction of their better fit in the target. On the other hand, the later strategy uses the pharmacophore queries to screen compound libraries, and to select new promising molecules, by excluding those that do not fit the queries. Furthermore, pharmacophore model, as well as other ligand-based similarity methods may work as a pre-filter that is able to significantly reduce the size of compound database to screen, after which SBVS, namely docking calculations, can be applied with higher probability of success, aiming to find drug-like molecules for further *in vitro* evaluation [196, 201].

2. CHAPTER II

GENERAL OBJECTIVES

2. CHAPTER II

General objectives

Poly(ADP-ribose)polymerase-1 (PARP-1) plays a key role in DNA-repair and may contribute to the resistance phenomena to anti-cancer drugs that act as DNA-damaging drugs and, consequently promote the survival and proliferation of cancer cells. In line with this, the aim of this thesis is to identify new and selective PARP-1 inhibitors that can be used as anti-cancer agents.

In order to achieve this main goal, the following general purposes should be fulfilled:

Performing molecular dynamic (MD) simulations of the PARP-1 catalytic domain

MD studies will be carried out on the PARP-1 catalytic domain, to provide further insights into the PARP-1 binding site, which can ultimately contribute to the disclosure of important features involved in ligand binding.

Generation of structure-based pharmacophores of the PARP-1 catalytic domain

Pharmacophore model generation will be performed using the information retrieved from MD studies, to consider receptor flexibility and to disclose key features involved in PARP-1 ligand binding.

Pharmacophore-based virtual screening (VS) against different compound databases

Commercial compound libraries and a database designed by our research group will be used in pharmacophore-based VS to identify promising PARP-1 inhibitor candidates.

Docking studies of the hits retrieved from pharmacophore-based VS

The hits that fit the best pharmacophoric hypotheses and display drug-like properties will be subjected to docking calculations.

***In vitro* evaluation of the most promising hits obtained from molecular docking**

The top-ranking compounds, with a high predictable binding affinity to the PARP-1 catalytic domain, will be selected for *in vitro* assays to confirm the results obtained from *in silico* studies.

3. CHAPTER III

DESIGN OF STRUCTURE-BASED PHARMACOPHORES FOR THE PARP-1 CATALYTIC DOMAIN

3. CHAPTER III

Design of structure-based pharmacophores for PARP-1 catalytic domain

3.1. OVERVIEW

During the last five decades, poly(ADP-ribose)polymerase-1 (PARP-1) has been deeply studied as a key effector in different biological processes, namely in DNA-repair. In an attempt to overcome drug resistance (often associated with the ability of cancer cells in detecting and repairing DNA lesions triggered by cytotoxic drugs) and to discover novel treatments to fight cancer, PARP-1 inhibition has been pursued [178].

The PARP-1 inhibitors approved to date, or currently under clinical evaluation, are nicotinamide/benzamide derivatives that bind to the nicotinamide-binding pocket as competitive inhibitors. Nevertheless, none of those molecules is a specific PARP-1 inhibitor [150]. In fact, as mentioned before, the catalytic domain of the PARP family displays a high level of homology, mostly due to the conserved sequence of amino acids shared by PARP members, the PARP signature motif [95]. Moreover, resistance to PARP-1 inhibitors has emerged as an obstacle in the clinical application of these agents [156, 303]. Thus, deeper studies of the PARP-1 recognition features are required to identify novel and more selective PARP-1 inhibitors.

Computational methods have emerged as a critical tool in drug discovery, as they disclose essential features in the ligand-receptor binding interactions, allowing the identification of new druggable binding sites [200, 261]. A broadly applied method in drug development pipeline is molecular dynamics (MD). MD simulations have become a crucial tool to overcome a big challenge in the drug development pipeline, which is the use of a single crystal structure of a target to predict the putative ligand-binding site, not taking into account the flexibility engaged in the ligand-binding that can ultimately compromise its biological function [232]. Moreover, pharmacophore models generation has been amply applied in drug discovery, namely to screen compound databases in the attempt to find out new hits, to develop 3D-QSAR models, or even to guide the synthesis of new drug candidates in the course of the hit-to-lead optimization [304].

At early stages of drug discovery, virtual screening (VS) of large compound databases has become an useful method to find out new promising ligands, acting on a specific target, saving time and resources [200]. Both ligand- and structure-based approaches can be applied to identify promising drug candidates.

In this work, a dynamic receptor-based pharmacophore approach based on the calculation of molecular interaction fields (MIFs) minima points in the binding pocket was applied in the attempt to identify novel and selective PARP-1 inhibitors. The conformational flexibility of the unbound PARP-1 catalytic domain (wild-type and PARP-1 Val101Ala), previously subjected to MD simulations was considered during the pharmacophore models generation. Subsequently, VS of different compound databases was performed, and the most promising hits were subjected to molecular docking. The top-scoring molecules were further evaluated by using an *in vitro* PARP-1 inhibition assay.

It is worth mentioning that the combination of different VS tools, such as pharmacophore queries and molecular docking have been reported in diverse drug discovery projects, contributing to a better prediction of truly active molecules for further development [305-307]. In addition to this, the application of MD in the pharmacophore modelling, considering protein flexibility, has been described as a way of enhance the likelihood of finding potential leads for different targets [273-275].

3.2. MATERIALS AND METHODS

3.2.1. Molecular dynamics simulations

Four co-crystal structures of the PARP-1 catalytic domain in complex with different inhibitors were retrieved from the Protein Data Bank (PDB codes: 2RCW, 3GN7, 3GJW and 3L3L). The structures were processed using the Protein Preparation Wizard tool in Maestro Suite. Water molecules were removed and bond orders were assigned. Each ligand-receptor complex (2RCW, 3GN7, 3GJW and 3L3L), as well as the unbound receptor form of both structures with PDB codes 2RCW (wild-type PARP-1 catalytic domain) and 3GN7 (PARP-1 Val101Ala catalytic domain) was subjected to 20 ns MD simulations in explicit water using the Amber package. Amber FF99SB [308] and GAFF [262] were assigned to the protein and ligands, respectively. TIP3P water model was used to solvate all systems [309] in a truncated octahedral box. Na^+ counter ions were added to neutralize the system net charge, and periodic boundary conditions were applied. Two minimizations cycles were performed, followed by an equilibration time of 1 ns in NVT (constant volume, constant temperature) conditions, in which protein and ligand atoms were position restrained with a constant force of 10 kcal/mol, to allow relaxation of the solvent molecules. Subsequently, a final production phase of 20 ns was carried out and trajectory snapshots were saved at every 10 ps, for each system. Langevin method was used in the thermal control of the system to 300 K, and also for achieving a constant pressure at 1 atm. Particle Mesh Ewald summation method [310] and a cut-off of 10 Å, were used to assign Electrostatic and Lennard-Jones forces, respectively. The SHAKE algorithm [311] was implemented to constrain bonds that involved hydrogen atoms.

The trajectory analysis was carried out using GROMACS software package [312]. For each system, a conformational cluster analysis was performed with a backbone RMSD (root mean square deviation) cut-off of 0.15 nm. Cluster analysis was performed taking into account all snapshots saved from each MD trajectory.

3.2.2. MIFs calculation and pharmacophore modelling

GRID [301] was applied to calculate MIFs, aiming the detection of energetically favourable binding interactions in the PARP-1 catalytic domain. Four GRID cubic cages were applied, two for each representative structure of the most populated cluster (hereinafter referred to as MD reference snapshot) of both unbound PARP-1 catalytic domain, the wild-type (retrieved from 2RCW) and PARP-1 Val101Ala (retrieved from 3GN7). To define the size of the GRID cage, the most populated clusters of each ligand-bounded system after MD were inspected.

A first GRID cage was centred at Tyr246, taking into account all residues that are engaged in conserved binding interactions with the four co-crystallised inhibitors, namely Gly202, Ser243 and Tyr246. Additionally, a second GRID cage was settled in order to consider residues involved in different types of interactions with binding site, disclosed after MD simulations of four different inhibitors co-crystallised with PARP-1 catalytic domain.

The MIFs were generated by considering five chemical probes: DRY, O, N1, O^- and N^+, which describe hydrophobic centres, hydrogen bond acceptors (HBAs), hydrogen bond donors (HBDs), negative charged and positive charged centres, respectively.

The MIFs energy minima recorded were combined to generate four pharmacophore models, one by each GRID cubic cage generated. The selection of MIFs minima points to be converted into pharmacophoric features took into account the distance between each minimum point, in order to prevent that pharmacophoric features only map large molecules from database screening. Thus, a maximum of 15 Å of distance between each minimum was set to select MIFs minima points for pharmacophore generation. Furthermore, the determination of energy minima points was based on the proximity of residues with specific functional groups. This is particularly relevant for minimum points of O and N1 probes, since those have to be projected towards a specific donor and acceptor group, respectively, located at hydrogen bond distance.

Accelrys Discovery Studio (DS) was the software used to model pharmacophoric hypotheses. HBA, HBD, negative ionizable (NI), positive ionizable (PI), and ring aromatic (RA) features were considered in pharmacophore modelling. Default location constraints spheres were imposed to each pharmacophoric feature generated, in order to grant a certain level of tolerance during VS against compound databases. This is due to the fact GRID minima points works as the lowest energy representatives of several adjacent points that translate favourable binding regions rather than fixed isolated spots of favoured interactions between probes and protein residues.

3.2.3. Database preparation and pharmacophore-based virtual screening

The National Cancer Institute [313] (NCI2003 3D), DrugBank [314], Asinex [315] and natural compounds subset from ZINC [316] databases have been downloaded, and converted into multiconformer Catalyst databases. The “FAST” conformational analysis model of the catDB program in DS was used to build all databases, and a maximum of 255 conformations was set for each compound. An additional library formed by triterpenes and steroids derivatives, which was designed by our research group (ST database), was prepared in the same conditions.

The four pharmacophore models generated were used to screen the five databases, using Catalyst [291] in DS. A maximum of 300 hits were retrieved for each database searched. The QikProp module (Schrödinger, LLC, New York, NY, 2012) in Maestro Suite was applied in order to predict ADMET properties of the molecules retrieved, after which some drug-like filters were applied, such as Lipinski’s rule of five [289] and a polar surface area (PSA) not greater than 140 $Å^3$. Finally, all selected hits were prepared using the LigPrep module (Schrödinger, LLC, New York, NY, 2012). The pH was set to 7.4 (physiological pH) and the lowest energy ring conformation was kept for each molecule.

3.2.4. Docking studies

Molecular docking was carried out using Glide (version 5.8 Schrödinger, LLC, New York, NY, 2012). Standard precision (SP) mode was employed, using the OPLS-AA force field [317], and 10 poses per ligand were saved for each docking run. The protein crystal structures with PDB references 2RCW and 3GN7, as well as the corresponding MD reference snapshots previously identified were used to perform docking calculations. All water molecules were removed from both the structures. A grid was generated, considering all residues located within 6 Å of each inhibitor co-crystallised with PARP-1 catalytic domain after MD simulations, i.e., 2RCW, 3GN7, 3GJW, and 3L3L. Glu102, Asp105, Asp109, His201, Gly202, Ser203, Arg204, Arg217, Gly227, Tyr228, Tyr235, Phe236, Lys242, Ser243, Tyr246, Glu327 residues were included in this selection.

Control docking experiments were carried out using co-crystallised ligands A620223 and 3GN in the corresponding crystal structures, 2RCW and 3GN7, in order to validate and optimize docking parameter settings. As the best docking pose obtained for each co-crystallised ligand reproduce its crystal binding mode, docking studies with both protein structures were performed. The selected compounds that fit pharmacophore models generated from MIFs calculated on MD reference snapshot of wild-type PARP-1 catalytic domain were docked into that structure and the corresponding crystal one (2RCW). Similarly, molecules retrieved from the pharmacophoric hypotheses generated from MD reference snapshot of PARP-1 Val101Ala catalytic domain were docked into that structure and the corresponding crystal (3GN7).

After visual inspection of top-scoring molecules in all docking runs, the promising compounds that were only retrieved from pharmacophore models based on Val101Ala PARP-1 catalytic domain were re-docked into wild-type PARP-1 catalytic domain (crystal and MD reference snapshot).

3.2.5. PARP-1 enzyme assay

PARP-1 inhibition was evaluated using the HT Universal Colorimetric PARP Assay kit (Catalog #4677-096-K; Trevigen, Gaithersburg, MD, USA), in accordance with the instructions provided by the manufacturer. The assay evaluates the incorporation of biotinylated poly(ADP-ribose) onto histones proteins in a 96-well plate. In a few words, 10 µL of the test compounds were mixed with 15 µL of PARP-1 enzyme (0.5 U) into rehydrated histone-coated wells for 10 min at room temperature. Afterwards, 25 µL of PARP cocktail containing biotinylated NAD, activated DNA, and PARP buffer were added, and the solutions were incubated again for 60 min. Then, the wells were washed and the detection reaction was performed in line with the manufacturer’s protocol. The absorbance was recorded at 450 nm in a synergy HT plate reader. Stock solutions of the all test molecules were prepared in dimethyl sulfoxide (DMSO) and serially diluted to the required concentrations with 1X PARP buffer. Parallel experiments were performed by substituting the test compound with an equivalent volume of DMSO, in order to evaluate the effect of the vehicle on PARP-1 activity.

3.3. RESULTS AND DISCUSSION

3.3.1. Characterization of ligand-binding interactions in PARP-1 catalytic domain

PARP-1 catalytic domain co-crystallised with four different inhibitors were subjected to MD simulations to analyse active site–ligand interactions, and to identify which residues can be involved in ligand binding [107, 149]. After analysing the time-dependent distribution of the interactions between functional groups of the four ligands and PARP-1 binding pocket during MD simulations, it was observed that the interactions displayed in the crystal structures were consistent in all the four complexes studied. Specifically, three stable hydrogen bonds could be identified: two between the amide backbone of Gly202 and the amide moiety of the inhibitors and one between the Ser243 hydroxyl and the carbonyl group of inhibitors were established. Moreover, the well-known π–π stacking interaction between Tyr246 and the aromatic core of the inhibitors was also consistent throughout the MD simulations. Furthermore, additional interactions established between each inhibitor co-crystallised with PARP-1 catalytic domain could be identified in the MD simulations (shown in **Figure 3.1**).

Despite valines are not included in the set of residues involved in conserved interactions, Val101, located on the outskirts of the binding site, is involved in hydrophobic interactions with co-crystallised ligand (A620223) in the structure with PDB code 2RCW. These observations were revealed in the MD simulation (**Figure 3.1A**). The same was not observed for the other three ligand-bound systems (3GN7, 3GJW, and 3L3L) with Val101Ala mutations. In line with this, calculation of MIFs by using each MD reference snapshot of both wild-type and PARP-1 Val101Ala catalytic domain was settle, in order to understand the influence of that common single-nucleotide polymorphism (SNP) of PARP-1, which has been implicated in the reduction of PARP-1 catalytic activity [251].

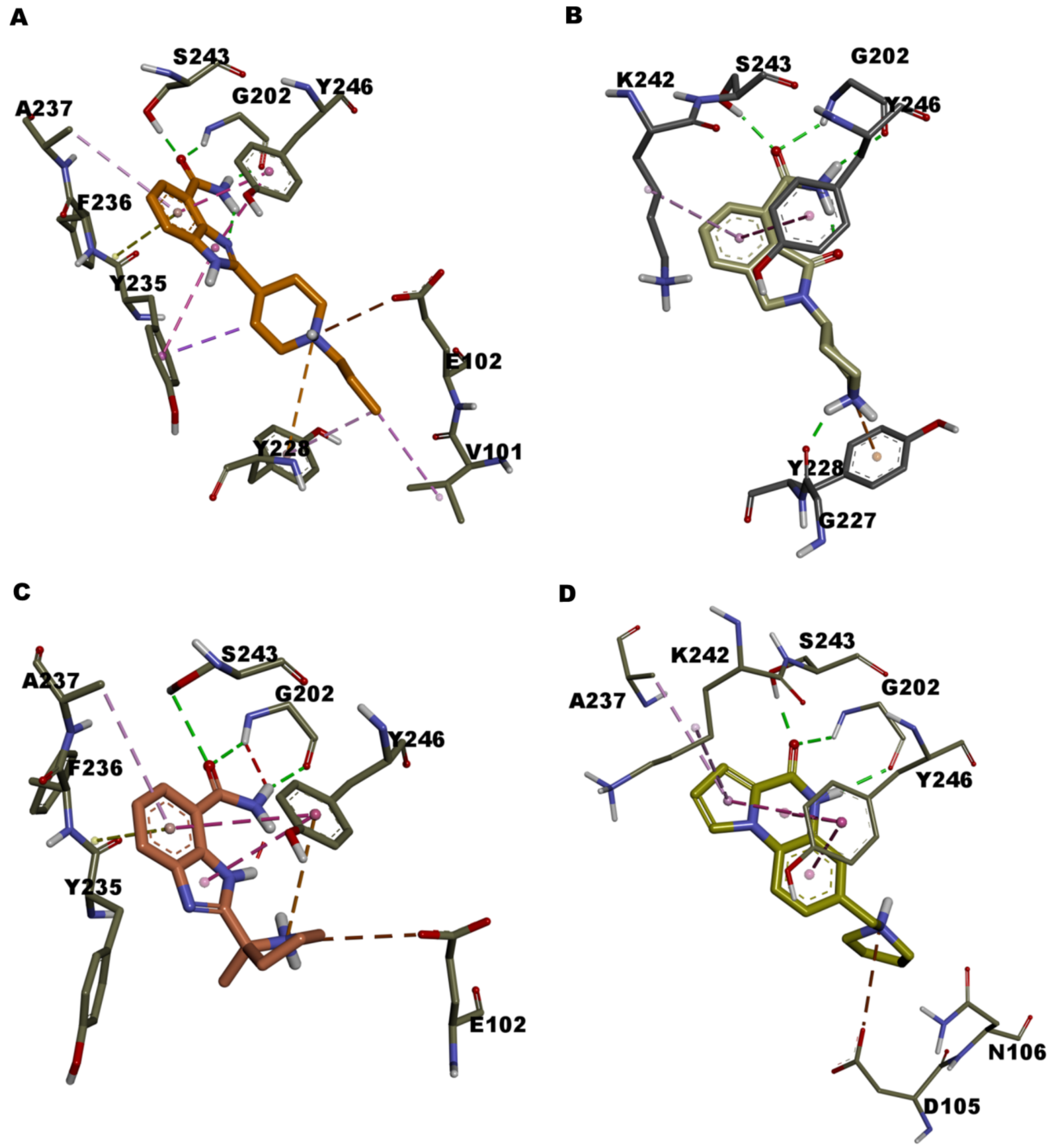
A
S243
A237
G202
Y246
F236
Y235
E102
Y228
V101
B
K242
S243
G202
Y246
Y228
G227
C
A237
S243
G202
Y246
F236
Y235
E102
D
K242
S243
A237
G202
Y246
N106
D105

Figure 3.1 Representation of the main interactions established for each co-crystallised ligand with PARP-1 catalytic domain along MD run. A) 2RCW. **B)** 3L3L. **C)** 3GN7. **D)** 3GJW. Dashed lines represent interactions between binding site residues and bound ligands. Green colour represents hydrogen bond interactions; Orange indicates π–cation interactions; yellow represents amide–π interactions; pink denotes π–π stacked; light pink denotes hydrophobic interactions (alkyl and π–alkyl); brown indicates charge-charge interactions. This figure was created using Discovery Studio Visualizer 16.1.0.

3.3.2. Molecular interaction fields calculation and receptor-based pharmacophore models generation

As long as all PARP-1 inhibitors approved to date display a nicotinamide-like pharmacophore, lacking of target specificity, especially among other PARP members, a dynamic structure-based pharmacophore approach was applied, in order to identify novel and selective PARP-1 inhibitors. In line with this strategy, MIFs between different chemical probes and PARP-1 catalytic domain, previously subjected to MD simulations, were computed to predict favourable regions for ligand binding. Four different 3D grids were used to explore PARP-1 binding site, two for each MD reference snapshot of PARP-1 catalytic domain (wild-type and Val101Ala polymorphism form). The use of the unbound PARP-1 catalytic domain after MD simulations in the MIFs calculation and pharmacophore generation was established to better understand the PARP-1 catalytic domain flexibility, namely its conformational changes in the absence of any inhibitor, and its effect on the ligand binding. Moreover, two different 3D GRID cages for the MD reference snapshot of each PARP-1 catalytic domain studied (wild-type and Val101Ala mutant) are settled to compute MIFs, in order to consider all residues displayed in the binding pocket able to be engaged in important interactions with ligands, without extend the MIFs calculation to those ones that likely did not interfere in the ligand binding. The first one (**Figure 3.2 A 1 and 3**) was centred on Tyr246 and considered all residues involved in conserved interactions with PARP-1 inhibitors, namely Gly202, Ser243 and Tyr246 [149]. The second GRID cage (**Figure 3.2 A 2 and 4**) was defined to consider the involvement of residues engaging additional interactions with PARP-1 inhibitors in the MD simulations with different co-crystallised ligands. Glu102 and Asp105, two of the few residues that are specific to PARP-1 (among its closest relatives) [149] seemed to be involved in specific interactions with ligands, a fact that can be relevant in the discovery and development of new selective PARP-1 inhibitors. Moreover, these residues are structurally placed at the periphery of NAD+ recognition site, which are also reported as less conserved among PARP family. One should highlight D-loop residues (like Tyr228) that lines the donor site and, to a certain extent, the acceptor site and shows structural variability among ARTDs [95, 149, 161, 318] (**Figure 3.3**).

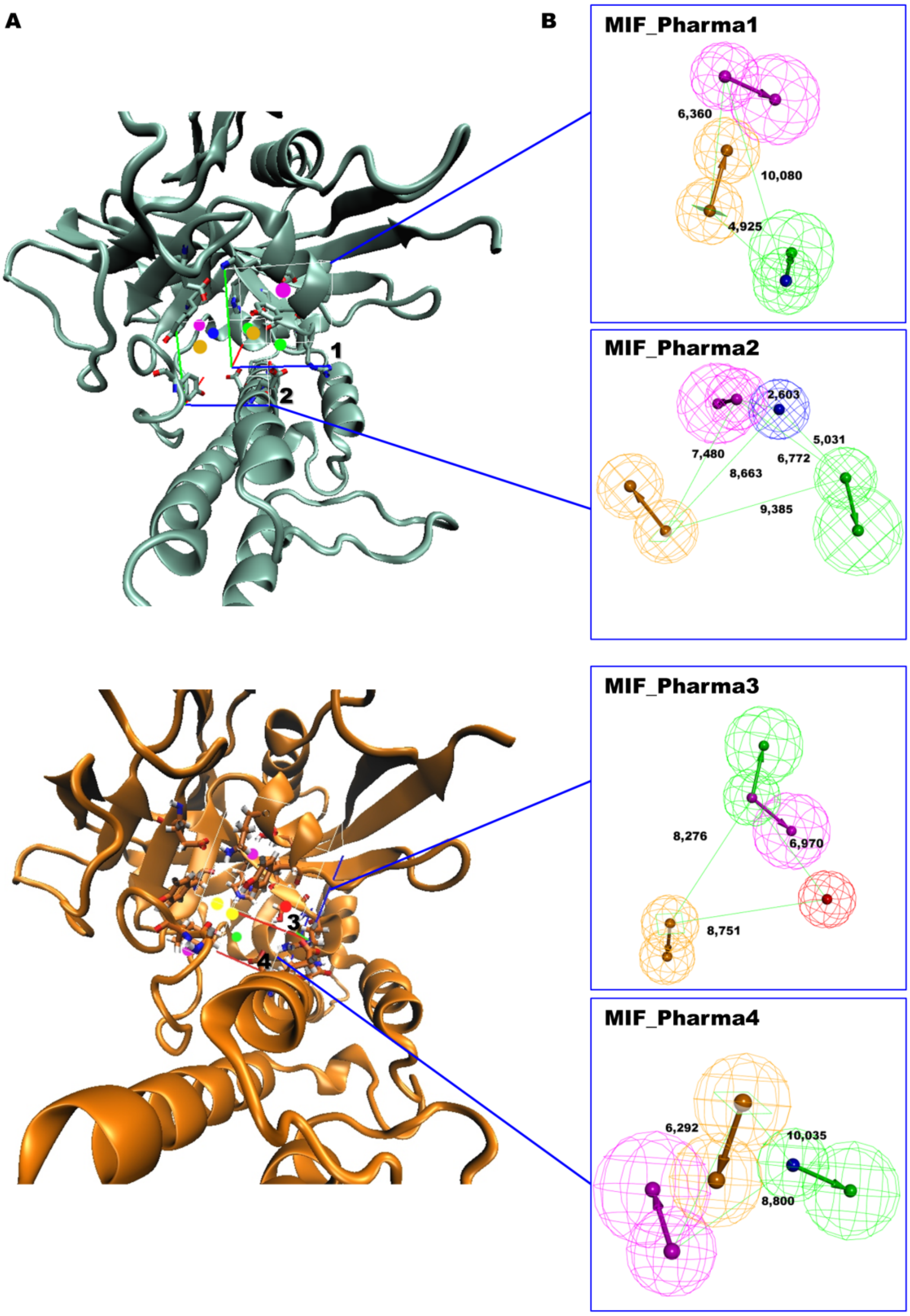
A
B
MIF_Pharma1
6,360
10,080
4,925
1
2
MIF_Pharma2
2,603
5,031
7,480
6,772
8,663
9,385
MIF_Pharma3
8,276
6,970
8,751
3
4
MIF_Pharma4
6,292
10,035
8,800

Figure 3.2 Pharmacophore models generated from MIFs calculation. A) Representation of GRID MIFs minima points calculated into MD reference snapshot of PARP-1 catalytic domain (wild-type (**1** and **2**) and PARP-1 Val101Ala (**3** and **4**)). N1 (magenta), O (green), DRY (yellow), N+ (red), O- (blue) probes are displayed. **B)** Representation of the pharmacophore models generated from MIFs energy minima recorded by each GRID cubic cage. Green colour indicates hydrogen bond acceptor (HBA); magenta denotes to hydrogen bond donor (HBD); yellow indicates ring aromatic (RA); red denotes to positive ionizable (PI) centre; and blue indicates negative ionizable (NI) centre. In both MIF_Pharma1 and MIF_Pharma4, HBA and NI points were superimposed. This figure was created using the program VMD [319].

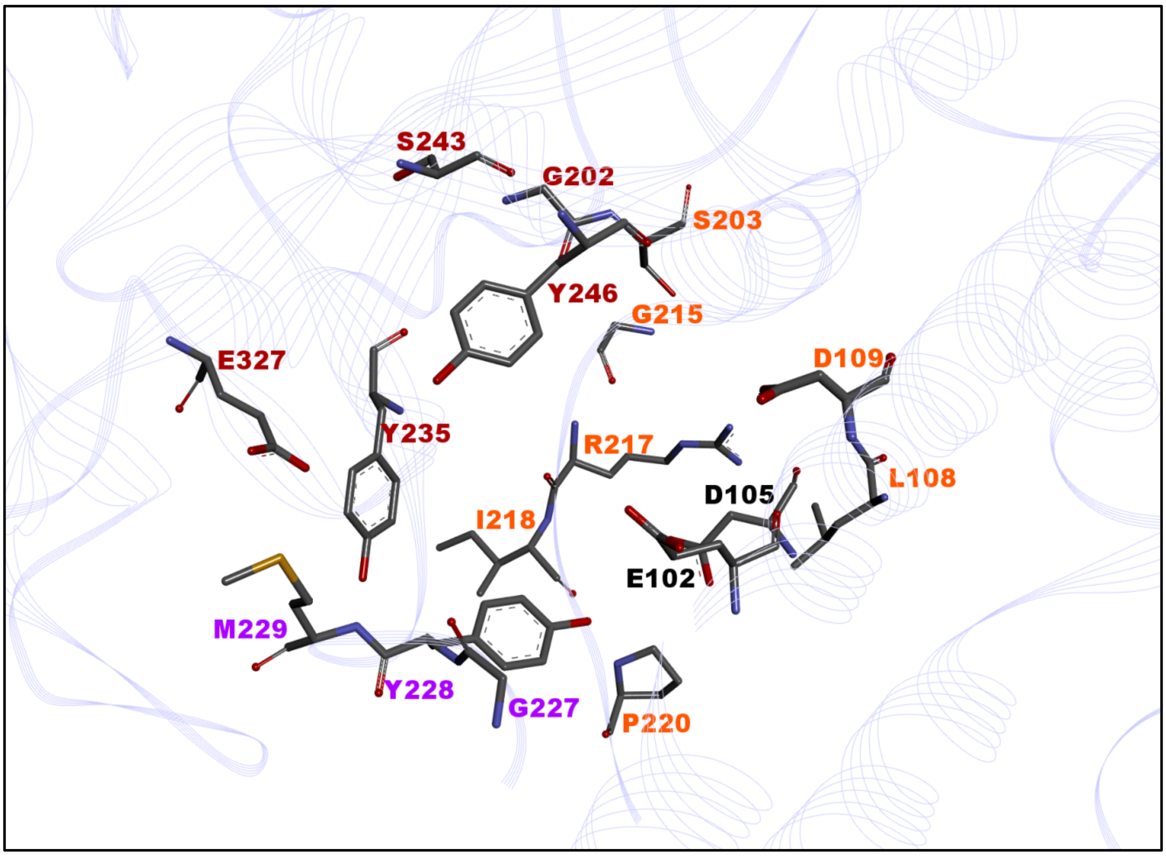

Figure 3.3 PARP-1 binding pocket. Nicotinamide and adenine-ribose binding residues are displayed in red and orange, respectively. Black is used to point out residues that lie in phosphate binding site. Violet indicates some important D-loop residues (215-233). This figure was created using Discovery Studio Visualizer 16.1.0.

The MIFs local energy minima retrieved from each probe (DRY, O, N1, O^- and N^+) were converted into pharmacophoric features, as they represent the points with the lowest interaction energy, and thus the locations at which the interaction between each probe and receptor are most favourable. Although five probes were used to explore the binding site, only the points of minimum of MIFs that correspond to four probes were retrieved for each pharmacophore model generated. This selection was based on the location of the MIFs minima points obtained for each probe and the distance among them, in order to choose the minima points placed in the regions of favourable interaction with important binding site residues, and to prevent the presence of probes too distant from each other. This was settled to prevent the mapping of only large molecules by the pharmacophoric features originated from those MIFs points.

Four pharmacophore models were generated, one by each MIFs local energy minima groups selected from each 3D GRID cage settled (**Figure 3.2 B**).

MIF_Pharma1 was the pharmacophore model based on the GRID minima points calculated for the MD reference snapshot of wild-type PARP-1 catalytic domain, which GRID cage was centred on the Tyr246. The four points of minimum were converted into four pharmacophoric features, which include an HBA pointed to the Ser203 hydroxyl, an HBD directed to the Lys242 (oxygen atom of the backbone carbonyl group), a NI pointed towards the Arg204, and an RA directed to the Tyr246.

MIF_Pharma2 was derived from minimum energy points of calculated MIFs in MD reference snapshot wild-type PARP-1 catalytic domain, in which the GRID cage was settled to consider residues involved in additional interactions (besides those ones retrieved from crystal structures) with the binding site. Four pharmacophoric features were recorded for this pharmacophore model, i.e., an HBA directed to the Ser203 hydroxyl, an HBD pointed towards the Arg217 (oxygen atom of the backbone carbonyl group), a NI also pointed to the Arg217 (guanidinium group), and a RA directed to the Tyr235.

MIF_Pharma3 and **MIF_Pharma4** were designed following the same principle of **MIF_Pharma1** and **MIF_Pharma2**, respectively, but using PARP-1 Val101Ala mutant instead of the wild-type PARP-1 catalytic domain. **MIF_Pharma3** displayed four pharmacophoric features, including an HBA, an HBD, a PI, and a RA. The projection points of the HBA and HDB, both recorded at the same GRID minima point, were directed to the Ser243 hydroxyl and the oxygen atom of the backbone carbonyl group of the Gly202, respectively. The PI was pointed to the Asp 105, and the RA was directed to the Tyr228. Finally, **MIF_Pharma4** exhibited four functional features: an HBA and a NI pointed to the guanidinium group of the Arg217, an HDB, which projection was directed to the oxygen atom of the backbone carbonyl group of the Gly233, and a RA pointed towards theTyr228.

Interestingly, the analysis of the four pharmacophore models generated highlighted that three of the four pharmacophores displayed features pointing to the residues with lower identity among the PARP-1 catalytic domain. In fact, the

HBAs in **MIF_Pharma1** and **MIF_Pharma2**, as well as the PI in **MIF_Pharma3** were directed to the Ser203 and the Asp105, respectively, both selective residues of PARP-1, which are among the few differences between PARP-1 and its closest PARP relatives in the donor site of PARP-1 catalytic domain [149]. This fact may be important for the disclosure of selective PARP-1 inhibitors. Moreover, most pharmacophoric hypotheses (**MIF_Pharma2**, **MIF_Pharma3**, and **MIF_Pharma4**) displayed at the least a functional feature pointed towards D-loop residues (215-233), which can also contribute to the discovery of new selective PARP-1, since D-loop exhibits an important variability among PARP family, as mentioned above.

3.3.3. Pharmacophore-based virtual screening and docking studies

The four pharmacophore models generated were used to screen the four commercial databases (NCI2003 3D, DrugBank, Asinex and natural compounds subset from ZINC database), and a total of 2449 molecules were selected. Among these compounds, only 266 were able to successfully pass the pre-defined drug-like filters, being afterwards used in the docking calculations.

The ST database was also subjected to pharmacophore-based VS, but no hits were retrieved for any pharmacophore model. An explanation for these results might be the presence of a NI (**MIF_Pharma1**, **MIF_Pharma2** and **MIF_Pharma4**) or PI (**MIF_Pharma3**) pharmacophoric feature in all pharmacophores hypotheses. Since most of the compounds that are included in the ST database are not charged at pH 7.4, they were not able to map all pharmacophore features. Thus, all pharmacophore models were simplified, by removing the PI/NI feature. A new pharmacophore-based VS against ST database retrieved 74 hits.

Altogether, 340 hits were subjected to molecular docking using Glide SP-mode. The hits retrieved from the screening against **MIF_Pharma1** and/or **MIF_Pharma2** were docked into the wild-type PARP-1 catalytic domain (MD reference snapshot and crystal structure). On the other hand, hits resulting from pharmacophore-based VS using **MIF_Pharma3** and/or **MIF_Pharma4** were docked into PARP-1 Val101Ala catalytic domain (MD reference snapshot and crystal structure). Crystal structures were used for docking calculations in order to evaluate the effect of target flexibility in the binding mode and the binding affinity of selected hits (**Figure 3.4**).

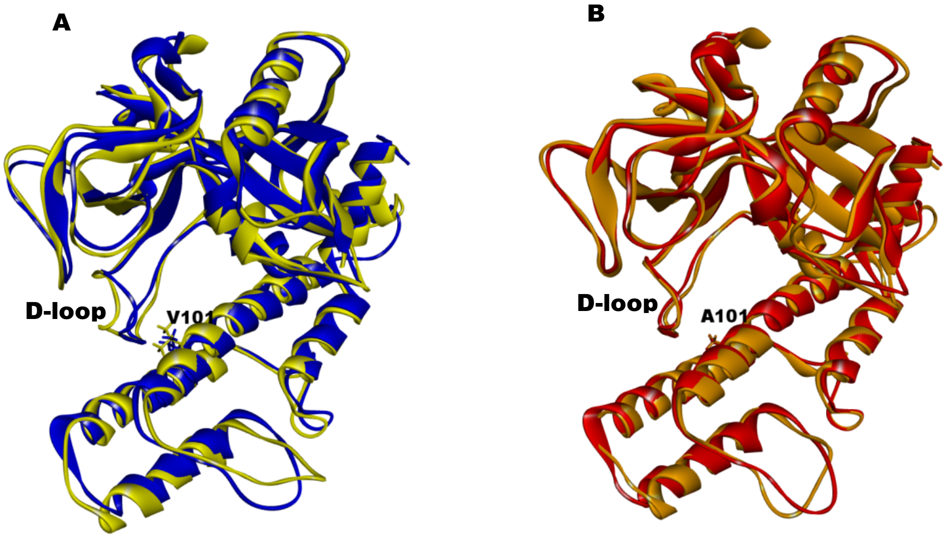

Figure 3.4 Superposition of crystal structure and MD reference snapshot of wild-type A) and PARP-1 Val101Ala B) catalytic domain. Blue and red represents the crystal structures (2RCW and 3GN7, respectively); yellow and orange indicate the MD reference snapshot of wild-type and PARP-1 Val101Ala catalytic domain. This figure was created using Discovery Studio Visualizer 16.1.0.

Moreover, the compounds that were only retrieved by **MIF_Pharma3** and **MIF_Pharma4** were subjected to molecular docking into MD reference snapshot of PARP-1 wild-type catalytic domain (and corresponding crystal structure) to evaluate the influence of Val101Ala mutation in their binding affinity with the PARP-1 binding site.

The top-scoring docked compounds for each docking calculation were subjected to careful visual inspection and seven (five from commercial databases and two from ST database), which are common among the top-ranking compounds for all docking runs, were selected for *in vitro* evaluation. This selection took into account molecules that are able to establish key interactions with the binding site, not only with highly conserved pocket residues (e.g., Gly202, Ser243 and Tyr246), but also with those ones displayed in the outer edges of the nicotinamide-binding pocket, which are less conserved (e.g., Glu102, Asp105 and D-loop residues (215-233)). The structural diversity was considered in the choice of potential hits, particularly in the molecules obtained from commercial databases.

The set of seven compounds selected was shortened to four molecules (**Figure 3.5**), as three of them were not acquired due to commercial availability limitations. The main interactions established between the four molecules, which effectively proceed to *in vitro* PARP-1 evaluation, with the MD reference snapshot of PARP-1 catalytic domain were displayed in **Figure 3.6**. As shown, all compounds were involved in different types of interactions with the PARP-1 binding site. Among the residues able to interact with the selected compounds, Glu102 and Asp105 (two non-conserved residues among PARP family) were particularly relevant, since they were involved in different types of interactions with all selected compounds. Additionally, the four molecules were able to interact with at least one D-loop residue, such as Arg217 (**3.1**, **3.3**, and **3.4**) and Tyr228 (**3.2**, **3.3**, and **3.4**).

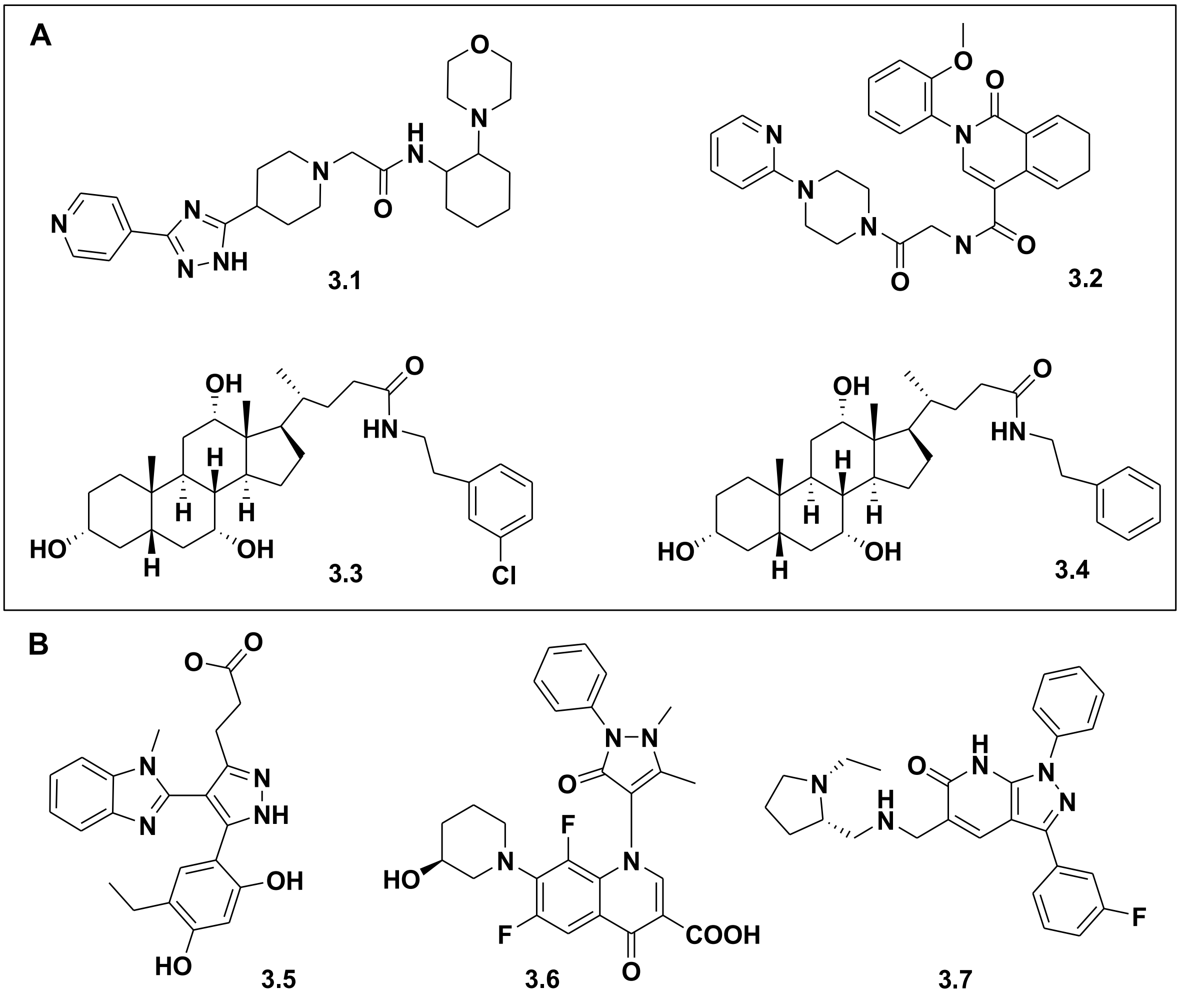

Figure 3.5 The top-scoring compounds selected from docking studies for further PARP-1 *in vitro* evaluation. A) The four compounds that were effectively evaluated. **B)** The three molecules discarded because of commercial availability issues.

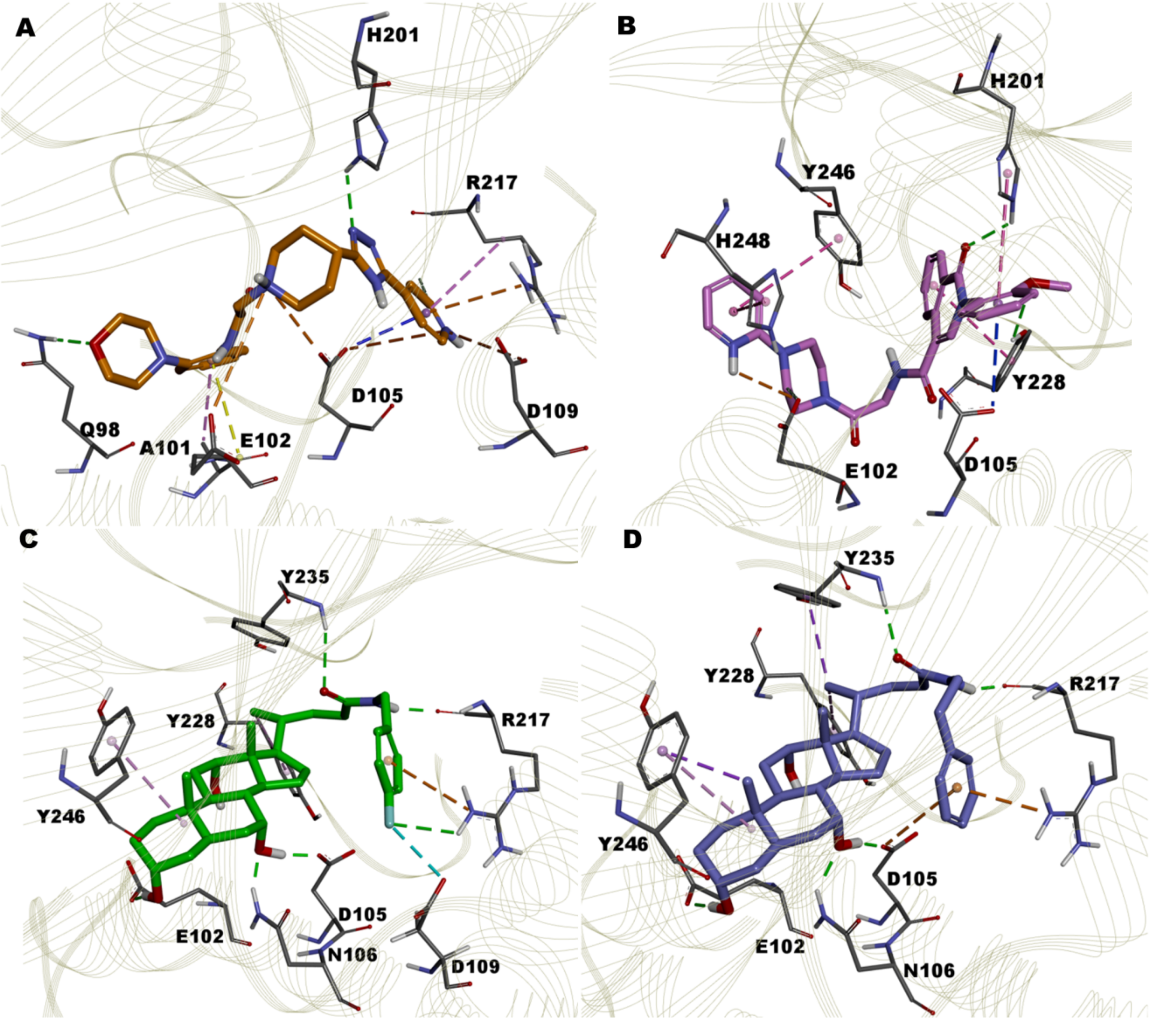
A
H201
R217
Q98
A101
E102
D105
D109
B
H201
Y246
H248
Y228
E102
D105
C
Y235
Y228
R217
Y246
D105
E102
N106
D109
D
Y235
Y228
R217
Y246
D105
E102
N106

Figure 3.6 Binding mode of the selected hits into MD reference snapshot of PARP-1 Val101Ala (A and B) and wild-type (C and D) PARP-1 catalytic domain. A) 3.1. **B)** 3.2. **C)** 3.3. **D)** 3.4. Dashed lines represent interactions between binding site residues and bound ligands. Green colour represents hydrogen bond interactions; Orange indicates π–cation interactions; blue denotes π–anion interactions pink denotes π–π stacked; yellow represents amide–π interactions; light pink denotes hydrophobic interactions (alkyl and π–alkyl); brown indicates charge-charge interactions. This figure was created using Discovery Studio Visualizer 16.1.0.

Concerning the impact of PARP-1 catalytic domain flexibility in the binding mode and binding affinity of the top retrieved hits, different results were obtained among the best ranking molecules (**Table 3.1**).

The compounds **3.1** and **3.2**, which were both retrieved from the screening against **MIF_Pharma3**, were first docked into crystal and MD reference snapshot of PARP-1 Val101Ala, with compound **3.1** showing similar binding affinities for both crystal structure and MD reference snapshot**.** Conversely, compound **3.2** exhibits a slight better affinity to the crystal structure.

Table 3.1 Docking score data and PARP-1 inhibition activity for the hits studied. [a]) PARP-1 inhibition was determined using HT Universal Colorimetric PARP Assay Kit (Cat #4677-096-k).

Compound code	**Docking score (Glide SP-mode)**				**PARP-1[a] inhibition (%, 100 μM)**
	PARP-1 wild-type crystal	**PARP-1 wild-type MD**	**PARP-1 Val101Ala crystal**	**PARP-1 Val101Ala MD**	
3.1	**-6.911**	**-9.634**	**-7.304**	**-7.358**	**12.68**
3.2	**-7.805**	**-7.838**	**-7.007**	**-6.025**	**17.30**
3.3	**-9.052**	**-7.093**	**-**	**-**	**16.80**
3.4	**-8.661**	**-7.092**	**-**	**-**	**19.64**
3.8	**-7.452**	**-**	**-**	**-**	**28.48**
3.9	**-7.747**	**-**	**-**	**-**	**31.87**

Interestingly, when docked into the wild-type PARP-1 catalytic domain, compound **3.1** showed a higher binding affinity to the MD reference snapshot when compared with the crystal structure.

Conversely, compounds **3.3** and **3.4** displayed a higher binding affinity when docked into the crystal structure of the wild-type PARP-1 catalytic domain, in comparison with MD reference snapshot. This is translated into a different binding mode of these molecules within the crystal structure or MD reference snapshot of wild-type PARP-1 catalytic domain. The two hits shared the same binding mode for the same target structure (crystal or MD reference snapshot) that suggests small protein conformational motions during MD, which were especially observed in D-loop residues, affects the binding mode of these molecules (**Figure 3.4 and 3.7**).

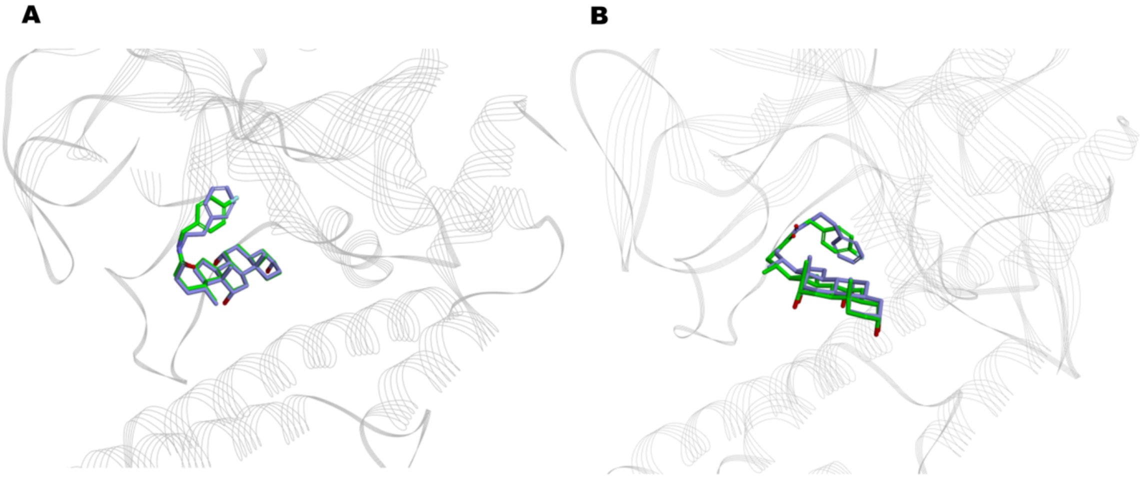

Figure 3.7 Binding mode of 3.3 and 3.4 into crystal structure A) and MD reference snapshot B) of wildtype PARP-1 catalytic domain. This figure was created using Discovery Studio Visualizer 16.1.0.

It is also worth mentioning that compounds **3.1** and **3.2**, both resulting from the screening against **MIF_Pharma3** and designed from MD reference snapshot PARP-1 Val101Ala catalytic domain, displayed strong binding affinities not only for PARP-1 Val101Ala, but also for wild-type PARP-1 catalytic domain. Although an aromatic group of compound **3.1** establish an π–alkyl and an amide–π interaction with Ala101 (**Figure 3.6A**), this did not seem essential for a strong binding affinity, since that molecule displayed higher docking score values when docked into MD reference snapshot of wild-type PARP-1 catalytic domain, when compared with PARP-1 Val101Ala (**Table 3.1**). In fact, the highest binding affinities for compounds **3.1** and **3.2** were obtained when these molecules were docked into MD reference snapshot of wild-type PARP-1 catalytic domain.

Taken together, deeper studies should be carried out in order to better understand the influence of Val101Ala mutation in PARP-1 activity.

3.3.4. PARP-1 inhibitory activity

In order to evaluate the ability of the four promising hits to inhibit PARP-1, the HT Universal Colorimetric PARP Assay was used. Two molecules chosen from commercial databases (**3.1** and **3.2**), as well as two cholic acid derivatives (**3.3** and **3.4**), which were obtained by chemical synthesis according to the literature [320], were screened at 100 μM. A maximum of 19.6% of PARP-1 inhibition activity was retrieved for compound **3.4** (**Table 3.1**). Because of the lack of strong inhibitory activity against PARP-1, IC_{50} values were not determined.

In another attempt to identify new promising PARP-1 inhibitor candidates, a new docking run with all compounds from the ST database and PARP-1 catalytic domain were conducted. Two compounds, **3.8** and **3.9** (**Figure 3.8**), were selected to evaluate PARP-1 inhibitory activity. Despite not fitting any of the pharmacophore models, these compounds showed promising docking results into wild-type PARP-1 catalytic domain (as shown in **Table 3.1**), interacting with key binding site residues, such as the Gly202 (**3.8**) and the Tyr246 (**3.8** and **3.9**). Interestingly, these molecules are betulinic acid derivatives. Since betulinic acid is a Pol β inhibitor [11], a key protein involved in BER, alongside PARP-1, their putative PARP-1 inhibitory activity could be an interesting achievement in the search for BER inhibitors. Nevertheless, the most promising PARP-1 inhibition activity was shown by **3.9**, which only inhibited 32% of PARP-1 activity at 100 μM.

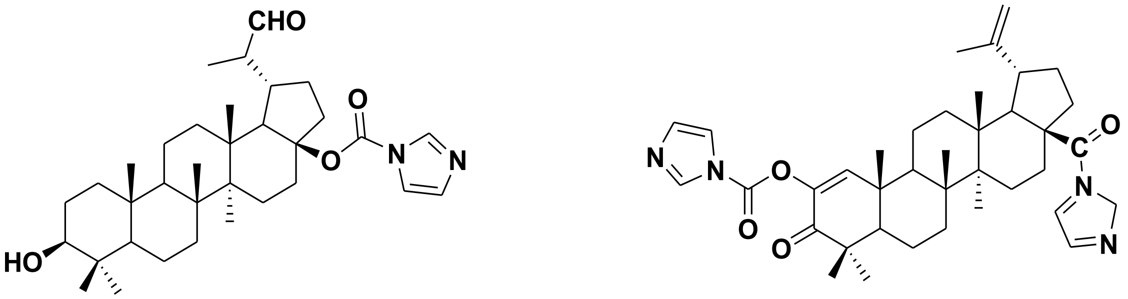

3.8 **3.9**

Figure 3.8 Betulinic acid derivatives selected from ST database for *in vitro* studies against PARP-1 due to their promising docking results.

After a deep analysis of all methodologies applied in the attempt to discover new PARP-1 inhibitors, some reasons may be pointed out to explain the unsuccessful results obtained. First of all, the use of a single structure resulting from MD simulations to design each pharmacophore model may not translate all the key binding site features. Although MD is essential to take into account the receptor flexibility and to better characterize the binding interface between PARP-1 and different ligands, an adequate sampling of conformational states usually involves a higher timescale MD run simulations, in the microsecond range [321]. This is particularly important in the presence of loops that display a relevant role in the enzyme activity, since they are one of the most flexible parts of an enzyme [322]. Considering that three of the four pharmacophore models (**MIF_Pharma2**, **MIF_Pharma3**, and **MIF_Pharma4)** displayed at least a feature directed to the D-loop residues, and only the representative structure of the main cluster of uncomplexed PARP-1 catalytic domain (MD reference snapshot of wild-type and PARP-1 Val101Ala catalytic domain), subjected to 20 ns MD simulations, was considered in the pharmacophore modelling, an increased simulation time running and/or the use of representative structures of the clusters that include almost all of the conformation sampling, should be considered.

On the other hand, the use of only the minima points of favourable interactions with the PARP-1 catalytic domain to model pharmacophoric hypotheses, without considering the shape and steric hindrance of the binding site may have also contributed to a higher number of false positives, and compounds with low inhibition, as those ones evaluated. Thus, the application of excluded volume spheres in the pharmacophore models generation could have overcome this issue, since they represent steric regions of binding site where the presence of ligand substituent groups is not allowed, being directly associated with a lower number of hits and false positives in the VS pipeline [323].

A further point to be taken into consideration is the molecular docking strategy applied. Even though docking calculations are performed in order to reproduce experimental binding affinities, the scoring functions used in these calculations are often not able to correctly predict them. This is the reason why docking is used to hit identification rather than lead optimization, since it is unable to accurately discriminate between true potent and weakly active molecules [324]. This might explain the weak PARP-1 inhibitory activity displayed by all compounds under investigation, despite their promising docking results. Nevertheless, the rescoring of the putative best poses identified by an initial docking run was reported as a way to improve the correctly distinction of true potential and weakly active compounds [324]. Thus, the rescoring of the top-scoring poses for the best ranked compounds may have led to a more accurate hit selection, which could lead to the identification of truly potent PARP-1 inhibitor candidates.

It is also worth noting that the high flexibility showed by the lateral chain of cholic acid derivatives **3.3**, and **3.4** might have contributed to an overestimated binding affinity prediction, which resulted in a weak PARP-1 inhibitory activity showed by these molecules.

3.4. CONCLUSIONS AND FURTHER DEVELOPMENTS

A receptor-based pharmacophore approach was applied in an attempt to find out novel and selective PARP-1 inhibitors. MIFs calculated on the PARP-1 catalytic domain (wild-type and Val101Ala) subject to MD simulations were used for the pharmacophore modelling.

After VS calculations using structure-based pharmacophore models, docking studies with the top-scoring compounds were performed. Even though promising binding affinities were shown by the selected molecules, none of them revealed a promising PARP-1 inhibitory activity.

Nonetheless, some limitations of the methodology used were pointed out in order to develop a new approach, able to conveniently identify promising PARP-1 inhibitor candidates.

4. CHAPTER IV

NOVEL PARP-1 INHIBITOR SCAFFOLDS DISCLOSED BY A DYNAMIC STRUCTURE-BASED PHARMACOPHORE APPROACH

Salete J. Baptista, Maria M.C. Silva, Elisabetta Moroni, Massimiliano Meli,
Giorgio Colombo, Teresa C.P. Dinis, Jorge A. R. Salvador

Novel PARP-1 inhibitors scaffolds disclosed by a dynamic structure-based pharmacophore approach

PLoS One, 2017 Jan 25;12(1):e0170846

https://doi.org/10.1371/journal.pone.0170846

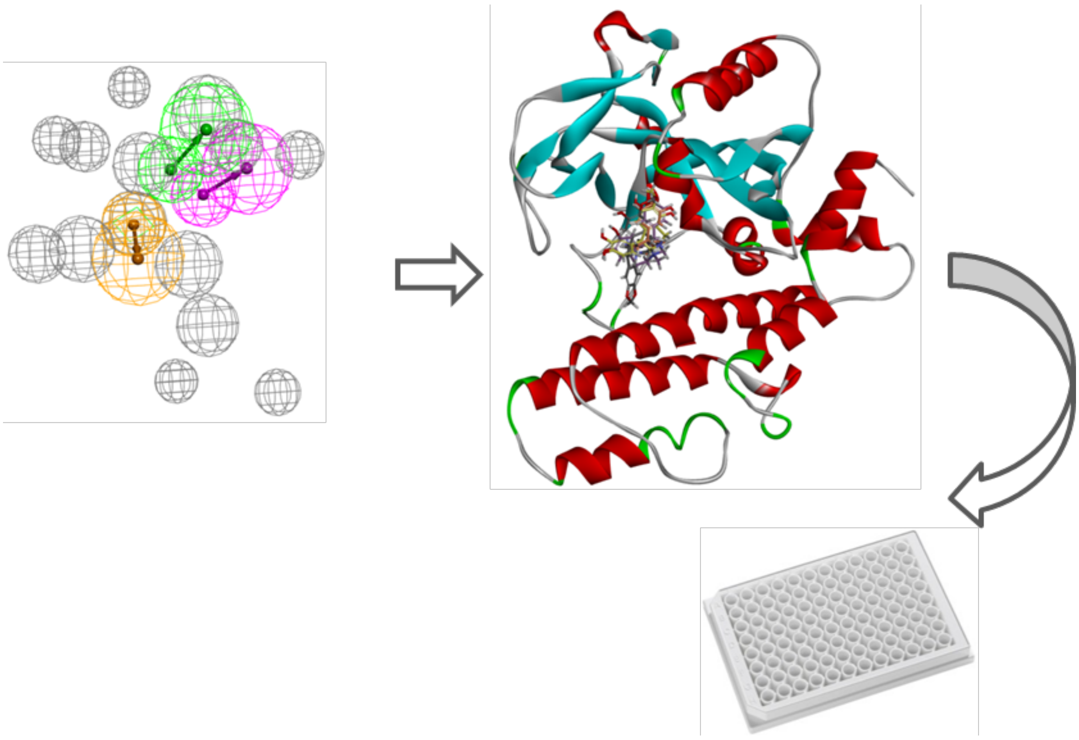

Highlights

- A dynamic structure-based strategy was applied to discover novel PARP-1 inhibitors.
- Three novel PARP-1 inhibitor scaffolds were disclosed, **NSC131753**, **NSC86342**, and **NSC121848**.
- **NSC131753** was the most active PARP-1 inhibitor.

4. CHAPTER IV

Novel PARP-1 inhibitor scaffolds disclosed by a dynamic structure-based pharmacophore approach

4.1. OVERVIEW

The development of poly(ADP-ribose)polymerase-1 (PARP-1) inhibitors as a therapy for several pathologies has been pursued, with special relevance in cancer and ischemic diseases [254]. The by-product of NAD+ cleavage, nicotinamide, has been used as the structural basis for the discovery of PARP-1 inhibitors. A large number of nicotinamide/benzamide derivatives have been studied, and some compounds have entered clinical trials as chemopotentiators in combination with anti-cancer drugs, as well as stand-alone agents in tumours with BRCA1/2 mutations, taking advantage of synthetic lethality [89, 238, 255, 256]. The drug candidate olaparib **1.1** (Lynparza^{TM}) was recently approved as the first PARP-1/2 inhibitor to treat advanced ovarian cancer in women with defects in the BRCA1/2 genes, who were previously treated with three or more chemotherapeutic lines [257]. Nevertheless, a polypharmacological profile has been assigned to PARP-1 drug candidates. The inhibition of other PARP isoforms, or even the interaction with other inter-family targets, was noted for several inhibitors in clinical trials [13, 254]. Moreover, olaparib **1.1** was reported to act as a substrate of the p-glycoprotein (P-gp) efflux pump, one of the mechanisms that are associated with resistance to PARP inhibitors [238, 258]. Clearly, more in-depth studies of the determinants of the PARP-1 recognition features are needed to develop novel and more selective PARP-1 inhibitors.

Computational methods have emerged as an important tool in drug discovery, as they disclose key features in the ligand-receptor binding interactions and allow the screening of large compound libraries, thus saving time and resources [195]. Moreover, molecular dynamics (MD) simulations have become an important method to solve one of the biggest challenges in drug discovery, i.e., the use of a single crystal structure of a protein to predict the putative ligand-binding site, not considering the target plasticity that is involved in ligand binding [141].

Different studies have combined MD with pharmacophore modelling, taking advantage of receptor flexibility to build structured-based pharmacophore models. In general, a wide array of drug discovery examples based on this approach have shown that they provide a better prediction of truly active compounds compared with inactive ones and are able to find potential leads for different targets under investigation [10, 228, 246, 259-261] .

In this work, a dynamic structure-based pharmacophore methodology was pursued to identify new scaffolds with PARP-1 inhibitory activity. A virtual screening of the available compounds databases was performed using the pharmacophore models generated, and the top-scoring compounds identified by molecular docking studies were validated through an *in vitro* PARP-1 inhibition assay.

4.2. MATERIALS AND METHODS

4.2.1. MD simulations

Four inhibitors that bound to the PARP-1 catalytic domain were retrieved from the Protein Data Bank (PDB codes: 2RCW, 3GN7, 3GJW, 3L3L). Crystal structures were processed using the Protein Preparation Wizard tool in Maestro Suite (Release 2013-1-9.4, Schrödinger, LLC, New York, NY, 2013). Water molecules were removed and bond orders were assigned.

For each ligand-bound system, MD simulations in explicit water were performed using the Amber package, v12. Amber FF99SB [62] and Generalized Amber Force Field (GAFF) [48] were assigned to the protein and ligands, respectively. Systems were solvated with TIP3P water molecules [22] in a truncated octahedral box, counter ions were added to neutralize the system net charge, and the periodic boundary conditions were applied. The final systems were composed of ~ 33400 atoms.

After minimizations, systems were submitted to an equilibration phase for 1 ns in NVT conditions, in which protein and ligand atoms were position restrained with a constant force of 10 kcal/mol, to allow relaxation of the solvent molecules. A final production phase of 20 ns was performed and trajectory snapshots were saved at every 10 ps, for each system. The Langevin temperature equilibration scheme was used to keep the temperature constant (300 K), and a constant pressure periodic boundary was applied (1 atm). Electrostatic and Lennard-Jones forces were assessed using the Particle Mesh Ewald summation method [42] and a cut-off of 10 Å, respectively. The SHAKE algorithm [311] was applied to constrain bonds that involved hydrogen atoms.

GROMACS [262] was used to perform the trajectory analysis. For each system, a conformational cluster analysis was carried out using a cut-off of 0.06-0.07 nm RMSD (root mean square deviation) between the backbone superposition of different structures. All snapshots saved from each MD trajectory were extracted and used to perform cluster analysis. To characterize the dynamics features of active site–ligand interactions in the PARP-1 catalytic domain, only the residues that were set to 5 Å around the inhibitor were taken into account in the cluster analysis.

4.2.2. Structure-based pharmacophore modelling and validation

Four different pharmacophore models were built based on the protein-ligand interactions observed after MD simulations. For each ligand-bound system, the clusters that represented more than 80% of the protein structural variability for each simulated system were selected to generate structure-based pharmacophores, using The Receptor-Ligand Pharmacophore Generation protocol of Accelrys Discovery Studio (DS), Accelrys, San Diego, USA. This protocol uses receptor-ligand interactions to create selective pharmacophore models. Hydrogen bond acceptor (HBA), hydrogen bond donor (HBD), hydrophobic (HY), negative ionizable (NI), positive ionizable (PI), and ring aromatic (RA) features, as well as the excluded volume spheres set to 5 Å around the inhibitor, were considered in the generation of the pharmacophore models. The hypotheses created were validated by a set of known PARP-1 ligands and decoys obtained from Database Useful Decoys Enhanced (DUD_E) – http://dude.docking.org/, using the validation option incorporated in the protocol. For each cluster, the hypotheses were ranked based on specificity and sensitivity, and the one that presented the best accuracy was chosen.

The best hypotheses that were retained for each cluster of a specified complex were superimposed, and the average coordinate point for each feature, including the excluded volumes spheres, was determined.

Four final pharmacophore models were created, one for each complex. As a final validation, the pharmacophore models were screened against the PARP-1 actives and decoys, to evaluate how well they discriminate active molecules from inactive ones. Moreover, the presence of chemical features that were essential for the interaction with key residues in the PARP-1 catalytic domain was taken into account in the validation of the pharmacophore models.

4.2.3. Database preparation and pharmacophore-based virtual screening

The National Cancer Institute (NCI) [313] – https://cactus.nci.nih.gov/download/nci/ and DrugBank [314] (http://www.drugbank.ca/) databases were downloaded. PARP-1 ligands and decoys were downloaded from the DUD_E database [325]. Seven hundred and forty-two actives (affinity ≤1 μM) and 30403 decoys (affinity ≥30 μM) were divided and converted into two databases, DUD_PARP1_ligands and DUD_PARP1_decoys, respectively. The “FAST” conformational analysis model of the catDB program was used to build the four databases, and a maximum of 255 conformations were generated for each molecule.

The four pharmacophore models obtained were used to screen the NCI and DrugBank databases using the “fast flexible database search” settings of Catalyst [291], to search for novel structural scaffolds with an ability to inhibit PARP-1.

The retrieved hits were subjected to different drug-like filters. Lipinski’s rule of five [263] and the modified Veber rule [17] (not more than 7 routable bonds) were applied. A maximum polar surface area was set to 140.

4.2.4. Docking Studies

The docking studies were performed using Glide (version 5.8). Standard precision (SP) and extra precision (XP) modes were applied, using the OPLS-AA force field [26].

The protein retrieved from the crystal structure of A620223 binding to PARP-1 (PDB code: 2RCW) was used to define the binding site. The Preparation Wizard tool was applied and all water molecules were removed from the crystal. A 15×15×15 Å receptor grid centred on the co-crystallised ligand was generated.

The final selected hits, as well as a set of know PARP-1 inhibitors (downloaded from BindingDB database (http://www.bindingdb.org)), were prepared using the LigPrep module (Schrödinger, LLC, New York, NY, 2013). The pH was set to 7.4 and a maximum of 5 stereoisomers per ligand were generated. The lowest energy ring conformation was kept for each stereoisomer.

An initial docking was performed using the SP-mode and 25 poses were kept for each molecule. A cut-off based on the docking score of reference PARP-1 inhibitors was used, and ligands with the highest score were subjected to XP docking.

4.2.5. PARP-1 enzyme assay

PARP-1 inhibition was evaluated using the HT Universal Colorimetric PARP Assay kit (Catalog #4677-096-K; Trevigen, Gaithersburg, MD, USA), in line with the instructions provided by the manufacturer. The assay evaluates the incorporation of biotinylated poly(ADP-ribose) onto histones proteins in a 96-well plate. Briefly, 10 μL of the test compounds were mixed with 15 μL of PARP-1 enzyme (0.5 U) into rehydrated histone-coated wells for 10 min at room temperature. Subsequently, 25 μL of PARP cocktail containing biotinylated NAD, activated DNA, and PARP buffer were added, and the solutions were incubated again for 60 min. After washing the wells, the detection reaction was performed according to the manufacturer’s protocol and absorbance was recorded at 450nm in a synergy HT plate reader. Stock solutions of the test compounds were prepared in DMSO and serially diluted to the required concentrations with 1× PARP buffer. To assess the effect of the vehicle on enzyme activity, parallel experiments were performed by substituting the test compound with an equivalent volume of DMSO. IC_{50} values for the most promising hits were determined by plotting the inhibition data of each compound at different concentrations against the log of the concentration of the inhibitor, using the GraphPad Prism software, version 5. At least six different concentrations of the test compounds were used. A minimum of three independent assays were performed for each sample, and the results are displayed as mean ± standard error of the mean (SEM).

4.2.6. Nuclear Magnetic Resonance studies

1D and 2D nuclear magnetic resonance (NMR) structure elucidation of the NSC86342, NSC121848, and NSC131753 compounds was obtained using a Brucker Digital NMR-Avance 400 spectrometer, with CD_3OD as the internal standard.

4.2.7. NSC131753 MD simulations

MD simulations were performed using (*R*)-NSC131753 and (*S*)-NSC131753 complexed with the PARP-1 catalytic domain, using top XP Glide poses as input structures. The MD simulations were performed according to the protocol described above for the four complexes taken from PDB, with equilibration and production phases of 50 ps and 100 ns, respectively. Three replicas (100 ns) were run for each system with different initial velocities, to increase sampling.

MD trajectory analysis was performed using the GROMACS package.

4.3. RESULTS AND DISCUSSION

4.3.1. Structural and dynamic characterization of different complexes with known inhibitors.

In this work, MD simulations with different known small-molecule inhibitors were carried out to characterize the dynamic features of active site–ligand interactions in the PARP-1 catalytic domain. In this context, the aim of MD simulations was not the full sampling of the events underlying complex formation or the exploration of ligand induced conformational changes, which can be considered as being absent, given the high global similarity of the starting crystal structures, with a maximum RMSD (as calculated on protein backbone atoms) of 0.62 Å (**Figure 4.1**). Rather, a comparative analysis of the trajectories from the different complexes was used to identify the salient features of the dynamic adaptation of PARP-1 to diverse active site inhibitors. Our general goal was to characterize the cross-talk between the ligands and the protein and highlight the binding interactions that were consistently preserved in multiple configurations, in addition to the ones that were immediately evident from crystal structures. Those conserved binding interactions were then used to develop dynamic pharmacophore models aimed at expanding the chemical diversity space of PARP-1 inhibitors.

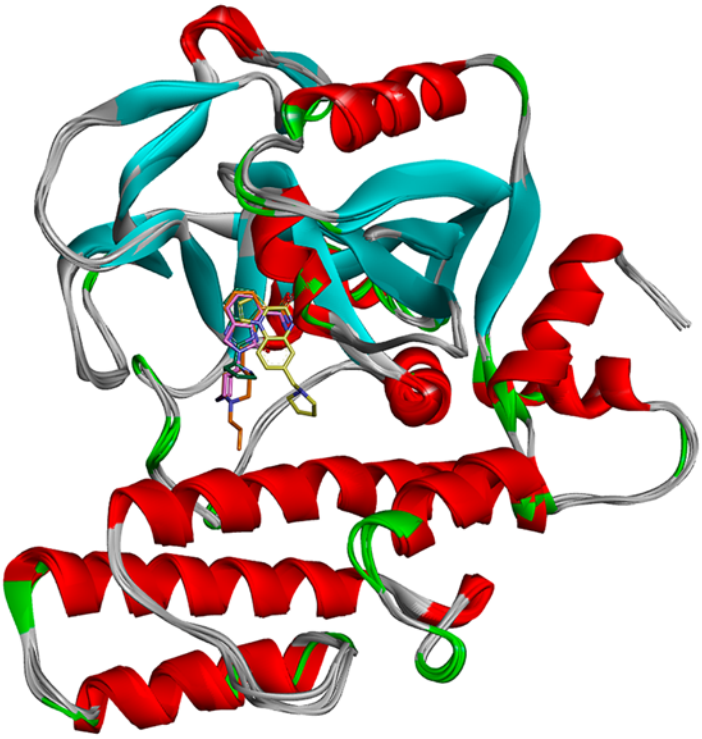

Figure 4.1 Superposition of the starting crystal structures of 2RCW, 3L3L, 3GN7 and 3GJW. This figure was created using Discovery Studio Visualizer 16.1.0.

The analysis of the main clusters revealed that the key interactions that were present in the co-crystal structures of PARP-1 with four different inhibitors were conserved. Such interactions consisted of three stable hydrogen bonds: two between the amide backbone of Gly202 and the amide moiety of the inhibitors and one between the OH group of Ser243 and the carbonyl group of inhibitors, as presented in **Table 4.1A**, as well as a π–π stacking interaction involving Tyr246 and the aromatic core of the ligands. Furthermore, MD simulations showed that the tyrosine residues present in the binding site were involved in different π–

interactions. To define the importance of the tyrosine residues, the contacts between Tyr228, Tyr235, and Tyr246 and the ligands were monitored during 20 ns MD run (**Figure 4.2**). Depending on the bound inhibitors, different tyrosine residues were engaged. Tyr228 appeared to be essential for the π–cation interaction with the protonated amine moiety of the 2RCW and 3L3L ligands, with occupancy of 99% and 100%, respectively, during MD trajectories. For the 3GN7 inhibitor, both Tyr228 and Tyr246 were implicated in this type of interactions, with occupancy of 65.45% and 47.50%, respectively. Moreover, Tyr235 and Phe236 were involved in amide–π interactions with the phenyl rings of the 2RCW, 3GN7, and 3GJW ligands. In addition, Ala237 and the alkyl side chain of Lys242 participated in hydrophobic interactions with the phenyl ring of each inhibitor along the MD trajectory for all ligand-bound systems analysed (**Table 4.1B**). The protonated amine group of each ligand also appeared to be important for the establishment of charge-charge interactions with some charged residues present in the binding site, such as Glu102, Asp105, and Asp109 (**Table 4.1C**). This type of interaction was especially relevant for 3GJW. The 3GJW ligand was involved in charge-charge interactions with Asp105 (:OD1) for 84.65% of the MD run time. The main interactions for each complex along MD trajectories (the first cluster) are shown in **Figure 4.3**.

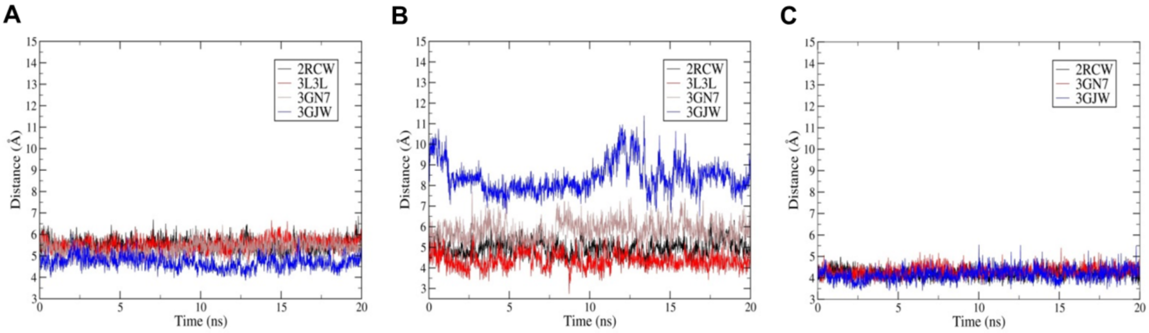

Figure 4.2 The plot distances involving the tyrosine residues and ligands along MD trajectories. A) Distance between Tyr246 centroid π ring and the aromatic core of ligands. **B)** Distance between Tyr228 centroid π ring and the protonate amine moiety of each ligand. **C)** Distance between the centroid of amide group (formed by the CO of Tyr235 and N of Phe236) and phenyl ring of each ligand.

Table 4.1 A) Hydrogen bonds, B) hydrophobic interactions (namely alkyl and π–alkyl interactions) and C) charge-charge interactions with greater occupancy during MD trajectories for 2RCW, 3L3L, 3GN7 and 3GJW complexes.

A

Hydrogen bonds			
PDB ID	**Donnor**	**Acceptor**	**%Occupancy**
2RCW	Gly202:N	AAI:O1	40.05
	Ser243:OG	AAI:O1	64.80
	AAI:N3	Gly202:O	73.55
3L3L	Gly202:N	L3L:O2	54.75
	Ser243:OG	L3L:N3	38.85
	L3L:N3	Gly202:O	64.35
	L3L:N1	Gly227:O	23.80
3GN7	Gly202:N	3GN:O12	38.80
	Ser243:OG	3GN:O12	44.50
	3GN:N1	Gly202:O	61.70
3GJW	Gly202:N	GJW:O1	27.15
	Ser243:OG	GJW:O1	62.65
	GJW:N3	Gly202:O	74.80

B

Alkyl and π–alkyl interactions		
PDB ID	**Residue**	**%Occupancy**
2RCW	Ala237	68.00
	Lys242	97.70
3L3L	Ala237	48.00
	Lys242	84.70
3GN7	Ala237	52.20
	Lys242	75.70
3GJW	Ala237	66.65
	Lys242	64.55

C

Charge-charge interactions			
PDB ID	**Residue**		**%Occupancy**
2RCW	Glu102	OE1	29.40
		OE2	32.50
	Asp105	OD1	30.30
		OD2	26.35
3L3L	Glu102	OE1	33.25
		OE2	37.60
3GN7	Glu102	OE1	29.15
		OE2	32.50
3GJW	Asp105	OD1	84.65
		OD2	19.65
	Asp109	OD1	30.95
		OD2	23.05

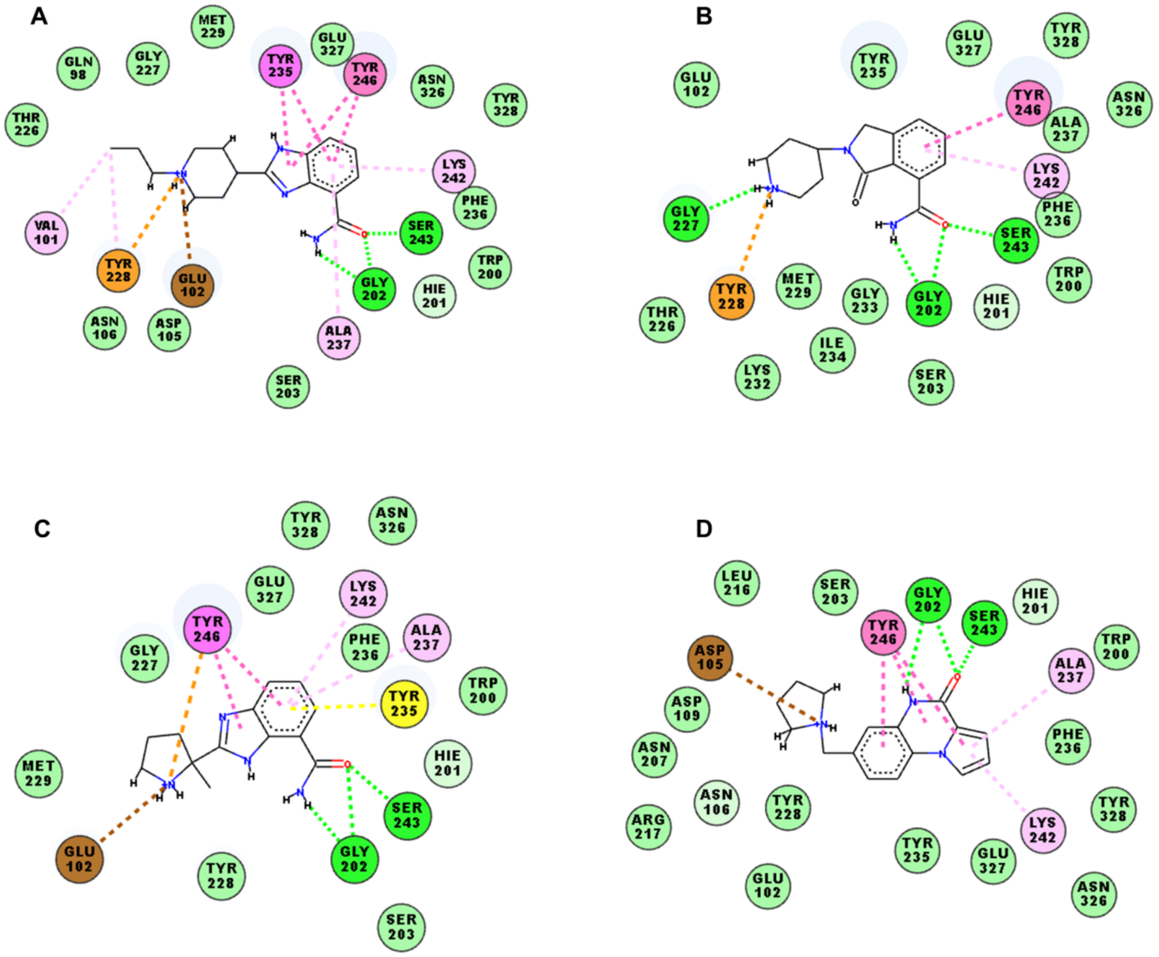
A
MET 229
GLN 98
GLY 227
TYR 235
GLU 327
TYR 246
ASN 326
TYR 328
THR 226
LYS 242
PHE 236
SER 243
TRP 200
VAL 101
TYR 228
GLU 102
GLY 202
HIE 201
ASN 106
ASP 105
ALA 237
SER 203
B
GLU 327
TYR 328
TYR 235
GLU 102
TYR 246
ASN 326
ALA 237
LYS 242
PHE 236
GLY 227
SER 243
TRP 200
MET 229
TYR 228
GLY 233
GLY 202
HIE 201
THR 226
ILE 234
LYS 232
SER 203
C
TYR 328
ASN 326
GLU 327
LYS 242
TYR 246
GLY 227
PHE 236
ALA 237
TRP 200
TYR 235
HIE 201
MET 229
SER 243
GLY 202
GLU 102
TYR 228
SER 203
D
LEU 216
SER 203
GLY 202
HIE 201
SER 243
TYR 246
TRP 200
ASP 105
ALA 237
ASP 109
ASN 207
PHE 236
ASN 106
TYR 228
ARG 217
TYR 328
TYR 235
LYS 242
GLU 327
GLU 102
ASN 326

Figure 4.3 2D-Ligand interaction diagrams for each ligand complexed with PARP-1 catalytic domain along MD run. Dashed lines represent interactions between binding site residues and bounded ligands. Green color pointed to hydrogen bond interactions; Orange indicates π–cation interactions; pink denotes π–π stacked; yellow pointed to amide–π interactions; light pink denotes hydrophobic interactions (alkyl and π–alkyl); brown indicates charge-charge interactions, and turquoise indicate Van der Waals interactions. **A)** 2RCW. **B)** 3L3L. **C)** 3GN7). **D)** 3GJW. This figure was created using Discovery Studio Visualizer 16.1.0.

By exploring the diversity and the motion of the ligands, as well as the flexibility of the binding site residues, four structure/dynamics-based pharmacophores were generated based on the ligand-protein interactions that were monitored during the MD trajectories. The conserved hydrogen bonds, as well as the π–π stacking, the π–cation and charge-charge interactions observed to a higher extent during MD, were considered to generate structure-based pharmacophores.

For each complex, seven representative structures (matching more than 80% of the structural variability) were taken into account to build the pharmacophore models.

For all pharmacophoric hypotheses, the Receptor-Ligand Pharmacophore Generation protocol in DS pointed key interactions between the PARP-1 catalytic domain and the ligand, and generated excluded volume spheres that were correlated with steric regions in the binding site that may not be engaged by the ligand substituent groups. In this context, the characterization of the mechanisms of the formation/disappearance of pockets around the ligands due to the immediate conformational response of the protein to known inhibitors can aptly indicate the positions at which the addition/modification of specific substituent groups may allow optimal extensions of binding interactions into previously uncharacterized regions.

The comparison of the excluded volume spheres obtained based on the crystal and the representative structure after MD simulations for each ligand-bound system (**Figure 4.4**) revealed that the excluded volume spheres were generally pointed to the same residues, especially in the nicotinamide-binding pocket, which comprises residues such as Gly202, Ser243 and Tyr246 (**Figure 3.3**). Analyses of root mean square fluctuation (RMSF) for all four complexes (**Figure 4.5**) revealed that the regions containing nicotinamide-binding residues were quite stable. The highest fluctuations were observed in loop regions (60-67; 78-94; and 118-128).

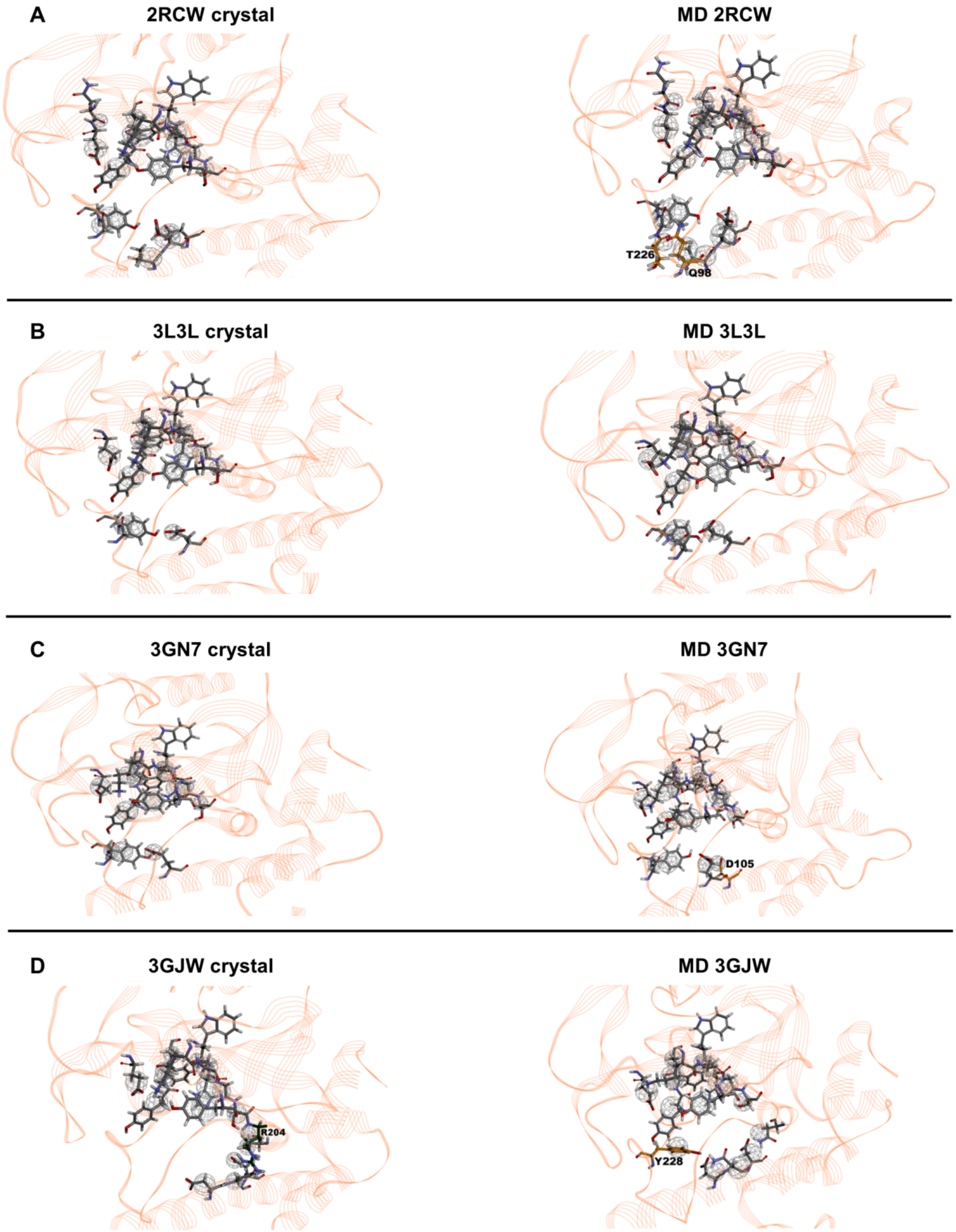
A
2RCW crystal
MD 2RCW
T226
Q98
B
3L3L crystal
MD 3L3L
C
3GN7 crystal
MD 3GN7
D105
D
3GJW crystal
MD 3GJW
R204
Y228

Figure 4.4 Representation of the PARP-1 binding site with excluded volume spheres. The excluded volume spheres, set to 5 Å around each inhibitor complexed with the binding site, were obtained from the crystal and the representative structure after MD simulations for 2RCW, 3L3L, 3GN7 and 3GJW complexes. This figure was created using Discovery Studio Visualizer 16.1.0.

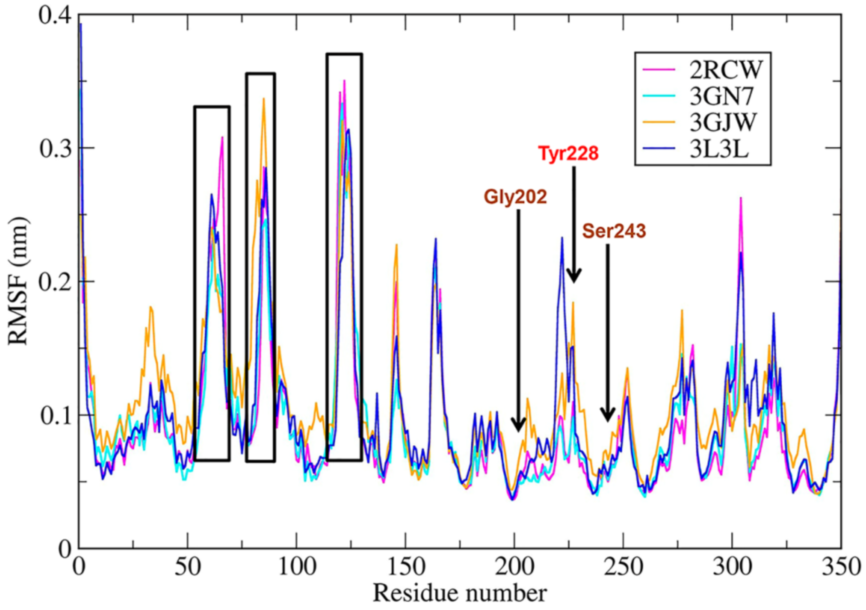

Figure 4.5 RMSFs of complexes along 20 ns MD run.

4.3.2. Pharmacophore model building

SB_Pharma1, which was based on the 2RCW complex, displayed five functional features, including an HBD and an HBA pointed to Gly202, an HY pointed towards Ala237 and Lys242 (alkyl side chain), an RA directed to Tyr246, and a PI pointed to Tyr228. Nineteen excluded volume spheres were identified, which represented an additional two spheres compared with the crystal structure. One of them was directed to Gln98 (side chain) and the other to Thr226 (backbone). **SB_Pharma2**, which was the pharmacophore model obtained from 3L3L, exhibited four features and 14 excluded volume spheres, pointed to the same residues of the crystal structure. One HBA and one HBD directed to Gly202, an HY pointed towards Ala237 and Lys242 (alkyl side chain), and a PI pointed to Tyr228 were observed. **SB_Pharma3** and **SB_Pharma4** were generated from 3GN7 and 3GJW, respectively. Both pharmacophore models exhibited three similar features: an HBA and an HBD pointed to Gly202, an HY centre directed towards Ala237 and Lys242 (alkyl side chain) and an RA also directed to Tyr246. A PI centre was pointed to Tyr228 or even Tyr 246 in **SB_Pharma3**, and to Asp105 in **SB_Pharma4**. Excluded volume spheres (15 and 16, respectively) were also identified. **SB_Pharma3** displayed an extra excluded volume (compared with the 3GN7 crystal structure) pointing towards the Asp105 side chain that changed side chain orientation during the MD simulation (**Figure 4.6**). Moreover, **SB_Pharma4** also showed an additional excluded volume sphere, directed to Tyr228, which side chain exhibited considerable flexibility along the MD trajectory (**Figure 4.4D and 4.5**). The excluded volume directed to Arg204, which was observed in the 3GJW crystal structure, was not set in the final pharmacophore model obtained after MD. As illustrated in **Figure 4.3D**, pointing to this active site residue did not appear to be essential for productive interaction. The final structure-based pharmacophore models (**SB_Pharma1**, **SB_Pharma2**, **SB_Pharma3**, and **SB_Pharma4**) obtained from the superposition of dominant conformations for each ligand-bound system, as well as those obtained from PDB crystal structures, are elucidated in **Figure 4.7**.

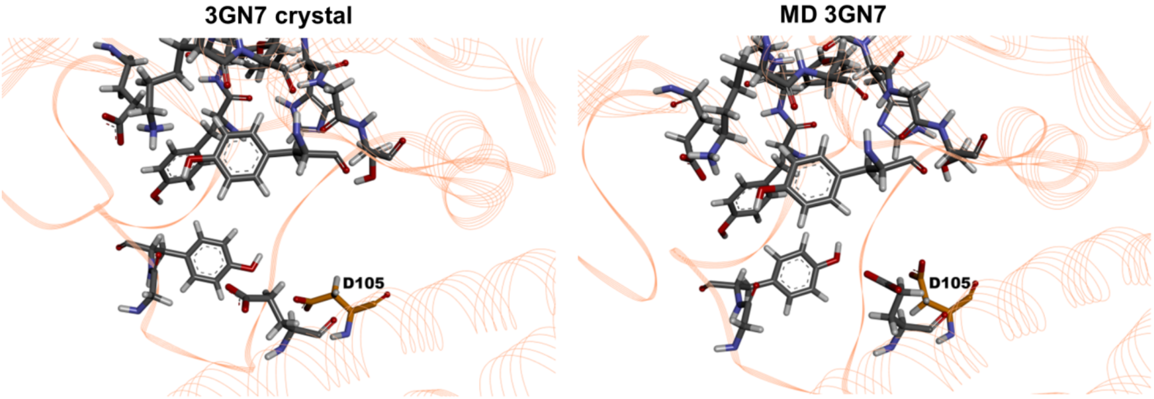

Figure 4.6 Asp105 side chain orientation in the crystal structure and after MD simulations (representative structure). This figure was created using Discovery Studio Visualizer 16.1.0.

The analysis of four structure-based pharmacophore models supported the essential role of Gly202 as an HBD and HBA, as well as the presence of important hydrophobic residues, namely Ala237 and Lys242 (alkyl side chain). Moreover, Tyr228, Tyr235, and Tyr246 were shown to be important for the establishment of different types of π-interactions. The aromatic feature directed to Tyr246, for instance, was necessary to mimic the relevant role of stacking interactions in driving effective binding to the PARP-1 catalytic domain. Finally, the presence of charge-charge interactions mediated by charged residues, as exemplified by Asp105, may be important for the identification of additional interactions that increase the binding affinity between the ligand and the protein.

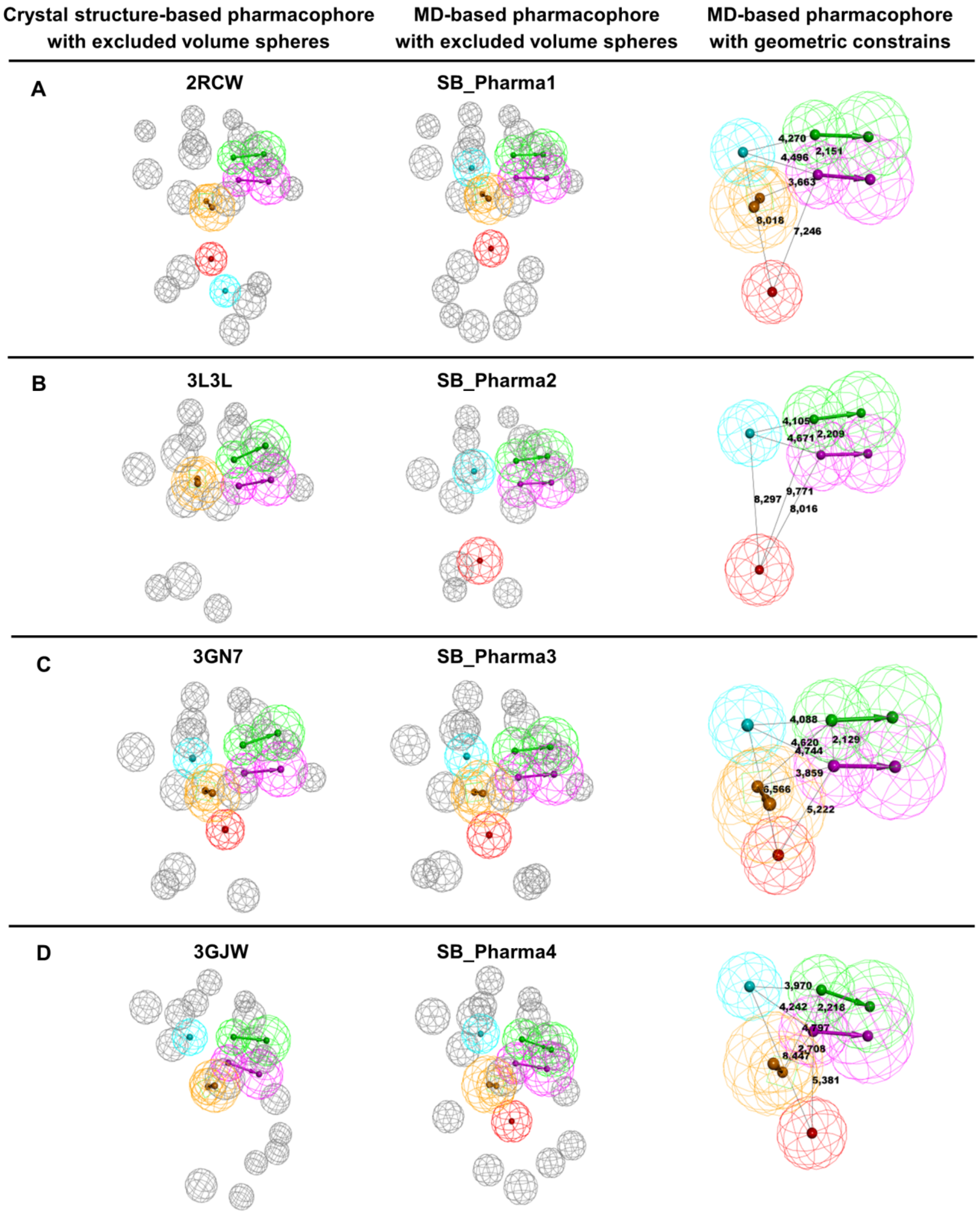
Crystal structure-based pharmacophore with excluded volume spheres
MD-based pharmacophore with excluded volume spheres
MD-based pharmacophore with geometric constrains
A
2RCW
SB_Pharma1
4,270
2,151
4,496
3,663
8,018
7,246
B
3L3L
SB_Pharma2
4,105
4,671
2,209
8,297
9,771
8,016
C
3GN7
SB_Pharma3
4,088
4,620
2,129
4,744
3,859
6,566
5,222
D
3GJW
SB_Pharma4
3,970
4,242
2,218
4,797
2,708
8,447
5,381

Figure 4.7 Representation of structure-based pharmacophore models obtained from crystal structures and the dominant conformations after MD simulations. Green color indicates hydrogen bond acceptor (HBA); magenta denotes to hydrogen bond donor (HBD); cyan shows hydrophobic center (HY); yellow indicates ring aromatic (RA); and red denotes to positive ionizable center (PI). This figure was created using Discovery Studio Visualizer 16.1.0.

4.3.3. Pharmacophore-based virtual screening and validation

The four pharmacophore models were validated against DUD_PARP1_ligands and DUD_PARP1_decoys, which were generated by Catalyst [291], and both sensitivity and specificity were calculated (**Table 4.2**). Sensitivity was related to the fraction of PARP-1 binders that correctly fit the pharmacophore models. Specificity was related to the fraction of molecules that did not fully fit the pharmacophoric hypotheses and were identified as decoys. The comparison of the values obtained for the four structure-based pharmacophore models showed that **SB_Pharma1** and **SB_Pharma4** displayed a better accuracy compared with the already good one characterizing all pharmacophore models, in general. Therefore, all four hypotheses generated were used to screen the NCI and DrugBank databases. However, to increase the ability to distinguish between active and inactive molecules, only hits with fit values above 2.0 and those that were retrieved by more than one pharmacophore model (in which at least one of them displayed the best accuracy (**SB_Pharma1** or **SB_Pharma4**)), were retained for further docking studies. Overall, 915 and 175 hits were obtained from the NCI and DrugBank databases, respectively.

Table 4.2 Statistical data of structure-based pharmacophore models.

Pharmacophore Model	TA	TI	TP	TN	FP	FN	Se	Sp	Acc
SB_Pharma1	742	30403	346	27926	2477	396	0.466	0.918	**0.908**
SB_Pharma2	742	30403	364	26037	4366	378	0.491	0.856	0.848
SB_Pharma3	742	30403	275	25873	4530	467	0.371	0.851	0.840
SB_Pharma4	742	30403	225	28073	2330	517	0.303	0.923	**0.908**

TA: Total number of actives; TI: Total number of inactives; TP: True positives; TN: True negatives; FP: False positives; FN: False negatives; Se: Sensitivity; Sp: Specificity; Acc: Accuracy.

Importantly, inspection of the retrieved hits identified 3 known PARP-1 inhibitors among the 175 molecules that were obtained from the screening of the DrugBank database: DB0372 (FR257517) [60], DB07787 (FR255595) [49], and D08348 (PJ34) [254]. It is worth noting here that these ligands were not part of the initial training set of ligands that was used to start MD simulations and pharmacophore design. The presence of these inhibitors, which have a higher potency regarding the inhibition of PARP-1 activity, constituted a first important validation of the capacity of our pharmacophore models to recapitulate the chemical and stereoelectronic determinants that underlie the activity of drug molecules.

4.3.4. Docking studies

The overall 1090 retrieved hits (from the NCI and DrugBank databases) were docked at the PARP-1 binding site using Glide SP-mode. To validate and optimize the docking parameters, A620223 co-crystallised with the PARP-1 catalytic domain (PDB code: 2RCW), as well as 14 reference PARP-1 inhibitors, were re-docked. The SP docking results showed that the binding pose of A620223 in the crystal could be optimally reproduced, with an RMSD of 0.64 Å (**Figure 4.8**). Furthermore, the top poses of hits retrieved from the NCI and DrugBank databases were inspected, and a docking score cut-off of -7 was applied, based on the docking score range of the PARP-1 inhibitors that were docked ([-7.5;-11.6]). The remaining compounds were subjected to a second docking run, using Glide XP-mode. To select promising hits, a visual inspection of the compounds was performed. The interaction with key residues, such as Gly202 and Tyr246, as well as the structural diversity between the molecules, was taken into account when choosing potential hits. A total of 60 compounds were chosen for further evaluation.

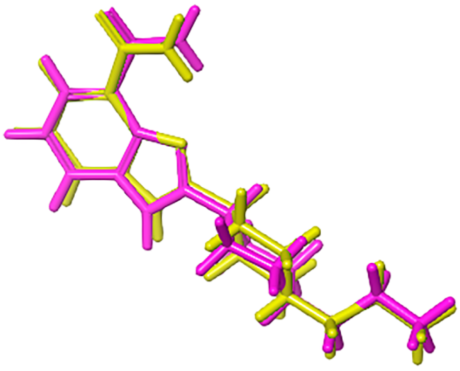

Figure 4.8 Superposition of the docked pose (magenta) of A620223 with its crystal structure conformation (yellow). This figure was created using Discovery Studio Visualizer 16.1.0.

4.3.5. PARP-1 inhibition and structure-activity relationship

The HT Universal Colorimetric PARP Assay Kit was used to screen and to determine the IC_{50} values of the promising hits obtained. Only 39 compounds among the 60 chosen above were effectively tested, because of commercial availability or solubility problems. After an initial screening at a concentration of 100 µM, seven compounds displayed a PARP-1 inhibition activity >90%. A new screening at 10 µM was performed, and the IC_{50} was determined for the most promising hits (**Figure 4.9** and **Figure 4.10**).

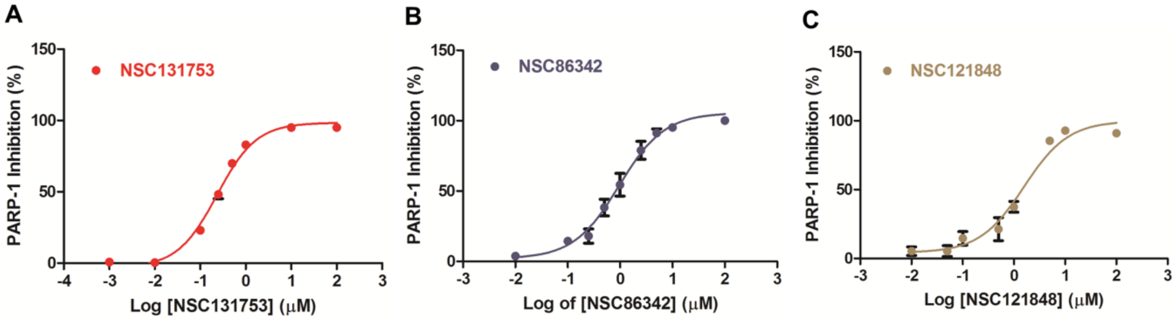

Figure 4.9 Dose-response curves of the three most promising hits: A) NSC131753; B) NSC86342; C) NSC121848. Each data point represents the mean ± SEM of at the least three independent experiments.

Among the promising molecules, three of them exhibited one or more chiral centres. To determine which isomer was acquired from NCI, the NSC86342, NSC131753, and NSC121848 compounds were characterized by NMR. The ^{1}H NMR and ^{13}C NMR spectra showed that only an isomeric form was present for each sample.

Compound code	2D Structure	PARP-1 Inhibition[a] (IC_{50}, µM)	Docking score (glide XP-mode)
NSC131753 (*R* or *S*)	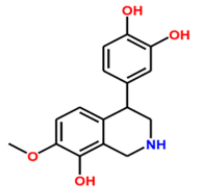	0.24±0.04	-9.582/-8.151
NSC86342 (*cis*)	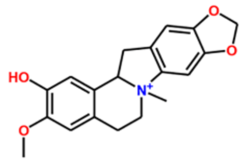	0.96±0.4	-6.121/-6.108*
NSC121848 (*R*)	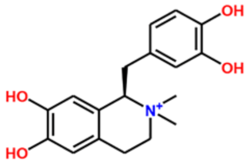	1.6±0.8	-9.045
NSC153161	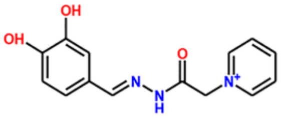	9±4	-8.504
NSC11907	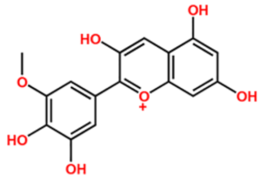	>10	-8.705
NSC65378	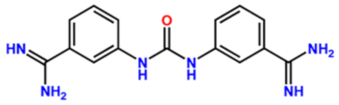	>10	-8.678
NSC102534	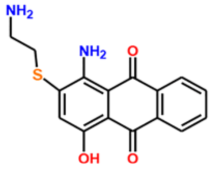	>10	-7.525

Figure 4.10 PARP-1 inhibitory activity and docking score data for the most promising hits. [a]PARP-1 inhibition was determined using HT Universal Colorimetric PARP Assay Kit (Cat #4677-096-k). *Docking score values of both possible NSC86342 *cis* diastereomers.

Moreover, the NOESY spectrum allowed the characterization of the enantiomeric form obtained for NSC121848. The H9 proton observed in the

NOESY spectrum was correlated with both methyl groups at N1, which indicates that the (*R*)-enantiomer was present (**Figure 4.11**). Similarly, in the NOESY spectrum of NSC86342, a correlation between H10 and the methyl group at N1 was observed. This demonstrates that these two groups have the same orientation, which reveals that NSC86342 is a cis diastereomer (**Figure 4.12**). As can be observed, there was a huge structural variability between the most promising compounds, with NSC131753 showing the highest PARP-1 inhibitory activity (IC_{50} = 0.24 μM). Moreover, PARP-1 inhibition was well correlated with the XP docking scores of three among the top four most promising hits (**Figure 4.10**). Despite the fact that NSC86342 showed the lowest docking score, it displayed π–cation and π–π interactions with key tyrosine residues (Tyr235 and Tyr246), which have been described as being essential for the binding of PARP-1 inhibitors to the catalytic domain. Moreover, some poses revealed π–charge interactions with Glu102, Glu327, and Tyr228. Taken together, these findings may explain the stability of this compound at the binding site and its high PARP-1 inhibitory activity (**Figure 4.10** and **Figure 4.13A**).

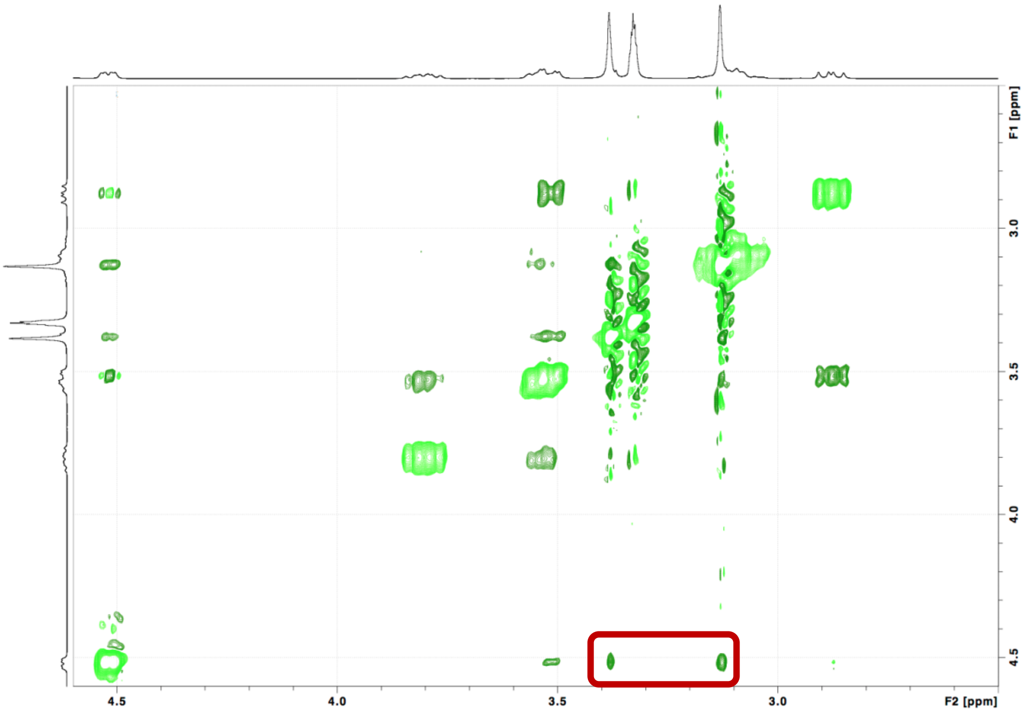

Figure 4.11 NOESY spectrum of NSC121848.

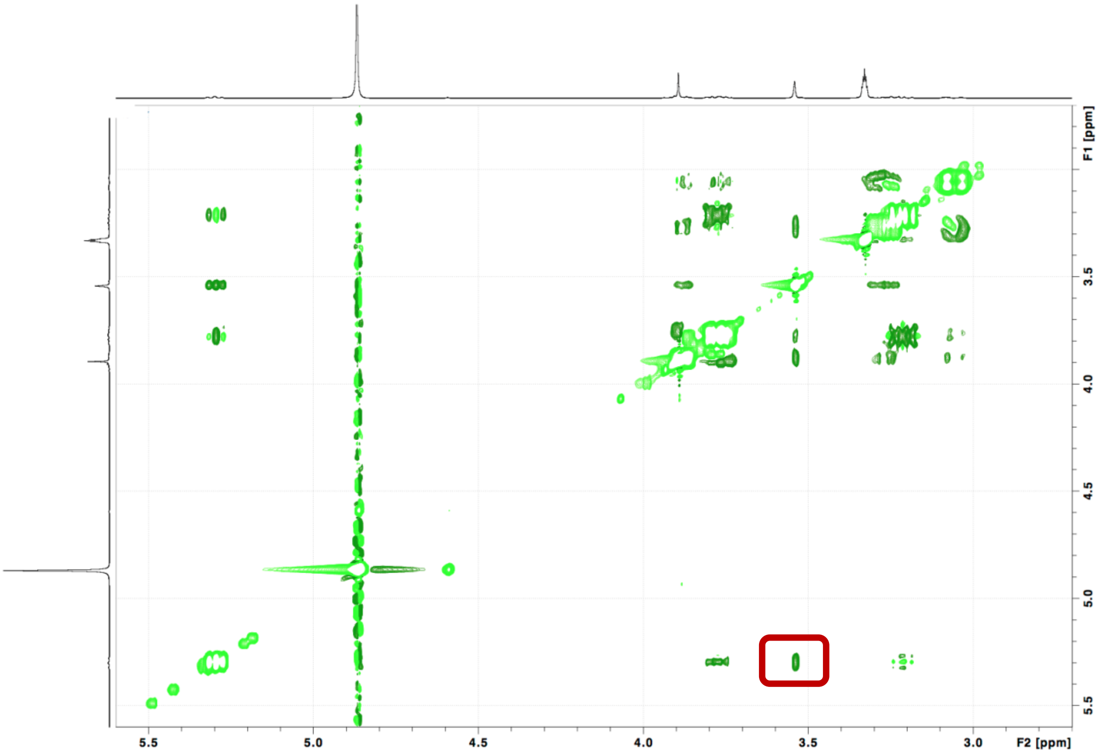

Figure 4.12 NOESY spectrum of NSC86342.

As expected, all promising hits were involved in interactions with conserved binding residues, such as Gly202, Tyr246, or even Tyr235. The presence of donor-acceptor aromatic systems appeared to be essential for PARP-1 inhibition, which is in line with the hydrophilic environment that surrounded the NAD+ binding pocket, with a remarkable presence of aromatic residues (**Figure 3.3**). Consequently, it is easy to understand why the best PARP-1 inhibition activities were displayed by molecules with an aromatic polycyclic skeleton with several HBAs or HBDs, such as NSC131753 and NSC121848 (**Figure 4.10**). The latter established hydrogen bonds with a vast number of residues, such as Phe236, Gly227, and Glu327, in addition to the π–cation and π–π interactions with the key Tyr235 and Tyr246 residues. Although the NMR analysis did not determine which NSC131753 enantiomer was evaluated, both (*R*) and (*S*) enantiomeric forms may be involved in different types of interactions with the catalytic domain, in spite of the differences in docking scores. Hydrogen bond interactions involving Gly233 and Phe236 were stablished with the (*R*)-enantiomer (**Figure 4.13C**), while Gly227 and Met229 were implicated in this type of interactions with the (*S*)-enantiomer

(**Figure 4.13D**). Moreover, Glu327 played an important role in the interaction profile of both enantiomeric forms, by establishing π–cation interactions with (*R*)-NSC131753 and H-bond with (*S*)-NSC131753. Further insights into the binding mode of the two enantiomeric forms will be discussed in the description of the NSC131753 MD simulations analysis.

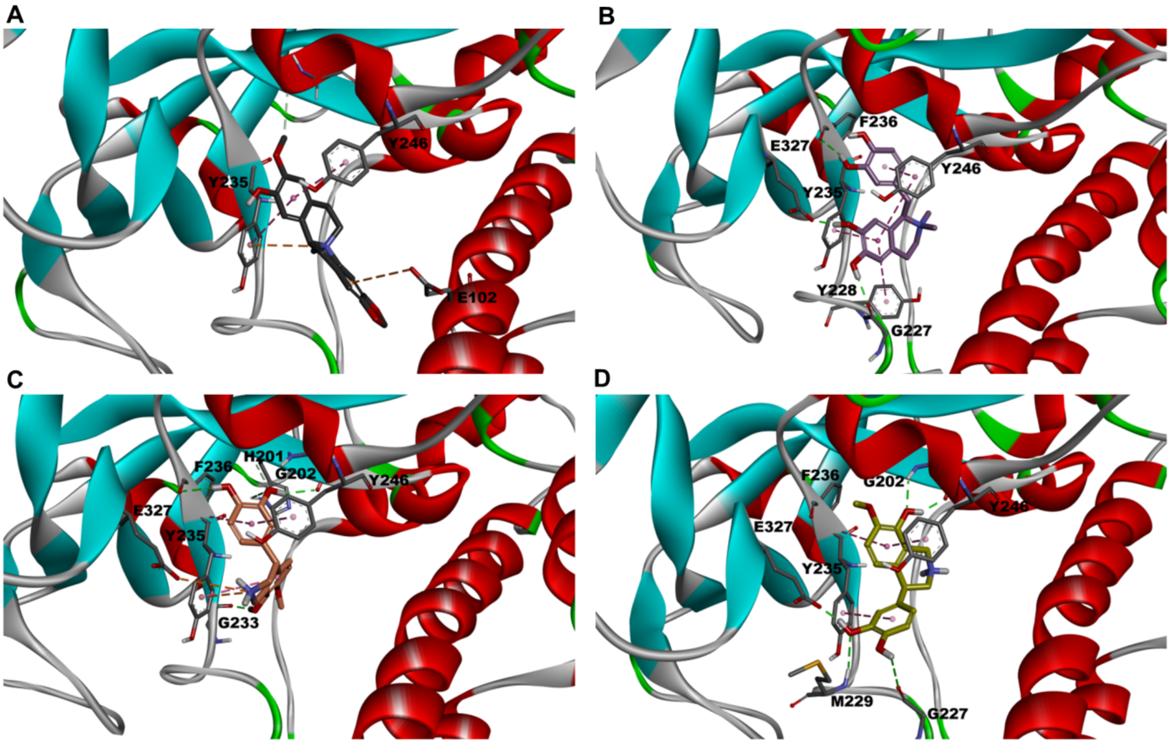

Figure 4.13 The binding mode of the most promising PARP-1 inhibitors at the PARP-1 catalytic domain. The molecular interactions of the top scored poses were displayed. **A)** NSC86342. **B)** NSC121848. **C)** (*R*)-NSC131753. **D)** (*S*)-NSC131753. This figure was created using Discovery Studio Visualizer 16.1.0.

It is worth mentioning that anthraquinone derivatives, of which NSC102534 is an example, have been recently reported as being PARP-1 inhibitors [243]. The polycyclic aromatic core of these compounds was crucial for the interaction with the binding site (**Figure 4.14**).

The most promising hit, NSC131753, contains a chiral centre. Despite the performance of 1D and 2D NMR studies, it was not possible to identify the enantiomeric form evaluated against the PARP Assay kit. To determine which enantiomer is more stable at the binding site and to attest the interaction profile obtained from the docking studies, 100 ns long MD simulations were carried out for (R)- and (S)-NSC131753 complexed with the catalytic domain.

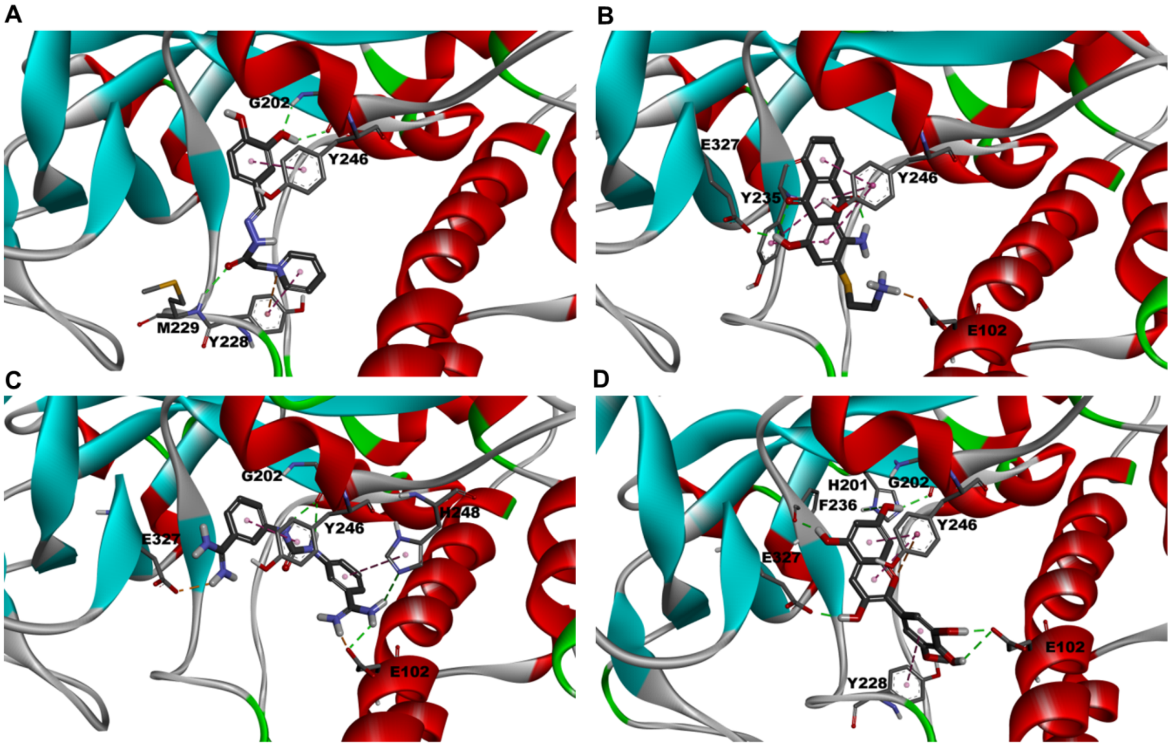

Figure 4.14 The binding mode of A) NSC153161, B) NSC102534, C) NSC65378 and D) NSC11907 at the PARP-1 catalytic domain. The molecular interactions of the top scored poses were displayed. This figure was created using Discovery Studio Visualizer 16.1.0.

The RMSD was lower for (S)-NSC131753 (around 0.05 nm compared with 0.09 nm for (*R*)-NSC131753), even though the two enantiomers revealed being quite stable (**Figure 4.15A** and 15D). However, the average RMSD calculated on the Cα atoms was lower and more stable for the (*R*)-enantiomer complex, along the three 100 ns MD replicas (**Figure 4.15B** and **15E**)). Conversely, a similar RMSF distribution (**Figure 4.15C** and **15F**) was observed for both enantiomeric forms, with the highest fluctuation observed in two loop regions of the catalytic domain (78-94; 118-128). Nevertheless, a highlighted mobility was observed from residues 317 to 322 in the RMSF plot of (*S*)-NSC131753, which was not observed for (*R*)-NSC131753. This may indicate a conformational change induced by the (*S*)-enantiomer. It is also worth noting that the D-loop residues (215-233) presented higher flexibility in the case of (R)-NSC131753 (at least 0.02 nm) compared with (*S*)-NSC131753 (around 0.015 nm). This difference may be due to the interaction of (*S*)-NSC131753 with Tyr228 (through π–π and π–cation interactions) and Met229 (hydrogen bond). In fact, the analysis of the interaction profile during MD showed that both enantiomers established an important number of interactions. Moreover, the main interactions proposed by the docking studies were maintained for both enantiomers, with high occupancy. Tyr235 and Tyr246 were involved in π–π interactions with both enantiomers, with occupancies above 65%. Glu327 was essential for the establishment of hydrogen bonding with both enantiomeric forms, and for charge-charge interactions with (*R*)-NSC131753, as demonstrated by the docking studies described above. MD trajectories analysis also revealed that Glu102 established a hydrogen bond interaction with the (*R*)-enantiomer for 41.5% of the MD run time, and with the (*S*)-enantiomer for 35.01%. A similar type of interaction was identified between ASP105 and (S)-NSC131753, with an occupancy of 38.55% along 100 ns MD simulations.

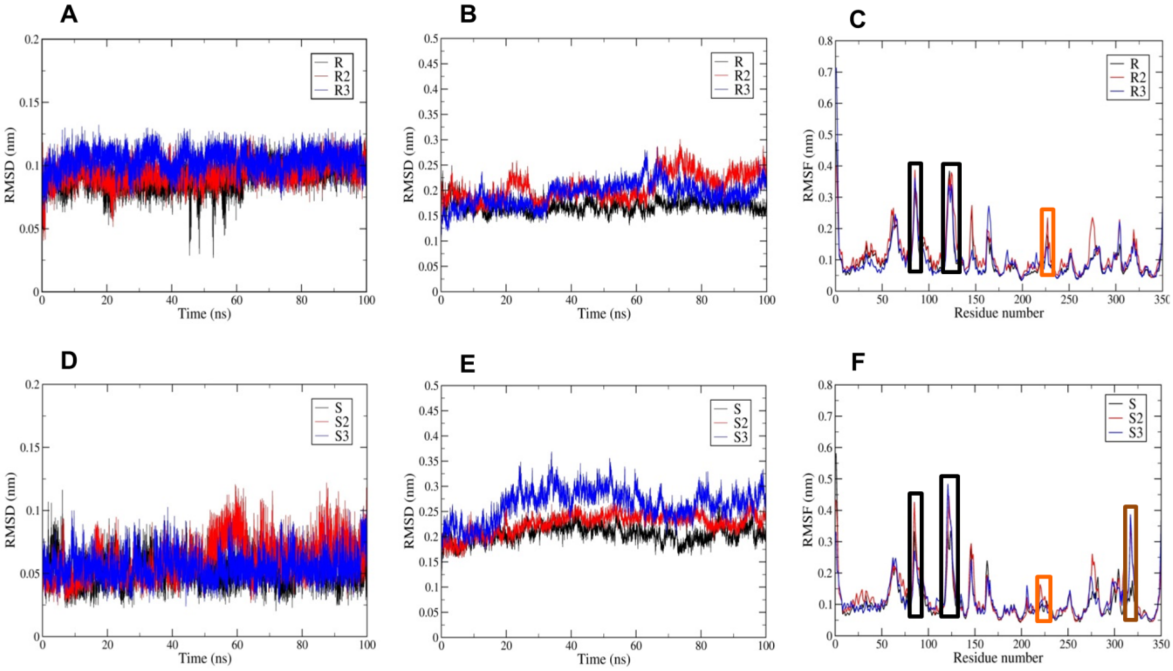

Figure 4.15 Conformational statistics obtained for (*R*)- and (*S*)-NSC131753, along 100 ns MD run. A), D) RMSDs of ligands. B), E) RMSDs of complexes. C), F) RMSFs of Cα atoms of catalytic domain.

In summary, the data showed that both enantiomers were able to interact with the catalytic domain with relative stability, via different types of interactions with binding site residues, some of which were revealed only during MD simulations. An example of this is the interaction between (*S*)-NSC131753 and

Tyr228, which was important to stabilize the D-loop and may explain the differences in docking scores observed between (*R*)- and (*S*)-NSC131753.

4.4. CONCLUSIONS AND FURTHER DEVELOPMENTS

A dynamic structure-based pharmacophore strategy was used to identify novel PARP-1 inhibitors. The pharmacophore models based on the interactions between the PARP-1 catalytic domain and four different inhibitors during MD simulations provided new insights in the ligand binding mode, taking into account the flexibility of both the enzyme and the ligand. Subsequently, the validated pharmacophore models were screened against two virtual compound libraries, to retrieve hits with novel chemical scaffolds. After molecular docking studies using Glide, the top scored drug-like molecules were tested against the PARP kit assay to determine PARP-1 inhibitory activity. Structurally diverse hits with important PARP-1 inhibitory activity were found. Moreover, the dynamic structure-based pharmacophore approach applied here led to the identification of three new PARP-1 inhibitor candidates with skeletons that had not been reported previously: NSC86342, NSC131753, and NSC121848. These candidates will be useful for guiding the further development of novel, selective and more potent PARP-1 inhibitors.

5. CHAPTER V

BILE ACID DERIVATIVES: FROM WEAK PARP-1 INHIBITORS TO NOVEL FXR MODULATORS

Salete J. Baptista, Maria M.C. Silva, Jorge A. R. Salvador, et al.

Bile acid derivatives: from weak PARP-1 inhibitors to novel FXR modulators

Article in Preparation

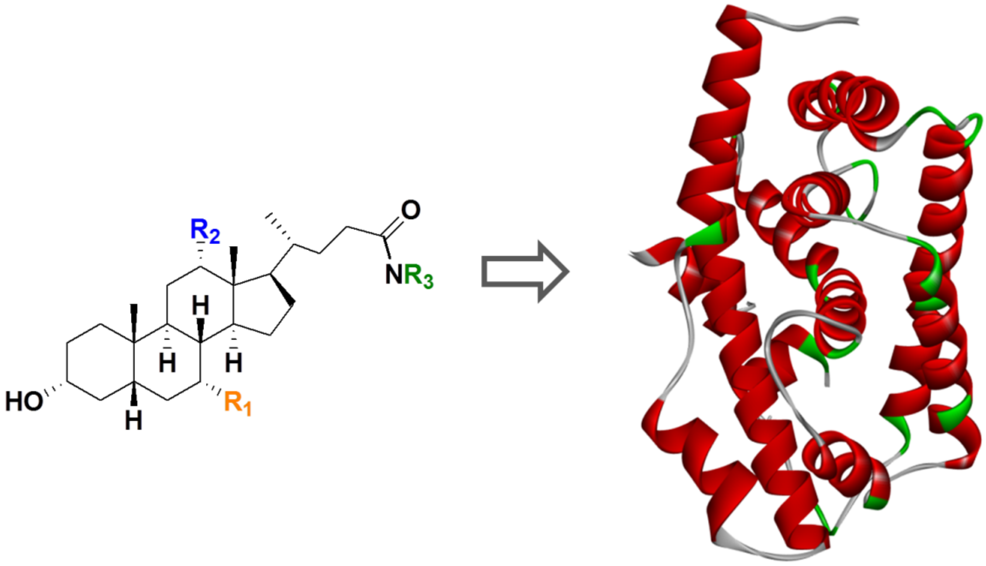

Highlights

- Design of a bile acid virtual library, taking as starting point the compounds **3.3** and **3.4**.
- Molecular docking of bile acid compound database against FXR ligand-binding domain.
- The 2-(3-chlorophenyl)ethyl substituents generally displayed the highest binding affinity predictions.
- Compounds **5.10** and **5.13** showed the highest binding affinities and were selected for further *in vitro studies*.

5. CHAPTER V

Bile acid derivatives: from weak PARP-1 inhibitors to novel FXR modulators

5.1. OVERVIEW

The Farnesoid X receptor (FXR) was firstly identified in 1995 as an orphan receptor that forms a heterodimeric complex with the retinoid X receptor after activation by farnesyl pyrophosphate which, in turn, is a metabolic intermediate of the mevalonate pathway [326]. Few years later, bile acids (BA), the end-products of cholesterol catabolism, were found to be the physiological ligands of this receptor, which granted it the denomination of BA receptor (BAR), as well [327, 328].

FXR is a nuclear hormone receptor, which is encoded by the *NR1H4* gene. Like other nuclear receptor (NR) members, FXR displays five domains: a N-terminal ligand-independent activation function 1 domain (AF1), a DNA-binding domain (DBD), a ligand-binding domain (LBD), a C-terminal ligand-dependent activation function 2 domain (AF2), and a flexible hinge region, which links the DBD and the LBD [329]. Four FXR isoforms (FXRα1–4), resulting from an alternative splicing and the use of different promoters have been identified [330]. As shown in **Figure 5.1**, the differences among the isoforms lie on the amino acid sequence of the initial region of the receptor, displaying the LBD 100% of homology among the four isoforms. Being highly expressed in the liver, intestines, adipose tissues, kidneys and vasculature [331], differences in the FXR isoforms expression were reported among different tissues. Thus, while FXRα1 and FXRα2 isoforms are predominantly expressed in the liver and adrenals, FXα3 and FXα4 are the leading isoforms in the colon and kidney. All the four isoforms are identified in the small intestine [329].

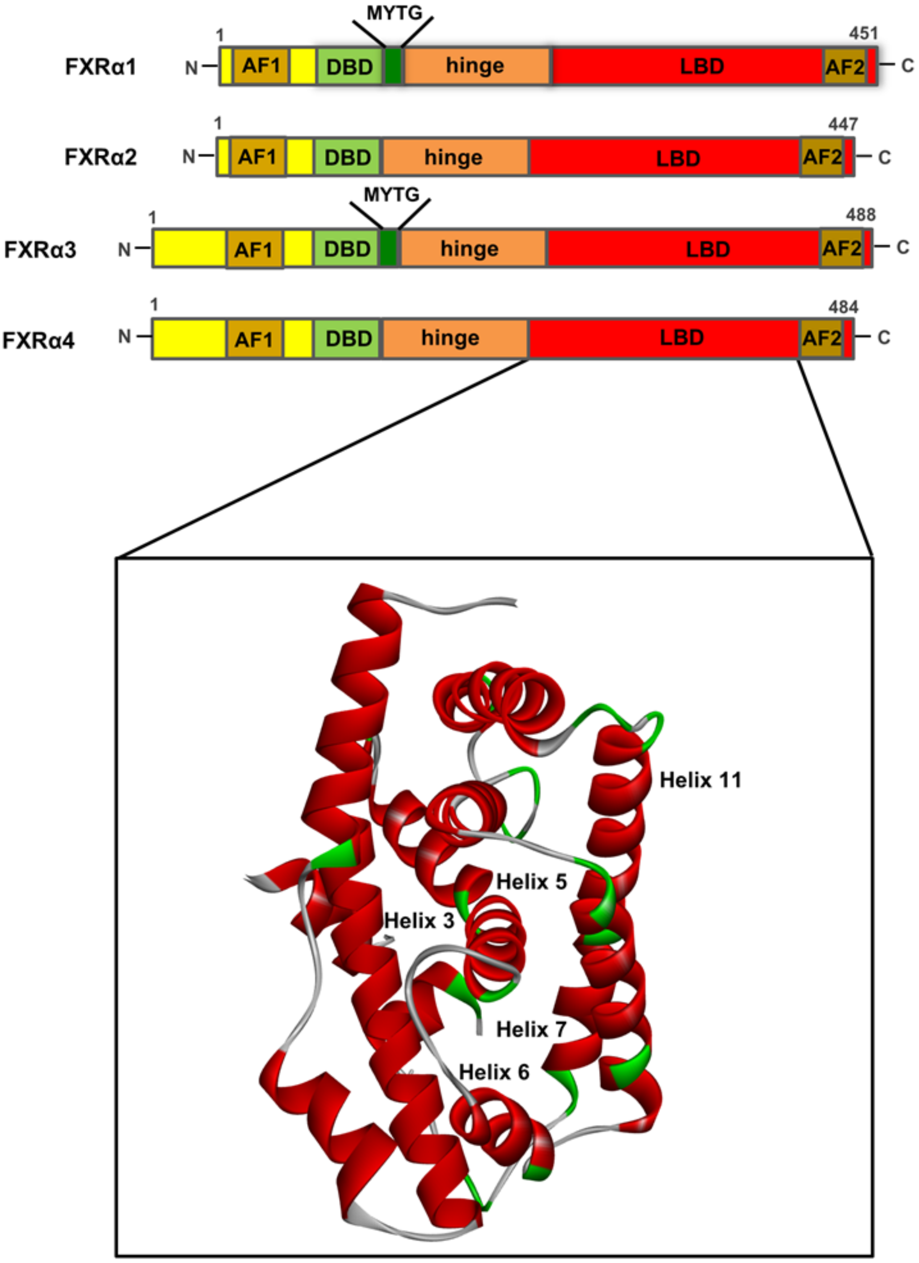
MYTG
1
451
FXRα1
N
AF1
DBD
hinge
LBD
AF2
C
1
447
FXRα2
N
AF1
DBD
hinge
LBD
AF2
C
MYTG
1
488
FXRα3
N
AF1
DBD
hinge
LBD
AF2
C
1
484
FXRα4
N
AF1
DBD
hinge
LBD
AF2
C
Helix 11
Helix 5
Helix 3
Helix 7
Helix 6

Figure 5.1 The different FXR isoforms and the 3D structure of FXR-LBD, which is conserved among all isoforms (PDB code: 4QE6).

FXR plays a key role in the regulation of several metabolic pathways, by regulating bile acid and glucose homeostasis, as well as lipoprotein and lipid metabolism. Furthermore, this NR has been implicated in cell proliferation, inflammation, hepatic regeneration, control of gut microbiome, and in the regulation of vascular tone [329, 332-334]. Therefore, FXR represents an attractive therapeutic target for cholestatic liver disease, diabetes mellitus, dyslipidemia as well as atherosclerosis prevention [335].

FXR is activated by both conjugated and unconjugated BAs at physiological concentrations, being the chenodeoxycholic acid (CDCA) **5.1** (**Figure 5.2**) the most active endogenous FXR agonist, followed by deoxycholic acid (DCA) **5.3** and lithocholic acid (LCA) **5.4** [336]. Due to their amphipathic character with detergent properties, BAs facilitate the intestinal absorption of lipophilic nutrients, including dietary cholesterol and fat-soluble vitamins. Despite this important role, the accumulation of high levels of those compounds, particularly of secondary BAs, DCA **5.3** and LCA **5.4** induces cytotoxicity. Nevertheless, the BAs homeostasis is critically regulated by FXR. In the presence of excessive levels of BAs, FXR is activated by the binding of endogenous BAs, following a feedback mechanism that ultimately regulates the synthesis, the uptake and the elimination of BAs from the cells, in order to return the level of BAs to homeostasis [337]. The key role played by BA-FXR interaction in glucose and lipid metabolism, as well as in the regulation of hepatic and intestinal inflammation and in atherosclerosis [338, 339], supports the therapeutic interest of using FXR agonists in several pathologies, such as non-alcoholic fatty liver disease (NAFLD). This is an emerging global epidemic with a huge medical and economic burden, which prevalence is rapidly increasing, and can culminate in more serious diseases, such as cirrhosis and hepatocellular carcinoma [340].

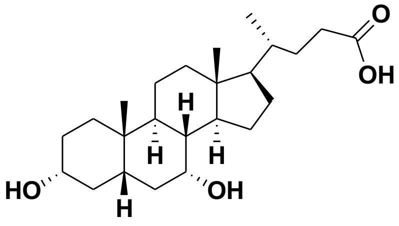

CDCA **5.1**

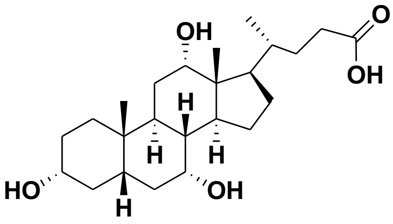

CA **5.2**

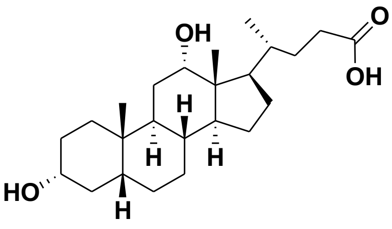

DCA **5.3**

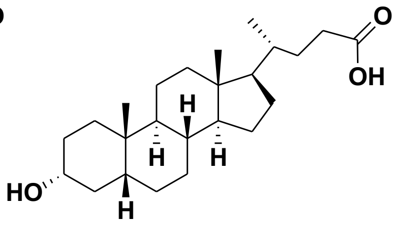

LCA **5.4**

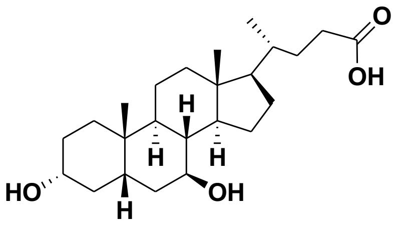

UDCA **5.5**

Figure 5.2 Primary (CDCA **5.1 and** CA **5.2) and secondary (**DCA **5.3, LCA 5.4 and** UDCA **5.5) endogenous bile acids.**

In an effort to discover more potent FXR agonists, the semi-synthesis of BA derivatives has been pursued, with the identification of a potent and selective FXR agonist, the 6α-ethyl-chenodeoxycholic acid (6-ECDCA), also called obeticholic acid (OCA) **5.6** (**Figure 5.3**) [341], recently approved in USA to treat primary biliary cholangitis (PBC) in combination with ursodeoxycholic acid (UDCA) **5.5** (**Figure 5.2**), or in monotherapy in individuals unable to tolerate UDCA [342].

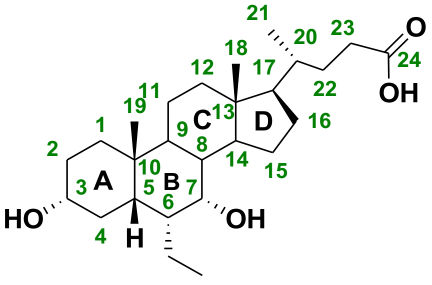

OCA **5.6**

Figure 5.3 The first-in class FXR agonist, OCA.

OCA, which is ~100-fold more potent than CDCA as FXR agonist, is under investigation for the treatment of other diseases. An improvement in hepatic fibrosis in non-alcoholic steatohepatitis (NASH) patients was observed in a phase II clinical trial, using OCA [343]. An increase in insulin sensitivity, as well as anti-inflammatory and anti-fibrotic effects were reported by using OCA in animal studies [339, 344, 345].

Despite the promising results obtained with OCA, some adverse events are associated with the therapeutic use of this molecule, such as fatigue, diarrhoea, constipation, as well as pruritus, which severity led to the suspension of treatment in some clinical studies [346]. Thus, the search for more selective FXR agonists is worth it.

In this study, a docking approach was used to identify novel and potent semi-synthetic BAs, acting on FXR. Taking as starting point the molecules **3.3** and **3.4**, which previously failed as PARP-1 inhibitors, a small library of 19 BA derivatives (including compounds **3.3** and **3.4**) was designed. All the molecules displayed an aromatic side chain extension, in order to better explore the surrounding hydrophobic cavities of the FXR binding pocket, and ultimately identify new potent FXR ligands, with improved ligand binding affinity.

5.2. MATERIALS AND METHODS

5.2.1. Database design and preparation

A small database composed of 19 BAs derivatives was built. The side chain of four different BAs, CDCA **5.1**, cholic acid (CA) **5.2**, DCA **5.3** and UDCA **5.5** were virtually extended with different aromatic substituents, creating a series of amide derivatives (**Figure 5.4**).

A

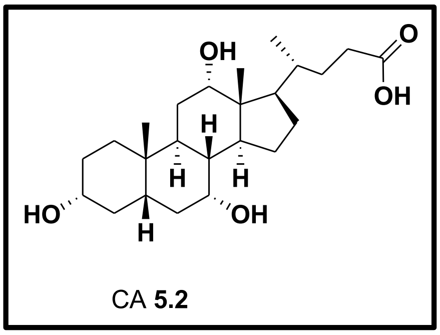

CA **5.2**

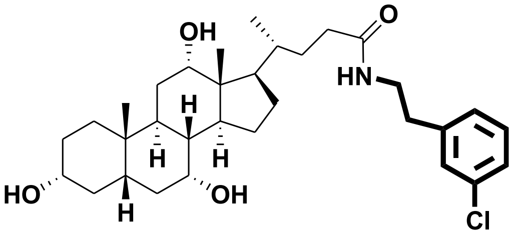

3.3

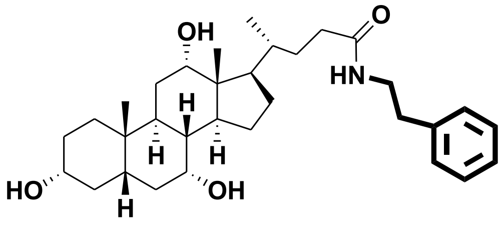

3.4

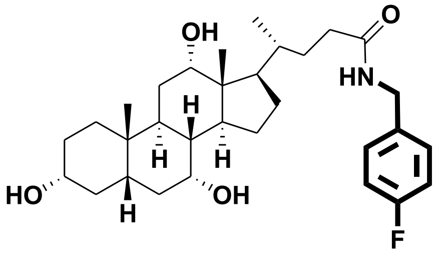

5.7

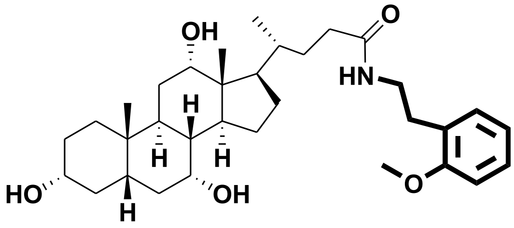

5.8

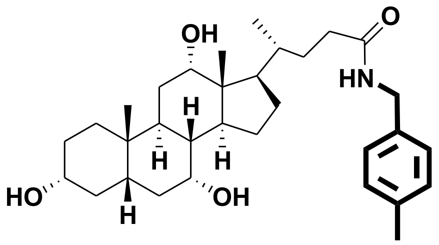

5.9

B

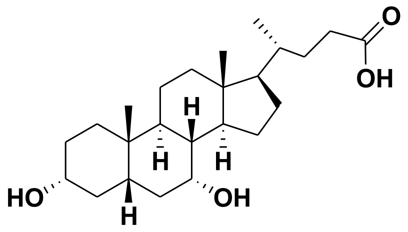

CDCA **5.1**

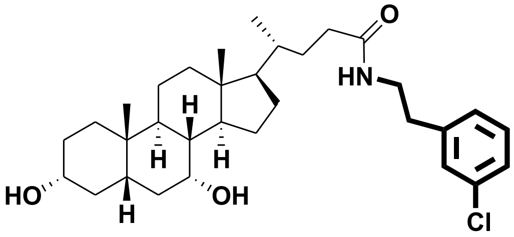

5.10

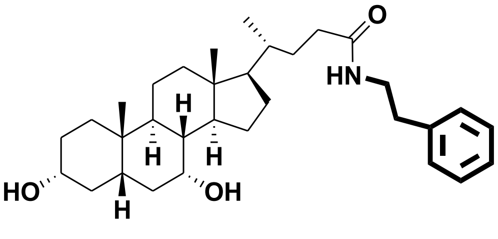

5.11

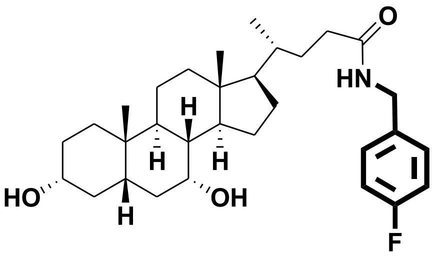

5.12

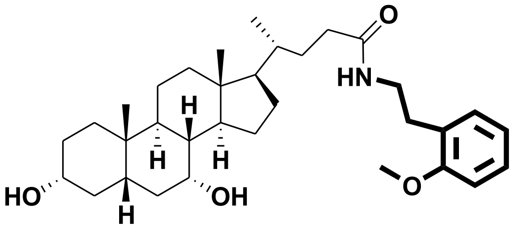

5.13

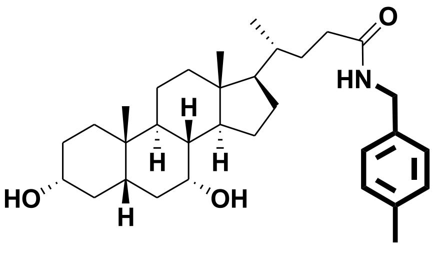

5.14

C

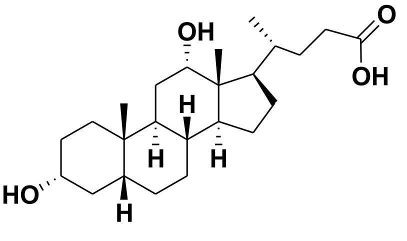

DCA **5.3**

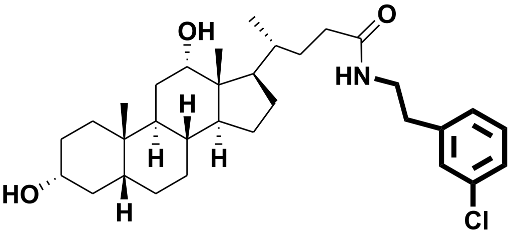

5.15

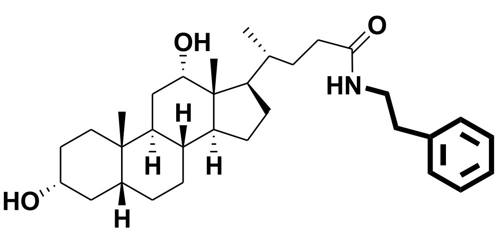

5.16

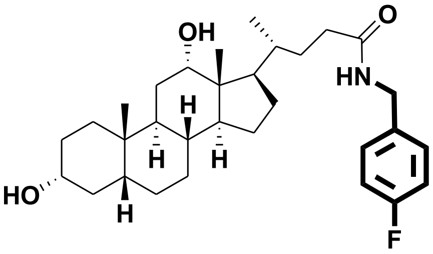

5.17

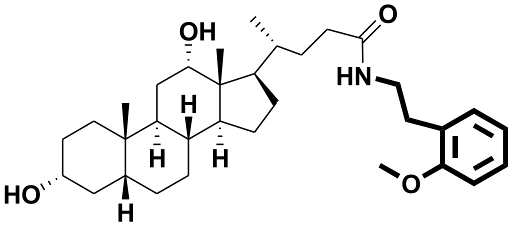

5.18

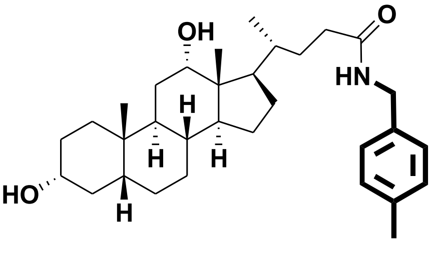

5.19

D

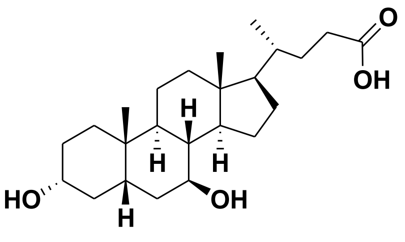

UDCA **5.5**

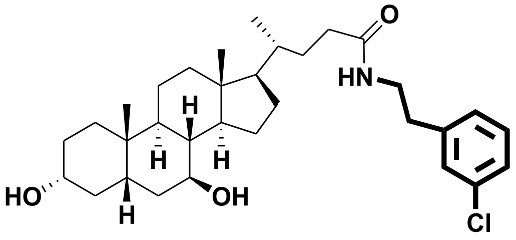

5.20

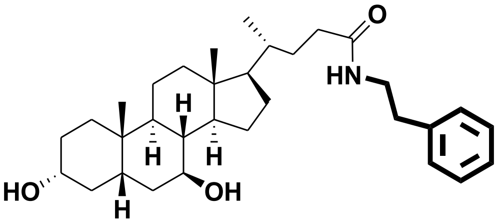

5.21

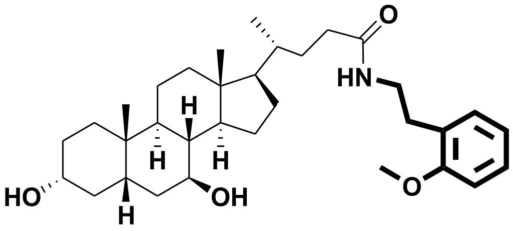

5.22

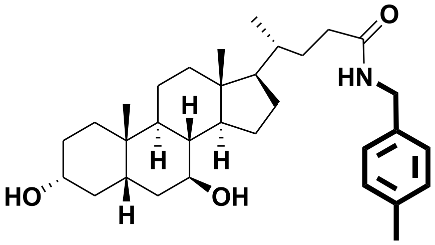

5.23

Figure 5.4 Virtual database of BAs derivatives including the endogenous BAs used as starting point to their preparation. A) CA derivatives; **B)** CDCA derivatives**; C)** DCA derivatives; **D)** UDCA derivatives. The amide side chain extension of each derivative designed is displayed in bold font.

All the structures were prepared using ChemAxon Calculator Plugin. The pH was set to 7.4 and the lowest energy conformation was saved for further docking studies.

5.2.2. Docking studies

The docking studies were performed using GOLD 5.2.2 (Genetic Optimization for Ligand Docking) software [246, 247].

The X-ray crystallographic structures of rat FXR-LBD (PDB code: 1OSV) and human FXR-LBD (PDB code: 4QE6) complexed with OCA and CDCA, respectively, were retrieved from the PDB to perform docking calculations. The use of two different LBD structures is supported by the conformational changes induced by ligand-binding into FXR-LBD. In fact, it has been reported that different ligand scaffolds induce different conformational changes in the LBD since specific helices may be involved in the interactions depending on the ligand binding. This is ultimately responsible for the recruitment of co-activators (because of ligand-induced protein-protein interactions) and the FRX activity regulation [347].

Moreover, it was demonstrated that minor structural variations displayed by the binding of different BAs have significant impact on the FXR affinity and consequently on its activation [337]. By using the FXR-LBD of the most potent endogenous and semi-synthetic BAs FXR agonists, CDCA and OCA (**Figure 5.3**), respectively, further insights into the ligand-dependent conformational changes able to influence the binding mode of the novel BAs derivatives, might be disclosed. It is worth mentioning that an attempt to use a FXR-LDB complexed with a non BA, but still a potent FXR agonist, MFA-1 [348] (PDB code: 3BEJ) was made. Nevertheless, neither OCA nor CDCA were correctly docked into the LDB, which demonstrates the high flexibility of the LDB upon ligand binding.

Discovery Studio (DS) was used to prepare both complex crystal structures at 7.4 pH. The water molecules were removed from the crystal structures. The residues within 6 Å of the co-crystallised ligands were taken into account to define the binding site of each protein structure used. Despite the high level of homology observed between the two FXR-LBD structures, two residues among ones that define the binding site were different between the rat and human structures. Thus, the Ser258 and the Ile294 in PDB entry 1OSV (rat) were substituted by Asn258 and Val294 in PDB entry 4QE6 (human).

All the 19 BAs derivatives in the virtual database, as well the four endogenous BAs used as starting points to their design (CA, CDCA, DCA and UDCA) and the first-in-class FXR agonist OCA were subjected to 100 molecular docking runs using the default ChemPLP fitness function and a search efficiency set to 200%. The top 10 scored poses were kept for each ligand. After visual inspection, the molecules that displayed the highest docking scores in both FXR-LDB structures, as well as an appropriate pocket fitting and conserved binding mode, were submitted to a second round of docking. The best ranked solution of the four selected BAs derivatives (**3.3**, **5.10**, **5.13**, and **5.20**) was submitted to 1000 molecular docking runs with the search efficiency set to 200%.

To evaluate the ability of the GOLD scoring functions to reproduce the crystal ligand poses, as well as to optimize all docking parameters, the two co-crystallised ligands OCA and CDCA were re-docked into the corresponding LDB-FXR, 1OSV and 4QE6, using all scoring functions available in GOLD (ChemPLP, GoldScore [245], ChemScore, and ASP). The best results were obtained for ChemPLP scoring function, which was therefore chosen to perform the docking calculations in this study.

5.3. RESULTS AND DISCUSSION

5.3.1. Structural characterization of the binding interactions of a series of bile acid derivatives into nuclear farnesoid receptor (FXR)

A SBVS approach was applied in order to identify novel BAs derivatives as potent FXR ligands. Twenty four compounds were subjected to molecular docking, using exhaustive settings (100 GA runs and a search efficiency of 200%). After careful visual inspection of all poses kept for each ligand in the docking runs, important findings were settled. As expected, all compounds docked into the FXR-LBD displayed a similar binding mode, with the A-ring 3α-hydroxyl group of the steroid skeleton, which is conserved among all BAs, oriented towards the helix 12, establishing a hydrogen bond with the His447 residue in the 4QE6 LBD (His474 in 1OSV), which is present on helix 11. An additional hydrogen bond was settled between the Asp333 (helix 5) in 4QE6 (Asp328 in 1OSV) and the C-24 carboxyl group (in CA, DCA, CDCA, UDCA, and OCA) or the C-24 amide oxygen in the novel BAs derivatives. Moreover, several alkyl interactions were established between the polycyclic steroid core of all compounds and binding site residues, such as Leu287 and Met290 (helix 3), Leu348 and Ile352 (helix 6), and Trp454 (in 4QE6). The corresponding residues of 1OSV were involved in the same interactions with the LBD. Since the interactions described below are observed in both FRX-LDB analysed, only the nomenclature of 4QE6 will be written down.

It is important to mention that the 7α-hydroxyl group was involved in hydrogen bond interactions with the FXR-LBD (Tyr366, Ser333, or Met292), which might explain the higher binding affinities (**Table 5.1**) showed by the BAs that display an α-hydroxyl moiety in that position (OCA, CDCA, and their amide derivatives), as opposed to those that display a 7β-hydroxyl (UDCA) or no hydroxyl group at position 7 (DCA and its amide derivatives). This supports the reported highest agonist activity by CDCA among the endogenous BAs, followed by a lower activity of DCA and UCDA [336]. Importantly, the 12α-hydroxyl group does not seem to interfere in the binding affinity, since no hydrogen bond was established between that group and neighbouring residues, as observed for DCA, CA and derivatives, at the FXR-LBD.

An additional interesting point disclosed by docking calculations was the higher binding affinity exhibited by OCA in comparison with the other BAs under investigation. Unlike the other BAs, all poses kept for OCA acquired the same binding mode, with fewer variations. The additional alkyl interactions stablished between the 6α-ethyl group and different hydrophobic residues (e.g. Ile349, Ile359, Met262, and Phe363) might explain the constant binding mode.

Comparing the binding affinities of the novel BAs derivatives with the BAs used as a starting point for their design, or even OCA, higher *in silico* binding affinities predictions were disclosed for the first ones. In fact, in all the novel BAs derivatives the aromatic extension of the side chain is directed towards the entry of the FRX-LDB, interacting with the hydrophobic residues of the internal face of helix 3, such as the His294, Val297, and Leu298 residues. Moreover, different aromatic residues, such as the Tyr260, His294, Phe301, surround the small hydrophobic pocket where the BAs side chain lie and are involved in π–π interactions with the aromatic portion of the side chain of the different BAs derivatives (**Figure 5.5**). This might be ultimately responsible for the stability exhibited by the side chain into the binding pocket and the higher affinities displayed, in general, by these molecules (**Table 5.1**).

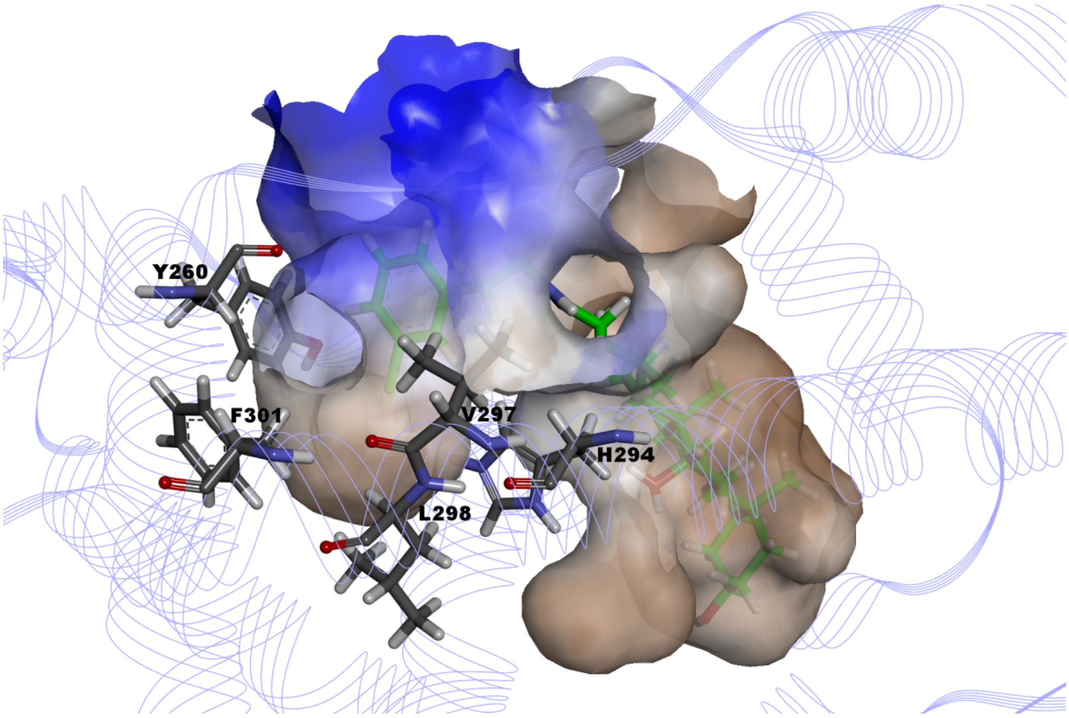

Figure 5.5 Representation of the hydrophobic receptor surface (PDB code: 4QE6) around 3.3. The brown represents the hydrophobic area, while blue points the polar part. This figure was created using Discovery Studio Visualizer 16.1.0.

Moreover, among the different substituents of the amide side chain, the 2-(3-chlorophenyl)ethyl moiety, seems to contribute to an enhancement in the binding affinity of the BAs derivatives. In fact, among the derivatives of each natural BA studied (CA, DCA, CDCA, and UDCA) the 2-(3-chlorophenyl)ethyl amides were generally the top scored ranking compounds, in both docking calculations. This might be related with the ability of the chlorine moiety to establish several alkyl interactions with the hydrophobic residues that lie in the small pocket that accommodates the amide side chain, namely His294, Val297, and Leu298 (**Figure 5.5**). This observation was further explored by a second exhaustive docking run (1000GA, 200% of efficiency), involving the three top-scored 2-(3-chlorophenyl)ethyl BA derivatives **3.3**, **5.10**, and **5.20** and the FXR-LDB. The compound **5.13**, which is a 2-methoxyphenethylamide derivative, was also included in the calculation, since it is the second molecule with a higher predicted binding affinity, among all BAs derivatives evaluated.

Table 5.1 Docking score data for the BAs under investigation. A first docking run was performed using 100GA and an efficiency of 200% for all 24 compounds into FXR-LDB 1OSV and 4QE6. The top four compounds were further submitted to a most exhaustive docking calculation, using 1000GA, with 200% of efficiency.

Compound code	**Docking score (CHEMPLP)**			
	1OSV 100GA, 200%	**4QE6 100GA, 200%**	**1OSV 1000GA,200%**	**4QE6 1000GA, 200%**
3.3	105.06	106.57	106.03	110.49
3.4	99.34	103.89	-	-
5.1	77.47	81.82	82.06	82.68
5.2	76.25	87.76	-	-
5.3	73.00	80.70	-	-
5.5	73.44	74.23	-	-
5.6	93.46	97.35	94.74	97.53
5.7	102.89	104.07	-	-
5.8	105.56	106.47	-	-
5.9	99.22	105.57	-	-
5.10	110.02	111.13	110.02	116.16
5.11	105.58	112.72	-	-
5.12	108.27	107.72	-	-
5.13	108.29	112.07	109.15	113.56
5.14	105.71	107.87	-	-
5.15	98.87	100.83	-	-
5.16	94.80	98.19	-	-
5.17	95.61	95.44	-	-
5.18	94.77	99.91	-	-
5.19	97.23	98.44	-	-
5.20	101.55	107.04	101.23	107.03
5.21	97.96	101.30	-	-
5.22	99.22	105.29	-	-
5.23	99.43	100.75	-	-

The visual inspection of all poses kept by each molecule revealed that all compounds display a stable binding mode into FXR-LDB, particularly in the amide side chain. In fact, the small differences in the docking scores seem to be related with the nature of the BA core structure, in which the CDCA derivatives **5.10** and **5.13** were the most promising molecules (**Table 5.1**). This is in line with the highest FXR agonist activity revealed by CDCA among all endogenous BAs [336]. Furthermore, the chlorine substituent at *para* position of the benzyl side chain appeared to be slightly more favourable than the *ortho* 2-methoxyphenethylamide substituent, likely due to the closer proximity of several hydrophobic residues able to interact with chlorine. In fact, the three 2-(3-chlorophenyl)ethyl amides derivatives **3.3**, **5.10** and **5.20**, as well as **5.13** display superposed poses. Nevertheless, while the chlorine moiety in **3.3**, **5.10** and **5.20** was always directed to the hydrophobic residues located at helix 5 (Ala327, Arg331) and helix 3 (His294, Val297, Leu298, Phe301) in both docking calculations, the methoxy group was positioned differently in the different docking runs, because of the rotation of the phenyl ring (**Figure 5.6)**.

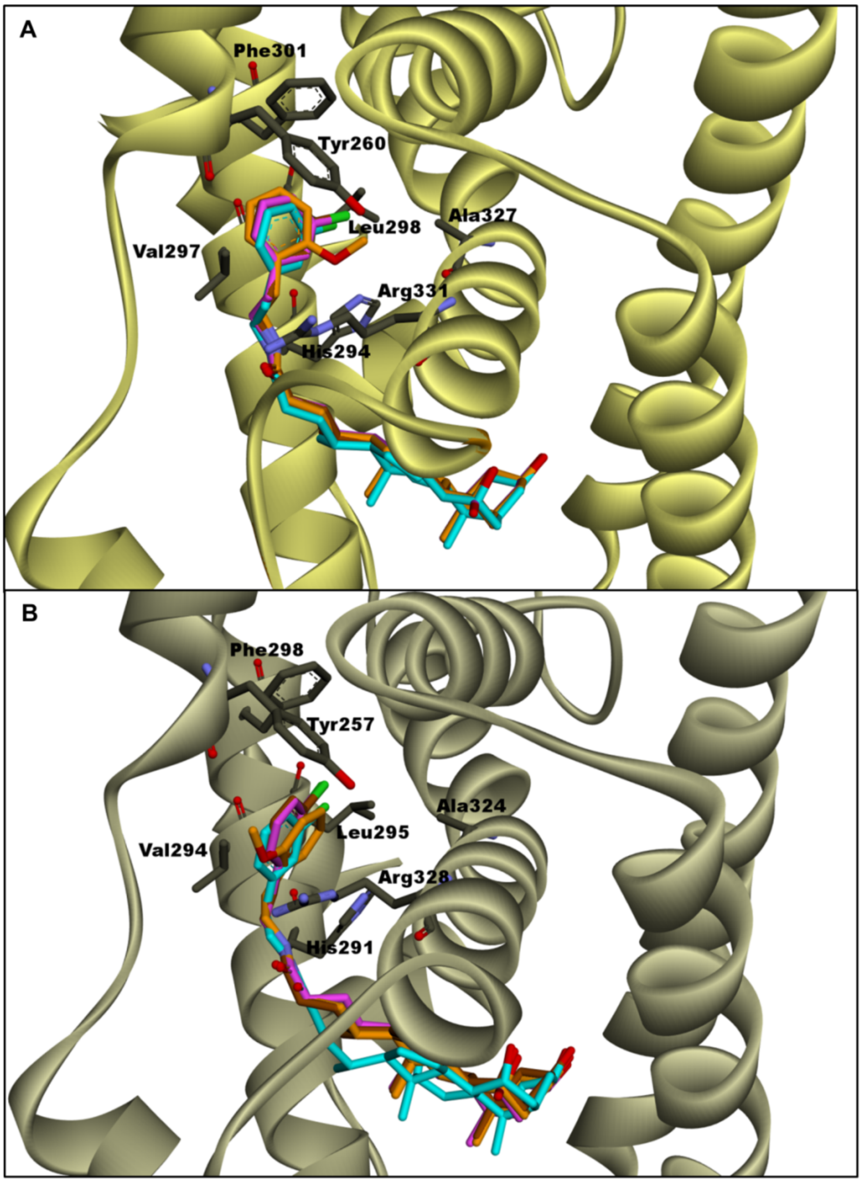
A
Phe301
Tyr260
Ala327
Leu298
Val297
Arg331
His294
B
Phe298
Tyr257
Ala324
Leu295
Val294
Arg328
His291

Figure 5.6 The binding mode of the 3.3, 5.10, 5.13, and 5.20 at the FXR-LBD. A) 4QE6; **B)** 1OSV. All the compounds display superposed poses. The 2-(3-chlorophenyl)ethyl BA derivatives **3.3** (brown), **5.10** (turquoise), and **5.20** (magenta) display the same binding mode in both FXR-LBD 4QE6 and 1OSV. The 2-methoxyphenethyl group of compound **5.13** (orange) at 4QE6 LBD rotates in comparison with 1OSV LBD. This figure was created using Discovery Studio Visualizer 16.1.0.

Although, the methoxy group of **5.13** was directed to the same side of the chlorine moiety in the 4QE6 LBD, that moiety was not able to establish any interaction with the target residues (**Figure 5.7**).

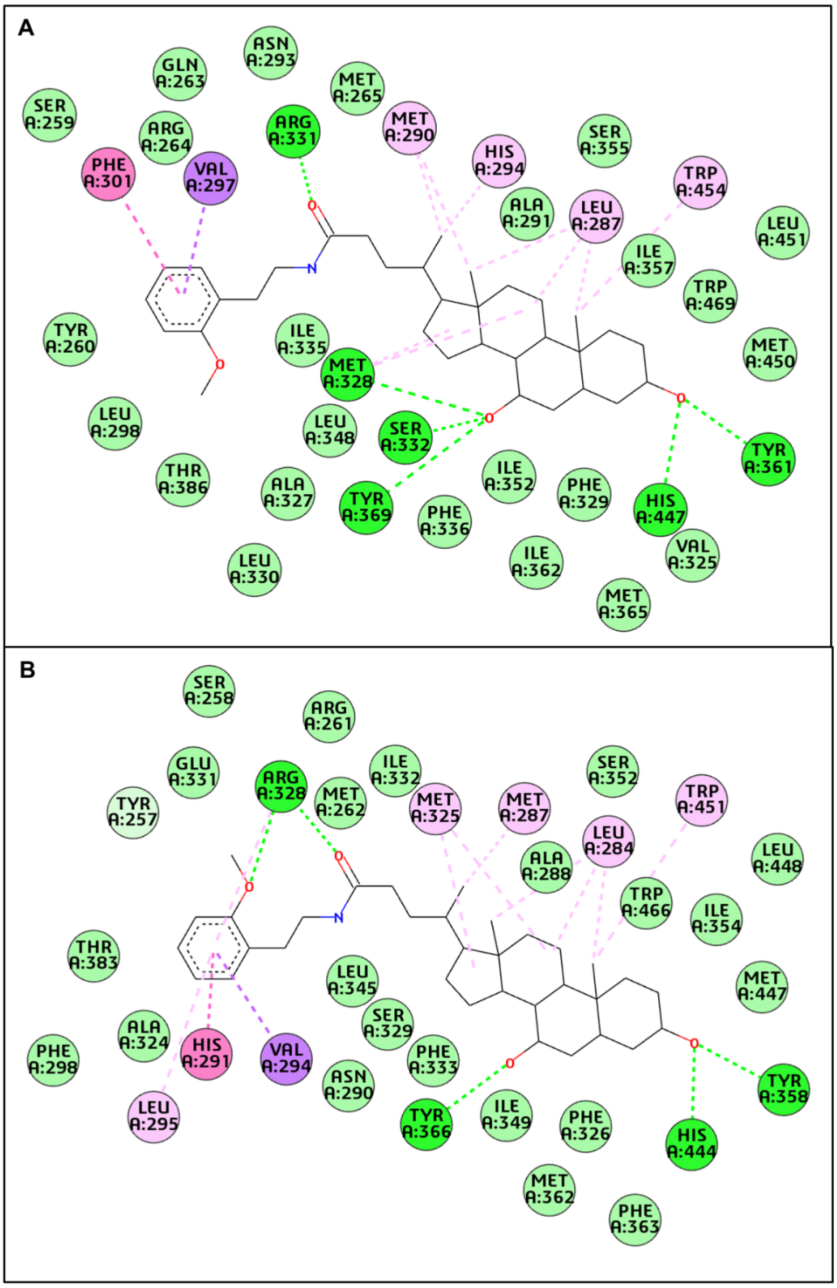
A
ASN A:293
GLN A:263
MET A:265
SER A:259
ARG A:331
MET A:290
ARG A:264
HIS A:294
SER A:355
PHE A:301
VAL A:297
TRP A:454
ALA A:291
LEU A:287
LEU A:451
ILE A:357
TRP A:469
TYR A:260
ILE A:335
MET A:450
MET A:328
LEU A:298
LEU A:348
SER A:332
TYR A:361
THR A:386
ILE A:352
PHE A:329
ALA A:327
TYR A:369
PHE A:336
HIS A:447
VAL A:325
ILE A:362
LEU A:330
MET A:365
B
SER A:258
ARG A:261
GLU A:331
ILE A:332
SER A:352
ARG A:328
MET A:262
TYR A:257
MET A:325
MET A:287
TRP A:451
LEU A:284
ALA A:288
LEU A:448
TRP A:466
ILE A:354
THR A:383
LEU A:345
MET A:447
SER A:329
PHE A:298
ALA A:324
HIS A:291
VAL A:294
PHE A:333
ASN A:290
LEU A:295
TYR A:366
ILE A:349
PHE A:326
HIS A:444
TYR A:358
MET A:362
PHE A:363

Figure 5.7 2D-Ligand interaction diagrams for 5.13 complexed with the FXR-LBD. A) 4QE6; **B)** 1OSV. Dashed lines represent interactions between binding site residues and bounded ligands. Green colour pointed to hydrogen bond interactions; pink denotes π–π stacked; light pink pointed to alkyl interactions; violet indicates π–alkyl interactions. This figure was created using Discovery Studio Visualizer 16.1.0.

On the other hand, in the 1OSV LBD the oxygen of the methoxy group was directed in an opposite way, establishing a hydrogen bond with Arg328. In line with the above, more in-depth studies are required to accurately predict the differences in protein-ligand binding energies between the most promising virtual compounds, **5.10** and **5.13**. Free energy perturbation (FEP) [349] using MD sampling would be a reliable approach to achieve this goal, taking also into account the conformational changes induced upon ligand binding to FXR-LBD, which ultimately determine the activation of this NR.

5.4. CONCLUSIONS AND FURTHER DEVELOPMENTS

A docking approach was used to disclose the binding affinity of a series of virtual BAs derivatives into the FXR-LBD.

Two CA derivatives, **3.3** and **3.4,** which display a phenyl amide side chain, were firstly evaluated against PARP-1, and failed as PARP-1 inhibitors (**Chapter 3**). Since BAs have been reported as FXR agonists, a virtual compound library, which included **3.3** and **3.4**, was designed and subjected to molecular docking calculations, in order to predict the binding affinity of **3.3** and **3.4**, as well as the other BAs derivatives into FXR-LDB.

A first docking run was performed with all 19 BAs derivatives, as well as the BAs used as starting point to their design, CDCA **5.1**, CA **5.2**, DCA **5.3** and UDCA **5.5**, and the first-in-class selective FXR agonist OCA **5.6**. It was observed that all BAs derivatives, including **3.3** and **3.4** displayed a higher binding affinity than the natural BAs CDCA **5.1**, CA **5.2**, DCA **5.3** and UDCA **5.5**, as well as the OCA **5.6**. The aromatic amide side extension displayed by all BAs derivatives established several interactions with the LBD, showing a stable binding mode into a small hydrophobic pocket formed by several hydrophobic residues, such as His294, Val297, Leu298, Phe301 (helix 3), Ala327, and Ala 334 (helix 5). Moreover, the 2-(3-chlorophenyl)ethyl substituents generally displayed the highest binding affinity predictions, mostly due to the ability of the chlorine moiety to interact with different residues in the small hydrophobic cavity mentioned before.

In line with this, the top three ranking 2-(3-chlorophenyl)ethyl amide derivatives and the second top-ranking compound **5.13**, which display a 2-methoxyphenethylamide, were subjected to an exhaustive docking in order to select the most promising derivative for *in vitro* evaluation against FXR. Despite a slightly higher binding affinity prediction revealed by **5.10**, which were determined by a higher number of interactions between this compound and the LBD, both **5.10** and **5.13**, CDCA derivatives, are promising candidates for further *in vitro* studies against FXR.

6. CHAPTER VI

CONCLUDING REMARKS

6. CHAPTER VI

Concluding remarks

Despite several years of research of, and important advances in cancer treatment, this multifactorial disease is still a leading cause of death worldwide. Among the different approaches used to fight cancer, targeting DNA-repair has appeared as a promising strategy, as DNA-repair inhibition may compromise cancer cells survival and ultimately lead to their death. PARP-1 has been extensively reported as playing a key role in several DNA-repair pathways. However, the PARP-1 inhibitors discovered to date are not selective, especially among the PARP family, and are associated with resistance phenomena. For these reasons, the identification of new and selective PARP-1 inhibitors remains an important strategy to fight cancer.

In a first attempt, a receptor-based pharmacophore strategy was applied in which MIFs calculated on the PARP-1 catalytic domain (wild-type and Val101Ala) after MD were used as a starting point for pharmacophore generation (**Chapter 3)**. Despite the initial promising docking results, *in vitro* evaluation of the putative hits revealed weak PARP-1 inhibition. Nonetheless, some important findings were pointed out, leading to a change in the pharmacophore modelling approach used. Thus, a dynamic structure-based pharmacophore strategy was explored to identify novel and selective PARP-1 inhibitors. Different pharmacophore models were generated taking into consideration the interactions established between different inhibitors and the PARP-1 catalytic domain, the complexes of which were previously subjected to MD simulations. After pharmacophore-based VS against two compound databases, the molecules that fit two of the four pharmacophores generated, in each one of them showed the best accuracy, were selected. The subsequent molecular docking studies performed using the molecules chosen led to the discovery of three novel PARP-1 hits, which will be further used as a starting point to disclose novel, selective and more potent PARP-1 inhibitors (**Chapter 4**).

On the other hand, among the compounds resulting from the first pharmacophore-based VS (**Chapter3**), there were two CA derivatives, which were used as a starting point for the design of a virtual BA derivatives database. This was further subjected to molecular docking, to predict the binding affinity of those compounds to FXR, an NR that is activated by BAs. From the evaluated molecules, two CDCA derivatives showed promising binding affinities (**Chapter 5**).

In summary, this thesis encompasses an integrated medicinal chemistry approach that used dynamic structure-based pharmacophore modelling and molecular docking to identify new PARP-1 inhibitory scaffolds with promising activities, which were validated using *in vitro* studies. Moreover, it allowed the identification of new potential FXR agonists, taking as a starting point two CA derivatives that were previously designed and evaluated as PARP-1 inhibitors and did not exhibit a significant PARP-1 inhibitory activity.

Finally, this thesis contributes for drug discovery process by opening new pathways to the identification of effective and selective PARP-1 inhibitors, as well as novel FXR agonists.

7. CHAPTER VII

REFERENCES

7. CHAPTER VII

References

1. Hanahan, D.; Weinberg, R.A. *Hallmarks of cancer: the next generation.* Cell, **2011**. 144(5): p. 646-74.

2. Connolly, J. L.; Schnitt, S. J.; Wang, H. H.; Dvorak, A. M.; Dvorak, H. F. *Principles of Cancer Pathology. In Holland-Frei Cancer Medicine.; Kufe DW, Pollock RE, W. R., Ed.; ISBN: 1-55009-213-8: Hamilton,* **2000**.

3. Ferlay J, Soerjomataram I, Ervik M, Dikshit R, Eser S, M. C. *GLOBOCAN 2012, Cancer Incidence and Mortality Worldwide: IARC CancerBase No. 11.* **2012**.

4. *WHO. http://www.who.int/mediacentre/factsheets/fs297/en/ (accessed March 21, 2017).*

5. Siegel, R.L.; Miller, K.D.; Jemal, A. *Cancer Statistics, 2017.* CA Cancer J Clin, **2017**. 67(1): p. 7-30.

6. *Bradbury,R.H. Cancer. Topics in medicinal chemistry. ISBN-13 978-3-540-33119-3: Springer Berlin Heidelberg New York,* ***2007****.*

7. Stewart, B. W.; Wild, C. P. *World cancer report 2014. WHO* **2014**, 1–2.

8. Brown, J.S.; O'Carrigan, B.; Jackson, S.P.; Yap, T.A. *Targeting DNA Repair in Cancer: Beyond PARP Inhibitors.* Cancer Discov, **2017**. 7(1): p. 20-37.

9. Jackson, S.P.; Bartek, J. *The DNA-damage response in human biology and disease.* Nature, **2009**. 461(7267): p. 1071-8.

10. Hoeijmakers, J.H. *DNA Damage, Aging, and Cancer.* N Engl J Med, **2009**. 361(15): p. 1475-1485.

11. Nikitaki, Z.; Michalopoulos, I.; Georgakilas, A.G. *Molecular inhibitors of DNA repair: searching for the ultimate tumor killing weapon.* Future Med Chem, **2015**. 7(12): p. 1543-58.

12. Hosoya, N.; Miyagawa, K. *Targeting DNA damage response in cancer therapy.* Cancer Sci, **2014**. 105(4): p. 370-88.

13. Akbari, M.; Krokan, H.E. *Cytotoxicity and mutagenicity of endogenous DNA base lesions as potential cause of human aging.* Mech Ageing Dev, **2008**. 129(7-8): p. 353-65.

14. Tian, H.; Gao, Z.; Li, H.; Zhang, B.; Wang, G.; Zhang, Q.; Pei, D.; Zheng, J. *DNA damage response-a double-edged sword in cancer prevention and cancer therapy.* Cancer Lett, **2015**. 358(1): p. 8-16.

15. Stover, E.H.; Konstantinopoulos, P.A.; Matulonis, U.A.; Swisher, E.M. *Biomarkers of Response and Resistance to DNA Repair Targeted Therapies.* Clin Cancer Res, **2016**.

16. Kelley, M.R.; Logsdon, D.; Fishel, M.L. *Targeting DNA repair pathways for cancer treatment: what's new?* Future Oncol, **2014**. 10(7): p. 1215-37.

17. Fan, C.H.; Liu, W.L.; Cao, H.; Wen, C.; Chen, L. Jiang, G. *O6-methylguanine DNA methyltransferase as a promising target for the treatment of temozolomide-resistant gliomas.* Cell Death Dis, **2013**. 4: p. e876.

18. Shen, L.; Kondo, Y.; Rosner, G.L.; Xiao, L.; Hernandez, N.S.; Vilaythong, J.; Houlihan, P.S.; Krouse, R.S.; Prasad, A.R.; Einspahr, J.G.; Buckmeier, J.; Alberts, D.S.; Hamilton, S.R. Issa, J.P. *MGMT promoter methylation and field defect in sporadic colorectal cancer.* J Natl Cancer Inst, **2005**. 97(18): p. 1330-8.

19. Ksiaa, F.; Ziadi, S.; Amara, K.; Korbi, S.; Trimeche, M. *Biological significance of promoter hypermethylation of tumor-related genes in patients with gastric carcinoma.* Clin Chim Acta, **2009**. 404(2): p. 128-33.

20. Pierini, S.; Jordanov, S.H.; Mitkova, A.V.; Chalakov, I.J.; Melnicharov, M.B.; Kunev, K.V.; Mitev, V.I.; Kaneva, R.P.; Goranova, T.E. *Promoter hypermethylation of CDKN2A, MGMT, MLH1, and DAPK genes in laryngeal squamous cell carcinoma and their associations with clinical profiles of the patients.* Head Neck, **2014**. 36(8): p. 1103-8.

21. Esteller, M.; Garcia-Foncillas, J.; Andion, E.; Goodman, S.N.; Hidalgo, O.F.; Vanaclocha, V.; Baylin, S.B.; Herman, J.G. *Inactivation of the DNA-repair gene MGMT and the clinical response of gliomas to alkylating agents.* N Engl J Med, **2000**. 343(19): p. 1350-4.

22. Kaina, B.; Margison, G.P.; Christmann, M. *Targeting O(6)-methylguanine-DNA methyltransferase with specific inhibitors as a strategy in cancer therapy.* Cell Mol Life Sci, **2010**. 67(21): p. 3663-81.

23. Robertson, A.B.; Klungland, A.; Rognes, T.; Leiros, I. *DNA repair in mammalian cells: Base excision repair: the long and short of it.* Cell Mol Life Sci, **2009**. 66(6): p. 981-93.

24. Quinones, J.L.; Demple, B. *When DNA repair goes wrong: BER-generated DNA-protein crosslinks to oxidative lesions.* DNA Repair (Amst), **2016**. 44: p. 103-9.

25. Carter, R.J.; Parsons, J.L. *Base Excision Repair, a Pathway Regulated by Posttranslational Modifications.* Mol Cell Biol, **2016**. 36(10): p. 1426-37.

26. Narciso, L.; Parlanti, E.; Racaniello, M.; Simonelli, V.; Cardinale, A.; Merlo, D.; Dogliotti, E. *The Response to Oxidative DNA Damage in Neurons: Mechanisms and Disease.* Neural Plast, **2016**. 2016: p. 3619274.

27. El-Khamisy, S.F.; Masutani, M.; Suzuki, H.; Caldecott, K.W. *A requirement for PARP-1 for the assembly or stability of XRCC1 nuclear foci at sites of oxidative DNA damage.* Nucleic Acids Res, **2003**. 31(19): p. 5526-33.

28. Gagne, J.P.; Isabelle, M.; Lo, K.S.; Bourassa, S.; Hendzel, M.J.; Dawson, V.L.; Dawson, T.M.; Poirier, G.G. *Proteome-wide identification of poly(ADP-ribose) binding proteins and poly(ADP-ribose)-associated protein complexes.* Nucleic Acids Res, **2008**. 36(22): p. 6959-76.

29. Timinszky, G.; Till, S.; Hassa, P.O.; Hothorn, M.; Kustatscher, G.; Nijmeijer, B.; Colombelli, J.; Altmeyer, M.; Stelzer, E.H.; Scheffzek, K.; Hottiger, M.O.; Ladurner, A.G. *A macrodomain-containing histone rearranges chromatin upon sensing PARP1 activation.* Nat Struct Mol Biol, **2009**. 16(9): p. 923-9.

30. Fortini, P.; Dogliotti, E. *Base damage and single-strand break repair: mechanisms and functional significance of short- and long-patch repair subpathways.* DNA Repair (Amst), **2007**. 6(4): p. 398-409.

31. ClinicalTrials.gov. *https://clinicaltrials.gov/. (accessed 7/11/2017)*.

32. Reed, A.M.; Fishel, M.L.; Kelley, M.R. *Small-molecule inhibitors of proteins involved in base excision repair potentiate the anti-tumorigenic effect of existing chemotherapeutics and irradiation.* Future Oncol, **2009**. 5(5): p. 713-26.

33. Research, A.T. *http://apextherapeutics.com/research*.

34. Gao, Z.; Maloney, D.J.; Dedkova, L.M.; Hecht, S.M. *Inhibitors of DNA polymerase beta: activity and mechanism.* Bioorg Med Chem, **2008**. 16(8): p. 4331-40.

35. Tsutakawa, S.E.; Classen, S.; Chapados, B.R.; Arvai, A.S.; Finger, L.D.; Guenther, G.; Tomlinson, C.G.; Thompson, P.; Sarker, A.H.; Shen, B.; Cooper, P.K.; Grasby, J.A.; Tainer, J.A. *Human flap endonuclease structures, DNA double-base flipping, and a unified understanding of the FEN1 superfamily.* Cell, **2011**. 145(2): p. 198-211.

36. Spivak, G. *Nucleotide excision repair in humans.* DNA Repair, **2015**. 36: p. 13-18.

37. Sugasawa, K. *Molecular mechanisms of DNA damage recognition for mammalian nucleotide excision repair.* DNA Repair (Amst), **2016**. 44: p. 110-7.

38. Fadda, E. *Role of the XPA protein in the NER pathway: A perspective on the function of structural disorder in macromolecular assembly.* Comput Struct Biotechnol J, **2016**. 14: p. 78-85.

39. Ogi, T.; Limsirichaikul, S.; Overmeer, R.M.; Volker, M.; Takenaka, K.; Cloney, R.; Nakazawa, Y.; Niimi, A.; Miki, Y.; Jaspers, N.G.; Mullenders, L.H.F.; Yamashita, S.; Fousteri, M.I.; Lehmann, A.R. *Three DNA*

Polymerases, Recruited by Different Mechanisms, Carry Out NER Repair Synthesis in Human Cells. Mol. Cell, **2010**. 37(5): p. 714-727.

40. Lehmann, A.R. *DNA polymerases and repair synthesis in NER in human cells.* DNA Repair, **2011**. 10(7): p. 730-733.

41. Scharer, O.D. *Nucleotide excision repair in eukaryotes.* Cold Spring Harb Perspect Biol, **2013**. 5(10): p. a012609.

42. Kamileri, I.; Karakasilioti, I.; Garinis, G.A. *Nucleotide excision repair: new tricks with old bricks.* Trends Genet, **2012**. 28(11): p. 566-73.

43. Barakat, K.; Tuszynski, J. *Nucleotide Excision Repair Inhibitors: Still a Long Way to Go*. New Research Directions in DNA Repair. **2013**.

44. Barret, J.M.; Cadou, M.; Hill, B.T. *Inhibition of nucleotide excision repair and sensitisation of cells to DNA cross-linking anticancer drugs by F 11782, a novel fluorinated epipodophylloid.* Biochem Pharmacol, **2002**. 63(2): p. 251-8.

45. Jiang, H.; Yang, L.Y. *Cell cycle checkpoint abrogator UCN-01 inhibits DNA repair: association with attenuation of the interaction of XPA and ERCC1 nucleotide excision repair proteins.* Cancer Res, **1999**. 59(18): p. 4529-34.

46. Aune, G.J.; Furuta, T.; Pommier, Y. *Ecteinascidin 743: a novel anticancer drug with a unique mechanism of action.* Anticancer Drugs, **2002**. 13(6): p. 545-55.

47. Martin, S.A.; Lord, C.J.; Ashworth, A. *Therapeutic targeting of the DNA mismatch repair pathway.* Clin Cancer Res, **2010**. 16(21): p. 5107-13.

48. Stojic, L.; Brun, R.; Jiricny, J. *Mismatch repair and DNA damage signalling.* DNA Repair (Amst), **2004**. 3(8-9): p. 1091-101.

49. Hsieh, P.; Yamane, K. *DNA mismatch repair: molecular mechanism, cancer, and ageing.* Mech Ageing Dev, **2008**. 129(7-8): p. 391-407.

50. Li, G.M. *Mechanisms and functions of DNA mismatch repair.* Cell Res, **2008**. 18(1): p. 85-98.

51. de Wind, N.; Dekker, M.; Berns, A.; Radman, M.; te Riele, H. *Inactivation of the mouse Msh2 gene results in mismatch repair deficiency, methylation tolerance, hyperrecombination, and predisposition to cancer.* Cell, **1995**. 82(2): p. 321-30.

52. Khanna, K.K.; Jackson, S.P. *DNA double-strand breaks: signaling, repair and the cancer connection.* Nat Genet, **2001**. 27(3): p. 247-54.

53. Hartlerode, A.J.; Scully, R. *Mechanisms of double-strand break repair in somatic mammalian cells.* Biochem J, **2009**. 423(2): p. 157-68.

54. Meek, K.; Dang, V.; Lees-Miller, S.P. *Chapter 2 DNA-PK: The Means to Justify the Ends?*, in *Advances in Immunology*. **2008**, Academic Press. p. 33-58.

55. Helleday, T.; Petermann, E.; Lundin, C.; Hodgson, B.; Sharma, R.A. *DNA repair pathways as targets for cancer therapy.* Nat Rev Cancer, **2008**. 8(3): p. 193-204.

56. Krejci, L.; Altmannova, V.; Spirek, M.; Zhao, X. *Homologous recombination and its regulation.* Nucleic Acids Res, **2012**. 40(13): p. 5795-818.

57. Mimitou, E.P.; Symington, L.S. *Nucleases and helicases take center stage in homologous recombination.* Trends Biochem Sci, **2009**. 34(5): p. 264-72.

58. Ceccaldi, R.; Rondinelli, B.; D'Andrea, A.D. *Repair Pathway Choices and Consequences at the Double-Strand Break.* Trends Cell Biol, **2016**. 26(1): p. 52-64.

59. Chernikova, S.B.; Game, J.C.; Brown, J.M. *Inhibiting homologous recombination for cancer therapy.* Cancer Biol Ther, **2012**. 13(2): p. 61-8.

60. Helleday, T. *Homologous recombination in cancer development, treatment and development of drug resistance.* Carcinogenesis, **2010**. 31(6): p. 955-60.

61. Konecny, G.E.; Kristeleit, R.S. *PARP inhibitors for BRCA1/2-mutated and sporadic ovarian cancer: current practice and future directions.* Br J Cancer, **2016**. 115(10): p. 1157-1173.

62. Farmer, H.; McCabe, N.; Lord, C.J.; Tutt, A.N.; Johnson, D.A.; Richardson, T.B.; Santarosa, M.; Dillon, K.J.; Hickson, I.; Knights, C.; Martin, N.M.; Jackson, S.P.; Smith, G.C.; Ashworth, A. *Targeting the DNA repair defect in BRCA mutant cells as a therapeutic strategy.* Nature, **2005**. 434(7035): p. 917-21.

63. Bryant, H.E.; Schultz, N.; Thomas, H.D.; Parker, K.M.; Flower, D.; Lopez, E.; Kyle, S.; Meuth, M.; Curtin, N.J.; Helleday, T. *Specific killing of BRCA2-deficient tumours with inhibitors of poly(ADP-ribose) polymerase.* Nature, **2005**. 434(7035): p. 913-7.

64. Huang, F.; Motlekar, N.A.; Burgwin, C.M.; Napper, A.D.; Diamond, S.L.; Mazin, A.V. *Identification of specific inhibitors of human RAD51 recombinase using high-throughput screening.* ACS Chem Biol, **2011**. 6(6): p. 628-35.

65. Budke, B.; Logan, H.L.; Kalin, J.H.; Zelivianskaia, A.S.; Cameron McGuire, W.; Miller, L.L.; Stark, J.M.; Kozikowski, A.P.; Bishop, D.K.; Connell, P.P. *RI-1: a chemical inhibitor of RAD51 that disrupts homologous recombination in human cells.* Nucleic Acids Res, **2012**. 40(15): p. 7347-57.

66. Deakyne, J.S.; Huang, F.; Negri, J.; Tolliday, N.; Cocklin, S.; Mazin, A.V. *Analysis of the activities of RAD54, a SWI2/SNF2 protein, using a specific small-molecule inhibitor.* J Biol Chem, **2013**. 288(44): p. 31567-80.

67. Noguchi, M.; Yu, D.; Hirayama, R.; Ninomiya, Y.; Sekine, E.; Kubota, N.; Ando, K.; Okayasu, R. *Inhibition of homologous recombination repair in irradiated tumor cells pretreated with Hsp90 inhibitor 17-allylamino-17-demethoxygeldanamycin.* Biochem Biophys Res Commun, **2006**. 351(3): p. 658-63.

68. Weterings, E.; Chen, D.J. *The endless tale of non-homologous end-joining.* Cell Res, **2008**. 18(1): p. 114-24.

69. Kim, H.S.; Hromas, R.; Lee, S.H. *Emerging Features of DNA Double-Strand Break Repair in Humans*, in *New Research Directions in DNA Repair*, Chen, C., Editor. **2013**, InTech: Rijeka. p. Ch. 07.

70. Lieber, M.R. *The mechanism of human nonhomologous DNA end joining.* J Biol Chem, **2008**. 283(1): p. 1-5.

71. Ahrabi, S.; Sarkar, S.; Pfister, S.X.; Pirovano, G.; Higgins, G.S.; Porter, A.C.; Humphrey, T.C. *A role for human homologous recombination factors in suppressing microhomology-mediated end joining.* Nucleic Acids Res, **2016**. 44(12): p. 5743-57.

72. Dueva, R.; Iliakis, G. *Alternative pathways of non-homologous end joining (NHEJ) in genomic instability and cancer.* Transl Cancer Res, **2013**. 2(3): p. 163-177.

73. Shintani, S.; Mihara, M.; Li, C.; Nakahara, Y.; Hino, S.; Nakashiro, K.; Hamakawa, H. *Up-regulation of DNA-dependent protein kinase correlates with radiation resistance in oral squamous cell carcinoma.* Cancer Sci, **2003**. 94(10): p. 894-900.

74. Sirzen, F.; Nilsson, A.; Zhivotovsky, B.; Lewensohn, R. *DNA-dependent protein kinase content and activity in lung carcinoma cell lines: correlation with intrinsic radiosensitivity.* Eur J Cancer, **1999**. 35(1): p. 111-6.

75. Davidson, D.; Amrein, L.; Panasci, L.; Aloyz, R. *Small Molecules, Inhibitors of DNA-PK, Targeting DNA Repair, and Beyond.* Front Pharmacol, **2013**. 4: p. 5.

76. Srivastava, M.; Nambiar, M.; Sharma, S.; Karki, S.S.; Goldsmith, G.; Hegde, M.; Kumar, S.; Pandey, M.; Singh, R.K.; Ray, P.; Natarajan, R.; Kelkar, M.; De, A.; Choudhary, B.; Raghavan, S.C. *An inhibitor of nonhomologous end-joining abrogates double-strand break repair and impedes cancer progression.* Cell, **2012**. 151(7): p. 1474-87.

77. Chen, X.; Zhong, S.; Zhu, X.; Dziegielewska, B.; Ellenberger, T.; Wilson, G.M.; MacKerell, A.D., Jr.; Tomkinson, A.E. *Rational design of human DNA*

ligase inhibitors that target cellular DNA replication and repair. Cancer Res, **2008**. 68(9): p. 3169-77.

78. Groselj, B.; Sharma, N.L.; Hamdy, F.C.; Kerr, M.; Kiltie, A.E. *Histone deacetylase inhibitors as radiosensitisers: effects on DNA damage signalling and repair.* Br J Cancer, **2013**. 108(4): p. 748-54.

79. Adimoolam, S.; Sirisawad, M.; Chen, J.; Thiemann, P.; Ford, J.M.; Buggy, J.J. *HDAC inhibitor PCI-24781 decreases RAD51 expression and inhibits homologous recombination.* Proc Natl Acad Sci U S A, **2007**. 104(49): p. 19482-7.

80. Kuroda, S.; Urata, Y.; Fujiwara, T. *Ataxia-telangiectasia mutated and the Mre11-Rad50-NBS1 complex: promising targets for radiosensitization.* Acta Med Okayama, **2012**. 66(2): p. 83-92.

81. Dulaney, C.; Marcrom, S.; Stanley, J.; Yang, E.S. *Poly(ADP-ribose) Polymerase Activity and Inhibition in Cancer.* Semin Cell Dev Biol, **2017**.

82. Davis, A.J.; Chen, D.J. *DNA double strand break repair via non-homologous end-joining.* Transl Cancer Res, **2013**. 2(3): p. 130-143.

83. Lopez-Martinez, D.; Liang, C.C.; Cohn, M.A. *Cellular response to DNA interstrand crosslinks: the Fanconi anemia pathway.* Cell Mol Life Sci, **2016**. 73(16): p. 3097-114.

84. Walden, H.; Deans, A.J. *The Fanconi anemia DNA repair pathway: structural and functional insights into a complex disorder.* Annu Rev Biophys, **2014**. 43: p. 257-78.

85. Chen, C.C.; Taniguchi, T.; D'Andrea, A. *The Fanconi anemia (FA) pathway confers glioma resistance to DNA alkylating agents.* J Mol Med (Berl), **2007**. 85(5): p. 497-509.

86. Yao, C.; Du, W.; Chen, H.; Xiao, S.; Huang, L.; Chen, F. *The Fanconi anemia/BRCA pathway is involved in DNA interstrand cross-link repair of adriamycin-resistant leukemia cells.* Leuk Lymphoma, **2015**. 56(3): p. 755-62.

87. Burkitt, K.; Ljungman, M. *Phenylbutyrate interferes with the Fanconi anemia and BRCA pathway and sensitizes head and neck cancer cells to cisplatin.* Mol Cancer, **2008**. 7: p. 24.

88. Chen, Q.; Van der Sluis, P.C.; Boulware, D.; Hazlehurst, L.A.; Dalton, W.S. *The FA/BRCA pathway is involved in melphalan-induced DNA interstrand cross-link repair and accounts for melphalan resistance in multiple myeloma cells.* Blood, **2005**. 106(2): p. 698-705.

89. Voter, A.F.; Manthei, K.A.; Keck, J.L. *A High-Throughput Screening Strategy to Identify Protein-Protein Interaction Inhibitors That Block the*

Fanconi Anemia DNA Repair Pathway. J Biomol Screen, **2016**. 21(6): p. 626-33.

90. Waters, L.S.; Minesinger, B.K.; Wiltrout, M.E.; D'Souza, S.; Woodruff, R.V.; Walker, G.C. *Eukaryotic translesion polymerases and their roles and regulation in DNA damage tolerance.* Microbiol Mol Biol Rev, **2009**. 73(1): p. 134-54.

91. McVey, M.; Khodaverdian, V.Y.; Meyer, D.; Cerqueira, P.G.; Heyer, W.D. *Eukaryotic DNA Polymerases in Homologous Recombination.* Annu Rev Genet, **2016**. 50: p. 393-421.

92. Korzhnev, D.M.; Hadden, M.K. *Targeting the Translesion Synthesis Pathway for the Development of Anti-Cancer Chemotherapeutics.* J Med Chem, **2016**. 59(20): p. 9321-9336.

93. Passeri, D.; Camaioni, E.; Liscio, P.; Sabbatini, P.; Ferri, M.; Carotti, A.; Giacche, N.; Pellicciari, R.; Gioiello, A.; Macchiarulo, A. *Concepts and Molecular Aspects in the Polypharmacology of PARP-1 Inhibitors.* ChemMedChem, **2016**. 11(12): p. 1219-26.

94. Yelamos, J.; Farres, J.; Llacuna, L.; Ampurdanes, C.; Martin-Caballero, J. *PARP-1 and PARP-2: New players in tumour development.* Am J Cancer Res, **2011**. 1(3): p. 328-346.

95. Papeo, G.; Casale, E.; Montagnoli, A.; Cirla, A. *PARP inhibitors in cancer therapy: an update.* Expert Opin Ther Pat, **2013**. 23(4): p. 503-14.

96. Riffell, J.L.; Lord, C.J.; Ashworth, A. *Tankyrase-targeted therapeutics: expanding opportunities in the PARP family.* Nat Rev Drug Discov, **2012**. 11(12): p. 923-36.

97. Langelier, M.F.; Riccio, A.A.; Pascal, J.M. *PARP-2 and PARP-3 are selectively activated by 5' phosphorylated DNA breaks through an allosteric regulatory mechanism shared with PARP-1.* Nucleic Acids Res, **2014**. 42(12): p. 7762-75.

98. Hassa, P.O.; Haenni, S.S.; Elser, M.; Hottiger, M.O. *Nuclear ADP-ribosylation reactions in mammalian cells: where are we today and where are we going?* Microbiol Mol Biol Rev, **2006**. 70(3): p. 789-829.

99. Liscio, P.; Camaioni, E.; Carotti, A.; Pellicciari, R.; Macchiarulo, A. *From polypharmacology to target specificity: the case of PARP inhibitors.* Curr Top Med Chem, **2013**. 13(23): p. 2939-54.

100. Hottiger, M.O.; Hassa, P.O.; Luscher, B.; Schuler, H.; Koch-Nolte, F. *Toward a unified nomenclature for mammalian ADP-ribosyltransferases.* Trends Biochem Sci, **2010**. 35(4): p. 208-19.

101. Xu, S.; Bai, P.; Little, P.J.; Liu, P. *Poly(ADP-ribose) polymerase 1 (PARP1) in atherosclerosis: from molecular mechanisms to therapeutic implications.* Med Res Rev, **2014**. 34(3): p. 644-75.

102. Rodriguez, M.I.; Majuelos-Melguizo, J.; Marti Martin-Consuegra, J.M.; Ruiz de Almodovar, M.; Lopez-Rivas, A.; Javier Oliver, F. *Deciphering the insights of poly(ADP-ribosylation) in tumor progression.* Med Res Rev, **2015**. 35(4): p. 678-97.

103. Morales, J.; Li, L.; Fattah, F.J.; Dong, Y.; Bey, E.A.; Patel, M.; Gao, J.; Boothman, D.A. *Review of poly (ADP-ribose) polymerase (PARP) mechanisms of action and rationale for targeting in cancer and other diseases.* Crit Rev Eukaryot Gene Expr, **2014**. 24(1): p. 15-28.

104. Scott, C.L.; Swisher, E.M.; Kaufmann, S.H. *Poly (ADP-ribose) polymerase inhibitors: recent advances and future development.* J Clin Oncol, **2015**. 33(12): p. 1397-406.

105. Verdone, L.; La Fortezza, M.; Ciccarone, F.; Caiafa, P.; Zampieri, M.; Caserta, M. *Poly(ADP-Ribosyl)ation Affects Histone Acetylation and Transcription.* PLoS One, **2015**. 10(12): p. e0144287.

106. Lupo, B.; Trusolino, L. *Inhibition of poly(ADP-ribosyl)ation in cancer: old and new paradigms revisited.* Biochim Biophys Acta, **2014**. 1846(1): p. 201-15.

107. Ferraris, D.V. *Evolution of poly(ADP-ribose) polymerase-1 (PARP-1) inhibitors. From concept to clinic.* J Med Chem, **2010**. 53(12): p. 4561-84.

108. Bai, P.; Houten, S.M.; Huber, A.; Schreiber, V.; Watanabe, M.; Kiss, B.; de Murcia, G.; Auwerx, J.; Menissier-de Murcia, J. *Poly(ADP-ribose) polymerase-2 [corrected] controls adipocyte differentiation and adipose tissue function through the regulation of the activity of the retinoid X receptor/peroxisome proliferator-activated receptor-gamma [corrected] heterodimer.* J Biol Chem, **2007**. 282(52): p. 37738-46.

109. Dantzer, F.; Mark, M.; Quenet, D.; Scherthan, H.; Huber, A.; Liebe, B.; Monaco, L.; Chicheportiche, A.; Sassone-Corsi, P.; de Murcia, G.; Menissier-de Murcia, J. *Poly(ADP-ribose) polymerase-2 contributes to the fidelity of male meiosis I and spermiogenesis.* Proc Natl Acad Sci U S A, **2006**. 103(40): p. 14854-9.

110. Yelamos, J.; Monreal, Y.; Saenz, L.; Aguado, E.; Schreiber, V.; Mota, R.; Fuente, T.; Minguela, A.; Parrilla, P.; de Murcia, G.; Almarza, E.; Aparicio, P.; Menissier-de Murcia, J. *PARP-2 deficiency affects the survival of CD4+CD8+ double-positive thymocytes.* EMBO J, **2006**. 25(18): p. 4350-60.

111. Haikarainen, T.; Krauss, S.; Lehtio, L. *Tankyrases: structure, function and therapeutic implications in cancer.* Curr Pharm Des, **2014**. 20(41): p. 6472-88.

112. Miknyoczki, S.; Chang, H.; Grobelny, J.; Pritchard, S.; Worrell, C.; McGann, N.; Ator, M.; Husten, J.; Deibold, J.; Hudkins, R.; Zulli, A.; Parchment, R.; Ruggeri, B. *The selective poly(ADP-ribose) polymerase-1(2) inhibitor, CEP-8983, increases the sensitivity of chemoresistant tumor cells to temozolomide and irinotecan but does not potentiate myelotoxicity.* Mol Cancer Ther, **2007**. 6(8): p. 2290-302.

113. Awada, A.; Campone, M.; Varga, A.; Aftimos, P.; Frenel, J.S.; Bahleda, R.; Gombos, A.; Bourbouloux, E.; Soria, J.C. *An open-label, dose-escalation study to evaluate the safety and pharmacokinetics of CEP-9722 (a PARP-1 and PARP-2 inhibitor) in combination with gemcitabine and cisplatin in patients with advanced solid tumors.* Anticancer Drugs, **2016**. 27(4): p. 342-8.

114. Lechaftois, M.; Dreano, E.; Palmier, B.; Margaill, I.; Marchand-Leroux, C.; Bachelot-Loza, C.; Lerouet, D. *Another "string to the bow" of PJ34, a potent poly(ADP-Ribose)polymerase inhibitor: an antiplatelet effect through P2Y12 antagonism?* PLoS One, **2014**. 9(10): p. e110776.

115. Bedikian, A.Y.; Papadopoulos, N.E.; Kim, K.B.; Hwu, W.J.; Homsi, J.; Glass, M.R.; Cain, S.; Rudewicz, P.; Vernillet, L.; Hwu, P. *A phase IB trial of intravenous INO-1001 plus oral temozolomide in subjects with unresectable stage-III or IV melanoma.* Cancer Invest, **2009**. 27(7): p. 756-63.

116. McGonigle, S.; Chen, Z.; Wu, J.; Chang, P.; Kolber-Simonds, D.; Ackermann, K.; Twine, N.C.; Shie, J.L.; Miu, J.T.; Huang, K.C.; Moniz, G.A.; Nomoto, K. *E7449: A dual inhibitor of PARP1/2 and tankyrase1/2 inhibits growth of DNA repair deficient tumors and antagonizes Wnt signaling.* Oncotarget, **2015**. 6(38): p. 41307-23.

117. Jones, P.; Wilcoxen, K.; Rowley, M.; Toniatti, C. *Niraparib: A Poly(ADP-ribose) Polymerase (PARP) Inhibitor for the Treatment of Tumors with Defective Homologous Recombination.* J Med Chem, **2015**. 58(8): p. 3302-14.

118. Penning, T.D.; Zhu, G.D.; Gandhi, V.B.; Gong, J.; Liu, X.; Shi, Y.; Klinghofer, V.; Johnson, E.F.; Donawho, C.K.; Frost, D.J.; Bontcheva-Diaz, V.; Bouska, J.J.; Osterling, D.J.; Olson, A.M.; Marsh, K.C.; Luo, Y.; Giranda, V.L. *Discovery of the Poly(ADP-ribose) polymerase (PARP) inhibitor 2-[(R)-2-methylpyrrolidin-2-yl]-1H-benzimidazole-4-carboxamide (ABT-888) for the treatment of cancer.* J Med Chem, **2009**. 52(2): p. 514-23.

119. Wang, B.; Chu, D.; Feng, Y.; Shen, Y.; Aoyagi-Scharber, M.; Post, L.E. *Discovery and Characterization of (8S,9R)-5-Fluoro-8-(4-fluorophenyl)-9-(1-methyl-1H-1,2,4-triazol-5-yl)-2,7,8,9-te trahydro-3H-pyrido[4,3,2-de]phthalazin-3-one (BMN 673, Talazoparib), a Novel, Highly Potent, and Orally Efficacious Poly(ADP-ribose) Polymerase-1/2 Inhibitor, as an Anticancer Agent.* J Med Chem, **2016**. 59(1): p. 335-57.

120. Kim, G.; Ison, G.; McKee, A.E.; Zhang, H.; Tang, S.; Gwise, T.; Sridhara, R.; Lee, E.; Tzou, A.; Philip, R.; Chiu, H.J.; Ricks, T.K.; Palmby, T.; Russell, A.M.; Ladouceur, G.; Pfuma, E.; Li, H.; Zhao, L.; Liu, Q.; Venugopal, R.; Ibrahim, A.; Pazdur, R. *FDA Approval Summary: Olaparib Monotherapy in Patients with Deleterious Germline BRCA-Mutated Advanced Ovarian Cancer Treated with Three or More Lines of Chemotherapy.* Clin Cancer Res, **2015**. 21(19): p. 4257-61.

121. Ledermann, J.; Harter, P.; Gourley, C.; Friedlander, M.; Vergote, I.; Rustin, G.; Scott, C.; Meier, W.; Shapira-Frommer, R.; Safra, T.; Matei, D.; Macpherson, E.; Watkins, C.; Carmichael, J.; Matulonis, U. *Olaparib maintenance therapy in platinum-sensitive relapsed ovarian cancer.* N Engl J Med, **2012**. 366(15): p. 1382-92.

122. Ledermann, J.; Harter, P.; Gourley, C.; Friedlander, M.; Vergote, I.; Rustin, G.; Scott, C.L.; Meier, W.; Shapira-Frommer, R.; Safra, T.; Matei, D.; Fielding, A.; Spencer, S.; Dougherty, B.; Orr, M.; Hodgson, D.; Barrett, J.C.; Matulonis, U. *Olaparib maintenance therapy in patients with platinum-sensitive relapsed serous ovarian cancer: a preplanned retrospective analysis of outcomes by BRCA status in a randomised phase 2 trial.* Lancet Oncol, **2014**. 15(8): p. 852-61.

123. Gelmon, K.A.; Tischkowitz, M.; Mackay, H.; Swenerton, K.; Robidoux, A.; Tonkin, K.; Hirte, H.; Huntsman, D.; Clemons, M.; Gilks, B.; Yerushalmi, R.; Macpherson, E.; Carmichael, J.; Oza, A. *Olaparib in patients with recurrent high-grade serous or poorly differentiated ovarian carcinoma or triple-negative breast cancer: a phase 2, multicentre, open-label, non-randomised study.* Lancet Oncol, **2011**. 12(9): p. 852-61.

124. Kaufman, B.; Shapira-Frommer, R.; Schmutzler, R.K.; Audeh, M.W.; Friedlander, M.; Balmana, J.; Mitchell, G.; Fried, G.; Stemmer, S.M.; Hubert, A.; Rosengarten, O.; Steiner, M.; Loman, N.; Bowen, K.; Fielding, A.; Domchek, S.M. *Olaparib monotherapy in patients with advanced cancer and a germline BRCA1/2 mutation.* J Clin Oncol, **2015**. 33(3): p. 244-50.

125. Audeh, M.W.; Carmichael, J.; Penson, R.T.; Friedlander, M.; Powell, B.; Bell-McGuinn, K.M.; Scott, C.; Weitzel, J.N.; Oaknin, A.; Loman, N.; Lu, K.; Schmutzler, R.K.; Matulonis, U.; Wickens, M.; Tutt, A. *Oral poly(ADP-ribose) polymerase inhibitor olaparib in patients with BRCA1 or BRCA2 mutations and recurrent ovarian cancer: a proof-of-concept trial.* Lancet, **2010**. 376(9737): p. 245-51.

126. Tutt, A.; Robson, M.; Garber, J.E.; Domchek, S.M.; Audeh, M.W.; Weitzel, J.N.; Friedlander, M.; Arun, B.; Loman, N.; Schmutzler, R.K.; Wardley, A.; Mitchell, G.; Earl, H.; Wickens, M.; Carmichael, J. *Oral poly(ADP-ribose) polymerase inhibitor olaparib in patients with BRCA1 or BRCA2 mutations and advanced breast cancer: a proof-of-concept trial.* Lancet, **2010**. 376(9737): p. 235-44.

127. Mateo, J.; Carreira, S.; Sandhu, S.; Miranda, S.; Mossop, H.; Perez-Lopez, R.; Nava Rodrigues, D.; Robinson, D.; Omlin, A.; Tunariu, N.; Boysen, G.; Porta, N.; Flohr, P.; Gillman, A.; Figueiredo, I.; Paulding, C.; Seed, G.; Jain, S.; Ralph, C.; Protheroe, A.; Hussain, S.; Jones, R.; Elliott, T.; McGovern, U.; Bianchini, D.; Goodall, J.; Zafeiriou, Z.; Williamson, C.T.; Ferraldeschi, R.; Riisnaes, R.; Ebbs, B.; Fowler, G.; Roda, D.; Yuan, W.; Wu, Y.M.; Cao, X.; Brough, R.; Pemberton, H.; A'Hern, R.; Swain, A.; Kunju, L.P.; Eeles, R.; Attard, G.; Lord, C.J.; Ashworth, A.; Rubin, M.A.; Knudsen, K.E.; Feng, F.Y.; Chinnaiyan, A.M.; Hall, E.; de Bono, J.S. *DNA-Repair Defects and Olaparib in Metastatic Prostate Cancer.* N Engl J Med, **2015**. 373(18): p. 1697-708.

128. Choy, E.; Butrynski, J.E.; Harmon, D.C.; Morgan, J.A.; George, S.; Wagner, A.J.; D'Adamo, D.; Cote, G.M.; Flamand, Y.; Benes, C.H.; Haber, D.A.; Baselga, J.M.; Demetri, G.D. *Phase II study of olaparib in patients with refractory Ewing sarcoma following failure of standard chemotherapy.* BMC Cancer, **2014**. 14: p. 813.

129. Bixel, K.; Hays, J.L. *Olaparib in the management of ovarian cancer.* Pharmgenomics Pers Med, **2015**. 8: p. 127-35.

130. Bang, Y.-J.; Im, S.-A.; Lee, K.-W.; Cho, J.Y.; Song, E.-K.; Lee, K.H.; Kim, Y.H.; Park, J.O.; Chun, H.G.; Zang, D.Y.; Fielding, A.; Rowbottom, J.; Hodgson, D.; O'Connor, M.J.; Yin, X.; Kim, W.H. *Randomized, Double-Blind Phase II Trial With Prospective Classification by ATM Protein Level to Evaluate the Efficacy and Tolerability of Olaparib Plus Paclitaxel in Patients With Recurrent or Metastatic Gastric Cancer.* J Clin Oncol, **2015**. 33(33): p. 3858-3865.

131. Liu, J.F.; Tolaney, S.M.; Birrer, M.; Fleming, G.F.; Buss, M.K.; Dahlberg, S.E.; Lee, H.; Whalen, C.; Tyburski, K.; Winer, E.; Ivy, P.; Matulonis, U.A. *A Phase 1 trial of the poly(ADP-ribose) polymerase inhibitor olaparib (AZD2281) in combination with the anti-angiogenic cediranib (AZD2171) in recurrent epithelial ovarian or triple-negative breast cancer.* Eur J Cancer, **2013**. 49(14): p. 2972-8.

132. Liu, J.F.; Barry, W.T.; Birrer, M.; Lee, J.M.; Buckanovich, R.J.; Fleming, G.F.; Rimel, B.; Buss, M.K.; Nattam, S.; Hurteau, J.; Luo, W.; Quy, P.; Whalen, C.; Obermayer, L.; Lee, H.; Winer, E.P.; Kohn, E.C.; Ivy, S.P.; Matulonis, U.A. *Combination cediranib and olaparib versus olaparib alone for women with recurrent platinum-sensitive ovarian cancer: a randomised phase 2 study.* Lancet Oncol, **2014**. 15(11): p. 1207-14.

133. Matulonis, U.; Wulf, G.M.; Birrer, M.J.; Westin, S.N.; Quy, P.; Bell-Mcguinn, K.M.; Lasonde, B.; Whalen, C.; Aghajanian, C.; Solit, D.B.; Mills, G.B.; Cantley, L.; Winer, E.P. *Phase I study of oral BKM120 and oral olaparib for high-grade serous ovarian cancer (HGSC) or triple-negative breast cancer (TNBC).* J Clin Oncol, **2014** . 32(15 suppl.).

134. Fong, P.C.; Boss, D.S.; Yap, T.A.; Tutt, A.; Wu, P.; Mergui-Roelvink, M.; Mortimer, P.; Swaisland, H.; Lau, A.; O'Connor, M.J.; Ashworth, A.; Carmichael, J.; Kaye, S.B.; Schellens, J.H.; de Bono, J.S. *Inhibition of poly(ADP-ribose) polymerase in tumors from BRCA mutation carriers.* N Engl J Med, **2009**. 361(2): p. 123-34.

135. Yamamoto, N.; Nokihara, H.; Yamada, Y.; Goto, Y.; Tanioka, M.; Shibata, T.; Yamada, K.; Asahina, H.; Kawata, T.; Shi, X.; Tamura, T. *A Phase I, dose-finding and pharmacokinetic study of olaparib (AZD2281) in Japanese patients with advanced solid tumors.* Cancer Sci, **2012**. 103(3): p. 504-9.

136. Bundred, N.; Gardovskis, J.; Jaskiewicz, J.; Eglitis, J.; Paramonov, V.; McCormack, P.; Swaisland, H.; Cavallin, M.; Parry, T.; Carmichael, J.; Dixon, J.M. *Evaluation of the pharmacodynamics and pharmacokinetics of the PARP inhibitor olaparib: a phase I multicentre trial in patients scheduled for elective breast cancer surgery.* Invest New Drugs, **2013**. 31(4): p. 949-58.

137. Lee, J.M.; Hays, J.L.; Annunziata, C.M.; Noonan, A.M.; Minasian, L.; Zujewski, J.A.; Yu, M.; Gordon, N.; Ji, J.; Sissung, T.M.; Figg, W.D.; Azad, N.; Wood, B.J.; Doroshow, J.; Kohn, E.C. *Phase I/Ib study of olaparib and carboplatin in BRCA1 or BRCA2 mutation-associated breast or ovarian cancer with biomarker analyses.* J Natl Cancer Inst, **2014**. 106(6): p. dju089.

138. Balmana, J.; Tung, N.M.; Isakoff, S.J.; Grana, B.; Ryan, P.D.; Saura, C.; Lowe, E.S.; Frewer, P.; Winer, E.; Baselga, J.; Garber, J.E. *Phase I trial of olaparib in combination with cisplatin for the treatment of patients with advanced breast, ovarian and other solid tumors.* Ann Oncol, **2014**. 25(8): p. 1656-63.

139. Del Conte, G.; Sessa, C.; von Moos, R.; Vigano, L.; Digena, T.; Locatelli, A.; Gallerani, E.; Fasolo, A.; Tessari, A.; Cathomas, R.; Gianni, L. *Phase I study of olaparib in combination with liposomal doxorubicin in patients with advanced solid tumours.* Br J Cancer, **2014**. 111(4): p. 651-9.

140. Rajan, A.; Carter, C.A.; Kelly, R.J.; Gutierrez, M.; Kummar, S.; Szabo, E.; Yancey, M.A.; Ji, J.; Mannargudi, B.; Woo, S.; Spencer, S.; Figg, W.D.; Giaccone, G. *A phase I combination study of olaparib with cisplatin and gemcitabine in adults with solid tumors.* Clin Cancer Res, **2012**. 18(8): p. 2344-51.

141. Samol, J.; Ranson, M.; Scott, E.; Macpherson, E.; Carmichael, J.; Thomas, A.; Cassidy, J. *Safety and tolerability of the poly(ADP-ribose) polymerase (PARP) inhibitor, olaparib (AZD2281) in combination with topotecan for the treatment of patients with advanced solid tumors: a phase I study.* Invest New Drugs, **2012**. 30(4): p. 1493-500.

142. Plummer, R.; Jones, C.; Middleton, M.; Wilson, R.; Evans, J.; Olsen, A.; Curtin, N.; Boddy, A.; McHugh, P.; Newell, D.; Harris, A.; Johnson, P.;

Steinfeldt, H.; Dewji, R.; Wang, D.; Robson, L.; Calvert, H. *Phase I study of the poly(ADP-ribose) polymerase inhibitor, AG014699, in combination with temozolomide in patients with advanced solid tumors.* Clin Cancer Res, **2008**. 14(23): p. 7917-23.

143. Plummer, R.; Lorigan, P.; Steven, N.; Scott, L.; Middleton, M.R.; Wilson, R.H.; Mulligan, E.; Curtin, N.; Wang, D.; Dewji, R.; Abbattista, A.; Gallo, J.; Calvert, H. *A phase II study of the potent PARP inhibitor, Rucaparib (PF-01367338, AG014699), with temozolomide in patients with metastatic melanoma demonstrating evidence of chemopotentiation.* Cancer Chemother Pharmacol, **2013**. 71(5): p. 1191-9.

144. Falzacappa, M.V.; Ronchini, C.; Faretta, M.; Iacobucci, I.; Di Rora, A.G.; Martinelli, G.; Meyer, L.H.; Debatin, K.M.; Orecchioni, S.; Bertolini, F.; Pelicci, P.G. *The Combination of the PARP Inhibitor Rucaparib and 5FU Is an Effective Strategy for Treating Acute Leukemias.* Mol Cancer Ther, **2015**. 14(4): p. 889-98.

145. Liu, J.F.; Konstantinopoulos, P.A.; Matulonis, U.A. *PARP inhibitors in ovarian cancer: current status and future promise.* Gynecol Oncol, **2014**. 133(2): p. 362-9.

146. *Rucaparib Approved for Ovarian Cancer.* Cancer Discovery, **2017**.

147. Scott, L.J. *Niraparib: First Global Approval.* Drugs, **2017**. 77(9): p. 1029-1034.

148. *European Medicines Agency: EMA/CHMP/574018/2017 - Committee for Medicinal Products for Human Use (CHMP).* *http://www.ema.europa.eu/docs/en_GB/document_library/Summary_of_opinion_-_Initial_authorisation/human/004249/WC500234797.pdf*. **2017**.

149. Steffen, J.D.; Brody, J.R.; Armen, R.S.; Pascal, J.M. *Structural Implications for Selective Targeting of PARPs.* Front Oncol, **2013**. 3: p. 301.

150. Wang, Y.Q.; Wang, P.Y.; Wang, Y.T.; Yang, G.F.; Zhang, A.; Miao, Z.H. *An Update on Poly(ADP-ribose)polymerase-1 (PARP-1) Inhibitors: Opportunities and Challenges in Cancer Therapy.* J Med Chem, **2016**. 59(21): p. 9575-9598.

151. Banasik, M.; Komura, H.; Shimoyama, M.; Ueda, K. *Specific inhibitors of poly(ADP-ribose) synthetase and mono(ADP-ribosyl)transferase.* J Biol Chem, **1992**. 267(3): p. 1569-75.

152. Iglesias, P.; Costoya, J.A. *The antimitotic potential of PARP inhibitors, an unexplored therapeutic alternative.* Curr Top Med Chem, **2014**. 14(20): p. 2346-65.

153. Watson, C.Y.; Whish, W.J.; Threadgill, M.D. *Synthesis of 3-substituted benzamides and 5-substituted isoquinolin-1(2H)-ones and preliminary*

evaluation as inhibitors of poly(ADP-ribose)polymerase (PARP). Bioorg Med Chem, **1998**. 6(6): p. 721-34.

154. Suto, M.J.; Turner, W.R.; Arundel-Suto, C.M.; Werbel, L.M.; Sebolt-Leopold, J.S. *Dihydroisoquinolinones: the design and synthesis of a new series of potent inhibitors of poly(ADP-ribose) polymerase.* Anticancer Drug Des, **1991**. 6(2): p. 107-17.

155. Jaspers, J.E.; Kersbergen, A.; Boon, U.; Sol, W.; van Deemter, L.; Zander, S.A.; Drost, R.; Wientjens, E.; Ji, J.; Aly, A.; Doroshow, J.H.; Cranston, A.; Martin, N.M.; Lau, A.; O'Connor, M.J.; Ganesan, S.; Borst, P.; Jonkers, J.; Rottenberg, S. *Loss of 53BP1 causes PARP inhibitor resistance in Brca1-mutated mouse mammary tumors.* Cancer Discov, **2013**. 3(1): p. 68-81.

156. Lawlor, D.; Martin, P.; Busschots, S.; Thery, J.; O'Leary, J.J.; Hennessy, B.T.; Stordal, B. *PARP Inhibitors as P-glyoprotein Substrates.* J Pharm Sci, **2014**. 103(6): p. 1913-20.

157. Williams, R. *Discontinued drugs in 2011: oncology drugs.* Expert Opin Investig Drugs, **2013**. 22(1): p. 9-34.

158. Pescatore, G.; Branca, D.; Fiore, F.; Kinzel, O.; Bufi, L.L.; Muraglia, E.; Orvieto, F.; Rowley, M.; Toniatti, C.; Torrisi, C.; Jones, P. *Identification and SAR of novel pyrrolo[1,2-a]pyrazin-1(2H)-one derivatives as inhibitors of poly(ADP-ribose) polymerase-1 (PARP-1).* Bioorg Med Chem Lett, **2010**. 20(3): p. 1094-9.

159. Ferrigno, F.; Branca, D.; Kinzel, O.; Lillini, S.; Llauger Bufi, L.; Monteagudo, E.; Muraglia, E.; Rowley, M.; Schultz-Fademrecht, C.; Toniatti, C.; Torrisi, C.; Jones, P. *Development of substituted 6-[4-fluoro-3-(piperazin-1-ylcarbonyl)benzyl]-4,5-dimethylpyridazin-3(2H)-ones as potent poly(ADP-ribose) polymerase-1 (PARP-1) inhibitors active in BRCA deficient cells.* Bioorg Med Chem Lett, **2010**. 20(3): p. 1100-5.

160. Zhu, G.D.; Gong, J.; Gandhi, V.B.; Liu, X.; Shi, Y.; Johnson, E.F.; Donawho, C.K.; Ellis, P.A.; Bouska, J.J.; Osterling, D.J.; Olson, A.M.; Park, C.; Luo, Y.; Shoemaker, A.; Giranda, V.L.; Penning, T.D. *Discovery and SAR of orally efficacious tetrahydropyridopyridazinone PARP inhibitors for the treatment of cancer.* Bioorg Med Chem, **2012**. 20(15): p. 4635-45.

161. Aoyagi-Scharber, M.; Gardberg, A.S.; Yip, B.K.; Wang, B.; Shen, Y.; Fitzpatrick, P.A. *Structural basis for the inhibition of poly(ADP-ribose) polymerases 1 and 2 by BMN 673, a potent inhibitor derived from dihydropyridophthalazinone.* Acta Crystallogr F Struct Biol Commun, **2014**. 70(Pt 9): p. 1143-9.

162. Park, C.H.; Chun, K.; Joe, B.Y.; Park, J.S.; Kim, Y.C.; Choi, J.S.; Ryu, D.K.; Koh, S.H.; Cho, G.W.; Kim, S.H.; Kim, M.H. *Synthesis and evaluation of tricyclic derivatives containing a non-aromatic amide as inhibitors of poly(ADP-ribose)polymerase-1 (PARP-1).* Bioorg Med Chem Lett, **2010**. 20(7): p. 2250-3.

163. Gangloff, A.R.; Brown, J.; de Jong, R.; Dougan, D.R.; Grimshaw, C.E.; Hixon, M.; Jennings, A.; Kamran, R.; Kiryanov, A.; O'Connell, S.; Taylor, E.; Vu, P. *Discovery of novel benzo[b][1,4]oxazin-3(4H)-ones as poly(ADP-ribose)polymerase inhibitors.* Bioorg Med Chem Lett, **2013**. 23(16): p. 4501-5.

164. Chen, J.; Peng, H.; He, J.; Huan, X.; Miao, Z.; Yang, C. *Synthesis of isoquinolinone-based tricycles as novel poly(ADP-ribose) polymerase-1 (PARP-1) inhibitors.* Bioorg Med Chem Lett, **2014**. 24(12): p. 2669-73.

165. Ye, N.; Chen, C.H.; Chen, T.; Song, Z.; He, J.X.; Huan, X.J.; Song, S.S.; Liu, Q.; Chen, Y.; Ding, J.; Xu, Y.; Miao, Z.H.; Zhang, A. *Design, synthesis, and biological evaluation of a series of benzo[de][1,7]naphthyridin-7(8H)-ones bearing a functionalized longer chain appendage as novel PARP1 inhibitors.* J Med Chem, **2013**. 56(7): p. 2885-903.

166. Giannini, G.; Battistuzzi, G.; Vesci, L.; Milazzo, F.M.; De Paolis, F.; Barbarino, M.; Guglielmi, M.B.; Carollo, V.; Gallo, G.; Artali, R.; Dallavalle, S. *Novel PARP-1 inhibitors based on a 2-propanoyl-3H-quinazolin-4-one scaffold.* Bioorg Med Chem Lett, **2014**. 24(2): p. 462-6.

167. Zhou, Q.; Ji, M.; Zhou, J.; Jin, J.; Xue, N.; Chen, J.; Xu, B.; Chen, X. *Poly (ADP-ribose) polymerases inhibitor, Zj6413, as a potential therapeutic agent against breast cancer.* Biochem Pharmacol, **2016**. 107: p. 29-40.

168. Griffin, R.J.; Pemberton, L.C.; Rhodes, D.; Bleasdale, C.; Bowman, K.; Calvert, A.H.; Curtin, N.J.; Durkacz, B.W.; Newell, D.R.; Porteous, J.K. et al. *Novel potent inhibitors of the DNA repair enzyme poly(ADP-ribose)polymerase (PARP).* Anticancer Drug Des, **1995**. 10(6): p. 507-14.

169. Zhu, Q.; Wang, X.; Chu, Z.; He, G.; Dong, G.; Xu, Y. *Design, synthesis and biological evaluation of novel imidazo[4,5-c]pyridinecarboxamide derivatives as PARP-1 inhibitors.* Bioorg Med Chem Lett, **2013**. 23(7): p. 1993-1996.

170. Patel, M.R.; Bhatt, A.; Steffen, J.D.; Chergui, A.; Murai, J.; Pommier, Y.; Pascal, J.M.; Trombetta, L.D.; Fronczek, F.R.; Talele, T.T. *Discovery and structure-activity relationship of novel 2,3-dihydrobenzofuran-7-carboxamide and 2,3-dihydrobenzofuran-3(2H)-one-7-carboxamide derivatives as poly(ADP-ribose)polymerase-1 inhibitors.* J Med Chem, **2014**. 57(13): p. 5579-601.

171. Cincinelli, R.; Musso, L.; Merlini, L.; Giannini, G.; Vesci, L.; Milazzo, F.M.; Carenini, N.; Perego, P.; Penco, S.; Artali, R.; Zunino, F.; Pisano, C.; Dallavalle, S. *7-Azaindole-1-carboxamides as a new class of PARP-1 inhibitors.* Bioorg Med Chem, **2014**. 22(3): p. 1089-103.

172. Lee, Y.-R.; Yu, D.-S.; Liang, Y.-C.; Huang, K.-F.; Chou, S.-J.; Chen, T.-C.; Lee, C.-C.; Chen, C.-L.; Chiou, S.-H.; Huang, H.-S. *New Approaches of PARP-1 Inhibitors in Human Lung Cancer Cells and Cancer Stem-Like Cells by Some Selected Anthraquinone-Derived Small Molecules.* PLoS ONE, **2013**. 8(2): p. e56284.

173. Song, M.; Li, J.L.; Li, X.P.; Kan, S.F. *Targeting Human Poly(ADP-Ribose) Polymerase-1 with Natural Medicines and Its Potential Applications in Ovarian Cancer Therapeutics.* Arch Pharm (Weinheim), **2015**.

174. Ishida, J.; Yamamoto, H.; Kido, Y.; Kamijo, K.; Murano, K.; Miyake, H.; Ohkubo, M.; Kinoshita, T.; Warizaya, M.; Iwashita, A.; Mihara, K.; Matsuoka, N.; Hattori, K. *Discovery of potent and selective PARP-1 and PARP-2 inhibitors: SBDD analysis via a combination of X-ray structural study and homology modeling.* Bioorg Med Chem, **2006**. 14(5): p. 1378-90.

175. Eltze, T.; Boer, R.; Wagner, T.; Weinbrenner, S.; McDonald, M.C.; Thiemermann, C.; Burkle, A.; Klein, T. *Imidazoquinolinone, imidazopyridine, and isoquinolindione derivatives as novel and potent inhibitors of the poly(ADP-ribose) polymerase (PARP): a comparison with standard PARP inhibitors.* Mol Pharmacol, **2008**. 74(6): p. 1587-98.

176. Papeo, G.M.E.; BORGHI, D.; Caruso, M.; Posteri, H.; Krasavin, M.Y. *3-oxo-2,3-dihydro-1h-indazole-4-carboxamide derivatives as PARP-1 inhibitors*. US Patent 9,073,893 (July 15, 2015).

177. Papeo, G.; Posteri, H.; Borghi, D.; Busel, A.A.; Caprera, F.; Casale, E.; Ciomei, M.; Cirla, A.; Corti, E.; D'Anello, M.; Fasolini, M.; Forte, B.; Galvani, A.; Isacchi, A.; Khvat, A.; Krasavin, M.Y.; Lupi, R.; Orsini, P.; Perego, R.; Pesenti, E.; Pezzetta, D.; Rainoldi, S.; Riccardi-Sirtori, F.; Scolaro, A.; Sola, F.; Zuccotto, F.; Felder, E.R.; Donati, D.; Montagnoli, A. *Discovery of 2-[1-(4,4-Difluorocyclohexyl)piperidin-4-yl]-6-fluoro-3-oxo-2,3-dihydro-1H-isoindole-4-carboxamide (NMS-P118): A Potent, Orally Available, and Highly Selective PARP-1 Inhibitor for Cancer Therapy.* J Med Chem, **2015**. 58(17): p. 6875-98.

178. Kumar, C.; Rani, N.; Velan Lakshmi, P.T.; Arunachalam, A. *A comprehensive look of poly(ADP-ribose) polymerase inhibition strategies and future directions for cancer therapy.* Future Med Chem, **2017**. 9(1): p. 37-60.

179. Murai, J.; Huang, S.Y.; Das, B.B.; Renaud, A.; Zhang, Y.; Doroshow, J.H.; Ji, J.; Takeda, S.; Pommier, Y. *Trapping of PARP1 and PARP2 by Clinical PARP Inhibitors.* Cancer Res, **2012**. 72(21): p. 5588-99.

180. Shen, Y.; Aoyagi-Scharber, M. Wang, B. *Trapping Poly(ADP-Ribose) Polymerase.* J Pharmacol Exp Ther, **2015**. 353(3): p. 446-57.

181. Murai, J.; Huang, S.Y.; Renaud, A.; Zhang, Y.; Ji, J.; Takeda, S.; Morris, J.; Teicher, B.; Doroshow, J.H.; Pommier, Y. *Stereospecific PARP trapping by BMN 673 and comparison with olaparib and rucaparib.* Mol Cancer Ther, **2014**. 13(2): p. 433-43.

182. Hopkins, T.A.; Shi, Y.; Rodriguez, L.E.; Solomon, L.R.; Donawho, C.K.; DiGiammarino, E.L.; Panchal, S.C.; Wilsbacher, J.L.; Gao, W.; Olson, A.M.; Stolarik, D.F.; Osterling, D.J.; Johnson, E.F.; Maag, D. *Mechanistic*

Dissection of PARP1 Trapping and the Impact on In Vivo Tolerability and Efficacy of PARP Inhibitors. Mol Cancer Res, **2015**. 13(11): p. 1465-77.

183. Kaelin, W.G. *The Concept of Synthetic Lethality in the Context of Anticancer Therapy.* Nat. Rev. Cancer, **2005**. 5(9): p. 689-698.

184. Ashworth, A. *A synthetic lethal therapeutic approach: poly(ADP) ribose polymerase inhibitors for the treatment of cancers deficient in DNA double-strand break repair.* J Clin Oncol, **2008**. 26(22): p. 3785-90.

185. Ahel, I.; Ahel, D.; Matsusaka, T.; Clark, A.J.; Pines, J.; Boulton, S.J.; West, S.C. *Poly(ADP-ribose)-binding zinc finger motifs in DNA repair/checkpoint proteins.* Nature, **2008**. 451(7174): p. 81-5.

186. Gagne, J.P.; Pic, E.; Isabelle, M.; Krietsch, J.; Ethier, C.; Paquet, E.; Kelly, I.; Boutin, M.; Moon, K.M.; Foster, L.J.; Poirier, G.G. *Quantitative proteomics profiling of the poly(ADP-ribose)-related response to genotoxic stress.* Nucleic Acids Res, **2012**. 40(16): p. 7788-805.

187. Wang, M.; Wu, W.; Wu, W.; Rosidi, B.; Zhang, L.; Wang, H.; Iliakis, G. *PARP-1 and Ku compete for repair of DNA double strand breaks by distinct NHEJ pathways.* Nucleic Acids Res, **2006**. 34(21): p. 6170-82.

188. Hochegger, H.; Dejsuphong, D.; Fukushima, T.; Morrison, C.; Sonoda, E.; Schreiber, V.; Zhao, G.Y.; Saberi, A.; Masutani, M.; Adachi, N.; Koyama, H.; de Murcia, G.; Takeda, S. *Parp-1 protects homologous recombination from interference by Ku and Ligase IV in vertebrate cells.* EMBO J, **2006**. 25(6): p. 1305-14.

189. Paddock, M.N.; Bauman, A.T.; Higdon, R.; Kolker, E.; Takeda, S.; Scharenberg, A.M. *Competition between PARP-1 and Ku70 control the decision between high-fidelity and mutagenic DNA repair.* DNA Repair (Amst), **2011**. 10(3): p. 338-43.

190. Patel, A.G.; Sarkaria, J.N.; Kaufmann, S.H. *Nonhomologous end joining drives poly(ADP-ribose) polymerase (PARP) inhibitor lethality in homologous recombination-deficient cells.* Proc Natl Acad Sci U S A, **2011**. 108(8): p. 3406-11.

191. De Lorenzo, S.B.; Patel, A.G.; Hurley, R.M.; Kaufmann, S.H. *The Elephant and the Blind Men: Making Sense of PARP Inhibitors in Homologous Recombination Deficient Tumor Cells.* Front Oncol, **2013**. 3: p. 228.

192. Lord, C.J.; Ashworth, A. *Mechanisms of resistance to therapies targeting BRCA-mutant cancers.* Nat Med, **2013**. 19(11): p. 1381-8.

193. Montoni, A.; Robu, M.; Pouliot, E.; Shah, G.M. *Resistance to PARP-Inhibitors in Cancer Therapy.* Front Pharmacol, **2013**. 4: p. 18.

194. Dufour, R.; Daumar, P.; Mounetou, E.; Aubel, C.; Kwiatkowski, F.; Abrial, C.; Vatoux, C.; Penault-Llorca, F.; Bamdad, M. *BCRP and P-gp relay*

overexpression in triple negative basal-like breast cancer cell line: a prospective role in resistance to Olaparib. Sci Rep, **2015**. 5: p. 12670.

195. Volinia, S.; Galasso, M.; Sana, M.E.; Wise, T.F.; Palatini, J.; Huebner, K.; Croce, C.M. *Breast cancer signatures for invasiveness and prognosis defined by deep sequencing of microRNA.* Proc Natl Acad Sci U S A, **2012**. 109(8): p. 3024-9.

196. Liao, C.; Sitzmann, M.; Pugliese, A.; Nicklaus, M.C. *Software and resources for computational medicinal chemistry.* Future Med Chem, **2011**. 3(8): p. 1057-85.

197. Leelananda, S.P.; Lindert, S. *Computational methods in drug discovery.* Beilstein J Org Chem, **2016**. 12: p. 2694-2718.

198. Macalino, S.J.; Gosu, V.; Hong, S.; Choi, S. *Role of computer-aided drug design in modern drug discovery.* Arch Pharm Res, **2015**. 38(9): p. 1686-701.

199. Cerqueira, N.M.; Gesto, D.; Oliveira, E.F.; Santos-Martins, D.; Bras, N.F.; Sousa, S.F.; Fernandes, P.A.; Ramos, M.J. *Receptor-based virtual screening protocol for drug discovery.* Arch Biochem Biophys, **2015**. 582: p. 56-67.

200. Sliwoski, G.; Kothiwale, S.; Meiler, J.; Lowe, E.W., Jr. *Computational methods in drug discovery.* Pharmacol Rev, **2014**. 66(1): p. 334-95.

201. Ripphausen, P.; Nisius, B.; Peltason, L.; Bajorath, J. *Quo vadis, virtual screening? A comprehensive survey of prospective applications.* J Med Chem, **2010**. 53(24): p. 8461-7.

202. Jorgensen, W.L. *The many roles of computation in drug discovery.* Science, **2004**. 303(5665): p. 1813-8.

203. Voet, A.; Zhang, K.Y. *Pharmacophore modelling as a virtual screening tool for the discovery of small molecule protein-protein interaction inhibitors.* Curr Pharm Des, **2012**. 18(30): p. 4586-98.

204. Rognan, D. *The impact of in silico screening in the discovery of novel and safer drug candidates.* Pharmacol Ther, **2017**.

205. Cushman, D.W.; Cheung, H.S.; Sabo, E.F.; Ondetti, M.A. *Design of potent competitive inhibitors of angiotensin-converting enzyme. Carboxyalkanoyl and mercaptoalkanoyl amino acids.* Biochemistry, **1977**. 16(25): p. 5484-5491.

206. von Itzstein, M.; Wu, W.-Y.; Kok, G.B.; Pegg, M.S.; Dyason, J.C.; Jin, B.; Phan, T.V.; Smythe, M.L.; White, H.F.; Oliver, S.W.; Colman, P.M.; Varghese, J.N.; Ryan, D.M.; Woods, J.M.; Bethell, R.C.; Hotham, V.J.; Cameron, J.M. Penn, C.R. *Rational design of potent sialidase-based*

inhibitors of influenza virus replication. Nature, **1993**. 363(6428): p. 418-423.

207. Greer, J.; Erickson, J.W.; Baldwin, J.J.; Varney, M.D. *Application of the Three-Dimensional Structures of Protein Target Molecules in Structure-Based Drug Design.* J Med Chem, **1994**. 37(8): p. 1035-1054.

208. Craig, J.C.; Duncan, I.B.; Hockley, D.; Grief, C.; Roberts, N.A.; Mills, J.S. *Antiviral properties of Ro 31-8959, an inhibitor of human immunodeficiency virus (HIV) proteinase.* Antiviral Research, **1991**. 16(4): p. 295-305.

209. Turner, S.R.; Strohbach, J.W.; Tommasi, R.A.; Aristoff, P.A.; Johnson, P.D.; Skulnick, H.I.; Dolak, L.A.; Seest, E.P.; Tomich, P.K.; Bohanon, M.J.; Horng, M.-M.; Lynn, J.C.; Chong, K.-T.; Hinshaw, R.R.; Watenpaugh, K.D.; Janakiraman, M.N.; Thaisrivongs, S. *Tipranavir (PNU-140690): A Potent, Orally Bioavailable Nonpeptidic HIV Protease Inhibitor of the 5,6-Dihydro-4-hydroxy-2-pyrone Sulfonamide Class.* J Med Chem, **1998**. 41(18): p. 3467-3476.

210. de Béthune, M.-P. *Non-nucleoside reverse transcriptase inhibitors (NNRTIs), their discovery, development, and use in the treatment of HIV-1 infection: A review of the last 20 years (1989–2009).* Antiviral Research, **2010**. 85(1): p. 75-90.

211. Wood, J.M.; Maibaum, J.; Rahuel, J.; Grütter, M.G.; Cohen, N.-C.; Rasetti, V.; Rüger, H.; Göschke, R.; Stutz, S.; Fuhrer, W.; Schilling, W.; Rigollier, P.; Yamaguchi, Y.; Cumin, F.; Baum, H.-P.; Schnell, C.R.; Herold, P.; Mah, R.; Jensen, C.; O'Brien, E.; Stanton, A.; Bedigian, M.P. *Structure-based design of aliskiren, a novel orally effective renin inhibitor.* Biochem Biophys Res Commun, **2003**. 308(4): p. 698-705.

212. Weisberg, E.; Manley, P.W.; Breitenstein, W.; Brüggen, J.; Cowan-Jacob, S.W.; Ray, A.; Huntly, B.; Fabbro, D.; Fendrich, G.; Hall-Meyers, E.; Kung, A.L.; Mestan, J.; Daley, G.Q.; Callahan, L.; Catley, L.; Cavazza, C.; Mohammed, A.; Neuberg, D.; Wright, R.D.; Gilliland, D.G.; Griffin, J.D. *Characterization of AMN107, a selective inhibitor of native and mutant Bcr-Abl.* Cancer Cell, **2005**. 7(2): p. 129-141.

213. Zhexin, X. *Advances in Homology Protein Structure Modeling.* Curr Protein Pept Sci, **2006**. 7(3): p. 217-227.

214. Krieger, E.; Nabuurs, S.B.; Vriend, G. *Homology Modeling*, in *Structural Bioinformatics*. GU, J.; Bourne, P.E., Ed.; ISBN: 978-0-470-18105-8, **2005**, John Wiley & Sons, Inc. p. 509-523.

215. Lemer, C.M.R.; Rooman, M.J.; Wodak, S.J. *Protein structure prediction by threading methods: Evaluation of current techniques.* Proteins, **1995**. 23(3): p. 337-355.

216. Hardin, C.; Pogorelov, T.V.; Luthey-Schulten, Z. *Ab initio protein structure prediction.* Curr Opin Struct Biol, **2002**. 12(2): p. 176-181.

217. Lee, J.; Wu, S.; Zhang, Y. *Ab Initio Protein Structure Prediction*, in *From Protein Structure to Function with Bioinformatics*, Rigden, D.J., Ed.; ISBN 978-94-024-1069-3, **2009**, Springer Netherlands: Dordrecht. p. 3-25.

218. Kutchukian, P.S.; Shakhnovich, E.I. *De novo design: balancing novelty and confined chemical space.* Expert Opin Drug Discov, **2010**. 5(8): p. 789-812.

219. Rodrigues, T.; Schneider, G. *Flashback Forward: Reaction-Driven De Novo Design of Bioactive Compounds.* Synlett, **2014**. 25(02): p. 170-178.

220. Schneider, G.; Fechner, U. *Computer-based de novo design of drug-like molecules.* Nat Rev Drug Discov, **2005**. 4(8): p. 649-63.

221. Cheng, T.; Li, Q.; Zhou, Z.; Wang, Y.; Bryant, S.H. *Structure-based virtual screening for drug discovery: a problem-centric review.* AAPS J, **2012**. 14(1): p. 133-41.

222. Huang, S.Y.; Grinter, S.Z.; Zou, X. *Scoring functions and their evaluation methods for protein-ligand docking: recent advances and future directions.* Phys Chem Chem Phys, **2010**. 12(40): p. 12899-908.

223. May, A.; Sieker, F.; Zacharias, M. *How to Efficiently Include Receptor Flexibility During Computational Docking.* Curr Comput Aided Drug Des, **2008**. 4(2): p. 143-153.

224. Meng, X.Y.; Zhang, H.X.; Mezei, M.; Cui, M. Molecular docking: a powerful approach for structure-based drug discovery. Curr Comput Aided Drug Des, **2011**. 7(2): p. 146-57.

225. Kuntz, I.D.; Blaney, J.M.; Oatley, S.J.; Langridge, R.; Ferrin, T.E. *A geometric approach to macromolecule-ligand interactions.* J Mol Biol, **1982**. 161(2): p. 269-288.

226. Ritchie, D.W. *Recent progress and future directions in protein-protein docking.* Curr Protein Pept Sci, **2008**. 9(1): p. 1-15.

227. Hashmi, I.; Shehu, A. *HopDock: a probabilistic search algorithm for decoy sampling in protein-protein docking.* Proteome Sci, **2013**. 11(1): p. S6.

228. Totrov, M.; Abagyan, R. *Flexible ligand docking to multiple receptor conformations: a practical alternative.* Curr Opin Struct Biol, **2008**. 18(2): p. 178-84.

229. Amaro, R.E.; Baron, R.; McCammon, J.A. *An improved relaxed complex scheme for receptor flexibility in computer-aided drug design.* J Comput Aided Mol Des, **2008**. 22.

230. Bolstad, E.S.D.; Anderson, A.C. *In pursuit of virtual lead optimization: Pruning ensembles of receptor structures for increased efficiency and accuracy during docking.* Proteins, **2009**. 75(1): p. 62-74.

231. N. Cavasotto, C.; Singh, N. *Docking and High Throughput Docking: Successes and the Challenge of Protein Flexibility*. Curr Comput Aided Drug Des, **2008**. 4(3): p. 221-234.

232. Cozzini, P.; Kellogg, G.E.; Spyrakis, F.; Abraham, D.J.; Costantino, G.; Emerson, A.; Fanelli, F.; Gohlke, H.; Kuhn, L.A.; Morris, G.M.; Orozco, M.; Pertinhez, T.A.; Rizzi, M.; Sotriffer, C.A. *Target flexibility: an emerging consideration in drug discovery and design.* J Med Chem, **2008**. 51(20): p. 6237-55.

233. Hansson, T.; Oostenbrink, C.; van Gunsteren, W. *Molecular dynamics simulations.* Curr Opin Struct Biol, **2002**. 12(2): p. 190-6.

234. Karplus, M.; McCammon, J.A. *Molecular dynamics simulations of biomolecules.* Nat Struct Biol, **2002**. 9(9): p. 646-52.

235. Leach, A.L. *Monte Carlo simulation methods. In Molecular Modelling: Principles and Applications. 2nd ed*. ISBN: 0582382106, **2001**: Pearson Education. 410-456.

236. Trosset, J.-Y.; Scheraga, H.A. *Prodock: Software package for protein modeling and docking.* J Comput Chem, **1999**. 20(4): p. 412-427.

237. Pak, Y.; Wang, S. *Application of a Molecular Dynamics Simulation Method with a Generalized Effective Potential to the Flexible Molecular Docking Problems.* J. Phys. Chem. B, **2000**. 104(2): p. 354-359.

238. Schnecke, V.; Swanson, C.A.; Getzoff, E.D.; Tainer, J.A.; Kuhn, L.A. *Screening a peptidyl database for potential ligands to proteins with side-chain flexibility.* Proteins, **1998**. 33(1): p. 74-87.

239. Cerqueira, N.M.F.S.A.; Bras, N.F.; Fernandes, P.A.; Ramos, M.J. *MADAMM: A multistaged docking with an automated molecular modeling protocol.* Proteins, **2009**. 74(1): p. 192-206.

240. Knegtel, R.M.A.; Kuntz, I.D.; Oshiro, C.M. *Molecular docking to ensembles of protein structures.* J Mol Biol, **1997**. 266(2): p. 424-440.

241. Heather, A.C. *Protein Flexibility is an Important Component of Structure-Based Drug Discovery.* Curr Pharm Des, **2002**. 8(17): p. 1571-1578.

242. Osterberg, F.; Morris, G.M.; Sanner, M.F.; Olson, A.J.; Goodsell, D.S. *Automated docking to multiple target structures: incorporation of protein mobility and structural water heterogeneity in AutoDock.* Proteins, **2002**. 46(1): p. 34-40.

243. Fischer, B.; Fukuzawa, K.; Wenzel, W. *Receptor-specific scoring functions derived from quantum chemical models improve affinity estimates for in-silico drug discovery.* Proteins, **2008**. 70(4): p. 1264-73.

244. Huang, N.; Kalyanaraman, C.; Bernacki, K.; Jacobson, M.P. *Molecular mechanics methods for predicting protein-ligand binding.* Phys Chem Chem Phys, **2006**. 8(44): p. 5166-5177.

245. Verdonk, M.L.; Cole, J.C.; Hartshorn, M.J.; Murray, C.W.; Taylor, R.D. *Improved protein-ligand docking using GOLD.* Proteins, **2003**. 52(4): p. 609-23.

246. Jones, G.; Willett, P.; Glen, R.C. *Molecular recognition of receptor sites using a genetic algorithm with a description of desolvation.* J Mol Biol, **1995**. 245(1): p. 43-53.

247. Jones, G.; Willett, P.; Glen, R.C.; Leach, A.R.; Taylor, R. *Development and validation of a genetic algorithm for flexible docking.* J Mol Biol, **1997**. 267(3): p. 727-48.

248. Makino, S.; Kuntz, I.D. *Automated flexible ligand docking method and its application for database search.* J Comput Chem, **1997**. 18(14): p. 1812-1825.

249. Morris, G.M.; Goodsell, D.S.; Huey, R.; Olson, A.J. *Distributed automated docking of flexible ligands to proteins: Parallel applications of AutoDock 2.4.* J Comput Aided Mol Des, **1996**. 10(4): p. 293-304.

250. Weiner, S.J.; Kollman, P.A.; Nguyen, D.T.; Case, D.A. *An all atom force field for simulations of proteins and nucleic acids.* J Comput Chem, **1986**. 7(2): p. 230-252.

251. Eldridge, M.D.; Murray, C.W.; Auton, T.R.; Paolini, G.V.; Mee, R.P. *Empirical scoring functions: I. The development of a fast empirical scoring function to estimate the binding affinity of ligands in receptor complexes.* J Comput Aided Mol Des, **1997**. 11(5): p. 425-445.

252. Artemenko, N. *Distance Dependent Scoring Function for Describing Protein−Ligand Intermolecular Interactions.* J Chem Inf Model, **2008**. 48(3): p. 569-574.

253. Martin, O.; Schomburg, D. *Efficient comprehensive scoring of docked protein complexes using probabilistic support vector machines.* Proteins, **2008**. 70(4): p. 1367-1378.

254. Friesner, R.A.; Murphy, R.B.; Repasky, M.P.; Frye, L.L.; Greenwood, J.R.; Halgren, T.A.; Sanschagrin, P.C.; Mainz, D.T. *Extra Precision Glide: Docking and Scoring Incorporating a Model of Hydrophobic Enclosure for Protein−Ligand Complexes.* J Med Chem, **2006**. 49(21): p. 6177-6196.

255. Huang, S.-Y.; Zou, X. *An iterative knowledge-based scoring function to predict protein–ligand interactions: I. Derivation of interaction potentials.* J Comput Chem, **2006**. 27(15): p. 1866-1875.

256. Gohlke, H.; Hendlich, M.; Klebe, G. *Knowledge-based scoring function to predict protein-ligand interactions.* J Mol Biol., **2000**. 295(2): p. 337-356.

257. Velec, H.F.G.; Gohlke, H.; Klebe, G. *DrugScore(CSD)-Knowledge-Based Scoring Function Derived from Small Molecule Crystal Data with Superior Recognition Rate of Near-Native Ligand Poses and Better Affinity Prediction.* J Med Chem, **2005**. 48(20): p. 6296-6303.

258. Charifson, P.S.; Corkery, J.J.; Murcko, M.A.; Walters, W.P. *Consensus scoring: A method for obtaining improved hit rates from docking databases of three-dimensional structures into proteins.* J Med Chem, **1999**. 42(25): p. 5100-9.

259. Wang, R.; Lai, L.; Wang, S. *Further development and validation of empirical scoring functions for structure-based binding affinity prediction.* J Comput Aided Mol Des, **2002**. 16(1): p. 11-26.

260. Ganesan, A.; Coote, M.L.; Barakat, K. *Molecular dynamics-driven drug discovery: leaping forward with confidence.* Drug Discov Today, **2017**. 22(2): p. 249-269.

261. Moroni, E.; Paladino, A.; Colombo, G. *The Dynamics of Drug Discovery.* Curr Top Med Chem, **2015**. 15(20): p. 2043-55.

262. Wang, J.; Wolf, R.M.; Caldwell, J.W.; Kollman, P.A.; Case, D.A. *Development and testing of a general amber force field.* J Comput Chem, **2004**. 25(9): p. 1157-74.

263. Vanommeslaeghe, K.; Hatcher, E.; Acharya, C.; Kundu, S.; Zhong, S.; Shim, J.; Darian, E.; Guvench, O.; Lopes, P.; Vorobyov, I.; Mackerell, A.D., Jr. *CHARMM general force field: A force field for drug-like molecules compatible with the CHARMM all-atom additive biological force fields.* J Comput Chem, **2010**. 31(4): p. 671-90.

264. Daura, X.; Mark, A.E.; Van Gunsteren, W.F. *Parametrization of aliphatic CHn united atoms of GROMOS96 force field.* J Comput Chem, **1998**. 19(5): p. 535-547.

265. Childers, M.C. Daggett, V. *Insights from molecular dynamics simulations for computational protein design.* Mol Syst Des Eng, **2017**. 2(1): p. 9-33.

266. Gasteiger, J. *Of Molecules and Humans.* J Med Chem, **2006**. 49(22): p. 6429-6434.

267. Rizzo, R.C.; Toba, S.; Kuntz, I.D. *A molecular basis for the selectivity of thiadiazole urea inhibitors with stromelysin-1 and gelatinase-A from generalized born molecular dynamics simulations.* J Med Chem, **2004**. 47(12): p. 3065-74.

268. Chennubhotla, C.; Yang, Z.; Bahar, I. *Coupling between global dynamics and signal transduction pathways: a mechanism of allostery for chaperonin GroEL.* Mol Biosyst, **2008**. 4(4): p. 287-92.

269. Smock, R.G.; Gierasch, L.M. *Sending signals dynamically.* Science, **2009**. 324(5924): p. 198-203.

270. Carlson, H.A.; Masukawa, K.M.; Rubins, K.; Bushman, F.D.; Jorgensen, W.L.; Lins, R.D.; Briggs, J.M.; McCammon, J.A. *Developing a dynamic pharmacophore model for HIV-1 integrase.* J Med Chem, **2000**. 43(11): p. 2100-14.

271. Meagher, K.L.; Carlson, H.A. *Incorporating protein flexibility in structure-based drug discovery: using HIV-1 protease as a test case.* J Am Chem Soc, **2004**. 126(41): p. 13276-81.

272. Bowman, A.L.; Nikolovska-Coleska, Z.; Zhong, H.; Wang, S.; Carlson, H.A. *Small molecule inhibitors of the MDM2-p53 interaction discovered by ensemble-based receptor models.* J Am Chem Soc, **2007**. 129(42): p. 12809-14.

273. Meli, M.; Pennati, M.; Curto, M.; Daidone, M.G.; Plescia, J.; Toba, S.; Altieri, D.C.; Zaffaroni, N.; Colombo, G. *Small-molecule targeting of heat shock protein 90 chaperone function: rational identification of a new anticancer lead.* J Med Chem, **2006**. 49(26): p. 7721-30.

274. Genoni, A.; Pennati, M.; Morra, G.; Zaffaroni, N.; Colombo, G. *Ligand selection from the analysis of protein conformational substates: new leads targeting the N-terminal domain of Hsp90.* RSC Advances, **2012**. 2(10): p. 4268-4282.

275. Colombo, G.; Margosio, B.; Ragona, L.; Neves, M.; Bonifacio, S.; Annis, D.S.; Stravalaci, M.; Tomaselli, S.; Giavazzi, R.; Rusnati, M.; Presta, M.; Zetta, L.; Mosher, D.F.; Ribatti, D.; Gobbi, M.; Taraboletti, G. *Non-peptidic thrombospondin-1 mimics as fibroblast growth factor-2 inhibitors: an integrated strategy for the development of new antiangiogenic compounds.* J Biol Chem, **2010**. 285(12): p. 8733-42.

276. Marhefka, C.A.; Moore, B.M., 2nd; Bishop, T.C.; Kirkovsky, L.; Mukherjee, A.; Dalton, J.T.; Miller, D.D. *Homology modeling using multiple molecular dynamics simulations and docking studies of the human androgen receptor ligand binding domain bound to testosterone and nonsteroidal ligands.* J Med Chem, **2001**. 44(11): p. 1729-40.

277. Huo, S.; Wang, J.; Cieplak, P.; Kollman, P.A.; Kuntz, I.D. *Molecular dynamics and free energy analyses of cathepsin D-inhibitor interactions: insight into structure-based ligand design.* J Med Chem, **2002**. 45(7): p. 1412-9.

278. Jitender, V.; Vijay, M.K.; Evans, C.C. *3D-QSAR in Drug Design - A Review.* Curr Top Med Chem, **2010**. 10(1): p. 95-115.

279. Verma, R.P.; Hansch, C. *Camptothecins: A SAR/QSAR Study.* Chem Rev, **2009**. 109(1): p. 213-235.

280. Damale, M.G.; Harke, S.N.; Kalam Khan, F.A.; Shinde, D.B.; Sangshetti, J.N. *Recent advances in multidimensional QSAR (4D-6D): a critical review.* Mini Rev Med Chem, **2014**. 14(1): p. 35-55.

281. Cherkasov, A.; Muratov, E.N.; Fourches, D.; Varnek, A.; Baskin, II; Cronin, M.; Dearden, J.; Gramatica, P.; Martin, Y.C.; Todeschini, R.; Consonni, V.; Kuz'min, V.E.; Cramer, R.; Benigni, R.; Yang, C.; Rathman, J.; Terfloth, L.; Gasteiger, J.; Richard, A.; Tropsha, A. *QSAR modeling: where have you been? Where are you going to?* J Med Chem, **2014**. 57(12): p. 4977-5010.

282. Melo-Filho, C.C.; Braga, R.C.; Andrade, C.H. *3D-QSAR approaches in drug design: perspectives to generate reliable CoMFA models.* Curr Comput Aided Drug Des, **2014**. 10(2): p. 148-59.

283. Klopmand, G. *Concepts and applications of molecular similarity. Journal of Computational Chemistry.; Johnson, M.A.; Maggiora, G.M., Ed., ISBN: 978-0-471-62175-1: John Wiley & Sons, New York, **1990**, 393 pp.*,13(4): p. 539-540.

284. Maggiora, G.; Vogt, M.; Stumpfe, D.; Bajorath, J. *Molecular Similarity in Medicinal Chemistry.* J Med Chem, **2014**. 57(8): p. 3186-3204.

285. Wermuth, C.G.; Ganellin, C.R.; Lindberg, P.; Mitscher, L.A. *Glossary of terms used in medicinal chemistry (IUPAC Recommendations 1998)*, in *Pure and Applied Chemistry*. **1998**. p. 1129.

286. Van Drie, J.H. *Strategies for the determination of pharmacophoric 3D database queries.* J Comput Aided Mol Des, **1997**. 11(1): p. 39-52.

287. Caporuscio, F.; Tafi, A. *Pharmacophore modelling: a forty year old approach and its modern synergies.* Curr Med Chem, **2011**. 18(17): p. 2543-53.

288. Bostrom, J. *Reproducing the conformations of protein-bound ligands: a critical evaluation of several popular conformational searching tools.* J Comput Aided Mol Des, **2001**. 15(12): p. 1137-52.

289. Lipinski, C.A.; Lombardo, F.; Dominy, B.W.; Feeney, P.J. *Experimental and computational approaches to estimate solubility and permeability in drug discovery and development settings.* Adv Drug Deliv Rev, **2001**. 46(1-3): p. 3-26.

290. Sun, H. *Pharmacophore-based virtual screening.* Curr Med Chem, **2008**. 15(10): p. 1018-24.

291. *Catalyst; Accelrys Software Inc. http://accelrys.com/.*

292. Dixon, S.L.; Smondyrev, A.M.; Rao, S.N. *PHASE: a novel approach to pharmacophore modeling and 3D database searching.* Chem Biol Drug Des, **2006**. 67(5): p. 370-2.

293. *Molecular Operating Environment (MOE), 2013.08; Chemical Computing Group ULC, 1010 Sherbooke St. West, Suite #910, Montreal, QC, Canada, H3A 2R7.*

294. Maga, G.; Falchi, F.; Garbelli, A.; Belfiore, A.; Witvrouw, M.; Manetti, F.; Botta, M. *Pharmacophore modeling and molecular docking led to the discovery of inhibitors of human immunodeficiency virus-1 replication targeting the human cellular aspartic acid-glutamic acid-alanine-aspartic acid box polypeptide 3.* J Med Chem, **2008**. 51(21): p. 6635-8.

295. Burnett, J.C.; Wang, C.; Nuss, J.E.; Nguyen, T.L.; Hermone, A.R.; Schmidt, J.J.; Gussio, R.; Wipf, P.; Bavari, S. *Pharmacophore-guided lead optimization: the rational design of a non-zinc coordinating, sub-micromolar inhibitor of the botulinum neurotoxin serotype a metalloprotease.* Bioorg Med Chem Lett, **2009**. 19(19): p. 5811-3.

296. Aronov, A.M. *Common pharmacophores for uncharged human ether-a-go-go-related gene (hERG) blockers.* J Med Chem, **2006**. 49(23): p. 6917-21.

297. Klabunde, T.; Evers, A. *GPCR antitarget modeling: pharmacophore models for biogenic amine binding GPCRs to avoid GPCR-mediated side effects.* Chembiochem, **2005**. 6(5): p. 876-89.

298. Steindl, T.M.; Schuster, D.; Wolber, G.; Laggner, C.; Langer, T. *High-throughput structure-based pharmacophore modelling as a basis for successful parallel virtual screening.* J Comput Aided Mol Des, **2006**. 20(12): p. 703-15.

299. Schuster, D.; Langer, T. *The identification of ligand features essential for PXR activation by pharmacophore modeling.* J Chem Inf Model, **2005**. 45(2): p. 431-9.

300. Artese, A.; Cross, S.; Costa, G.; Distinto, S.; Parrotta, L.; Alcaro, S.; Ortuso, F.; Cruciani, G. *Molecular interaction fields in drug discovery: recent advances and future perspectives.* WIRES COMPUT MOL SCI, **2013**. 3(6): p. 594-613.

301. Goodford, P.J. *A computational procedure for determining energetically favorable binding sites on biologically important macromolecules.* J Med Chem, **1985**. 28(7): p. 849-57.

302. Pastor, M.; Cruciani, G.; McLay, I.; Pickett, S.; Clementi, S. *GRid-INdependent Descriptors (GRIND): A Novel Class of Alignment-Independent Three-Dimensional Molecular Descriptors.* J Med Chem, **2000**. 43(17): p. 3233-3243.

303. Lupo, B.;Trusolino, L. *Review: Inhibition of poly(ADP-ribosyl)ation in cancer: Old and new paradigms revisited*. Biochim Biophys Acta, **2014**. 1846(1): p. 201-15.

304. Khedkar, S.A.; Malde, A.K.; Coutinho, E.C.; Srivastava, S. *Pharmacophore modeling in drug discovery and development: an overview.* Med Chem, **2007**. 3(2): p. 187-97.

305. John, S.; Thangapandian, S.; Sakkiah, S.; Lee, K.W. *Potent BACE-1 inhibitor design using pharmacophore modeling, in silico screening and molecular docking studies.* BMC Bioinformatics, **2011**. 12 Suppl 1: p. S28.

306. Vyas, V.K.; Ghate, M.; Goel, A. *Pharmacophore modeling, virtual screening, docking and in silico ADMET analysis of protein kinase B (PKB beta) inhibitors.* J Mol Graph Model, **2013**. 42: p. 17-25.

307. Sakkiah, S.; Thangapandian, S.; John, S.; Lee, K.W. *Pharmacophore based virtual screening, molecular docking studies to design potent heat shock protein 90 inhibitors.* Eur J Med Chem, **2011**. 46(7): p. 2937-47.

308. Hornak, V.; Abel, R.; Okur, A.; Strockbine, B.; Roitberg, A.; Simmerling, C. *Comparison of multiple Amber force fields and development of improved protein backbone parameters.* Proteins, **2006**. 65(3): p. 712-25.

309. Jorgensen, W.L.; Chandrasekhar, J.; Madura, J.D.; Impey, R.W.; Klein, M.L. *Comparison of simple potential functions for simulating liquid water.* J Chem Phys, **1983**. 79(2): p. 926-935.

310. Darden, T.; York, D.; Pedersen, L. *Particle mesh Ewald: An N·log(N) method for Ewald sums in large systems.* J Chem Phys, **1993**. 98(12): p. 10089-10092.

311. Ryckaert, J.-P.; Ciccotti, G.; Berendsen, H.J.C. *Numerical integration of the cartesian equations of motion of a system with constraints: molecular dynamics of n-alkanes.* J Comput Phys, **1977**. 23(3): p. 327-341.

312. Hess, B.; Kutzner, C.; van der Spoel, D.; Lindahl, E. *GROMACS 4: Algorithms for Highly Efficient, Load-Balanced, and Scalable Molecular Simulation.* J Chem Theory Comput, **2008**. 4(3): p. 435-47.

313. Developmental Therapeutics Program NCI/NIH *Developmental Therapeutics Program NCI/NIH.* http://dtp.nci.nih.gov/.

314. Knox, C.; Law, V.; Jewison, T.; Liu, P.; Ly, S.; Frolkis, A.; Pon, A.; Banco, K.; Mak, C.; Neveu, V.; Djoumbou, Y.; Eisner, R.; Guo, A.C.; Wishart, D.S. *DrugBank 3.0: a comprehensive resource for 'omics' research on drugs.* Nucleic Acids Res, **2011**. 39(Database issue): p. D1035-41.

315. *Asinex.* http://www.asinex.com/.

316. Irwin, J.J.; Shoichet, B.K. *ZINC--a free database of commercially available compounds for virtual screening.* J Chem Inf Model, **2005**. 45(1): p. 177-82.

317. Jorgensen, W.L.; Maxwell, D.S.; Tirado-Rives, J. *Development and Testing of the OPLS All-Atom Force Field on Conformational Energetics and Properties of Organic Liquids.* J Am Chem Soc, **1996**. 118(45): p. 11225-11236.

318. Wahlberg, E.; Karlberg, T.; Kouznetsova, E.; Markova, N.; Macchiarulo, A.; Thorsell, A.G.; Pol, E.; Frostell, A.; Ekblad, T.; Oncu, D.; Kull, B.; Robertson, G.M.; Pellicciari, R.; Schuler, H.; Weigelt, J. *Family-wide chemical profiling and structural analysis of PARP and tankyrase inhibitors.* Nat Biotechnol, **2012**. 30(3): p. 283-8.

319. Humphrey, W.; Dalke, A.; Schulten, K. *VMD: visual molecular dynamics.* J Mol Graph, **1996**. 14(1): p. 33-8, 27-8.

320. Jiang, F.; Wang, H.-J.; Bao, Q.-C.; Wang, L.; Jin, Y.-H.; Zhang, Q.; Jiang, D.; You, Q.-D.; Xu, X.-L. *Optimization and biological evaluation of celastrol derivatives as Hsp90–Cdc37 interaction disruptors with improved druglike properties.* Bioorganic Med Chem, **2016**. 24(21): p. 5431-5439.

321. Durrant, J.D.; McCammon, J.A. *Molecular dynamics simulations and drug discovery.* BMC Biology, **2011**. 9(1): p. 71.

322. Nestl, B.M.; Hauer, B. *Engineering of Flexible Loops in Enzymes.* ACS Catalysis, **2014**. 4(9): p. 3201-3211.

323. Greenidge, P.A.; Carlsson, B.; Bladh, L.G.; Gillner, M. *Pharmacophores incorporating numerous excluded volumes defined by X-ray crystallographic structure in three-dimensional database searching: application to the thyroid hormone receptor.* J Med Chem, **1998**. 41(14): p. 2503-12.

324. Ramirez, D.; Caballero, J. *Is It Reliable to Use Common Molecular Docking Methods for Comparing the Binding Affinities of Enantiomer Pairs for Their Protein Target?* Int J Mol Sci, **2016**. 17(4).

325. Mysinger, M.M.; Carchia, M.; Irwin, J.J.; Shoichet, B.K. *Directory of useful decoys, enhanced (DUD-E): better ligands and decoys for better benchmarking.* J Med Chem, **2012**. 55(14): p. 6582-94.

326. Forman, B.M.; Goode, E.; Chen, J.; Oro, A.E.; Bradley, D.J.; Perlmann, T.; Noonan, D.J.; Burka, L.T.; McMorris, T.; Lamph, W.W.; Evans, R.M.; Weinberger, C. *Identification of a nuclear receptor that is activated by farnesol metabolites.* Cell, **1995**. 81(5): p. 687-93.

327. Makishima, M.; Okamoto, A.Y.; Repa, J.J.; Tu, H.; Learned, R.M.; Luk, A.; Hull, M.V.; Lustig, K.D.; Mangelsdorf, D.J.; Shan, B. *Identification of a nuclear receptor for bile acids.* Science, **1999**. 284(5418): p. 1362-5.

328. Parks, D.J.; Blanchard, S.G.; Bledsoe, R.K.; Chandra, G.; Consler, T.G.; Kliewer, S.A.; Stimmel, J.B.; Willson, T.M.; Zavacki, A.M.; Moore, D.D.; Lehmann, J.M. *Bile acids: natural ligands for an orphan nuclear receptor.* Science, **1999**. 284(5418): p. 1365-8.

329. Mazuy, C.; Helleboid, A.; Staels, B.; Lefebvre, P. *Nuclear bile acid signaling through the farnesoid X receptor.* Cell Mol Life Sci, **2015**. 72(9): p. 1631-50.

330. Huber, R.M.; Murphy, K.; Miao, B.; Link, J.R.; Cunningham, M.R.; Rupar, M.J.; Gunyuzlu, P.L.; Haws Jr, T.F.; Kassam, A.; Powell, F.; Hollis, G.F.; Young, P.R.; Mukherjee, R.; Burn, T.C. *Generation of multiple farnesoid-X-receptor isoforms through the use of alternative promoters.* Gene, **2002**. 290(1–2): p. 35-43.

331. Bishop-Bailey, D.; Walsh, D.T.; Warner, T.D. *Expression and activation of the farnesoid X receptor in the vasculature.* Proc Natl Acad Sci U S A, **2004**. 101(10): p. 3668-3673.

332. Zhang, R.; Ran, H.H.; Zhang, Y.X.; Liu, P.; Lu, C.Y.; Xu, Q.; Huang, Y. *Farnesoid X receptor regulates vascular reactivity through nitric oxide mechanism.* J Physiol Pharmacol, **2012**. 63(4): p. 367-72.

333. Zhang, R.; Ran, H.; Peng, L.; Zhang, Y.; Shen, W.; Sun, T.; Cao, F.; Chen, Y. *Farnesoid X receptor regulates vasoreactivity via Angiotensin II type 2 receptor and the kallikrein-kinin system in vascular endothelial cells.* Clin Exp Pharmacol Physiol, **2016**. 43(3): p. 327-334.

334. Adorini, L.; Pruzanski, M.; Shapiro, D. *Farnesoid X receptor targeting to treat nonalcoholic steatohepatitis.* Drug Discov Today, **2012**. 17(17): p. 988-997.

335. Ali, A.H.; Carey, E.J.; Lindor, K.D. *Recent advances in the development of farnesoid X receptor agonists.* Ann Transl Med, **2015**. 3(1): p. 5.

336. Vaquero, J.; Monte, M.J.; Dominguez, M.; Muntane, J.; Marin, J.J. *Differential activation of the human farnesoid X receptor depends on the pattern of expressed isoforms and the bile acid pool composition.* Biochem Pharmacol, **2013**. 86(7): p. 926-39.

337. Modica, S.; Gadaleta, R.M.; Moschetta, A. *Deciphering the nuclear bile acid receptor FXR paradigm.* Nucl Recept Signal, **2010**. 8: p. e005.

338. Carr, R.M.; Reid, A.E. *FXR agonists as therapeutic agents for non-alcoholic fatty liver disease.* Curr Atheroscler Rep, **2015**. 17(4): p. 500.

339. Ho, P.P.; Steinman, L. *Obeticholic acid, a synthetic bile acid agonist of the farnesoid X receptor, attenuates experimental autoimmune encephalomyelitis.* Proc Natl Acad Sci U S A, **2016**. 113(6): p. 1600-1605.

340. Younossi, Z.M.; Koenig, A.B.; Abdelatif, D.; Fazel, Y.; Henry, L.; Wymer, M. *Global epidemiology of nonalcoholic fatty liver disease-Meta-analytic assessment of prevalence, incidence, and outcomes.* Hepatology, **2016**. 64(1): p. 73-84.

341. Pellicciari, R.; Fiorucci, S.; Camaioni, E.; Clerici, C.; Costantino, G.; Maloney, P.R.; Morelli, A.; Parks, D.J.; Willson, T.M. *6α-Ethyl-*

Chenodeoxycholic Acid (6-ECDCA), a Potent and Selective FXR Agonist Endowed with Anticholestatic Activity. J Med Chem, **2002**. 45(17): p. 3569-3572.

342. Markham, A.; Keam, S.J. *Obeticholic Acid: First Global Approval.* Drugs, **2016**. 76(12): p. 1221-6.

343. Neuschwander-Tetri, B.A.; Loomba, R.; Sanyal, A.J.; Lavine, J.E.; Van Natta, M.L.; Abdelmalek, M.F.; Chalasani, N.; Dasarathy, S.; Diehl, A.M.; Hameed, B.; Kowdley, K.V.; McCullough, A.; Terrault, N.; Clark, J.M.; Tonascia, J.; Brunt, E.M.; Kleiner, D.E.; Doo, E. *Farnesoid X nuclear receptor ligand obeticholic acid for non-cirrhotic, non-alcoholic steatohepatitis (FLINT): a multicentre, randomised, placebo-controlled trial.* Lancet, **2015**. 385(9972): p. 956-65.

344. Cipriani, S.; Mencarelli, A.; Palladino, G.; Fiorucci, S. *FXR activation reverses insulin resistance and lipid abnormalities and protects against liver steatosis in Zucker (fa/fa) obese rats.* J Lipid Res, **2010**. 51(4): p. 771-84.

345. Verbeke, L.; Farre, R.; Trebicka, J.; Komuta, M.; Roskams, T.; Klein, S.; Elst, I.V.; Windmolders, P.; Vanuytsel, T.; Nevens, F.; Laleman, W. *Obeticholic acid, a farnesoid X receptor agonist, improves portal hypertension by two distinct pathways in cirrhotic rats.* Hepatology, **2014**. 59(6): p. 2286-98.

346. Issa, D.; Wattacheril, J.; Sanyal, A.J. *Treatment options for nonalcoholic steatohepatitis - a safety evaluation.* Expert Opin Drug Saf, **2017**. 16(8): p. 903-913.

347. Yang, L.; Broderick, D.; Jiang, Y.; Hsu, V.; Maier, C.S. *Conformational dynamics of human FXR-LBD ligand interactions studied by hydrogen/deuterium exchange mass spectrometry: insights into the antagonism of the hypolipidemic agent Z-guggulsterone.* Biochim Biophys Acta, **2014**. 1844(9): p. 1684-93.

348. Soisson, S.M.; Parthasarathy, G.; Adams, A.D.; Sahoo, S.; Sitlani, A.; Sparrow, C.; Cui, J.; Becker, J.W. *Identification of a potent synthetic FXR agonist with an unexpected mode of binding and activation.* Proc Natl Acad Sci U S A, **2008**. 105(14): p. 5337-42.

349. Zwanzig, R.W. *High-Temperature Equation of State by a Perturbation Method. I. Nonpolar Gases.* J Chem Phys, **1954**. 22(8): p. 1420-1426.